New approaches to ^{45}Ti, ^{64}Cu, ^{68}Ga, and ^{89}Zr purification by liquid-liquid extraction and development of a ^{45}Ti-labeled PET tracer for the diagnosis of prostate cancer

Pedersen, Kristina Søborg

Publication date:
2019

Document Version
Publisher's PDF, also known as Version of record

New approaches to ^{45}Ti, ^{64}Cu, ^{68}Ga, and ^{89}Zr purification by liquid-liquid extraction and development of a ^{45}Ti-labeled PET tracer for the diagnosis of prostate cancer

PhD Thesis by
Kristina Søborg Pedersen

October 2019

The Hevesy Laboratory, Center for Nuclear Technologies, DTU

Preface

This thesis represents the work conducted during my three years as a PhD student at the Hevesy Laboratory, DTU Nutech, Technical University of Denmark (DTU). The study has been supervised by Dr. Fedor Zhuravlev (main supervisor) and Prof. Mikael Jensen (co-supervisor). The work has mainly been carried out at the Hevesy Laboratory except for a six months external research stay in the group of Prof. Klavs F. Jensen at Massachusetts Institute of Technology (MIT), USA.

The focus of the work has been on the separation and utilization of four different positron emitting radiometals (titanium-45 (^{45}Ti), copper-64 (^{64}Cu), gallium-68 (^{68}Ga), and zirconium-89(^{89}Zr)). A separation technique applicable to radiometal purification and the synthesis and evaluation of a radiotracer for positron emission tomography (PET) have been studied. The separation technique has mainly been tested and optimized during the stay at MIT. This technique has later been applied to purification of radiometals, which was conducted at the Hevesy Laboratory together with the synthesis and production of the radiotracer. The preclinical studies of the radiotracer were conducted at Odense University Hospital.

Acknowledgements

During my three years as a PhD student, I have been introduced to numerous talented and helpful persons, who have supported and guided me. First, I would like to thank my main supervisor Dr. Fedor Zhuravlev for his guidance during these three years. His enthusiasm and determination has inspired me, and I appreciate the confidence he has shown in me, especially by planning an external stay in an early stage of the project. I would like to thank my co-supervisor Prof. Mikael Jensen for his helpful suggestions. His extensive knowledge of the field has helped me seeing new perspectives and the importance of the research within nuclear technologies. I would also like to thank my former co-supervisor Dr. Dennis R. Elema.

I would like to express gratitude to Prof. Klavs F. Jensen and his group at MIT. I appreciate the time I spend in the group and I would especially like to thank Dr. Joseph Imbrogno for introducing me to membrane separation and for making me feel welcome. Furthermore, I would like to thank Dr. Marcella Lusardi for performing ICP-OES measurements.

Special thanks to Dr. Karin Michaelsen Nielsen and Dr. Jesper Fonslet and the isotope production team at the Hevesy Laboratory for producing the radiometals for this project. I also want to thank Karin for helpful suggestions in the development and evaluation of a PET tracer and for her incredible motivation and support.

I would like to thank Christina Baun and Assoc. Prof. Helge Thisgaard at Odense University Hospital for performing and analyzing the preclinical studies and Dr. Andreas T. I. Jensen for help with the planning and organization of these studies.

I would like to thank the members of the Hevesy Laboratory for their support, and interest in the project. In particular I want to thank Dr. Mattia Siragusa for making me feel welcome from the first day, Dr. Pil Fredericia for sharing her thoughts and advice on PhD student life, Charlotte Busk Magnus for many enjoyable times at courses and conferences, and Dr. Claire Deville and Emanuel Sporer for creating a great work environment.

Finally, I would like to thank my family and friends for their great support and assistance and for visiting me whether it’s in Roskilde or Boston.

Abstract

Radiometals for positron emission tomography (PET) are of interest in the ongoing development of radiopharmaceuticals for the diagnosis of diseases. An important advantage of radiometals compared to non-metallic radionuclides is the relatively large variety of half-lives and chemical properties. Several radiometals with suitable physical properties exist; however, not all have been studied and applied for PET.

In this study, four different positron emitting radiometals including titanium-45 (^{45}Ti), copper-64 (^{64}Cu), gallium-68 (^{68}Ga), and zirconium-89 (^{89}Zr) are emphasized. Especially ^{45}Ti has not been extensively studied and applied for PET despite its suitable physical properties. A new approach for the purification of radiometals has been studied and applied in order to possibly improve the availability of radiometals for PET application. Additionally, the development of a ^{45}Ti-labeled PET tracer with a prostate-specific membrane antigen (PSMA) targeting moiety has been performed. The aim of this attempt was to increase the utilization of ^{45}Ti for PET and to improve the diagnosis of prostate cancer.

If the radiometal is produced on a cyclotron, the separation of radiometals from their cyclotron target material is essential for the further production of a PET radiopharmaceutical. The difference in chemical properties of the radiometal and the target material is utilized for the separation. In this study, liquid-liquid extraction (LLE) in flow has been applied to selectively extract the radiometal and a membrane-based separation technique has been used for the phase separation of the aqueous and organic phase. This technique can be automatized which reduces the danger of radiation exposure.

The development of the ^{45}Ti-labeled PET tracer included synthesis of the nonradioactive tracer, radiolabeling optimizations, and purification, analyses and stability studies of the ^{45}Ti-labeled PET tracer. Finally, the radiotracer was evaluated *in vivo* by µPET imaging.

The applied LLE method was optimized for each of the four radiometals and it was possible to extract the radiometals with extraction efficiencies of 84.8 ± 2.4 % for ^{45}Ti, 86.1 ± 5.5 % for ^{64}Cu, 95.7 ± 2.0 % for ^{68}Ga, and 53.7 ± 3.9 % for ^{89}Zr. The co-extraction of the respective cyclotron target materials (scandium, nickel, and yttrium) was not detectable, except for zinc, where $5 \cdot 10^{-3} \pm 3 \cdot 10^{-3}$ % was co-extracted with ^{68}Ga.

The purification method by LLE in flow was subsequently applied to obtain purified ^{45}Ti for the labeling of the synthesized PSMA-targeted radiotracer. Acceptable radiolabeling yield could be achieved and the radiotracer, [^{45}Ti]Ti-CAS-PSMA, was formed. Following purification, analyses of the radiotracer were performed, which led to a final preclinical *in vivo* evaluation of the radiotracer. The biodistribution of [^{45}Ti]Ti-CAS-PSMA was

evaluated in PSMA-positive tumor-bearing mice by µPET imaging. However, no tumor uptake was observed, which can be due to unstable chelation of ^{45}Ti or modifications of the binding motif of the radiotracer, potentially decreasing the affinity for PSMA.

In conclusion, the LLE and phase separation in flow could be applied for the purification of the four radiometals and can be an alternative purification method for radiometals, which are challenging to obtain with conventional purification methods. The availability of these radiometals can thereby be improved. The synthesized ^{45}Ti-labeled PET tracer could not be applied for the detection of prostate cancer. However, the development of the tracer displayed that the LLE method could be applied to obtain ^{45}Ti for the radiolabeling and it might lead to a further development of specific ^{45}Ti-labeled PET tracers.

Resumé

Nye fremgangsmåder til oprensning af ^{45}Ti, ^{64}Cu, ^{68}Ga og ^{89}Zr med væske-væske ekstraktion og udvikling af et ^{45}Ti-mærket PET-sporstof til diagnose af prostatakræft

Anvendelsen af radiometaller til positron emission tomografi (PET) er essentiel i forhold til den løbende udvikling af radioaktive sporstoffer til diagnose af sygdomme. Der findes stor variation i halveringstider og egenskaber bland radiometaller, hvilket er en afgørende fordel ved radiometaller i forhold til ikke-metalliske radionuklider. Der findes talrige radiometaller med velegnede fysiske egenskaber til PET-applikation, men ikke alle har endnu fundet anvendelse i radioaktive sporstoffer.

I dette projekt indgår fire forskellige positron emitterende radiometaller: titanium-45 (^{45}Ti), kobber-64 (^{64}Cu), gallium-68 (^{68}Ga) og zirconium-89 (^{89}Zr). Blandt disse radiometaller er det især ^{45}Ti, som ikke er blevet udførligt undersøgt og anvendt til PET, på trods af ellers velegnede fysiske egenskaber. En ny fremgangsmåde til oprensningen af radiometaller er blevet undersøgt og anvendt i dette studie med et formål om at øge tilgængeligheden af radiometaller til PET. Desuden indgår udviklingen af et nyt ^{45}Ti-mærket radioaktivt sporstof i dette studie. Sporstoffet indeholder en kemisk gruppe med bindingsaffinitet til prostata-specifik membranantigen (PSMA). Formålet med udviklingen af dette sporstof var at øge udbredelsen af ^{45}Ti til PET og at forbedre diagnosen af prostatakræft.

Oprensningen af radiometaller fra deres cyklotron targetmateriale er essentiel for den videre produktion af et radioaktivt sporstof til PET. Oprensningen og separationen af radiometaller fra deres cyklotron targetmateriale er mulig på grund af forskelle i de to metallers kemiske egenskaber. I dette studie er væske-væske ekstraktion i flow anvendt til selektivt at ekstrahere radiometallet, og en membranbaseret separationsteknik er blevet anvendt til at adskille den vandige og den organiske fase efter ekstraktionen. En fordel ved denne teknik er muligheden for at automatisere processen, hvilket kan reducere faren for eksponering til stråling.

I udviklingen af det ^{45}Ti-mærkede sporstof blev det ikke-radioaktive sporstof først syntetiseret og analyseret. Dernæst blev radiomærkningen optimeret, og det radioaktive sporstof blev fremstillet og oprenset. Derefter blev stabiliteten og biodistributionen af det ^{45}Ti-mærkede sporstof undersøgt. Biodistributionen blev evalueret præklinisk *in vivo* ved hjælp af µPET-scanning.

Den beskrevne væske-væske ekstraktionsmetode blev optimeret for hvert af de fire radiometaller, hvor henholdsvis 84,8 ± 2,4% ^{45}Ti, 86,1 ± 5,5% ^{64}Cu, 95,7 ± 2,0% ^{68}Ga og 53,7 ± 3,9% ^{89}Zr blev ekstraheres.

Ekstraktionen af det respektive cyklotron targetmateriale (scandium, nikkel, zink, og yttrium) var enten lav eller ikke mulig at detektere.

Væske-væske ekstraktion i flow blev derefter anvendt til at oprense ^{45}Ti til radiomærkningen af det syntetiserede PSMA-targeted sporstof. Det var muligt at radiomærke og oprense sporstoffet. Stabiliteten af det ^{45}Ti-mærkede sporstof blev analyseret, og det blev evalueret *in vivo* i fire PSMA-positiv-tumor-bærende mus. PET-scanningerne viste dog, at der ikke var et optag af det ^{45}Ti-mærkede sporstof i tumor. Dette kan skyldes ustabilitet af sporstoffet eller modifikationer af sporstoffet, som kan have reduceret affiniteten til PSMA.

Væske-væske ekstraktionen og faseseparationen i flow kunne anvendes til oprensningen af de fire radiometaller og kan derfor være en alternativ oprensningsmetode, især til radiometaller, som er vanskelige at oprense med konventionelle metoder. Tilgængeligheden kan derved forbedres. Det syntetiserede ^{45}Ti-mærkede sporstof kunne ikke anvendes til prostatakræftdiagnose, men udviklingen af sporstoffet viste, at ^{45}Ti kunne oprenses og anvendes til radiomærkningen ved hjælp af den undersøgte oprensningsmetode. Dette kan forhåbentlig føre til en videreudvikling af ^{45}Ti-mærkede sporstoffer til PET.

List of abbreviations

n-Am_2O	*n*-Amyl ether
ATSM	1-methyl-3-[(E)-[(3E)-3-(methylcarbamothioylhydrazinylidene)butane-2-ylidene]-amino]thio-urea
BFC	Bifunctional chelator
BPO	Benzoyl peroxide
n-Bu_2O	Dibutyl ether
BuOH	1-Buthanol
c.a.	Carrier-added
CA-PSMA	Chelidamic acid PSMA-targeted ligand
CAS-PSMA	Chelidamic acid and salan PSMA-targeted ligand
CB-TE2A	1,4,8,11-tetraazabicyclo[6.6.2]-hexadecane-4,11-diacetic acid
CT	Computed tomography
d.c.	Decay corrected
DCE	1,2-dichloroethane
DCM	Dichloromethane
DFO	Deferoxamine
DHN	2,3-dihydroxynaphtalene
DIPEA	*N*,*N*-Diisopropylethylamine
Dipic	Pyridine-2,6-dicarboxylic acid
DMF	*N*,*N*-dimethylformamide
DMSO	Dimethyl sulfoxide
DOTA	1,4,7,10-tetraazacyclododecane-1,4,7,10-tetraacetic acid
EC	Electron capture
EDTA	Ethylenediaminetetraacetic acid
EOB	End of bombardment
EOS	End of synthesis
Et_2O	Diethyl ether
eV	Electron volt
EXFOR	Experimental Nuclear Reaction Data
FDA	Food and Drug Administration
FDG	Fluorodeoxyglucose
GMP	Good Manufacturing Practice
HBED	*N*,*N*'-bis[2-hydroxybenzyl]ethylenediamine-*N*,*N*'-diacetic acid

HDEHP	Di-(2-ethylhexyl)phosphoric acid
HEPES	4-(2-hydroxyethyl)-1-piperazineethanesulfonic acid
HPLC	High-performance liquid chromatography
HSAB	Hard-soft acid-base
ICP-OES	Inductively coupled plasma optical emission spectrometry
$^{i}Pr_2O$	Diisopropyl ether
LLE	Liquid-liquid extraction
log P	logarithm of the partition coefficient
mb	millibarn (10^{-31} m^2)
mil	10^{-3} inch (1 mil = 25.4 µm)
MRI	Magnetic resonance imaging
MS	Mass spectrometry
n.c.a.	No-carrier-added
NBS	*N*-bromosuccinimide
n-BuOMe	*n*-Butyl methyl ether
n.d.c.	Non-decay corrected
n-HexOMe	Hexyl methyl ether
NMO	*N*-methylmorpholine-*N*-oxide
NMR	Nuclear magnetic resonance
NOTA	1,4,7-triazacyclononane-1,4,7-triacetic acid
p.i.	Post injection
PBS	Phosphate-buffered saline
PEEK	Polyether ether ketone
PEG	Polyethylene glycol
PET	Positron emission tomography
PMT	Photomultiplier tube
PP	Polypropylene
PSMA	Prostate-specific membrane antigen
PTFE	Polytetrafluoroethylene
PVDF	Polyvinylidene fluoride
QMA	Quaternary methyl ammonium
qNMR	Quantitative NMR
RCP	Radiochemical purity
RCY	Radiochemical yield

R_f	Retention factor
Rf_{10}-diol	3-(4,4,5,5,6,6,7,7,8,8,9,9,10,10,11,11,12,12,13,13,13-henicosafluorodecyl)-propane diol
Rf_6-ol	Perfluoro-*1H,1H,2H,2H*-1-octanol
rt	Room temperature
Salan	A diamino bis(phenolato) ligands
SPE	Solid phase extraction
SPECT	Single-photon emission computed tomography
SRIM	Stopping and Range of Ions in Matter
TFA	Trifluoroacetic acid
TFT	α,α,α-Trifluorotoluene
THF	Tetrahydrofuran
THP	Tetrahydropyran
TLC	Thin-layer chromatography
TOPO	Trioctylphosphine oxide
TPPO	Triphenyl phosphine oxide
UV-vis	Ultraviolet-visible

Table of Contents

PhD study objectives

Positron emission tomography (PET) is a medical imaging technique which has a broad diagnostic application especially in the field of oncology. [1] Short-lived radioisotopes are incorporated in radiopharmaceuticals, which can be small molecules or biomolecules targeting specific sites, e.g. tumors, or are involved in metabolic processes. Thereby a functional image of the patient can be obtained. [2] Both positron emitting nonmetallic radionuclides and radiometals can be incorporated in radiopharmaceuticals. Radiometals are gaining interest due to the large variety in half-lives making it possible to match the physical half-life of the radiometal with the biological half-life of the biomolecule. The purification of cyclotron-produced positron emitting radiometals used for PET is an essential step for the production of radiopharmaceuticals and the radiometals need to be separated from their respective cyclotron target material. [3] Due to radiation protection this separation requires automatic processes. Liquid-liquid extraction (LLE) is a chemical separation technique which can be used to selective extract radiometals from their target material, but the technique can be challenging to automate. [4] An automatic LLE method is made possible with a membrane-based separation technique [5], but has not been applied to radiometal extraction before this PhD study.

There are still radiometals which have not yet been widely used for PET despite their suitable physical properties. One of these is ^{45}Ti. Titanium is very oxophilic and its complexes hydrolyze easily. [6] The development of stable, specific ^{45}Ti-based radiopharmaceuticals is needed to evaluate the PET properties of ^{45}Ti. In recent years, a great interest in the development of radiopharmaceuticals for the detection of prostate cancer has been seen. Prostate-specific membrane antigen (PSMA) is a favorable biological target for the detection of prostate cancer and the development of small-molecule PSMA-targeted radiotracers is ongoing. [7] Thus, the development of a ^{45}Ti-labeled PSMA-targeted radiotracer will be of interest.

Therefore, the focus of this PhD study is on the recovery and activation of four different cyclotron-produced PET radiometals (^{45}Ti, ^{64}Cu, ^{68}Ga, and ^{89}Zr) and the development of a ^{45}Ti-labeled PSMA-targeted radiotracer for prostate cancer detection.

The thesis is divided into three main chapters. Chapter 1 is an introduction to the topic of the thesis, while chapter 2 and 3 each have an introduction and additionally describe the research and experiments conducted during the PhD study. The experimental section can be found at the end of the thesis. A summary after each chapter is given and a final conclusion and further perspectives for the complete PhD study are outlined at the end of the thesis.

Chapter 1 (section 1-3) contains an introduction to radiometal-based radiopharmaceuticals for PET. Here, the fundamentals of PET will be outlined and the production, purification, and application of radiometals for PET are discussed.

In chapter 2 (section 4-9), the study on the separation of the four radiometals: ^{68}Ga, ^{45}Ti, ^{64}Cu, and ^{89}Zr from their respective cyclotron target materials using liquid-liquid extraction (LLE) and a membrane-based separation technique is described. First, an introduction to the applied membrane-based separation method is given. A suitable LLE and separation method for the selective extraction of ^{45}Ti from scandium was developed and this work has been published during this PhD study and can be found in appendix A (*"Liquid–liquid extraction in flow of the radioisotope titanium-45 for positron emission tomography applications"* [8]). A description of the preliminary experiments and the published research are given in chapter 2. Next, the LLE and separation of ^{89}Zr and ^{64}Cu from their cyclotron target materials; yttrium and nickel are outlined and discussed. Lastly, the LLE and separation technique applied and optimized for the separation of ^{68}Ga from zinc is described and this research has led to a publication, which can be found in appendix B (*"Separation of Radiogallium from Zinc Using Membrane-Based Liquid-Liquid Extraction in Flow: Experimental and COSMO-RS Studies"* [9]). The results from the separation and purification of all four radiometals have been used to construct a patent application which has been filed as an international application (*"A method for continuous separation of radiometals for positron emission tomography"* PCT ref. EP2019/071156 [10]).

In chapter 3 (section 10-11), the development and preclinical evaluation of a novel ^{45}Ti-labeled PSMA-targeted radiotracer ([^{45}Ti]Ti-CAS-PSMA) are described. An introduction to PSMA-targeted PET radiotracers and their application for prostate cancer detection is given. Next, the development and synthesis of [^{45}Ti]Ti-CAS-PSMA and the following evaluation of the radiotracer are outlined. The final preclinical evaluation was performed shortly before the conclusion of the PhD and the research has not yet been published, however, chapter 3 contains a detailed description and the results of the experiments conducted.

Chapter 1

Radiometals for positron emission tomography

1 Medical imaging and positron emission tomography

Medical imaging is an important non-invasive diagnostic technology, which makes it possible to visualize the interior structure and function of the human body. The medical image is obtained by using techniques, which can display the area of interest, e.g. a tumor in contrast to healthy tissue. Different types of medical imaging exist e.g. ultrasound imaging, X-ray projection imaging, computed tomography (CT), magnetic resonance imaging (MRI), and nuclear imaging. Ultrasound imaging utilizes the refraction of sound waves in tissue. The contrast is obtained due to inhomogeneities in tissue forming echoes, which travels with various speeds in different tissues. Both X-ray projection imaging and CT are using an outer X-ray source for imaging. The interaction between the X-rays and soft matter, bone and air is visualized. The X-rays can interact with matter by scattering, photoelectric effect and pair production. The photoelectric effect is the most important for the imaging, since it depends on the density of the matter and thereby forms a contrast. CT differs from the X-ray projection imaging, since a 2D or 3D absorption image can be obtained by transforming the X-ray projections to cross-sectional images using computer techniques. MRI is in some ways similar to CT, but based on another principle. For MRI, the orientation of protons in a magnetic field is affected by applying a resonant radiofrequency. The relaxation back to equilibrium can be measured and the contrast is formed due to the difference in relaxation time, which is dependent on the tissue. MRI can be used to give anatomic information but also image physiological processes e.g. blood oxygenation. [2]

1.1 Nuclear imaging

Nuclear imaging uses radiation, as X-ray projection imaging and CT, but the radioactive source is internal, e.g. as a radiopharmaceutical. The radiopharmaceutical can contain a biological active molecule (targeting vector), which targets specific sites in the body, e.g. tumors and the image is obtained by measuring the distribution of the radiopharmaceutical. Thereby, metabolic processes can be visualized and a functional image is obtained. Scans from nuclear imaging are often combined with CT or MRI, since these can give structural information, be applied for attenuation correction, and have higher resolution making it possible to achieve a more informative image. [2]

1.1.1.1 Principles of single-photon emission computed tomography

Single-photon emission computed tomography (SPECT) is a nuclear imaging technique, where gamma emitting radionuclides are used as radioactive source. The gamma rays are measured by a gamma camera containing detectors, which consist of photomultiplier tubes (PMTs) that have a conversion layer and a collimator. The collimators decrease off-angle photons and the conversion layer converts the gamma photons to visible light. The signal from a visible-light photon is enhanced in the PMTs, since the photon releases an electron when hitting the photocathode in the PMT. The PMTs contain electron-multiplying dynodes, so when the electron reaches the first dynode secondary electrons will be released. These electrons reach the next dynode and more electrons are released. This process is repeated through the PMTs. A measurable current is formed at the anode at the end of the dynode chain. The gamma camera can be moved around the patient and a 3D image can be obtained. [2]

1.1.1.2 Principles of positron emission tomography

Positron emission tomography (PET) is another nuclear imaging method, which has a higher sensitivity and signal-to-noise ratio than SPECT. [2] PET is crucial in the field of oncology, but is also used in neurology and for diagnosis of cardiovascular disease. The administered radiopharmaceutical for PET imaging contains a radionuclide, which decays by positron emission (β^+ decay). The PET scanner detects the annihilation photons emitted when the positron interacts with an electron. The photons are emitted due to the annihilation of the positron (antimatter) with an electron (matter), where the rest mass is converted into two annihilation photons. These two photons have the same energy of 511 keV and are emitted simultaneously in the opposite direction of each other (approximately 180°) (Figure 1). These properties make it possible to determine a line on which the annihilation took place by annihilation coincidence detection. [11]

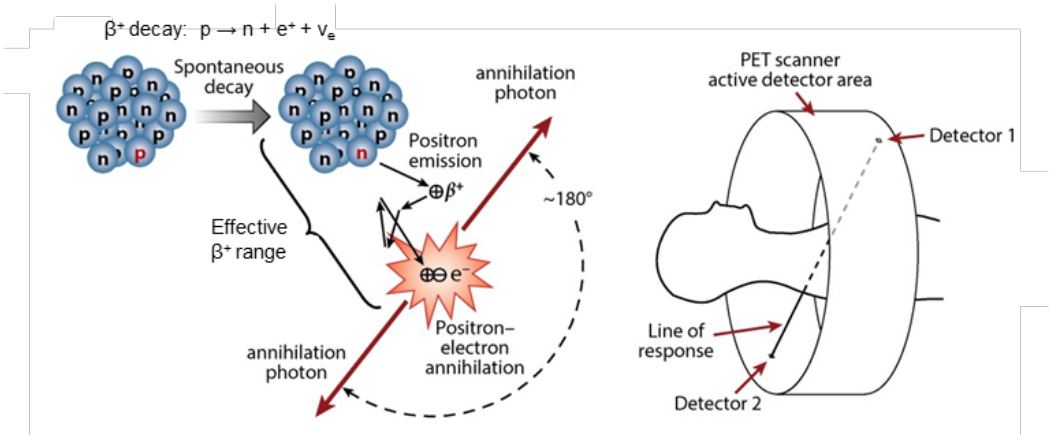

Figure 1: Left: Illustration of β^+ decay where a parent radionuclide decays to the daughter nuclide by positron emission. The positron annihilates with an electron, whereby two photons are emitted in opposite direction of each other. Right: Figure of the PET scanner detector ring. The annihilation is detected by two detectors and a line of response can be defined. The figure is modified from [12].

A PET scanner has a ring of detectors (Figure 1) consisting of PMTs with a conversion layer and a collimator as the detectors of the gamma camera for SPECT. When one detector detects an annihilation photon, a gate opens for a very short time period in order to detect the other photon by another detector. The annihilation coincidence detection disregards single photons, which are rejected as noise. [2] The distance between the annihilation event and the positron emission is short and depends on the energy of the positron. The resolution of the PET scan is higher when isotopes with low β^+ energy are used, since the range of the positron is shorter. [11], [13] The radionuclide must be chosen by evaluating its physical properties (half-life, β^+ energy and branching ratio) and compared to the properties of the targeting vector (as mentioned in section 2). The half-life must be long enough to produce the radiopharmaceutical, perform quality control, transport the radiopharmaceutical to the patient, distribute in the patient and conduct the scan. However, the half-life must be short in order to prevent the patient from unnecessary radiation. In 2000, PET started to be combined with CT, which increased the use of PET as a diagnostic tool. [14] Furthermore, the availabilities of PET scanners and cyclotron facilities have expanded in recent years, which have enabled an increased development of PET radiopharmaceuticals. [15]

1.2 Positron emitting radionuclides

Different positron emitting radionuclides, both metals and nonmetals, can be used for PET. Some of these are listed in Table 1. The main nonmetal used for PET is fluorine-18 (^{18}F), due to its suitable physical properties (half-life, β^+ energy and branching ratio). ^{18}F is used for the most common PET radiopharmaceutical: ^{18}F-fluorodeoxyglucose ([^{18}F]FDG), which is taken up by rapidly growing tumors since it is similar to glucose and subsequently accumulated in the cell due to changes in the metabolic pathway compared to glucose. [3] Other nonmetals used for PET are carbon-11 (^{11}C), nitrogen-13 (^{13}N), and oxygen-15 (^{15}O) (Table 1). However, the half-life of the PET nonmetals might not match the biological half-life of targeting vectors, which have longer circulation time. The production of these radionuclides also requires cyclotron facilities close to the patients due to their relative short half-life. The incorporation of nonmetals in the targeting vector can be challenging, since the synthesis needs to be fast. An attempt to overcome these challenges can be the development of radiopharmaceuticals based on positron emitting radiometals. One of the advantages of using positron emitting radiometals for PET is the larger variety of half-lives of different radiometals (Table 1). It is also possible to incorporate the radiometal easily and at a late stage of the synthesis of the radiopharmaceutical using suitable chelators. [14], [16] Here the focus will be on four different radiometals; ^{45}Ti, ^{64}Cu, ^{68}Ga, and ^{89}Zr and the advantages and challenges of using radiometals for PET radiopharmaceuticals will be described in the following sections.

Table 1: Physical properties of positron emitting radionuclides including half-life, decay mode and branching ratio, average and end-point energy of particle, and main production route, by generator or nuclear reaction, are listed. EC: electron capture. [3], [15], [17], [18]

Radionuclide	Half-life	Decay mode and branching ratio	Average energy of particle (keV)	End-point energy of particle (keV)	Main production
^{11}C	20 min	β^+ (100 %)	386	960	^{14}N(p,α)^{11}C
^{13}N	10 min	β^+ (100 %)	492	1199	^{16}O(p,α)^{13}N
^{15}O	2 min	β^+ (100 %)	735	1732	^{15}N(d,n)^{15}O
^{18}F	110 min	β^+ (97 %)	250	634	^{18}O(p,n)^{18}F
^{45}Ti	3.1 h	β^+ (85 %) EC (15 %)	439	1040	^{45}Sc(p,n)^{45}Ti
^{64}Cu	12.7 h	β^+ (18%) β^- (39%) EC (44 %)	278 191	653 579	^{64}Ni(p,n)^{64}Cu
^{68}Ga	68 min	β^+ (89 %) EC (11 %)	664	1900	^{68}Ge/^{68}Ga generator ^{68}Zn(p,n)^{68}Ga
^{89}Zr	78.4 h	β^+ (23%) EC (77 %)	396 γ (909 keV)	902	^{89}Y(p,n)^{89}Zr

1.3 Established and promising PET radiometals: ^{68}Ga, ^{45}Ti, ^{64}Cu, and ^{89}Zr

In the recent years, there has been an increased interested in radiometals for PET. This can be seen in a literature study, where the number of publications with ^{68}Ga, ^{45}Ti, ^{64}Cu, and ^{89}Zr for PET application from 2005 to 2018 has been found using Web of Science as database (Figure 2). An increase in the number of publications from 2005 to 2018, especially for ^{68}Ga, can be seen. This development might be attributed to the commercialization of the ^{68}Ge/^{68}Ga generator in 1996 and later the improved version became available in 2008. [19] The production of ^{68}Ga-DOTATOC/TATE (Figure 3) for imaging neuroendocrine tumors in the beginning of the 21st century showed that ^{68}Ga has an application as a PET radiopharmaceutical. Furthermore, the success of imaging prostate cancer by targeting prostate-specific membrane antigen (PSMA) with the ^{68}Ga radiopharmaceutical, ^{68}Ga-PSMA-11 (Figure 3), first published in 2012 [20], has further increased the interest in ^{68}Ga. A rise in the number of publications concerning ^{89}Zr and ^{64}Cu is also seen, while a limited number of ^{45}Ti studies has been published

(17 publications were found in total). There has been an enhanced interest in using antibodies for PET (immuno-PET) demanding radiometals with longer half-life such as ^{64}Cu and ^{89}Zr. However, ^{89}Zr seems to become the radiometal of choice for immuno-PET (Figure 3) and an almost equal number of publications with ^{64}Cu and ^{89}Zr was seen in 2018. ^{64}Cu-labeled small molecules, peptides, and nanoparticles have also been studied. One specific example is the imaging of hypoxia with ^{64}Cu-ATSM (Figure 3). [13] The increased research in radiometals for PET can also have been affected by the limited access to molybdenum-99 (^{99}Mo) in 2010 and thereby technetium-99m (^{99m}Tc), the most used radiometal for SPECT. This limitation increased the need to study other radiometals. [13]

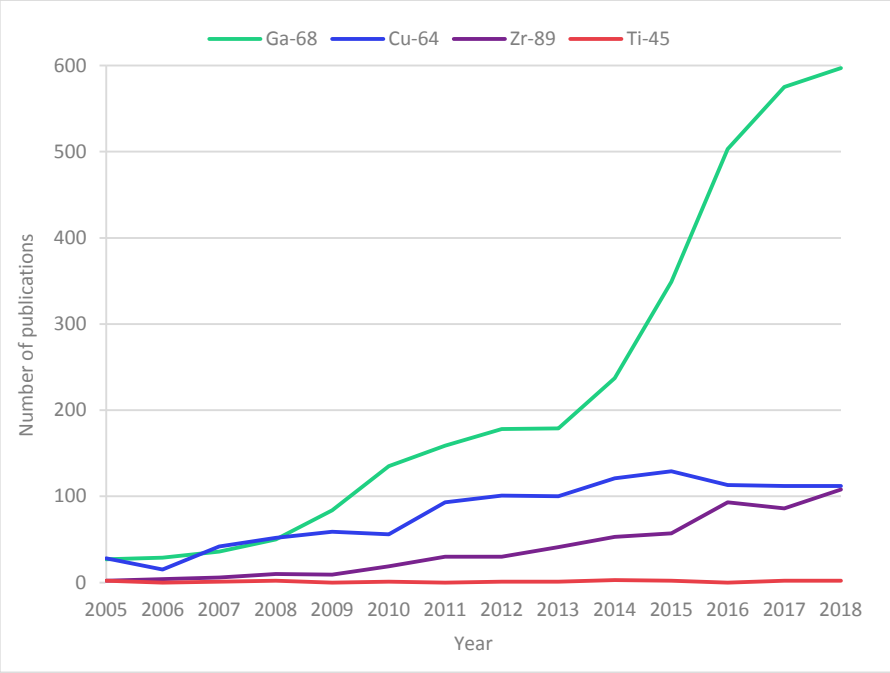

Figure 2: Number of publications with ^{68}Ga, ^{64}Cu, ^{89}Zr, and ^{45}Ti in PET from 2005-2018. Web of Science was used as database (example of search string: Ga-68 PET). A similar trend was seen by previous studies by Brandt et al. and Notni and Wester. [13], [19]

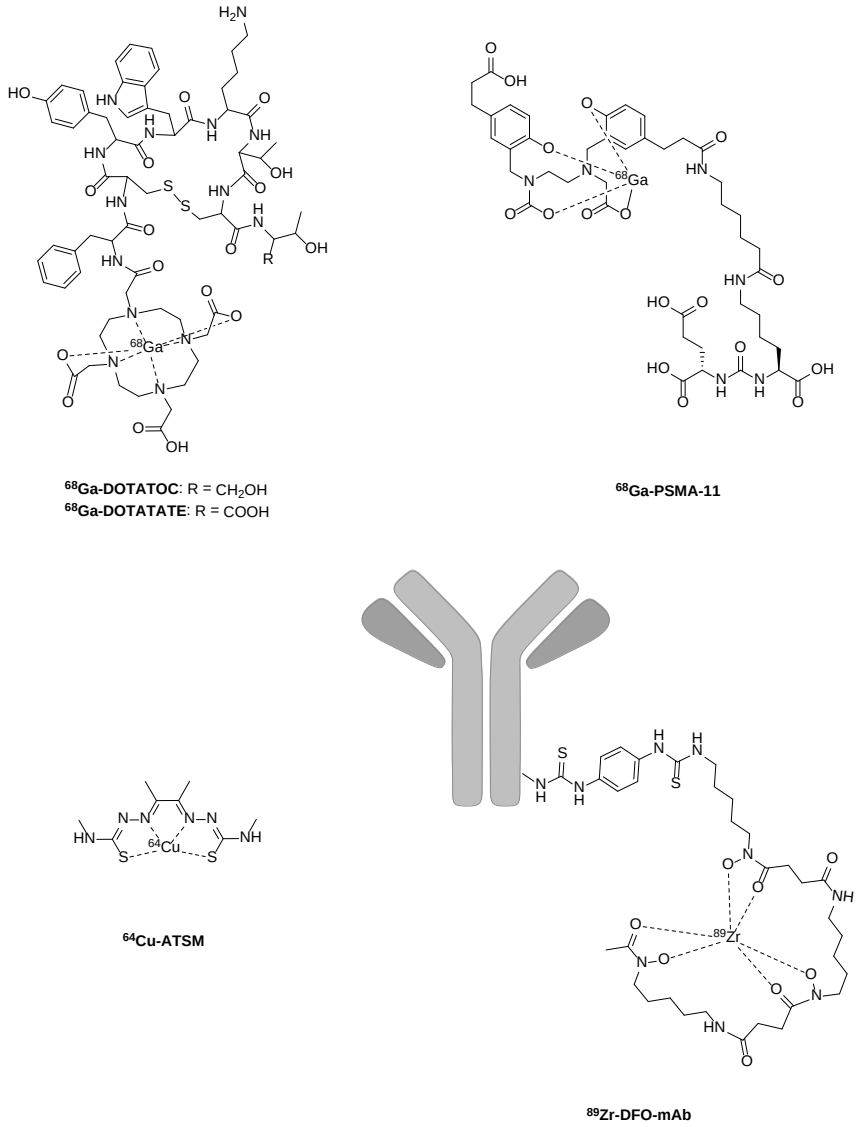

Figure 3: The structure of ^{68}Ga-DOTATOC/TATE, ^{68}Ga-PSMA-11, ^{64}Cu-ATSM, and an ^{89}Zr-labeled monoclonal antibody with deferoxamine (DFO) as chelator.

The number of clinical trials with ^{68}Ga, ^{64}Cu, and ^{89}Zr for PET from 2005 to 2018, found with clinicaltrials.gov as database, is shown in Figure 4. No clinical trials with ^{45}Ti for PET were found. The number of clinical trials with ^{68}Ga increased over the years, except for a small decrease in 2017. The first clinical trials with ^{68}Ga-DOTATOC/TATE were performed in the first decade of the 21st century [21], [22], which seems to start the application of ^{68}Ga in clinical trials. The number of clinical trials with ^{68}Ga further increased after the development and promising initial results with ^{68}Ga-PSMA-11 [23], [24] and a relative high number of clinical trials have been conducted since. A higher number of clinical trials have been conducted with ^{89}Zr than with ^{64}Cu in the past years, despite a higher number of publications found with ^{64}Cu. This could indicate an adoption

of mainly ^{89}Zr for immuno-PET application. [13], [25] Over the past years, a steady growth in the number of clinical trials and publications with radiometal-based PET tracers, has been observed, and it will be interesting to see if the development will continue.

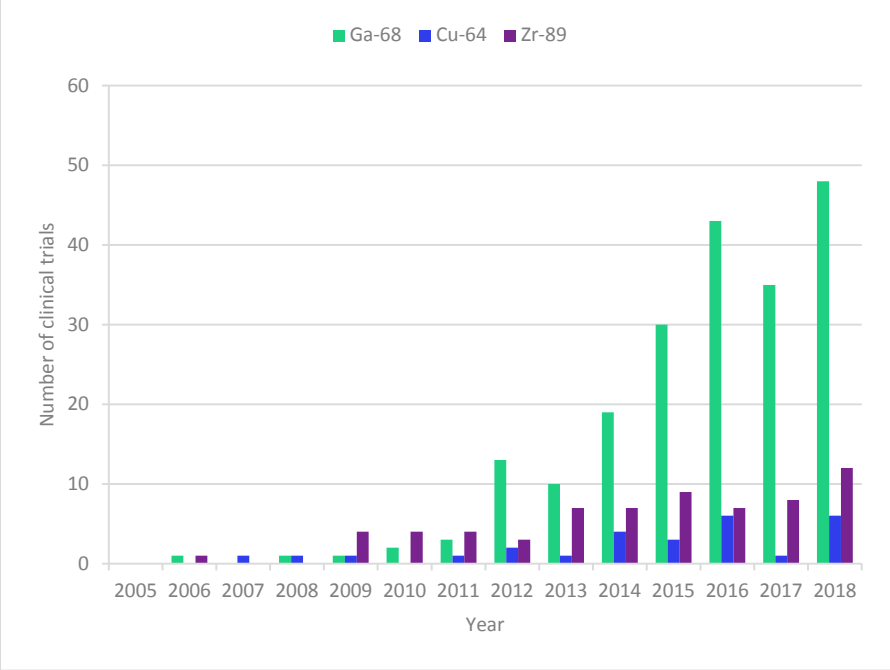

Figure 4: The number of clinical trials with ^{68}Ga, ^{64}Cu, and ^{89}Zr in PET application from 2005 to 2018. Clinicaltrials.gov was used as a database, with an example of search string: gallium-68 OR gallium 68 OR Ga-68 OR 68Ga OR Gallium68 OR Ga68.

2 Radiometal-based PET radiopharmaceuticals

One approach to apply radiometals for PET is to attach the radiometal to a targeting vector. In most cases a bifunctional chelator (BFC) is applied (Figure 5). A BFC consists of a chelator that can form a complex with the radiometal, while also containing a functional group, which can form a covalent linkage to the targeting vector. A spacer moiety between the targeting vector and the BFC is, in some cases, inserted to prevent the chelator to affect the binding of the vector to its target, or the targeting vector to disturb the complexation (Figure 5). [3] The purpose of the spacer can also be to modulate the lipophilicity of the radiopharmaceutical which can improve the binding of the radiopharmaceutical to the biological target or change the metabolic pathway of the radiopharmaceutical. [20]

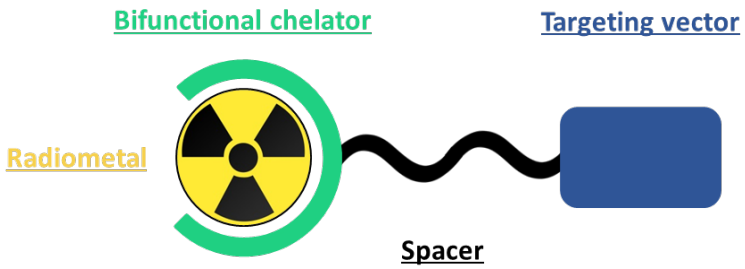

Figure 5: Illustration of a radiometal-based radiopharmaceutical consisting of a radiometal, a BFC, a spacer, and a targeting vector.

A suitable targeting vector has a high affinity for the biological target. The targeting vector can e.g. bind to a type of receptor, which is overexpressed on the target cells, while healthy cells have low or no expression of the receptors. Small molecules and different types of biomolecules such as peptides and proteins can be used as targeting vectors. The circulation time of large molecules, e.g. proteins and antibodies, is often longer compared to small molecules and peptides. [26] The targeting properties of antibodies are highly specific, while the clearance rate is slow, which makes longer waiting time necessary in order to obtain a high tumor-to-background ratio. The circulation time can be improved by using antibody fragments that still have a highly specific receptor binding as the targeting vector. [3] There exist different positron emitting radiometals, which gives access to a large variety of physical and chemical properties. This makes it possible to match the biological half-life of the targeting vector with a radiometal with a suitable physical half-life (Figure 6). Short-lived radiometals, such as ^{68}Ga, are suitable for the labeling of small molecules and peptides due to the rapid pharmacokinetics, while long-lived isotopes, such as ^{89}Zr, can be used for the labeling of antibodies, since they have a longer circulation and distribution time. [13] The large variety in physical half-life of radiometals is one of the main advantage of radiometal-based radiopharmaceuticals.

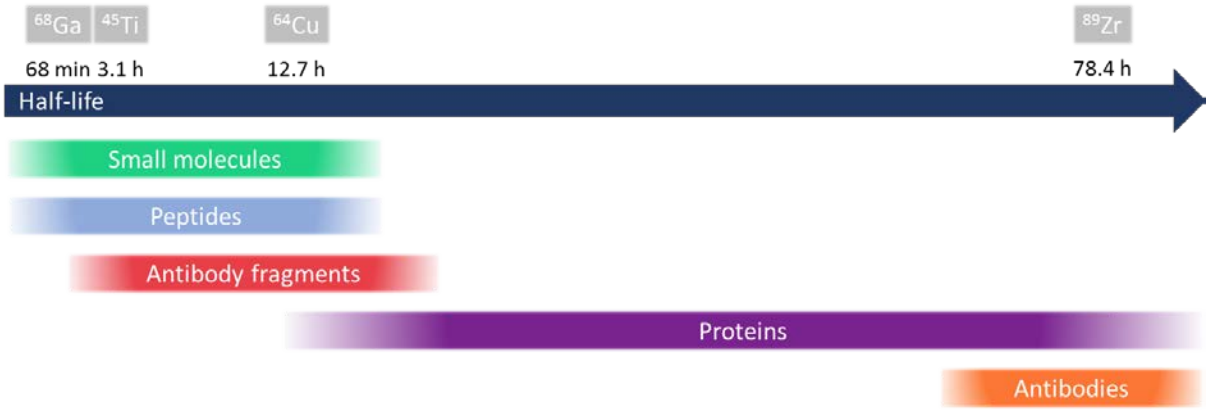

Figure 6: Illustration of matching the physical half-life of ^{68}Ga, ^{45}Ti, ^{64}Cu, and ^{89}Zr with the biological half-life of small molecules, peptides, antibody fragments, proteins, and antibodies. The biological half-life can vary depending on the specific biomolecule. [26]–[29]

2.1 Theranostic application

Another advantageous use of radiometals is for theranostic application. The positron emitting radiometal, which is used for the diagnostic PET scan, can be exchanged with a therapeutic radiometal, ideally of the same element. There are different types of theranostic approaches. In one approach, a radiometal that both emits diagnostic β^+ or γ radiation and therapeutic β^- or α radiation or low-energy electrons emitted by Auger effect, e.g. ^{64}Cu (β^+ and β^-), is used. Thereby, the same radiopharmaceutical can be used and to perform imaging during therapy. Another approach is to exchange a diagnostic radiometal, e.g. ^{68}Ga, with a therapeutic radiometal, e.g. luthetium-177 (^{177}Lu). [13] This approach is used e.g. for the detection and therapy of prostate cancer, where ^{68}Ga-PSMA-617 is used for the imaging and ^{177}Lu-PSMA-617 for the therapy. [30] The same targeting vector with the same spacer and chelator is used in this approach, but there can be an effect of exchanging the radiometal, which needs to be studied. A third approach is to use two different isotopes of the same radiometal e.g. yttrium-86 (^{86}Y) (β^+) and yttrium-90 (^{90}Y) (β^-), leading to chemical identical radiopharmaceuticals. [13] One example is $^{64/67}$Cu-SARTATE, where the ^{64}Cu-labeled SARTATE can be used for the detection of neuroendocrine tumors and ^{67}Cu-SARTATE has shown antitumor activity in preclinical studies, which is promising for the treatment of neuroendocrine tumors. [31]

2.2 Production of radiometal-based PET tracers

The following sections describe the production and purification of radiometals, the applications of BFCs and evaluation of the chelator-radiometal suitability for application as PET tracers.

2.2.1.1 Cyclotron production of radiometals

Positron emitting radiometals can be produced using different approaches of which cyclotrons are often used. In a cyclotron, a magnetic field placed perpendicular to an alternating electric field is used to accelerate charged particles, such as protons (p), deuterons (d), and α-particles (α). These particles are accelerated to reach an energy high enough to take part in a nuclear reaction when colliding with a target material. When a nuclear reaction takes place, the particle collides with a target nucleus, whereby a compound nucleus is formed. This compound nucleus can decompose in different ways leading to new nuclei. [32] An example is shown in Figure 7. An energetic proton and a nitrogen-14 (^{14}N) nucleus collide, whereby the compound nucleus ^{15}O is formed. ^{15}O can then decompose by emitting a neutron (n) forming oxygen-14 (^{14}O), an α-particle forming ^{11}C, or a proton together with a neutron (pn) or deuterium forming ^{13}N. The different nuclear reactions are written as follows: ^{14}N(p,n)^{14}O, ^{14}N(p,α)^{11}C, ^{14}N(p,pn)^{13}N, and ^{14}N(p,d)^{13}N.

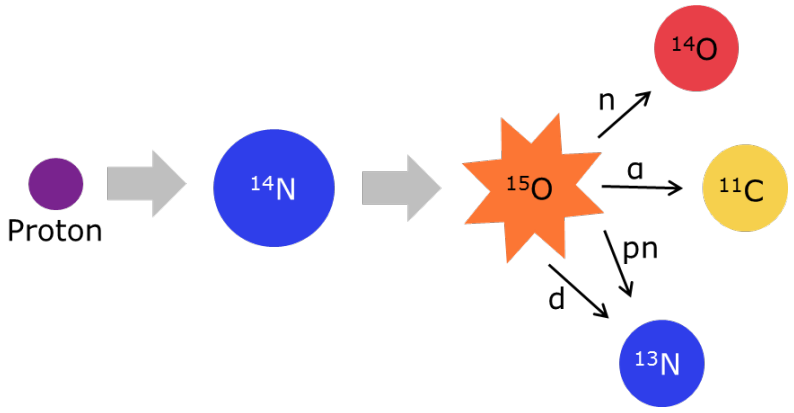

Figure 7: Illustration of the collision between a proton and a ^{14}N nucleus, whereby a compound nucleus (^{15}O) is formed. The decomposition of ^{15}O can be by the emission of a proton (p), an α-particle (α), a proton and neutron (pn), or deuterium (d). [33]

The individual nuclear reaction will occur if the threshold energy is reached. The threshold energy of a nuclear reaction depends on the Q value, which is the mass difference between the nuclear reactants and the products, and on the Coulomb barrier being the electrostatic repulsion between the accelerated particle and the target material. The amount of the radionuclide produced by the nuclear reaction is determined by the number of target nuclei, the beam intensity (number of accelerated particles e.g. protons), and the formation cross section for the specific nuclear reaction. The cross section describes the probability for a nuclear reaction to take place and is a function of the beam energy. [32] Therefore, by choosing the optimal beam energy, a higher yield can be obtained and/or the coproduction, e.g. for competing nuclear reactions, can be minimized.

The radionuclidic purity can also be increased by using isotopically enriched target materials but these can be expensive. Natural monoisotopic materials, e.g. scandium-45 (^{45}Sc) and yttrium-89 (^{89}Y) are preferable, but only few exist. The amount of the stable metal of the same element as the desired radiometal needs also to be considered during the radionuclide production and decreased, since the stable metal of the same element cannot be chemically separated from the radiometal. The ratio is described as the molar activity, which is the activity of the radiometal per amount of the element (Bq/mol). [3] A high molar activity is especially important when targeting a biological target with few sites since a high concentration of the nonradioactive tracer will occupy these sites. [34]

2.2.1.2 Solid and liquid cyclotron targets

The target material for the production of radiometals can be in a solid form as a metal foil, which can be used in solid targets, or as a metal salt solution used in liquid targets. There are different advantages and challenges using both approaches. The solid target produces a higher yield of the radiometal, due to the higher density of target nuclei. However, the denser target material often has a higher price compared to the solutions used in

liquid targets. It is also necessary to dissolve the solid target material after the irradiation in order to continue with the separation of the radiometal from the target material. This often requires strong acids which might introduce metal ions that might necessitate an additional purification. [35] Furthermore, the delivery of the irradiated material from the target to a hotcell for further processing is more complicated to automate. This process can easier be automated for liquid targets. The processing of the liquid target after the irradiation is also faster, since the dissolution of the target material is avoided. The acidic metal salt solution used for liquid targets places demands on the corrosive resistance of the target body and foil, containing and cooling the solution during irradiation. Therefore, most often niobium target body and foils are used, since it has a high corrosive resistance. [36], [37] Other challenges with liquid targets are the formation of gas during irradiation, which can cause a too high pressure buildup in the target, and the possibility of salt precipitation in the target. These effects can be reduced by using nitric acid and the nitrate salt of the target material instead of hydrochloric acid and the chloride salt. [38]

2.2.1.3 Radiometal generators

Some PET radionuclides can also be obtained using generators. The PET radiometals e.g. ^{68}Ga, rubidium-82 (^{82}Rb) ($T_{½}$ = 75 s), and scandium-44 (^{44}Sc) ($T_{½}$ = 3.97 h) can be obtained by the ^{68}Ge/^{68}Ga, ^{82}Sr/^{82}Rb, and ^{44}Ti/^{44}Sc generator, respectively. However, only a limited number of PET radiometals can be produced by this approach. [39] Generators consist of a long lived parent radionuclide which decays to the desired daughter radionuclide. The long lived parent radionuclide is bound to a resin from which the daughter radionuclide can be eluted selectively. Generators can be beneficial when there is no or limited access to cyclotron facilities. [3]

2.3 Recovery and purification of radiometals for PET

After the production of the radiometal, the radiometal needs to be separated from its target material in order to be incorporated in radiopharmaceuticals. The low concentration of the radiometal (pico- to nanomolar) and the large excess of the target material (millimolar to molar) demand an efficient chemical separation technique. A no-carrier-added (n.c.a.) production of radionuclides is desired, as only a low amount of stable isotopes of the same element, as the radiometal, is usually present. The stable isotopes of the same element as the radiometal cannot be separated chemically from the radiometal; therefore, an n.c.a. production leads to a higher molar activity than carrier-added (c.a.). [3] Different techniques can be used to separate and purify the radiometal from the target material. The properties of the target material and the produced radiometal need to be evaluated in order to find the optimal separation approach. Separation techniques, such as chromatography, liquid-liquid extraction (LLE), distillation, and precipitation, can be applied. [38] Two methods for the separation of the desired radiometal from its cyclotron target material will be described here. These are solid phase extraction

(SPE) (chromatography) and LLE, which both utilize the difference in affinity of the metals for either a stationary phase or an aqueous/organic phase, respectively.

2.3.1.1 Ion exchange chromatography

SPE, by ion exchange chromatography is a prevalent chromatographic technique for radiometal separation and purification. [38] Both cation- and anion-exchange resins can be used. Cation-exchange resin can contain functional groups, such as carboxylic acids or the resin can be sulfonated, while quaternary ammonium functional groups can be used for anion-exchange resin. The principle of cation- and anion-exchange chromatography is similar. Firstly, the ion exchange resin (R) is washed with an eluent, which contains an ion (E) (an anion for anion-exchange and a cation for cation-exchange). In this equilibration step the resin is converted to the eluent ion form (R-E). Then the sample ion (S) is loaded on the resin and the ion-exchange equilibrium takes place (Equation (1)).

$$R\text{-}E + S \rightleftharpoons R\text{-}S + E \tag{1}$$

The equilibrium constant (K) can be seen in the following equations (Equation (2)).

$$K = \frac{[R\text{-}S] \cdot [E]}{[R\text{-}E] \cdot [S]} \tag{2}$$

The sample ion can then be eluted by washing the column with the eluent, shifting the equilibrium (Equation (1)) to the left. The separation of different sample ions, e.g. the radiometal and the target material, is obtained by the difference in the ion-exchange equilibria between the eluent ion and the respective sample ions. The difference in the equilibria can be quite small for some metal ions, but the separation can be improved by using an eluent which has different ability to form complexes with the metal ions. [40]

The interactions between the cationic metal ions and cation-exchange columns are utilized in cation-exchange chromatography. Cations in a high charge state (e.g. 3+) are more retained by the cation-exchange resin than less charged cations (1+). The metal cations can be eluted with acidic solutions, e.g. HCl solutions, which can form neutral or anionic complexes that are not retained by the cation-exchange column. The difference in metal ion affinity for the resin can be quite small and it can be difficult to separate metal ions with similar charge. [40] Anion exchange chromatography can be used to separate metal ions in acidic aqueous solution, e.g. HCl solution. Many metal ions form anionic chloride species in aqueous HCl solution, but the tendency to form these species depends on the metal. Consequently, the metal ions can be separated due to their different tendency to form chloro-complexes. These anionic complexes interact with the anion-exchange column and are retained, but can subsequently be eluted in a solution with a lower HCl concentration or in water. [41]

2.3.1.2 Extraction chromatography

Extraction chromatography is a SPE chromatographic method with a different affinity principle compared to ion exchange chromatography. An organic extractant is bound to a porous polymeric or inorganic support. The organic extractant needs to be chosen according to the chemical properties of the radiometal, enabling it to chelate the desired radiometal but not the target material or other metal impurities. The dissolved solid target or the liquid target solution is here loaded on a resin-filled column in a suitable dilution, often an acidic solution. The resin can be washed after the loading, and the radiometal is then eluted with a solution capable of dissociating the radiometal from the organic extractant. [42]

2.3.1.3 Liquid-liquid extraction

LLE can also be used to separate radiometals from the cyclotron target material. This is a simple, inexpensive, and fast method that does not involve a stationary phase. LLE was frequently used for the separation of radiometals, but the separation by SPE methods became more widespread, since the automation of this method was easier. However, a recent development of LLE methods based on flow chemistry makes the automation simpler and a better control and efficiency can be achieved. One of these methods – a membrane-based separation technique – will be described. The method is applied to separate ^{45}Ti, ^{89}Zr, ^{64}Cu, and ^{68}Ga from their respective target materials, and is discussed further in chapter 2. For LLE, two immiscible liquids are mixed enabling the transfer of the metal ions or compounds from one phase to the other. The phases are subsequently separated. The transfer of metal ions between the phases can be due to chelation/compound formation, ion association or solvation. [4]

Extraction by chelation/compound formation can be described as cation exchange, where organic acidic extractants are used to exchange their acidic H^+ with the metal ion. Ion association is central for anion exchange extractants. The extractants are large cationic organic molecules and are useful for the extraction of metals, which form negatively charged complexes with inorganic ligands in the aqueous phase. Metal extraction by solvation requires that the metal is present as neutral species. These can be the metal acid species (HMX_y e.g. $HFeCl_4$) or neutral salt species. If the coordination of these species are unsaturated they will contain water of hydration ($ML_z(H_2O)_x$), which decreases the extraction. It is desirable to exchange the water of hydration with organic molecules to form more lipophilic complexes. In some cases, where no organic molecules are present capable of replacing the water molecules, the undissociated ligand (HL) can replace the water, forming a self-adduct ($ML_z(HL)_x$). The extraction of metal ions can also be a mixture of the different mechanisms. [43]

Extraction is affected by the pH of the aqueous phase, since the metal speciation depends on the pH. The distribution of a specific metal or compound is described with the distribution constant (K_d) which is the ratio of the concentration of the metal between the organic (c_{org}) and aqueous (c_{aq}) phase (Equation (3)).

$$K_d = \frac{c_{org}}{c_{aq}} \tag{3}$$

It is desirable to have a large K_d for the desired radiometal and small K_d for the target material and impurities, when extracting the radiometal from aqueous phase to organic phase. The K_d value depends on the temperature and phase volume ratio. The percent extraction (%E) can be calculated from the K_d value and the volumetric phase ratio (P) (organic phase volume divided by aqueous phase volume) (Equation (4)).

$$\%E = \frac{100\ (P)K_d}{1 + (P)K_d} \tag{4}$$

The percent extraction is increased when a higher (P) is used for the extraction. Furthermore, the concentration of the extractant, temperature, pH, and metal concentration in the aqueous phase can affect the extraction. The rate of the extraction depends on the surface area between the organic and aqueous phase, where a higher surface-to-volume ratio is desirable. Furthermore, the viscosity, mixing time, and temperature need to be altered according to the kinetics of the extraction. Another important term to describe the LLE is the separation factor β, which is the ratio between the K_d value of the desired metal and the K_d value of the target material or an impurity (Equation (5)). [4]

$$\beta = \frac{K_{d,radiometal}}{K_{d,target\ metal\ or\ impurity}} \tag{5}$$

The separation factor should be considered in regards to the amount of radiometal produced and the amount of target material present. For instance, a nickel-64 (^{64}Ni) target for ^{64}Cu production can contain ~50 mg nickel [44] while a zinc-68 (^{68}Zn) target for ^{68}Ga production can contain up to ~250 mg zinc [45]. When producing, e.g. 1 GBq of ^{64}Cu or ^{68}Ga, the amount of radiometal is in the picomol to nanomol range, while the amount of target material is in the millimol range. If assuming a $K_{d,radiometal}$ value of 19, corresponding to 95 % extraction of the radiometal to the organic phase, β needs to be higher than $1 \cdot 10^6$ in the case of ^{64}Cu and $1 \cdot 10^8$ in the case of ^{68}Ga to achieve the required purities of maximum 1 µg Ni per GBq ^{64}Cu and maximum 10 µg Zn per GBq ^{68}Ga. The requirement for ^{64}Cu is the internally set value at the Hevesy Laboratory and the requirement for ^{68}Ga is set by the European Pharmacopoeia monograph no. 2464. [46] Furthermore, the extraction of the radiometal needs to be relative fast due to the short physical half-life. The separation of radiometals can be challenging, but by

choosing a suitable purification method, the radiometal has the potential to be included in a radiopharmaceutical. The separation of the four radiometals; ^{45}Ti, ^{89}Zr, ^{64}Cu, and ^{68}Ga, from their respective target materials using LLE with a membrane-based separation method is described in chapter 2.

2.4 Bifunctional chelators

The purified radiometal can subsequently be attached to a targeting vector by the use of a BFC, as mentioned in section 2. The complexation should be fast, in very dilute solution, preferably at room temperature, and be relatively stable towards *in vivo* transmetallation and transchelation. Transmetallation refers to the exchange of the radiometal with competing metal ions, while transchelation refers to chelation of the radiometal by a different ligand, e.g. proteins. The chelator used to form the complex needs to suit the chemical properties of the radiometal.

2.4.1 Chelators for radiometals

Chelators with different donor atoms, geometry, and coordination number either currently exist or are being developed, in order to ensure a fast and stable complexation. [14] Examples of various chelators are shown in Figure 8.

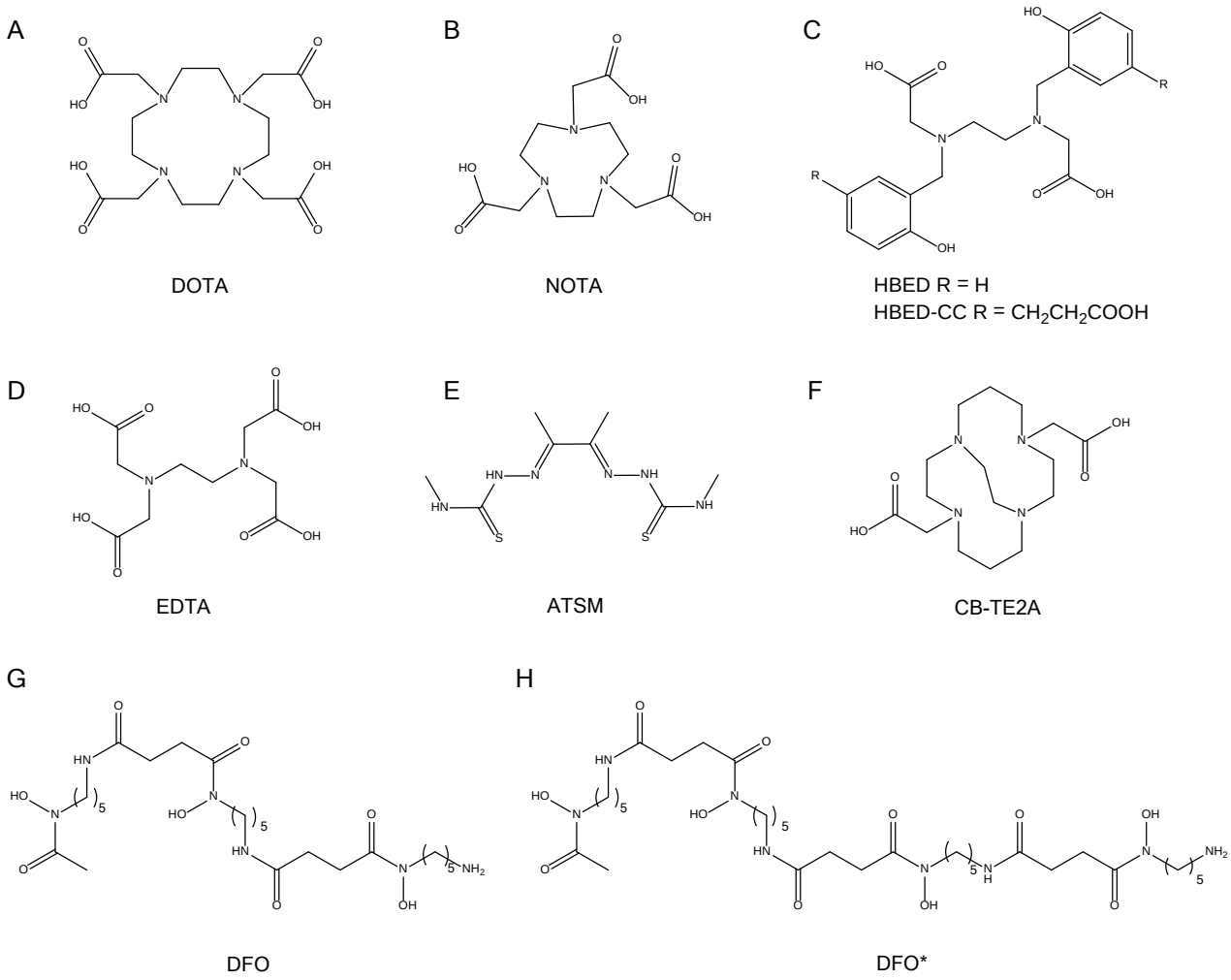

Figure 8: The chemical structure of nine different chelators: DOTA (A), NOTA (B), HBED (C), HBED-CC (C), EDTA (D), ATSM (E), CB-TE2A (F), DFO (G), and DFO* (H).

The hard-soft acid-base (HSAB) theory is useful in order to match the radiometal with a chelator. Hard metal ions are characterized by having a high charge density and the electron shells are non-polarizable. They preferably form ionic bonds, and thereby favor hard donor groups with dense anionic property. On the other hand, soft metal ions favor bonding with more covalent character. They have a low charge density and the electron shells are polarizable, and they prefer soft donor groups, which are electron-disperse. It is advantageous to use chelators since they can form more than one coordinate bond to the metal ion, which is more entropically favorable than multiple monodentate ligands (the “chelate effect”). The same applies to chelators with suitable metal binding pockets, such as macrocyclic chelators, e.g. DOTA (1,4,7,10-tetraazacyclododecane-1,4,7,10-tetraacetic acid) and NOTA (1,4,7-triazacyclononane-1,4,7-triacetic acid) (Figure 8) (the “macrocylic effect”). Macrocyclic chelators suffer from slow binding, often requiring high temperatures, which is not compatible with

temperature sensitive targeting vectors. However, they often afford more stable complexes *in vivo* than the acyclic chelators. [3]

2.4.1.1 Chelators for ^{68}Ga, ^{45}Ti, ^{64}Cu, and ^{89}Zr

Some of the chemical properties of titanium, copper, gallium, and zirconium are listed in Table 2. Cu^{2+} complexes are more common for PET radiopharmaceuticals than Cu^{+} [15] so the properties for Cu^{2+} are listed in this table. The ionic radius of the metal ion and it oxidation state indicates if the metal ion prefers chelators with soft or hard donor groups (HSAB theory). The coordination number is also important when choosing a chelator for the metal. The chemical properties can be used to choose suitable chelators for ^{68}Ga, ^{45}Ti, ^{64}Cu, and ^{89}Zr.

Table 2: The ionic radius , the oxidation state in aqueous solution at physiological pH, the coordination number, and the preferred chelator donor groups for titanium(IV), copper(II), gallium(III), and zirconium(IV) are listed. [3], [6], [15], [47]

	Titanium(IV)	**Copper(II)**	**Gallium(III)**	**Zirconium(IV)**
Ionic radius	0.42-0.74 Å	0.57-0.73 Å	0.47-0.62 Å	0.59-0.89 Å
Oxidation state in aqueous solution at physiological pH	+4	+2, +1	+3	+4
Coordination number	6-7	4-6	3-6	7-8
Donor groups	Carboxylates, hydroxides, phenolates	Aliphatic and aromatic amines	Hard donor groups containing oxygen and nitrogen	Hard donor groups containing oxygen

DOTA (Figure 8A) is commonly used as chelator for ^{68}Ga, even though the ring size of DOTA is larger than the optimal size and the radiolabeling requires elevated temperatures. NOTA (Figure 8B) has a smaller ring size, which fits the size of Ga^{3+} better, and the radiolabeling can be performed at room temperature. This difference can also be seen by comparing the thermodynamic stability of the Ga-NOTA complex (log K_{ML} = 29.0-31.0) with the one for the Ga-DOTA complex (log K_{ML} = 21.3-26.1). [3], [48] Furthermore, NOTA provides six donor groups affording a favorable coordination number for Ga^{3+} (Table 2). Acyclic chelators as HBED (*N,N'*-bis[2-hydroxybenzyl]ethylenediamine-*N,N'*-diacetic acid) (Figure 8C) are also applied for gallium. The complex has a high thermodynamic stability (log K_{ML} = 38.5-39.6) and the modified HBED chelator, HBED-CC, is used for one of the most studied PSMA tracers: ^{68}Ga-HBED-CC-PSMA (^{68}Ga-PSMA-11). [3] Additionally, the formed ^{68}Ga complexes need to be inert towards transchelation by e.g., transferrin which is challenging due to the

similarity between Ga^{3+} and Fe^{3+}. Gallium can also be hydrolyzed at neutral pH to $[Ga(OH)_4]^-$ which can lead to demetallation from the complex if the stability is too low. [3], [49]

Cu^{2+} is easily reduced to Cu^+ *in vivo* requiring the Cu^{2+} complex to be inert towards the one-electron reduction since this can lead to demetallation due to different coordination chemistry of Cu^{2+} and Cu^+. However, the easy reduction of Cu^{2+} to Cu^+ has been utilized for the diagnosis of hypoxic tumors with ^{64}Cu using the acyclic ATSM (1-methyl-3-[(E)-[(3E)-3-(methylcarbamothioylhydrazinylidene)butane-2-ylidene]-amino]thio-urea) as a ligand (Figure 8E). [50] DOTA and NOTA have also been widely used for ^{64}Cu in the 2+ oxidation state. However, dissociation from DOTA has been observed. [51] Using NOTA, is advantageous since it is possible to label NOTA with ^{64}Cu at room temperature, and the Cu-NOTA complex has similar thermodynamic stability as the Cu-DOTA complex (log K_{ML} = 19.8-21.6 (NOTA) and 22.7 (DOTA)). [15], [48] Cross-bridged chelators have been developed for Cu^{2+} e.g. CB-TE2A (1,4,8,11-tetraazabicyclo[6.6.2]-hexadecane-4,11-diacetic acid) (Figure 8F), which are more inert and have higher thermodynamic stability, while on the other hand they require higher temperature for the radiolabeling. The choice of chelator has therefore also to be evaluated according to the targeting vector. [15]

The most widely used chelator for ^{89}Zr is DFO. DFO has three hydroxamate donors which have a high affinity for Zr^{4+}. [15] However, release of ^{89}Zr from DFO *in vivo* has been seen over time (after days), by an uptake of ^{89}Zr in the bone. [52] The development of chelators, which form more inert complexes with ^{89}Zr is therefore ongoing. One example is a chelator called DFO* which is DFO modified by adding a fourth hydroxamate group (Figure 8G), providing now 8 donor groups instead of 6, which is more favorable for Zr^{4+} (Table 2), but also decreasing the water solubility. The *in vivo* stability of the Zr-DFO* complex has been studied and a lower bone uptake of ^{89}Zr was seen after long circulation time of 72 and 144 hours. [52]

Few chelators have been labeled with ^{45}Ti. The formation of stable titanium-complexes are challenging since titanium complexes tends to hydrolyze at aqueous conditions (section 5.2). [6] The complexations of nonradioactive titanium with DFO (Figure 8G) and EDTA (ethylenediaminetetraacetic acid) (Figure 8D) have previously been studied. The EDTA complex with titanium was found to precipitate at pH above 5, while the titanium-DFO complex was thermodynamically stable but the labeling with ^{45}Ti was not optimal for PET application. [6], [15], [53] The development towards stable titanium complexes is described in section 10 in chapter 3.

2.4.1.2 Conjugation of bifunctional chelators

The use of a suitable chelator gives the possibility to incorporate the radiometal at a late stage of the synthesis of the radiopharmaceutical. This is a great advantage, since only one or few radioactive synthesis step(s) is needed and the reaction time is often short and under mild conditions. In most cases, the purification is also simple. [54] The use of BFCs also makes it possible to label a large variety of targeting vectors. Different functional groups can be attached to the chelator, e.g. carboxylic acids, activated esters, and isothiocyanate. These groups can be coupled by a covalent bond to a targeting vector, e.g. a peptide by amide coupling or thiourea coupling. The position of the functional group on the chelator can in some cases affect the chelation of the metal ion, if one of the coordinating groups is modified. An example can be seen in Figure 9, where different BFCs with DOTA as chelator are shown. One of the carboxylic groups can be functionalized for the vector conjugation (e.g. DOTA-NHS-ester), but this decreases the possible coordination to a metal ion. Alternatively, DOTA can be functionalized at a different position (e.g. *p*-SCN-Bn-DOTA), which has less impact on the chelation of a metal ion. [55]

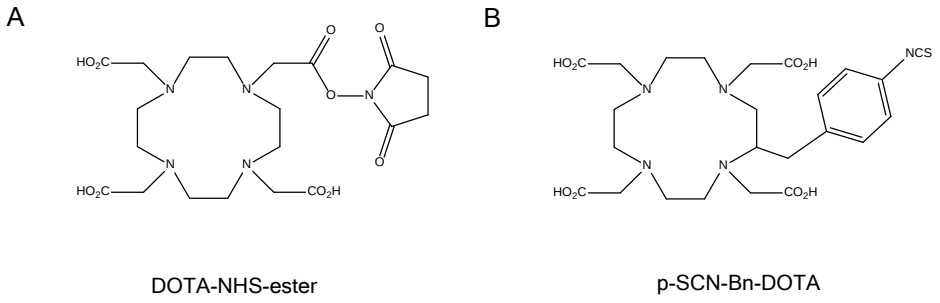

Figure 9: The chemical structure of two BFCs with DOTA as chelator: DOTA-NHS-ester (A) and *p*-SCN-Bn-DOTA (B).

2.4.2 Evaluation of radiometal and chelator suitability

Different studies can be performed in order to evaluate the suitability of the chelator for a given radiometal. First, radiolabeling experiments can be performed to evaluate the radiolabeling yield and the required reaction temperature and time. The temperature is important to consider if the chelator is supposed to be conjugated to temperature sensitive targeting vectors, such as antibodies. The time for the radiolabeling is especially important for short-lived radiometals. However, the kinetics of the radiolabeling needs to be evaluated, since a fast chelation at low temperature, in some cases, also involves fast dissociation of the radiometal and chelator. [55] The thermodynamic stability of the complex can be tested by various titrations techniques, e.g. by potentiometric, spectrophotometric or calorimetric measurements. [56] The stability constant (K_{ML}) of a metal complex (ML) is given by equation (6) and can be applied as a first indication of the radiometal-chelator suitability, but the kinetics of the dissociation needs to be evaluated. [55]

$$K_{ML} = \frac{[ML]}{[M][L]} \quad (6)$$

The kinetic inertness of the complex can be analyzed by performing competition studies. The competition between the metal ion and protons, and thereby the acid-catalyzed dissociation of the complex, can be evaluated by lowering the pH. The acid dissociation is, however, not as applicable, since the stability at physiological conditions is of interest. A competition study with an excess of various biological relevant metal ions, e.g. Fe^{3+} or Zn^{2+}, can be performed to evaluate the stability of the complex towards replacement of the radiometal with other metal ions. Furthermore, competition studies with possible biological relevant ligands, e.g. serum proteins *in vitro* can give an indication of the tendency of transchelation of the radiometal *in vivo*. In order to evaluate the amount of the radiometal-complex at different time points of the competition studies, thin-layer chromatography (TLC) or high-performance liquid chromatography (HPLC) can be applied. [3]

The most conclusive test, is the evaluation of the stability *in vivo* by PET imaging in animals. The radiometal-chelator complex can be studied *in vivo* without being conjugated to a targeting vector. The biodistribution and clearance of the compound can thereby be evaluated, but the clearance of the radiometal-chelator complex can be very fast, and it might therefore be necessary to conjugate it to a targeting vector to evaluate the stability. [55] An indication of dissociation of the radiometal and the chelator, can often be seen as an increased radioactivity in tissue where the metal has a high association, e.g. bone in the case of zirconium [57] or liver in the case of copper [58]. However, a high radioactivity in the liver can also be due to the excretion of lipophilic compounds. [58] It can thus be challenging to determine, whether an observed biodistribution is due to instability of the radiometal-chelator complex.

Another aspect, which needs to be evaluated, is if or how the addition of the BFC affects the pharmacokinetics and binding affinity of the targeting vector. The incorporation of the chelator can be a significant modification, especially for small molecules and peptides. Even changing or modifying the chelator and/or the radiometal can result in very different biological distribution of the radiopharmaceutical. [3] The binding affinity of the modified targeting vector with the BFC can be evaluated *in vitro* by binding assays; however, the binding affinity to the biological target needs to be subsequently studied *in vivo* to evaluate if the compound can be applied as a radiopharmaceutical. [59]

3 Summary – Radiometal-based radiopharmaceuticals

The production and application of PET radiometal-based radiopharmaceuticals is a multidisciplinary field requiring experience and knowledge from fields as physics, radiochemistry, organic and inorganic chemistry, biology, pharmacology, and engineering.

Positron emitting radiometals are suitable for PET radiopharmaceuticals due to a large variety of physical and chemical properties, making it possible to match the radiometal to the targeting vector (biology, pharmacology). The radiometal can be introduced easily and in a late stage of the synthesis of the radiopharmaceutical by using suitable BFCs (inorganic and organic chemistry). Several radiometals can be produced with 16-18 MeV cyclotrons, while a few radiometals are available from generators (nuclear physics and radiochemistry). The radiometal needs to be purified and separated from its target material, since impurities and other metal ions can affect the radiolabeling (radiochemistry and inorganic chemistry). Furthermore, the production of radiopharmaceuticals implies handling of high amounts of radioactivity, and processes, which should ideally be automatized (engineering). Finally, the stability and binding affinity of the radiopharmaceutical *in vitro* and *in vivo* need to be studied in order to evaluate the application of the radiopharmaceutical for PET (cell biology, pharmacology, radiochemistry and nuclear medicine).

Chapter 2

Liquid-liquid extraction in flow of positron emitting radiometals

4 Liquid-liquid extraction and membrane-based separation

The separation of radiometals from their cyclotron target material is an essential step towards the production of a radiometal-based radiotracer for PET. A high separation factor (10^6-10^8) between the produced radiometal and its cyclotron target material is necessary due to significantly lower concentration of the radiometal compared to the concentration of the cyclotron target metal (section 2.3.1.3). The chemical separation of the radiometal from the target material can be performed by different methods, e.g. SPE and LLE as described in section 2.3. Currently, LLE of radionuclides has in most cases been replaced by SPE resin-based separation methods, as these are more automation-friendly [4], which reduces the radiation exposure. In this chapter, the separation of ^{45}Ti, ^{89}Zr, ^{64}Cu, and ^{68}Ga from their cyclotron target materials is explored by performing LLE and phase separation in flow using a membrane-based separation technique, which has the advantage of being simpler to automate, compared to gravity-operated LLE. The membrane-based separation technique is described and the purification of each of the four radiometals is discussed in individual sections with an overall summary at the end of the chapter.

4.1 Liquid-liquid extraction and phase separation in flow

The phase mixing and separation for LLE can be performed in batch mode, where the separation is governed by gravity or external forces, such as centrifugation. It is also possible to perform the phase mixing and separation in flow. Here, an efficient mass transfer to the extracting phase is obtained by mixing the two phases continuously in flow. Different flow regimes can be obtained when the two immiscible phases are mixed in flow. Slug flow is one regime that is commonly used to obtain high mass transfer, as it gives a high surface-to-volume ratio between the phases. In slug flow, friction at the walls of the tubing, wherein the two phases are mixed, takes place. A constant exchange of the interface of each slug takes place, since the material within the slugs is circulated (Figure 10). [4]

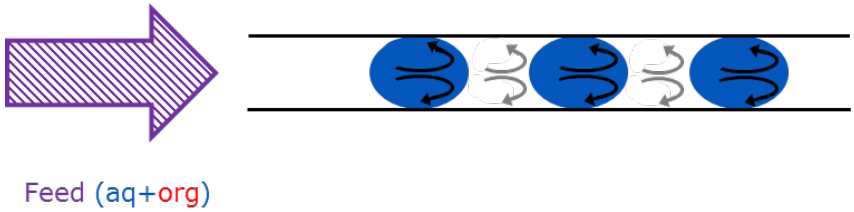

Figure 10: Illustration of slug flow of two immiscible phases. The feed (mixed aqueous (blue) and organic phase (white)) enters the tubing, where slug flow is developed. The friction on the walls creates a circulation within the slugs, which leads to a high surface-to-volume ratio between the two phases.

The phase separation in flow can be performed by utilizing the gravity force, but surface forces become more prevalent when the separation is performed in smaller scales (milli- and microscale). [4] For this study, a membrane-based separation technique with a microfiltration membrane and integrated pressure control is chosen. An image of the membrane separator and an illustration of the membrane and diaphragm can be seen in Figure 11. The aqueous phase and the organic phase are mixed (feed) and enter the membrane separator. Inside the membrane separator, the feed reaches the membrane, where the two phases are separated. In this case, a hydrophobic membrane is applied, allowing the organic phase to wet the membrane and permeate through the pores, while the aqueous phase is retained. The integrated pressure control is achieved by the use of a diaphragm. The diaphragm is placed over the stream of the retentate with the permeate stream on the other side (Figure 11, right). A certain pressure is necessary for the retentate to flow, since the diaphragm seals against the retentate flow path and needs to be deformed. Thereby, a pressure control with a constant pressure over the membrane is obtained. [5]

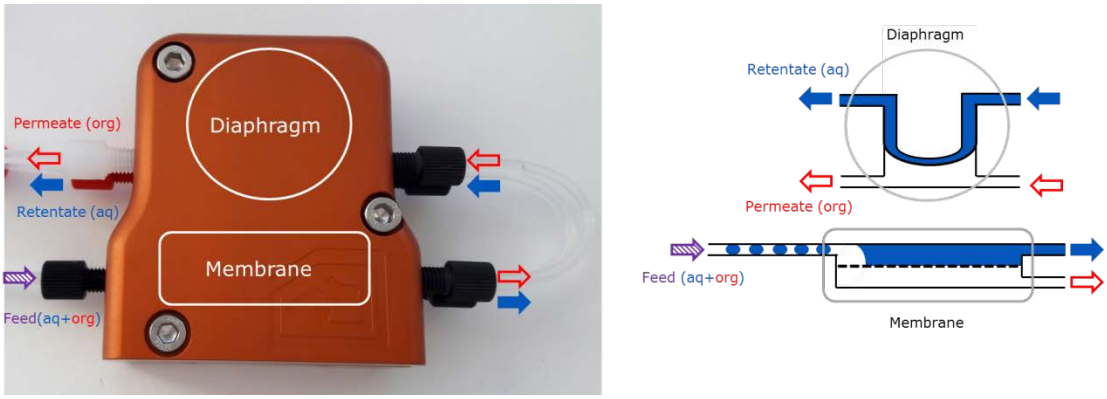

Figure 11: Left: Image with illustrations of the membrane separator used for the experiments in this study. The feed, which is mixed aqueous and organic phase (purple arrow) enters the membrane separator. The hydrophobic membrane retains the aqueous phase, while the organic phase permeates the membrane. A diaphragm is used as pressure control. The retentate (aqueous phase) (blue arrow) and the permeate (organic phase) (red arrow) exit the separator from two different outlets. Right: Illustration of the membrane and diaphragm.

The aqueous phase (blue) and organic phase (white) are mixed, separated over the membrane, passes the diaphragm and flow through the retentate and permeate outlet, respectively. The figure is adapted from [9].

The phase separation depends on the interfacial tension (γ) between the two phases. The capillary pressure (P_{cap}) needs to be modulated to obtain a suitable setup for the chosen solvent system. P_{cap} depends on γ, the contact angle (θ) between the membrane and the two phases, and the radius (R) of the pores of the membrane (equation (7)).

$$P_{cap} = \frac{2\gamma \cos(\theta)}{R} \tag{7}$$

To avoid breakthrough of the retained phase, P_{cap} needs to be greater than the transmembrane pressure (ΔP_{mem}) (Figure 12). It is also important that the pressure required to make the permeating phase flow through the membrane (P_{per}) is sufficient otherwise retention of the permeating phase is seen (Figure 12).

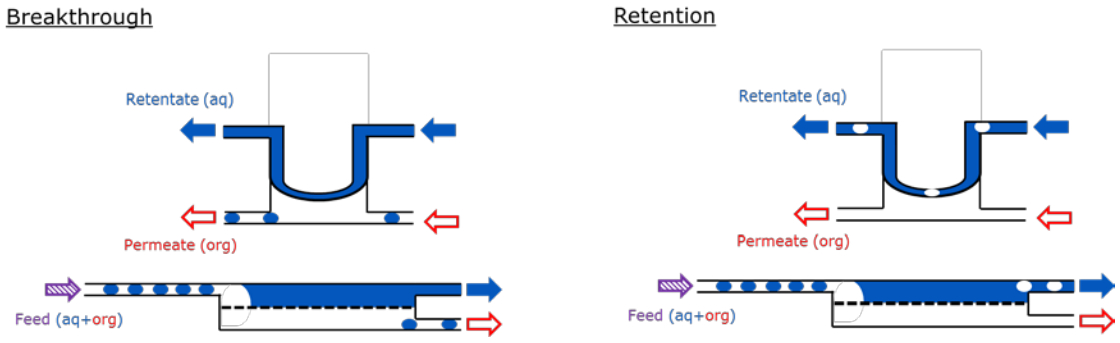

Figure 12: Illustration of two failure modes of the membrane separator. Left: Breakthrough of the retained phase in the permeate. Right: Retention of the permeating phase in the retentate.

P_{per} depends on the viscosity of the permeating phase (μ), the volumetric flow rate of the entering permeating phase (Q), the membrane thickness (L), and the number (n) and radius (R) of the pores (equation (8)).

$$P_{per} = \frac{8\mu QL}{n\pi R^4} \tag{8}$$

A combined inequality (equation (9)) can be outlined, if a negligible pressure drop along the channels of the membrane is present and under the assumption that ΔP_{mem} is constant along the membrane.

$$P_{cap} > \Delta P_{mem} > P_{per} \tag{9}$$

A higher P_{cap} than ΔP_{mem} can be obtained by choosing a suitable membrane material and pore size. ΔP_{mem} can be described as the difference between the pressure on the retentate side (P_1) and on the permeate side (P_2) (P_1 - P_2). By inserting P_1-P_2 in inequality (9), inequality (10) is obtained.

$$P_{cap} + P_2 > P_1 > P_{per} + P_2 \tag{10}$$

The diaphragm ensures that the retentate only flows when $P_1 > P_2$ and due to the tension on the diaphragm (P_{dia}), the retentate can be described by equation (11). P_{dia} depends on the properties of the diaphragm (thickness and elastic modulus) and the amount of deformation.

$$P_1 = P_{dia} + P_2 \tag{11}$$

Equation (12) is obtained by inserting the expression for P_{dia} into equation (10).

$$P_{cap} > P_{dia} > P_{per} \tag{12}$$

Thus, complete phase separation can be obtained if this inequality can be fulfilled. [5]

4.2 Design of the study

In this study, the establishment of a suitable solvent system, which ensures high extraction efficiency of the radiometal and enables phase separation in flow with the described membrane-based separation technique, was attempted. This development can be subdivided into different steps.

4.2.1.1 Preliminary LLE experiments

First, a suitable extraction system needed to be established. Here, the speciation of the radiometal and the cyclotron target material in acidic aqueous solution were taken into account, and the chemical properties were evaluated to choose a suitable extractant for the radiometal. The extraction was first tested in batch LLE primarily with the nonradioactive elements of the radiometal and cyclotron target material, e.g. Zr and Y, for the separation of ^{89}Zr separation, with the exception of the ^{68}Ga LLE, where the preliminary experiments were conducted with radioactive isotopes of gallium and zinc. The concentration of the nonradioactive elements needed to be significantly higher (millimolar) than the concentration of the radiometals (pico- to nanomolar) in order to be able to quantify the amount of the element. The extraction efficiencies of the nonradioactive metals were measured by Ultraviolet-visible (UV-vis) spectroscopy or inductively coupled plasma optical emission spectrometry (ICP-OES). For the quantification of a metal ion with UV-vis spectroscopy, the absorption spectrum of a colored complex, formed between the metal ion and specific ligands, was measured. The concentration of the complex could be calculated from a standard curve for the specific metal-complex.

However, only the amount of the metal forming the complex could be quantified. ICP-OES was applied to quantify the amount of the metals in the aqueous phase before and after the LLE. By ICP-OES, the total concentration of an element in the sample solution can be measured. The ICP-OES sample is converted to an aerosol by a nebulizer and injected into a plasma. Here, the aerosol is dried and vaporized, and the sample atomized and ionized. The atoms and ions are excited and the characteristic atomic emission of an element when relaxing back to ground state is used to quantify the elements in the sample. [60]

4.2.1.2 LLE and phase separation in flow

Next step was to evaluate and optimize the phase separation in flow by changing membrane material and pore size, and diaphragm thickness. An illustration of the setup for the LLE and membrane-based separation in flow is shown in Figure 13. The aqueous and the organic phase were loaded in two syringes, which each were connected to a piece of tubing, joined in a tee. The two phases were pumped using syringe pumps and the phases were mixed when reaching the tee, followed by a mixing through static mixers and by the development of slug flow in a mixing loop. The static mixers were added to improve the mixing of the two phases. The phases then entered the membrane separator, where the two phases had to be separated. The organic phase could be collected from the permeate outlet and the aqueous phase from the retentate outlet, if phase separation was obtained.

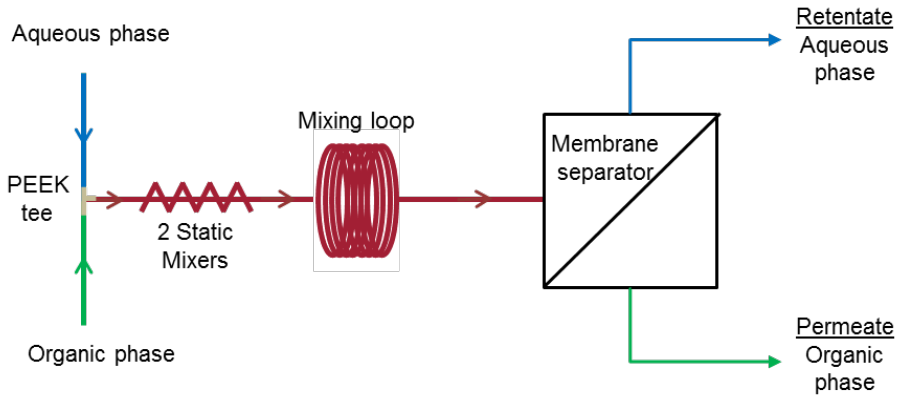

Figure 13: Illustration of the setup for the LLE and phase separation in flow. The aqueous phase (blue) and the organic phase (green) were each pumped using a syringe pump. The two streams were combined in a polyether ether ketone (PEEK) tee. The two phases were mixed by two 10-element static mixers and in a mixing loop. The mixed phases entered the membrane separator, where the organic phase permeated the membrane, while the aqueous phase was retained. The figure is modified from [8].

If complete phase separation could not be obtained, diluents were added to the organic phase to increase the interfacial tension between the phases and thereby P_{cap} (equation (7)). If phase separation was not possible after adding a diluent, other extractants were tested. The effect of flow rate, flow rate ratios, and residence times were evaluated in order to improve the extraction efficiency, when complete phase separation was obtained. In some

cases, the amount of organic phase in the aqueous phase after the LLE was measured, using quantitative nuclear magnetic resonance spectroscopy (qNMR), by the addition of an internal calibrant (see equation (18) in section 13.1.3.34). [61]

4.2.1.3 LLE of radiometals

The first steps were conducted with the stable elements, except for gallium, and it was thus necessary to subsequently evaluate, if similar extraction efficiency could be obtained, when changing to the radiometal, thereby decreasing the concentration significantly. The extraction efficiencies of the radiometals were calculated by measuring the amount of the radiometal in the two phases after the LLE using gamma spectroscopy or in the cases where only one radioactive isotope was present in the samples, a dose calibrator was applied.

Finally, attempts were made to obtain the radiometal in a solution suitable for the radiolabeling. This was performed by back-extraction (stripping) of the radiometal into an aqueous phase with a low HCl concentration or into an aqueous phase containing a chelator. Another approach was also tested, where the radiolabeling was performed in the organic phase from the LLE.

5 LLE of ^{45}Ti

^{45}Ti has suitable physical properties for PET with a half-life of 3.1 hours and a lower β^+ end-point energy than e.g. ^{68}Ga. However, only a limited number of *in vivo* studies with ^{45}Ti-based PET imaging have been published. [62]–[70] The application of ^{45}Ti for PET and the development of a specific ^{45}Ti-based PET tracer are described in chapter 3, while the production and purification of ^{45}Ti is described in the following sections.

5.1 Production of ^{45}Ti

^{45}Ti can be produced using a cyclotron by the ^{45}Sc(p,n)^{45}Ti nuclear reaction with a maximal cross section at 10-14 MeV (Figure 14). Scandium-45 (^{45}Sc) is the only naturally abundant isotope of scandium, which limits the coproduction of other isotopes. [71] However, as seen in Figure 14, at proton energies > 11 MeV competing nuclear reactions on ^{45}Sc will start to produce some radionuclidic impurities. Most significantly, titanium-44 (^{44}Ti) ($T_{½}$ = 60 y) is formed by the ^{45}Sc(p,2n)^{44}Ti nuclear reaction at proton beam energy higher than 13 MeV. [72] Additionally, ^{44}Sc ($T_{½}$ = 3.97 h) and scandium-44m (^{44m}Sc) ($T_{½}$ = 58.6 h) are produced by the ^{45}Sc(p,x)^{44m}Sc/^{44}Sc nuclear reactions at proton beam energies over 11 MeV. However, ^{44m}Sc/^{44}Sc can be chemically separated from ^{45}Ti, the same way as the scandium cyclotron target material.

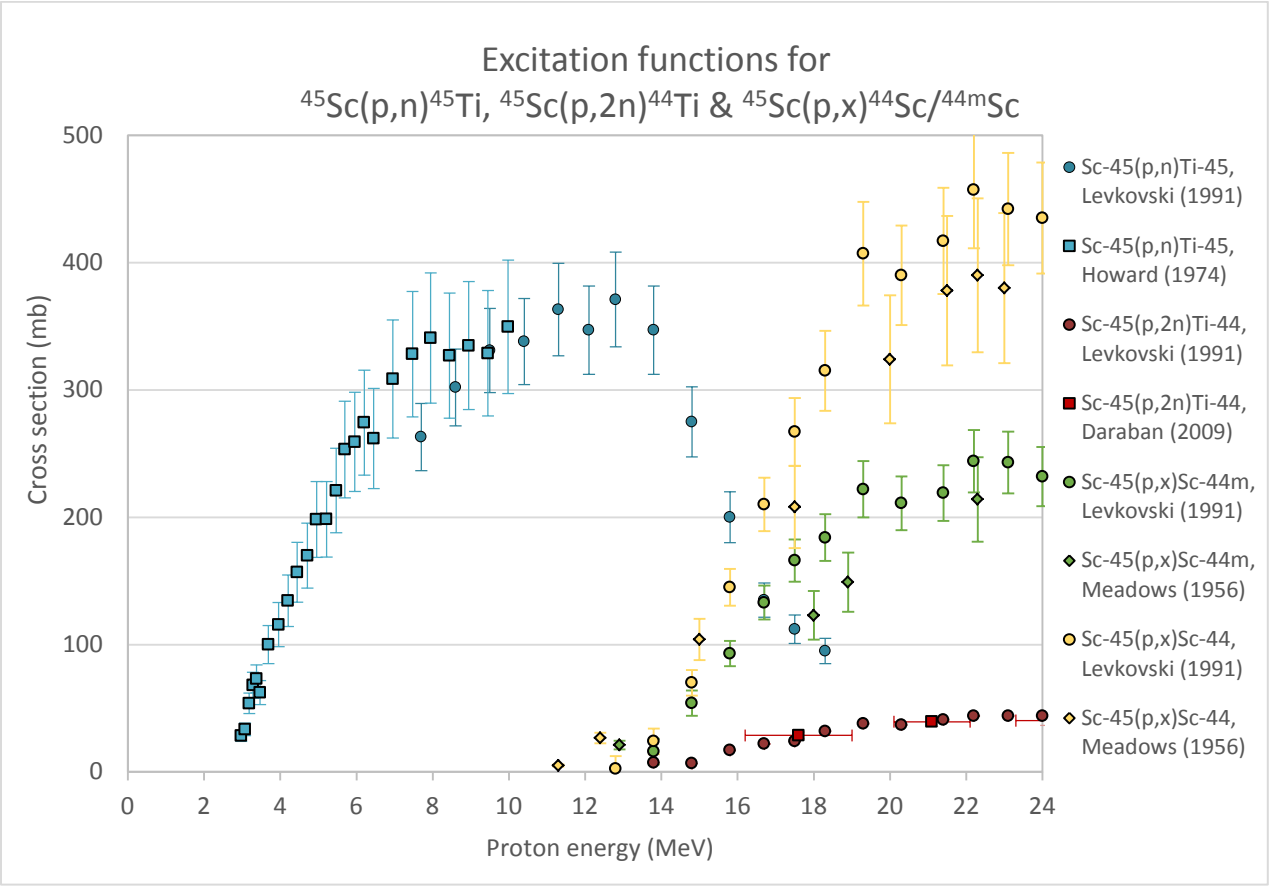

Figure 14: Excitation functions for the $^{45}Sc(p,n)^{45}Ti$ (blue), $^{45}Sc(p,2n)^{44}Ti$ (red), and $^{45}Sc(p,x)^{44m}Sc/^{44}Sc$ (green and yellow) nuclear reactions showing their energy dependent cross sections and the potential for co-production of radionuclide contaminations. The experimental cross section data is collected from the EXFOR (Experimental Nuclear Reaction Data) database [73] and published by [72], [74]–[76].

5.2 Chemical properties of titanium

Ti^{4+} is a very strong Lewis acid and titanium complexes tend to be hydrolyzed. At pH below 2, $[Ti(OH)_2]^{+2}$ exists, but gets further hydrolyzed to $[Ti(OH)_3]^{+}$ and $Ti(OH)_4$, which can be seen in Figure 15, illustrating a speciation diagram for titanium(IV) in aqueous solution and in HCl. The synthesis of stable titanium-complexes is challenging, since the formation of the hydroxide species can lead to demetallation. Due to the strong Lewis acidity, titanium prefers hard, strong Lewis bases, e.g. carboxylates, hydroxides, and phenolates. [6], [15]

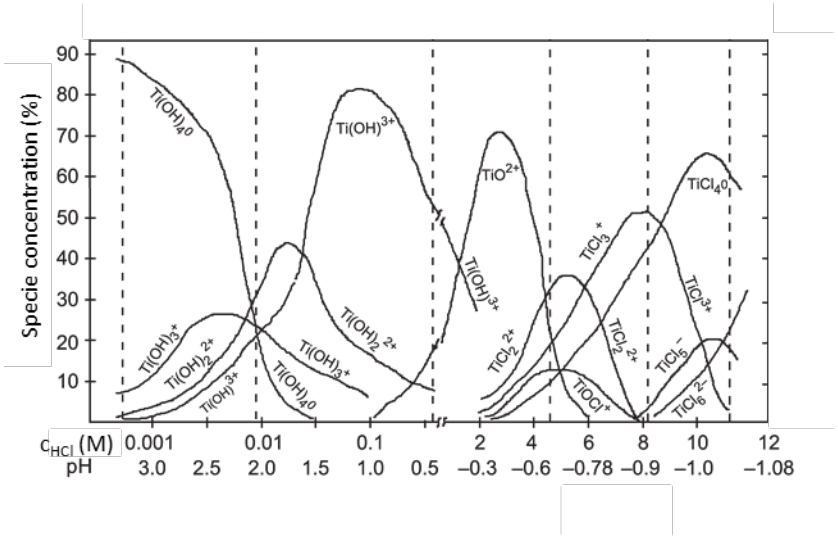

Figure 15: Speciation diagram of titanium(IV) in aqueous solution from pH 0.5 to 3.0 and in 2-12 M HCl. The figure has been modified from [77].

5.3 Purification of ^{45}Ti

^{45}Ti needs to be efficiently separated from the irradiated scandium, since the concentration of ^{45}Ti is very low compared to the concentration of scandium. The two metals can be separated from each other because of the different chemical properties. Scandium is in the group III (IIIB) in the periodic table and +3 is the most common oxidation state of scandium. [78] Separation of ^{45}Ti from scandium has previously been obtained with SPE and LLE methods. The separation of ^{45}Ti from scandium using cation exchange resin [67], [69], [79], e.g. AG 50W-X8, has been used with different success, where a high recovery of ^{45}Ti were found by Vavere et al. [67], while Price et al. experienced less efficient separation. [68] Hydroxamate resin has been applied with a ^{45}Ti recovery of 30-56 %, which can be further improved. [63], [68], [80] The separation using PEG (polyethylene glycol) functionalized 1,3-diol resin was found to be efficient, but it can be time consuming. [65], [81] LLE with alcohols, such as octanol and guaiacol, can also be used when the aqueous phase contains a high concentration of HCl. [8], [81]–[83] For the LLE of ^{45}Ti, high concentration of hydrochloric acid is needed, since the extractable species are expected to be $[TiCl_4 \cdot 2HCl]^0$, $[TiCl_4 \cdot 4HCl]^0$ or other neutral species, which predominate in the region of high concentration of HCl [84], as seen in Figure 15. At high HCl concentration (> 10 M) $TiCl_4$ is formed, while positively charged chloride species are present at HCl concentration below 10 M. [77]

The need for a high HCl concentration and the oxophilicity of titanium limits the choice of the organic phase to alcohols, diols, phenols, and certain organic acids. Different solvents and extractants including fluorinated compounds were tested in this study. As described in section 4.2, the LLEs were both performed using ^{45}Ti and nonradioactive titanium. First, a solvent system with high extraction efficiency of titanium, which could be

translated to LLE in flow, was found. Next, it was investigated if scandium was extracted by the chosen solvent system and the optimized conditions were applied to the LLE of ^{45}Ti in flow. The preliminary experiments are described in detail in the following sections, leading to the final and published experiments and results. The paper with the published results can be found in Appendix A (*"Liquid–liquid extraction in flow of the radioisotope titanium-45 for positron emission tomography applications"*). [8]

5.3.1 LLE of titanium with 1-octanol

The LLE with 1-octanol and with two different diol additives, 2,3-dihydroxynaphtalene (DHN) and 1,2-decanediol (Figure 16) was studied and subsequently attempted to be used for the LLE in flow, due to the promising extraction of ^{45}Ti with 1,3-diol resins and 1-octanol [81]–[83].

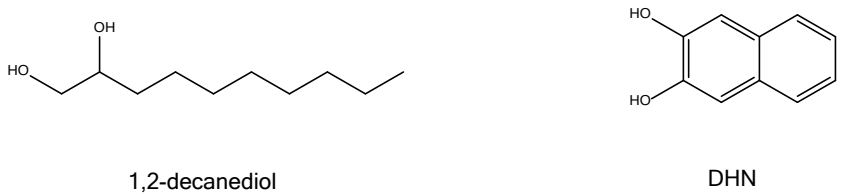

Figure 16: The chemical structure of 1,2-decanediol (left) and DHN (right).

In the first LLE experiments in batch mode it was tested, if the extraction of ^{45}Ti was possible using 1-octanol with and without additives, such as 1,2-decanediol and DHN. The extraction efficiencies of ^{45}Ti from 12 M HCl using 1-octanol, 1,2-decanediol, and DHN, can be seen in Figure 17. The LLE experiments were performed with 1-octanol, 1,2-decandiol, and DHN, where an additional volume of organic phase was added twice to the aqueous phase after the first LLE. The extraction efficiency after each LLE was calculated from the total activity in the organic phase(s) divided by the total activity in the aqueous and organic phases (section 13.1.3.3). The extraction efficiencies with 1-octanol when adding 1,2-decanediol and DHN were similar, but a small increase in efficiency was observed compared to the extraction efficiencies with 1-octanol alone. Up to 78 % extraction of ^{45}Ti was achieved after the three accumulative extractions.

Figure 17: The LLE in batch mode of ^{45}Ti from 12 M HCl containing the dissolved scandium foil using 1-octanol (blue circles), 0.1 M 1,2-decanediol in 1-octanol (red squares), and 0.1 M DHN in 1-octanol (green triangles). Number of extraction refers to the addition of a new portion of organic phase to the aqueous phase after each LLE run.

The extraction of ^{45}Ti from 6 M HCl with the same extractants, as mentioned above, was also studied, but was unsuccessful with practically no extraction (up to 3 %) into the organic phase. At this lower HCl concentration the titanium species are expected to be mainly positively charged, e.g. $TiOCl^{+}$, $TiCl_3^{+}$, and $TiCl_2^{2+}$, and with only a small concentration of the neutral $TiCl_4$ species (Figure 15). [77] Thus, the concentration of HCl was too low to prompt the formation of the extractable neutral $TiCl_4$ species.

The extraction efficiencies of titanium from 8, 10, and 12 M HCl were compared to evaluate the effect of the HCl concentration. The LLE was performed in batch mode using 1-octanol as extractant. As mentioned in section 4.2, the experiment was performed with nonradioactive titanium and the extraction efficiencies were evaluated by the UV-vis method described in section 13.1.3.13. Two consecutive LLE steps were performed for each HCl concentration, so the aqueous phase from the first LLE was mixed with an additional volume of organic phase. The extraction efficiencies, calculated from UV-vis spectroscopy, can be seen in Figure 18. This experiment illustrated that the HCl concentration played an important role in the extraction of titanium. The extraction efficiencies of titanium from 10 and 12 M HCl were both 43 % after the first LLE and were slightly increased after the second LLE, where the extraction from 10 M HCl was found to be higher, than from 12 M HCl. The LLE of titanium from 8 M HCl was on the other hand lower (up to 22 % after two LLEs) in both LLE runs. The observed difference was expected to be due to the lower concentration of neutral $TiCl_4$ species at 8 M HCl. A similar trend of HCl dependency was seen, when 10 mM 1,2-decanediol in 1-octanol was used as

extractant for titanium from 8, 10, and 12 M HCl. Here, an extraction efficiency of 18%, 56 %, and 70 %, respectively, was obtained after one LLE in batch.

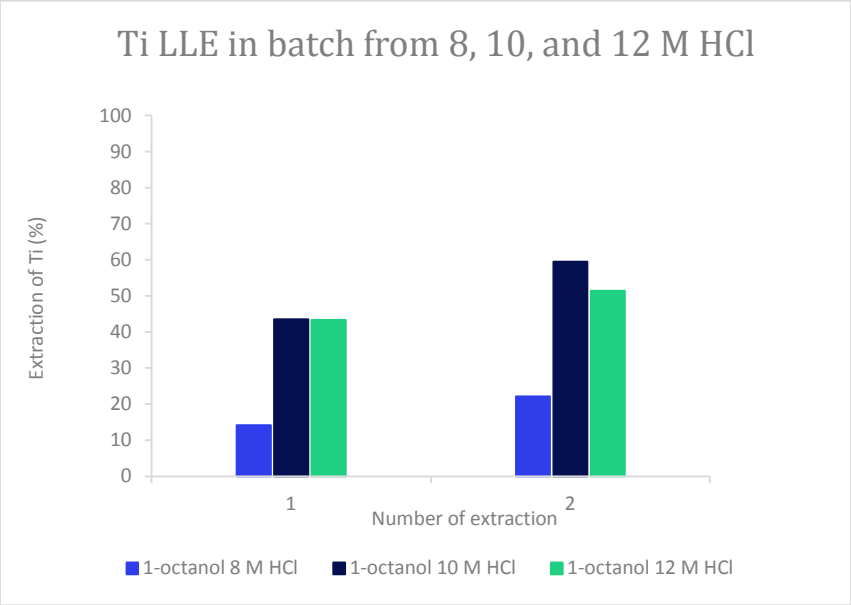

Figure 18: The LLE in batch mode of titanium from 8 M HCl (blue), 10 M HCl (dark blue), and 12 M HCl (green) using 1-octanol. The second extraction was when an additional volume of organic phase was added to the aqueous phase from the first extraction.

The LLE in flow of titanium from 12 M HCl using 1-octanol was attempted using the membrane-based separation technique described in section 4.1. Different membranes and diaphragm thicknesses were tested for the LLE of titanium shown in Table 3. The choice of membrane was limited to the compatibility of the membrane material with concentrated HCl and organic solvents. PTFE (polytetrafluoroethylene), PEEK, and PVDF (polyvinylidene fluoride) are compatible with concentrated HCl, while PP (polypropylene), which is a support material for some of the PTFE membranes with smaller pore size, might be affected over time. [85] Hence, it was important to examine the membranes after the LLE to ensure that the membranes had a sufficient resistance. Firstly, a PTFE membrane with a relative large pore size (0.5 µm) was used, but even with the thinnest diaphragm available (1 mil (10^{-3} inch (1 mil = 25.4 µm))) breakthrough was seen, where droplets of the aqueous phase in the organic phase was observed after the separation. The organic phase was modified by adding different amounts of hexane or octane as diluents to improve the phase separation. Unfortunately, these modifications did not lead to phase separation. Furthermore, the LLE of titanium in batch with 20, 50, and 80 % hexane in 1-octanol also showed a significant decrease in extraction efficiency (18 %, 12 %, and 7 %, respectively). Breakthrough was also seen when the HCl concentration was decreased to 10 M. Consequently, this approach was not pursued further. Instead, the membrane was changed to a membrane with a smaller pore size (0.1 µm) made out of PEEK. However, the separation of 1-octanol and 12 M HCl was still not possible. In

this case, retention was observed, when using a diaphragm thickness of 1 and 2 mil (Table 3). When changing to 5 mil both retention and breakthrough was seen. Membranes made out of PTFE and PVDF were used for the further study, but it was not possible to obtain complete phase separation with 0.1 or 0.2 µm pore size membranes made out of these materials.

Table 3: The LLE in flow of titanium from 0.01 M $TiCl_4$ and 0.01 M $ScCl_3$ in 10 M or 12 M HCl with 1-octanol can be seen. The membrane with pore size and material, diaphragm, and aqueous and organic phase used for each experiment are listed. The aqueous and organic flow rates were both 0.5 mL/min. The separation performance of each experiment is listed in the last column.

Membrane (pore size and material)	Diaphragm (mil)	Aqueous phase	Organic phase	Separation performance
0.5 µm, PTFE	1	12 M HCl	1-octanol	Breakthrough
			10mM DHN in 1-octanol	
			10 % hexane in 1-octanol	
			70 % hexane in 1-octanol	
			10 % octane in 1-octanol	
0.5 µm, PTFE	1	10 M HCl	1-octanol	Breakthrough
0.1 µm, PEEK	1	12 M HCl	1-octanol	Retention
	2			
0.1 µm, PEEK	5	12 M HCl	1-octanol	Retention and breakthrough
0.2 µm, PVDF	2	12 M HCl	1-octanol	Breakthrough
0.2 µm, PVDF	1	12 M HCl	1-octanol	Retention and breakthrough
0.1 µm, PTFE/PP	1	12 M HCl	1-octanol	Retention and breakthrough
0.2 µm, PTFE/PP	1	12 M HCl	1-octanol	Breakthrough

It was assumed that this challenging phase separation could be due to a too low interfacial tension between 1-octanol and concentrated HCl. A low interfacial tension would lead to a small P_{cap} (equation (7)) and it was not possible to decrease P_{dia} sufficiently to avoid breakthrough (inequality (12)). Furthermore, an increased volume of the organic phase after LLE in batch with 1-octanol and concentrated HCl was seen, indicating a migration of HCl into the organic phase. Due to the need of a high HCl concentration to form the extractable titanium species, a different extraction system was tested.

5.3.2 LLE of titanium with fluorinated compounds

Another possibility was the use of fluorous solvents which enables a high phase separation with the aqueous phase. Fluorous solvents are also immiscible with organic solvents and most organic extractants need to be fluorinated to be dissolved in the fluorous solvent. [86] Thus, fluorinated compounds containing hydroxy groups or diols might be suitable for the extraction of ^{45}Ti. The LLE of titanium with commercial available fluorinated 1-octanol (perfluoro-*1H,1H,2H,2H*-1-octanol) (Rf_6-ol) and a synthesized fluorinated diol (Rf_{10}-diol) were tested. The structure of the two fluorinated compounds can be seen in Figure 19.

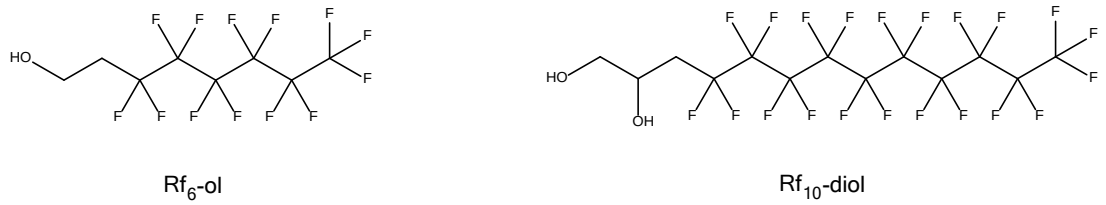

Figure 19: The structure of **Rf_6-ol** and of 3-(4,4,5,5,6,6,7,7,8,8,9,9,10,10,11,11,12,12,13,13,13-henicosafluorodecyl)-propane diol (**Rf_{10}-diol**).

The Rf_{10}-diol was synthesized by allylation of 1-iodoperfluorodecane with allyltributylstannane leading to compound **1** followed by dihydroxylation with *N*-methyl morpholine-*N*-oxide (NMO) catalyzed by osmium tetroxide (OsO_4) (Figure 20).

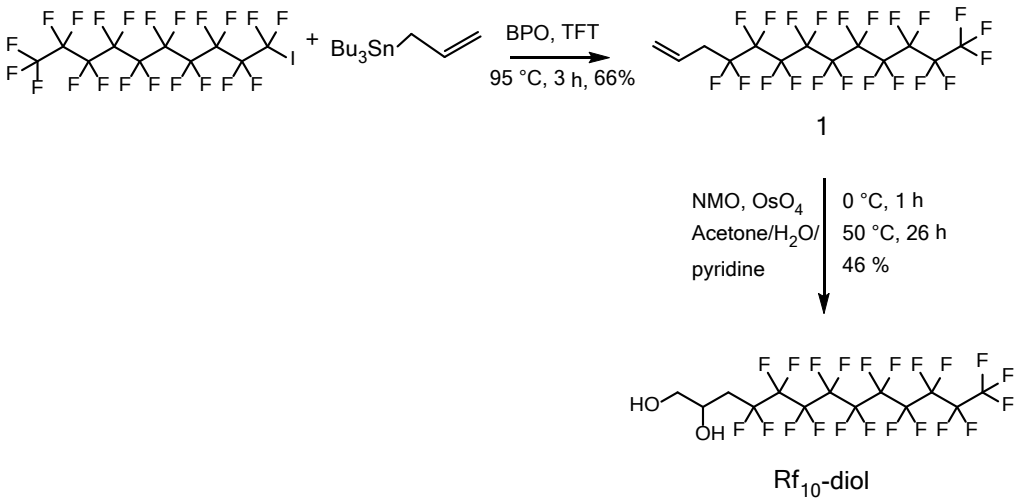

Figure 20: The 2-step synthesis of Rf_{10}-diol. BPO: benzoyl peroxide, TFT: α,α,α-trifluorotoluene, NMO: *N*-methyl morpholine-*N*-oxide.

The evaluation of the ^{45}Ti extraction using the fluorinated compounds Rf_6-ol and Rf_{10}-diol in batch LLE, showed no extraction of ^{45}Ti applying the Rf_{10}-diol as extractant. The Rf_{10}-diol was dissolved in α,α,α-trifluorotoluene (TFT)/hexafluoroisopropanol 1/1 (v/v) at a concentration of 0.05 M and the mixing time of the aqueous and fluorous phase was relative short (2 minutes). It was not investigated, if a higher concentration, different solvents or longer mixing time would have led to an increased extraction of titanium. Instead, the LLE of titanium in batch using neat Rf_6-ol was studied. The LLE was challenging, since the phase separation was very slow after mixing the two phases and it appeared as if an emulsion was formed. The same was seen when diluting Rf_6-ol with TFT or perfluoro(methylcyclohexane) (1:1). After a long waiting time, the titanium extraction efficiency using neat Rf_6-diol was measured to be 87 %. The LLE in flow with Rf_6-ol was attempted (Table 4). First, a PTFE membrane with a pore size of 0.5 µm was used. Three different diaphragm thicknesses (1, 2, and 5 mil) were tested, but breakthrough was seen when using a 5 or 2 mil diaphragm, while retention was observed with the 1 mil diaphragm. It was neither possible to obtain complete phase separation with a PTFE/PP membrane with a pore size of 0.2 µm and 2 mil diaphragm. Thus, another solvent system for the LLE of titanium was consequently evaluated.

Table 4: The LLE in flow of titanium from 0.01 M $TiCl_4$ and 0.01 M $ScCl_3$ in 12 M HCl using Rf_6-ol as organic phase can be seen. The membrane pore size and material, diaphragm thickness, and separation performance of the experiments are listed. The aqueous and organic flow rates were both 0.1 mL/min.

Membrane (pore size and material)	Diaphragm (mil)	Separation performance
0.5 µm, PTFE	1	Retention
0.5 µm, PTFE	5	Breakthrough
	2	
0.2 µm, PTFE/PP	2	Retention/ emulsion

5.3.3 LLE of titanium with guaiacol/anisole

The application of guaiacol as extractant for titanium was studied, since guaiacol can form complexes with titanium and guaiacol is compatible with 12 M HCl. A $TiCl_2$(guaiacolato)$_2$ complex has been synthesized by Sobota et al. using $TiCl_4$. [87] It was thus anticipated that guaiacol would have an affinity for neutral titanium species. From the LLE with 1-octanol, it was seen that the interfacial tension between the aqueous and organic phase could be challenging when efficient extraction of titanium requires concentrated HCl as the aqueous phase. Anisole was added as a diluent, since it is more hydrophobic than guaiacol but still is structurally similar. The phase separation in flow was possible between guaiacol/anisole 50/50 (v/v) and 12 M HCl with a PTFE/PP membrane with a 0.2 µm pore size and a diaphragm thickness of 2 mil (Table 5).

Table 5: The LLEs of titanium in flow from 0.01 M $TiCl_4$ and 0.01 M $ScCl_3$ in 12 M HCl with guaiacol/anisole as organic phase are listed. The membrane material and pore size, diaphragm thickness, organic phase composition, and aqueous and organic flow rates for each experiment and the separation performance can be seen.

Membrane (pore size and material)	Diaphragm (mil)	Organic phase	Aqueous flow rate (mL/min)	Organic flow rate (mL/min)	Separation performance
0.5 µm, PTFE	1	Guaiacol/anisole 50/50 (v/v)	0.1	0.1	Retention
0.5 µm, PTFE	2	Guaiacol/anisole 50/50 (v/v)	0.1	0.1	Breakthrough
0.2 µm,	2	Guaiacol/anisole	0.1	0.1	Complete phase

PTFE/PP		50/50 (v/v)			separation
0.2 µm, PTFE/PP	2	Guaiacol/anisole 75/25 (v/v)	0.1	0.1	Complete phase separation
			0.05	0.15	
			0.10	0.30	
			0.25	0.75	
0.2 µm, PTFE/PP	2	Guaiacol/anisole 95/5 (v/v)	0.1	0.1	Breakthrough/retention
0.05 µm, PTFE	2	Guaiacol	0.05	0.15	Retention
	5				
0.2 µm, PTFE/PP	2	Guaiacol/anisole 90/10 (v/v)	0.05	0.15	Complete phase separation
			0.0333	0.1667	
			0.25	0.75	

The extraction efficiency of different ratios of guaiacol and anisole was studied and calculated from ICP-OES measurements (Figure 21). The first attempt was a 50/50 (v/v) ratio of guaiacol and anisole. A titanium extraction efficiency of 61 % was achieved with this solvent system. The LLE and phase separation was tested with a higher guaiacol/anisole ratio in order to improve the efficiency. The phase separation was still possible with a 75/25 (v/v) guaiacol/anisole ratio (Table 5) and the extraction efficiency of titanium was improved to 68 %. It was then studied if a larger volumetric phase ratio (P) (equation (4)) could increase the extraction efficiency further, as described in section 2.3.1.3. A flow rate ratio of 1:3 (aq:org) was applied for the LLE with 75/25 (v/v) guaiacol/anisole, which led to an extraction efficiency of 85 %. The extraction efficiency was further improved by changing the ratio of guaiacol/anisole to 90/10 (v/v), while the phase separation was still complete with the same membrane and diaphragm thickness. The extraction of titanium was 90 % with a flow rate ratio of 1:3 (aq:org). However, the extraction efficiency was not improved when using a flow rate ratio of 1:5 (org:aq) and it was not possible to achieve complete phase separation between 12 M HCl and 95/5 (v/v) guaiacol/anisole (Table 5). Thus, the optimized conditions with highest titanium extraction efficiency was obtained by using 90/10 (v/v) guaiacol/anisole and a flow rate ratio of 1:3 (aq:org).

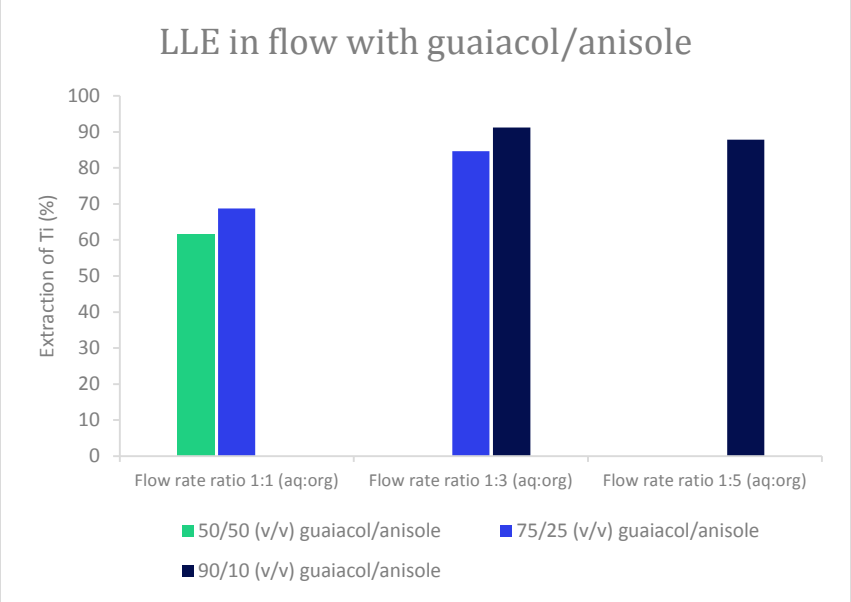

Figure 21: The LLE in flow of titanium from 12 M HCl with guaiacol/anisole at different flow rate ratios (1:1, 1:3, and 1:5 (aq:org)). Green: 50/50 (v/v) guaiacol/anisole, blue: 75/25 (v/v) guaiacol/anisole, and dark blue: 90/10 (v/v) guaiacol/anisole.

The effect of the residence time in the mixing tubing was analyzed with the optimal solvent system (guaiacol/anisole 90/10 (v/v)). The titanium extraction efficiency was 90.2 ± 0.7 % at all tested residence times ranging from 0.2 to 4.9 minutes. [8]

The extraction of scandium was also studied to ensure that an acceptable separation factor was obtained with this solvent system. The amount of scandium in the aqueous phase before and after the LLE was measured by ICP-OES and an average extraction of -1.1 ± 3.9 % was obtained. The negative value is expected to be due to the uncertainty when preparing the diluted samples for ICP-OES (section 13.1.3.12) or due to volume changes during the LLE, since a small decrease in the volume of the aqueous phase (5 %) and a small increase in the volume of the organic phase (6 %) were observed at a flow rate ratio of 1:3 (aq:org). Therefore, it was assumed that no measurable scandium extraction took place, but the separation factor could not be calculated.

5.3.4 LLE of ^{45}Ti with guaiacol/anisole

The LLE of ^{45}Ti in flow with guaiacol/anisole 90/10 (v/v) was tested, following the promising results with nonradioactive titanium. An extraction efficiency of 84.8 ± 2.4 % and still no scandium extraction could be measured. [8] Furthermore, it was studied if the extracted ^{45}Ti could be directly applied for the formation of a complex with two ligands: salan (a diamino bis(phenolato) ligand) and pyridine-2,6-dicarboxylic acid (dipic), which are described in section 10. The ^{45}Ti-complex, [^{45}Ti](salan)Ti(dipic), has previously been synthesized and applied as radiotracer. [65] The formation of [^{45}Ti](salan)Ti(dipic) was verified by radio-TLC and radio-HPLC

by comparing the retention factor (R_f) and retention time to the one for nonradioactive (salan)Ti(dipic) (Figure 22).

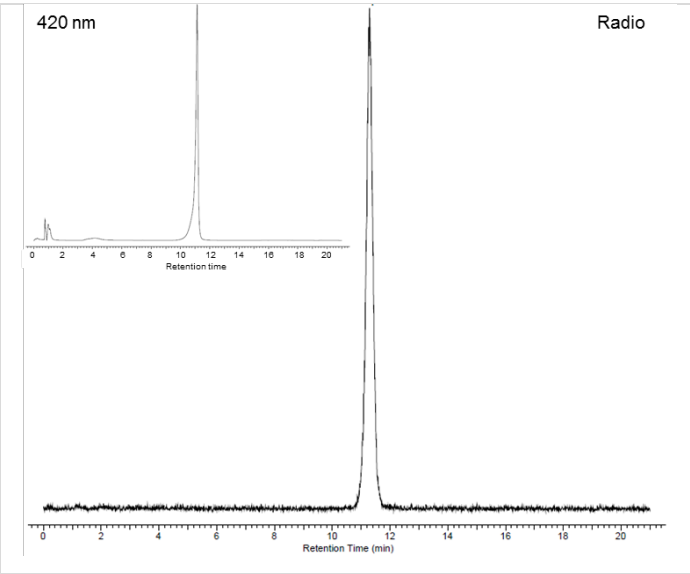

Retention time (min): 11.3 (radio) 11.2 (420 nm)

R_f–value: 0.49 (98.7 %)

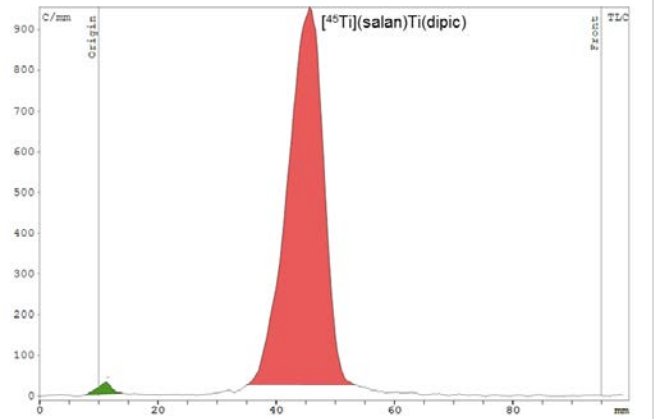

Figure 22: Left: Radio-signal for the HPLC chromatogram for [^{45}Ti](salan)Ti(dipic) formed after the LLE of ^{45}Ti. Top insert: UV-signal for the HPLC chromatogram for the reference material (salan)Ti(dipic). The retention times are listed next to the chromatograms. Right: The radio-TLC for [^{45}Ti](salan)Ti(dipic) where the R_f -value of the main peak (red) was 0.49, which corresponds to the value for the reference material (salan)Ti(dipic). The figure is modified from [8].

The LLE of ^{45}Ti and phase separation in flow was found to be efficient for the purification of ^{45}Ti from scandium. However, a relative large volume of high boiling point organic solvents was used for the LLE. It was expected that ^{45}Ti could be back-extracted (stripped) with an aqueous phase with a lower HCl concentration, but titanium can then form hydroxide species, which might not be suitable for the radiolabeling and formation of a radiotracer. Consequently, it might be necessary to perform the ^{45}Ti chelation in the organic solvent, as seen with salan and dipic, but subsequently the radiotracer needs to be isolated from the guaiacol/anisole mixture, which can be challenging. Finally, the use of organic solvents in the purification step necessitates an additional quality control analysis to ensure that the amount of residual solvents in the final radiotracer formulation of the radiotracer is below the limits specified by the European Pharmacopoeia monograph no. 50400. [88], [89]

6 LLE of ^{89}Zr

The encouraging results of the ^{45}Ti LLE in flow led to an interest in applying the method in the separation of other radiometals from their respective cyclotron target material. The first choice was ^{89}Zr, since the chemical properties of zirconium are similar to the properties of titanium. ^{89}Zr has a relative long half-life (78.4 hours) and is suitable for immuno-PET, due to the long circulation time of antibodies. Various antibodies have been labeled with ^{89}Zr and studied in clinical trials, but also antibody fragments and nanoparticles labeled with ^{89}Zr are investigated. [15] The production of ^{89}Zr and the separation from its cyclotron target material is described in the following sections.

6.1 Production of ^{89}Zr

As seen in Figure 23, ^{89}Zr can be produced on a cyclotron by the ^{89}Y(p,n)^{89}Zr nuclear reaction with the highest cross section at 12-14 MeV. ^{89}Y is the only natural abundant isotope of yttrium. This is advantageous in terms of decreased number of side nuclear reactions and price of the target material. However, at a proton energy >12 MeV competing nuclear reactions on ^{89}Y will start to produce some radionuclidic impurities. Most significant the co-production of zirconium-88 (^{88}Zr) ($T_{½}$ = 83 days) by the ^{89}Y(p,2n)^{88}Zr nuclear reaction at >13 MeV (Figure 23). Furthermore, yttrium-88 ($T_{½}$ = 106.6 days) can be produced by the ^{89}Y(p,pn)^{88}Y nuclear reaction at proton energy over 12 MeV. However, ^{88}Y can be chemically separated from ^{89}Zr together with the yttrium from the cyclotron target material. Instead of using yttrium foil, it is also possible to use pressed yttrium oxide powder targets [90] or a liquid target with $Y(NO_3)_3$ in solution [91], [92].

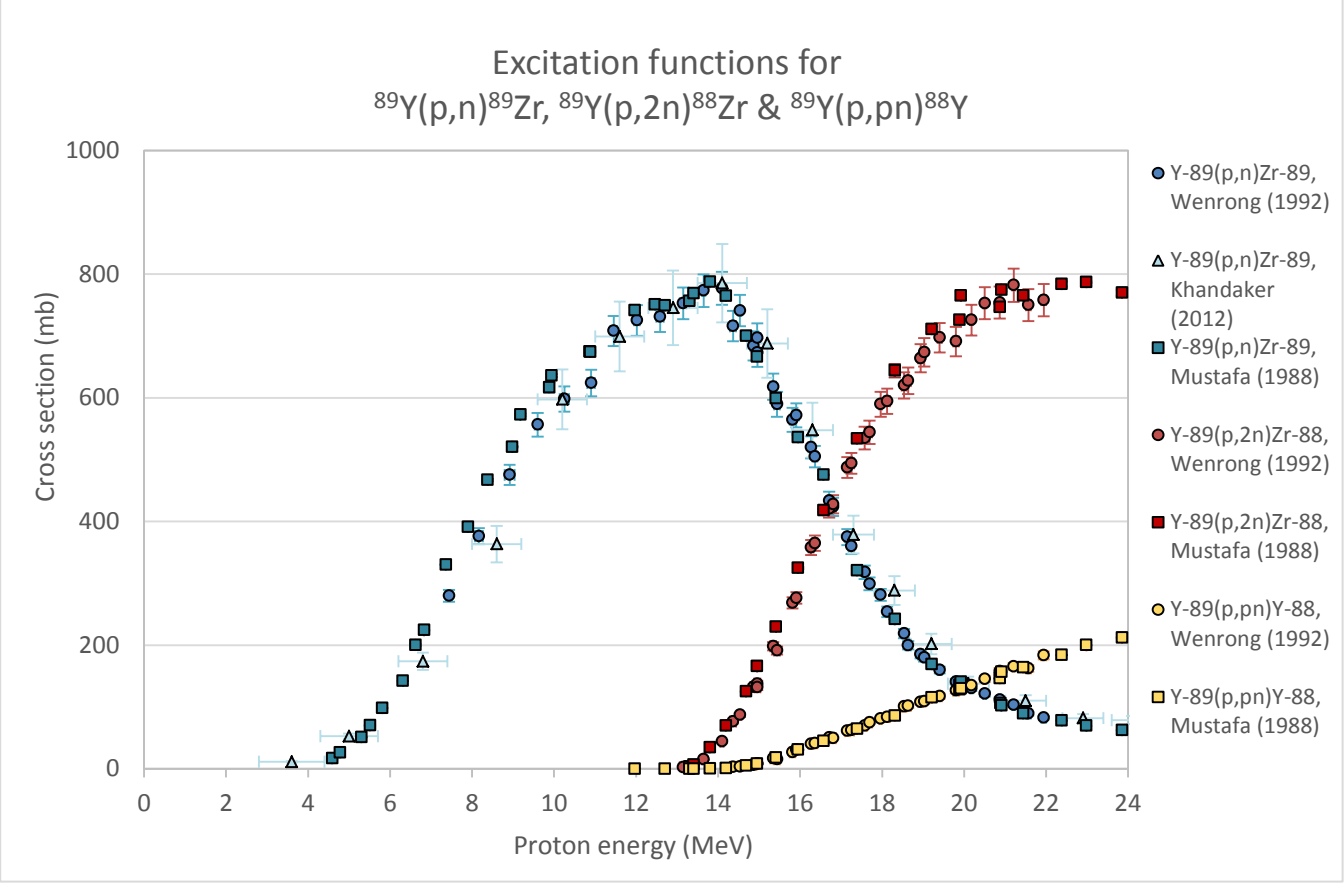

Figure 23: Excitation functions for the $^{89}Y(p,n)^{89}Zr$ (blue), $^{89}Y(p,2n)^{88}Zr$ (red), and $^{89}Y(p,pn)^{88}Y$ (yellow) nuclear reactions showing their energy dependent cross sections and the potential for co-production of radionuclide contaminations. The experimental cross section data is collected from the EXFOR database [73] and published by [93]–[95].

6.2 Chemical properties of zirconium

Zirconium is at physiological conditions present in the +4 oxidation state and is in the same group in the periodic table as titanium. Zr^{4+} is a hard metal (HSAB theory) due to the high charge density and relative small ionic radius. [15] Zirconium forms $Zr(OH)^{3+}$, $Zr(OH)_2^{2+}$, and $Zr(OH)_3^{+}$ species in aqueous media, and at low HCl concentration an outer-sphere of chloride ions is formed, e.g. $[Zr(OH)]^{3+}\cdot 3Cl^-$. Cation exchanger can be used to extract these species, but polymerization by formation of zirconium hydroxy-connected species has been observed at low HCl concentration (1-2 M), which challenges the extraction. The polymerization can be decreased at higher HCl concentration, where the hydroxide ions in the inner-sphere of the zirconium complex are replaced by chloride, as seen in equation (13), where i = 4, 5, or 6 and n = 1-4 or 6.

$$[Zr(OH)_n]^{(4-n)} + i\ Cl^- + n\ H^+ \rightleftharpoons [ZrCl_i]^{(4-i)} + n\ H_2O \qquad (13)$$

Thereby neutral or negatively charged species are formed, which can be extracted with neutral extractants or anion exchangers. [96]

6.3 Purification of ^{89}Zr

The differences in chemical properties between zirconium and yttrium have been utilized for the separation of ^{89}Zr from yttrium in cyclotron targets. Yttrium is in the same group in the periodic table as scandium and is most commonly present in the +3 oxidation state. [78] A common approach for the separation is by the use of hydroxamate resin. ^{89}Zr has a high affinity for the hydroxamate resin when loaded in 2 M HCl. Yttrium is removed by washing with dilute hydrochloric acid and water, while zirconium can be eluted with 1 M oxalic acid. The oxalic acid needs to be removed afterwards, since it is toxic, and thus not compatible with further *in vitro* and *in vivo* studies. This has been done using an quaternary methyl ammonium (QMA) strong anion exchange cartridge where ^{89}Zr was eluted in 1 M HCl. [97] Various commercially available extraction resins have also been applied for the separation of zirconium from yttrium. [98] The application of cation and anion exchange resins has likewise been investigated, but was found to be less efficient. Different extractants for the LLE of ^{89}Zr have also been applied. Di-(2-ethylhexyl)phosphoric acid (HDEHP) and triphenyl phosphine oxide (TPPO) have shown high extraction efficiencies of ^{89}Zr. [90] Additionally, LLE with anion exchange extractant, e.g. Aliquat 336, quaternary ammonium salts has shown high extraction efficiency of zirconium from 8-12 M HCl. [96] Furthermore, trioctylphosphine oxide (TOPO), which is a commonly used extractant for various metal ions, has shown high extraction efficiency of zirconium from aqueous HCl solution. [99]

6.3.1 LLE of zirconium with guaiacol/anisole

First, the LLE of zirconium from 12 M HCl, using guaiacol/anisole as organic phase, was attempted, due to the similarity between zirconium and titanium. The LLE was performed in flow using the optimized settings developed for the LLE of titanium (Table 6), where a diaphragm with a thickness of 2 mil and a PTFE/ PP membrane with a pore size of 0.2 µm were applied.

Table 6: The LLE in flow of zirconium from 0.01 M $ZrCl_4$ and 0.01 M YCl_3 in 12 M, 10 M, and 7 M HCl, respectively, with guaiacol/anisole 9/1 (v/v). The aqueous and organic flow rates, residence time in the mixing loop, and the separation performance are listed. A PTFE/PP membrane with a pore size of 0.2 µm and a diaphragm with a thickness of 2 mil were applied.

Aqueous phase	Organic phase	Aqueous flow rate (mL/min)	Organic flow rate (mL/min)	Residence time (min)	Separation performance
12 M HCl	Guaiacol/anisole 9/1 (v/v)	0.05	0.15	2.5	Complete phase separation
		0.25	0.75		
		0.033	0.167	2.5	

				10 1	
10 M HCl	Guaiacol/anisole 9/1 (v/v)	0.033	0.167	2.5	Complete phase separation
7 M HCl	Guaiacol/anisole 9/1 (v/v)	0.033	0.167	5.5	Complete phase separation

A guaiacol/anisole ratio of 9/1 (v/v) and a flow rate ratio of 1:3 (aq:org) was applied for the extraction of zirconium. The total flow rate of 0.2 mL/min and 1 mL/min were tested with the same residence time in the mixing loop (2.5 minutes).The extraction efficiency at both flow rates was above 60 % (Figure 24), however, it was notably lower than the extraction of titanium with the same setup. In an attempt to improve the extraction efficiency, a larger volumetric phase ratio (P) was applied by changing the flow rate ratio to 1:5 (aq:org). This improved the extraction of zirconium to 71 % (Figure 24).

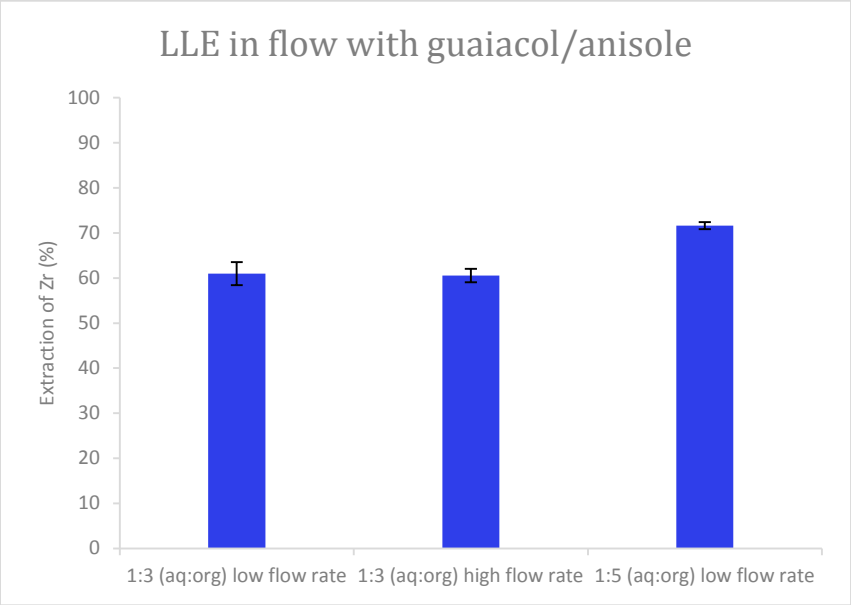

Figure 24: The LLE in flow of zirconium from 12 M HCl with guaiacol/anisole 9/1 (v/v) at different flow rate ratios (1:3 and 1:5 (aq:org)) and different total flow rates (low flow rate: 0.2 mL/min and high flow rate: 1 mL/min). The residence time in the mixing loop was 2.5 minutes.

It was not tested, if a higher volumetric phase ratio could improve the extraction of zirconium further, since a large volume of organic phase was already needed for the 1:5 (aq:org) ratio. A large difference in aqueous and organic flow rate might affect the separation over the membrane and lead to longer waiting time before steady state is reached. Instead, it was studied, if the residence time in the mixing loop and the concentration of HCl

affected the extraction efficiency. The extraction efficiency of zirconium from 10 M HCl using guaiacol/anisole 9/1 (v/v) was decreased to 18 ± 3.5 %; while no extraction of zirconium was observed when 7 M HCl was used as the aqueous phase. The LLE of zirconium in flow from 12 M HCl with guaiacol/anisole 9/1 (v/v) at a shorter (1 minute) and longer (12 minutes) residence time in the mixing loop was evaluated. The flow rate ratio of 1:5 (aq:org) was applied. The zirconium extraction efficiencies were 66.4 ± 0.7 % and 70.0 ± 1.8 %, respectively. A short residence time reduced the extraction efficiency, but a longer residence time did not improve the extraction compared to the extraction with a residence time of 2.5 minutes (Figure 24). The LLE of zirconium using guaiacol/anisole was not optimized further.

The extraction of yttrium was measured to ensure that zirconium was selectively extracted with guaiacol/anisole. The calculated extraction efficiency of yttrium was -10.5 ± 1.3 % for the 1:5 (aq:org) flow rate ratio. A negative value was obtained, which meant that a higher concentration of yttrium in the aqueous phase was measured after the LLE, than in the aqueous phase before the LLE. It was not expected that yttrium was present in guaiacol/anisole or in the tubing and membrane separator, which could have been dissolved or extracted to the aqueous phase during the LLE. Therefore, it was assumed that the negative value could be due to the uncertainty when preparing the diluted samples for ICP-OES. Another possibility was that the volume of the aqueous phase before and after the LLE might have been reduced during the LLE, if some of the aqueous phase had migrated to the organic phase. This would lead to a higher concentration of yttrium and zirconium in the aqueous phase after the LLE. The volume of the organic and aqueous phase after the LLE was measured during the LLE of titanium with guaiacol/anisole 9/1 (v/v) with a flow rate ratio of 1:3 (aq:org) (section 5.3.3). Here, a small decrease in the volume of the aqueous phase, while the volume of the organic phase was slightly increased after the LLE. The reduction of the volume of aqueous phase might be larger when a flow rate ratio of 1:5 (aq:org) was applied for the zirconium and yttrium, since a larger ratio of organic phase was used, which potentially could dissolve more of the aqueous phase, but this was not tested. Thus, it could be presumed that no measurable yttrium extraction took place, but that a correction for potential volume changes by measuring the volume of aqueous phase after the LLE needed to be performed.

6.3.2 LLE of zirconium with trioctylphosphine oxide

As described in the previous section, the LLE in flow of zirconium with guaiacol/anisole was possible; however, the extraction efficiency was modest even after the attempted optimizations. In order to improve the extraction efficiency further, a different extraction system was applied. As mentioned in section 6.3, TOPO (Figure 25) has been used as an extractant for the LLE of zirconium from aqueous HCl with high efficiency. [99] Thus, the LLE of zirconium with TOPO as extractant was studied.

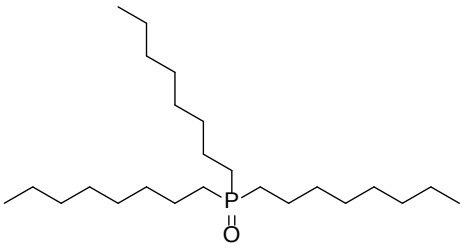

TOPO

Figure 25: Chemical structure of TOPO.

The extraction from 12 M HCl with 0.1 M TOPO in heptane led to a formation of three phases (Table 7). A light and a heavy organic phase were seen, which at first appeared to be breakthrough of the organic phase, but in the batch LLE, the three phases could be seen. The formation of a third phase has been observed in some cases when the concentration of the extracted metal ion exceeds a certain value in the organic phase, or if the HCl concentration is above a critical value. The diluent, in which the extractant was dissolved, additionally affected the formation of a third phase. [100]

Table 7: The LLE in flow of zirconium from 12 M or 6 M HCl with 0.1 M TOPO in heptane as extractant. The aqueous and organic phase, flow rates, and separation performance are shown. A PTFE/PP membrane with a 0.2 µm pore size and a 2 mil thick diaphragm were used.

Aqueous phase	Organic phase	Aqueous flow rate (mL/min)	Organic flow rate (mL/min)	Separation performance
0.01 M $ZrCl_4$ and YCl_3 12 M HCl	0.1 M TOPO in heptane	0.05	0.15	Formation of a third phase
0.001 M $ZrCl_4$ and YCl_3 6 M HCl	0.1 M TOPO in heptane	0.0.5	0.15	Complete phase separation
		0.033	0.167	

The extraction efficiency of zirconium with guaiacol/anisole 9/1 (v/v) was decreased when a lower concentration of HCl was in the aqueous phase. Thus, first the concentrations of zirconium and yttrium were decreased to evaluate, if the formation of a third phase was due to a high concentration of $ZrCl_4$ and YCl_3. The concentration was decreased to 0.0005 M; however, a third phase was still formed. Then, the HCl concentration of the aqueous phase was decreased to 10 M, 8 M, and 6 M. Three phases were formed when 10 M and 8 M HCl were used, but only two phases were seen when the concentration was 6 M HCl (Table 7). Compared to 6 M HCl, the extraction efficiency of zirconium was notably higher for the 10 M and 8 M HCl (Figure 26). The extraction efficiency of

yttrium with TOPO in heptane from 6 M HCl was -1.9 ± 2.8 %. This negative value was, as previously described, assumed to be due to the preparation of the ICP-OES samples or if the volume of the aqueous phase before and after the LLE was not constant. However, this tendency was not further studied.

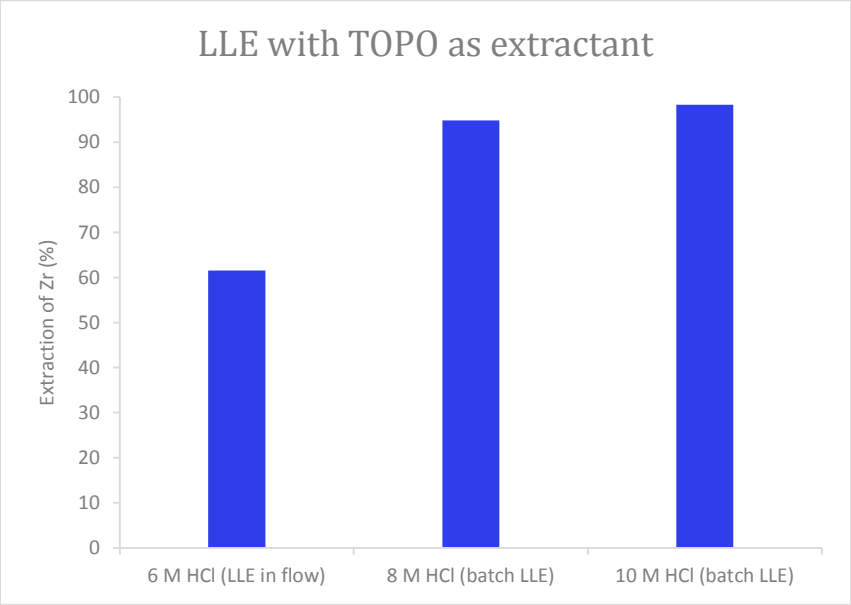

Figure 26: The LLE of zirconium with 0.1 M TOPO in heptane from 6 M HCl in flow (1:5 (aq:org)), from 8 M HCl in batch and from 10 M HCl in batch.

The extraction efficiency of zirconium using TOPO as extractant from 6 M HCl was not found to be higher than the extraction efficiency obtained with guaiacol/anisole 9/1 (v/v) and it was therefore not attempted to optimize the LLE with TOPO further. The effect of the diluent (only heptane was used for these zirconium experiments) was not studied, but it might be possible to prevent the formation of a third phase at high HCl concentration, if another diluent was used, which then could improve the extraction efficiency. Some studies have shown that aromatic diluents, e.g. toluene, have less tendency to form a third phase. [96], [100] Thus, the exchange of heptane with toluene might make it possible to prevent the formation of a third phase. Furthermore, the effect of temperature could be evaluated, since the work by T. Sato showed an increased extraction efficiency of zirconium with TOPO at elevated temperatures (50 °C). [99]

6.3.3 LLE of ^{89}Zr with guaiacol/anisole

The most suitable conditions tested for the LLE of zirconium was from 12 M HCl with guaiacol/anisole 9/1 (v/v) with a flow rate ratio of 1:5 (aq:org). These conditions were applied for the extraction of ^{89}Zr from 12 M HCl containing dissolved yttrium foil (Figure 27). The extraction of ^{89}Zr was higher than the extraction of nonradioactive zirconium, when a low total flow rate (0.2 mL/min) and long residence time (2.5 minutes) was

applied. The conditions for the extraction of the nonradioactive zirconium and ^{89}Zr were the same, although a significant lower concentration of ^{89}Zr was present. It was not expected that the extraction efficiency would have been higher for ^{89}Zr, since the opposite, a higher extraction efficiency of the nonradioactive titanium compared to ^{45}Ti, was observed, as described in section 5.3.3. The extractions efficiencies of zirconium and ^{89}Zr were calculated from two different analysis methods; ICP-OES and by measuring the activity in both phases after the LLE with a dose calibrator. With ICP-OES the concentration of zirconium and yttrium were measured and the extraction efficiency was calculated under the assumption that the volume of the two phases before and after the LLE was the same, which might not be correct. Furthermore, the LLE in flow of ^{89}Zr under these conditions was only tested once, therefore, the LLE at the same conditions needed to be repeated to ensure that the same extraction efficiency can be obtained. The LLE in flow of ^{89}Zr at high flow rate (1 mL/min) with a short residence time in the mixing loop (0.2 minutes) was also tested. Unfortunately, these conditions led to a less efficient ^{89}Zr extraction (around 50 %). This indicated that a relatively long residence time was needed to obtain a high extraction efficiency, which was also observed for the LLE of nonradioactive zirconium.

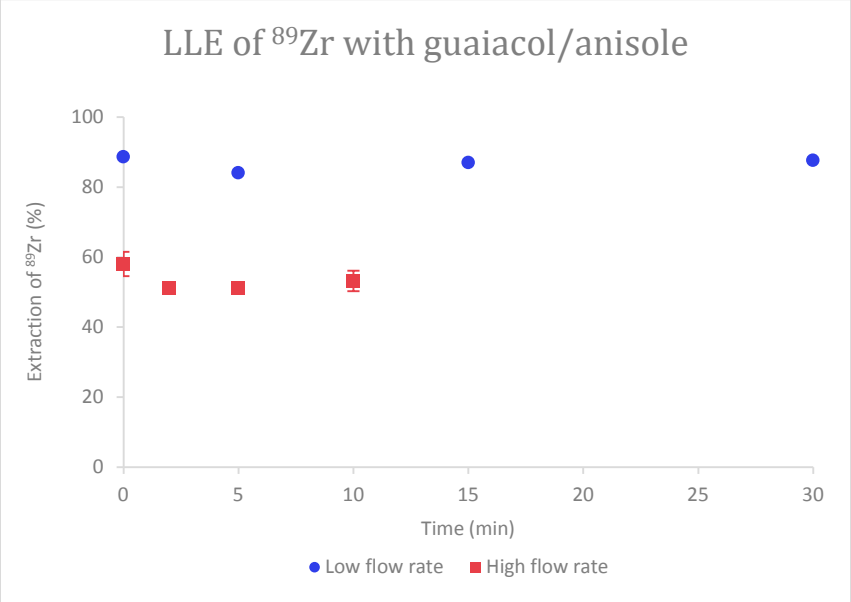

Figure 27: The LLE of ^{89}Zr in flow from 12 M HCl containing dissolved yttrium foil with guaiacol/anisole. A flow rate ratio of 1:5 (aq:org) was applied. A total flow rate of 0.2 mL/min and a residence time of 2.5 minutes (blue) and a total flow rate of 1 mL/min and a residence time of 0.2 minutes (red) were tested.

The LLE of ^{89}Zr needed to be studied further and optimized in order to evaluate if an efficient and reliable extraction of ^{89}Zr can be obtained with the LLE in flow technique. Furthermore, the back-extraction of ^{89}Zr and the labeling with the extracted ^{89}Zr should also be evaluated to assess the usability of the technique in the production of ^{89}Zr-labeled radiotracers.

7 LLE of ^{64}Cu

The membrane-based separation technique was applied for the LLE in flow of the two radiometals, titanium and zirconium, with similar chemical properties, showing promising results. It was therefore of interest, if the LLE in flow could be adapted to a radiometal, which was produced more routinely at our site, the Hevesy Laboratory. Thus, the LLE in flow was applied for the separation of ^{64}Cu from its cyclotron target material nickel-64 (^{64}Ni). ^{64}Cu has an intermediate half-life of 12.7 hours and is a promising PET radiometal despite its relative low β^+ branching ratio of 18 %. ^{64}Cu chelated by ATSM has been applied for the imaging of hypoxic tumors, where the Cu^{2+} ion in the ^{64}Cu-ATSM complex is reduced to Cu^+ in the reducing environment of hypoxic tumors, and thereby dissociated and trapped. [50]

7.1 Production of ^{64}Cu

^{64}Cu can be produced on the cyclotron from enriched ^{64}Ni by the ^{64}Ni(p,n)^{64}Cu nuclear reaction, which has the highest cross section at 9-12 MeV (Figure 28). In the same energy range, cobalt-61 (^{61}Co) ($T_{½}$ = 1.65 h) is co-produced on the ^{64}Ni by the ^{64}Ni(p,α)^{61}Co nuclear reaction. However, the ^{61}Co can be chemically separated from the ^{64}Cu after production. [101] The natural abundance of ^{64}Ni is low leading to high prices and thereby a need for reusing the ^{64}Ni target material. For the target preparation, the ^{64}Ni is electroplated onto a backing material, e.g. a Ag disc. The area of the plated ^{64}Ni is typically around 0.5 cm^2 and approximately 100 mg/cm^2 of ^{64}Ni has been used for thick targets. [44]

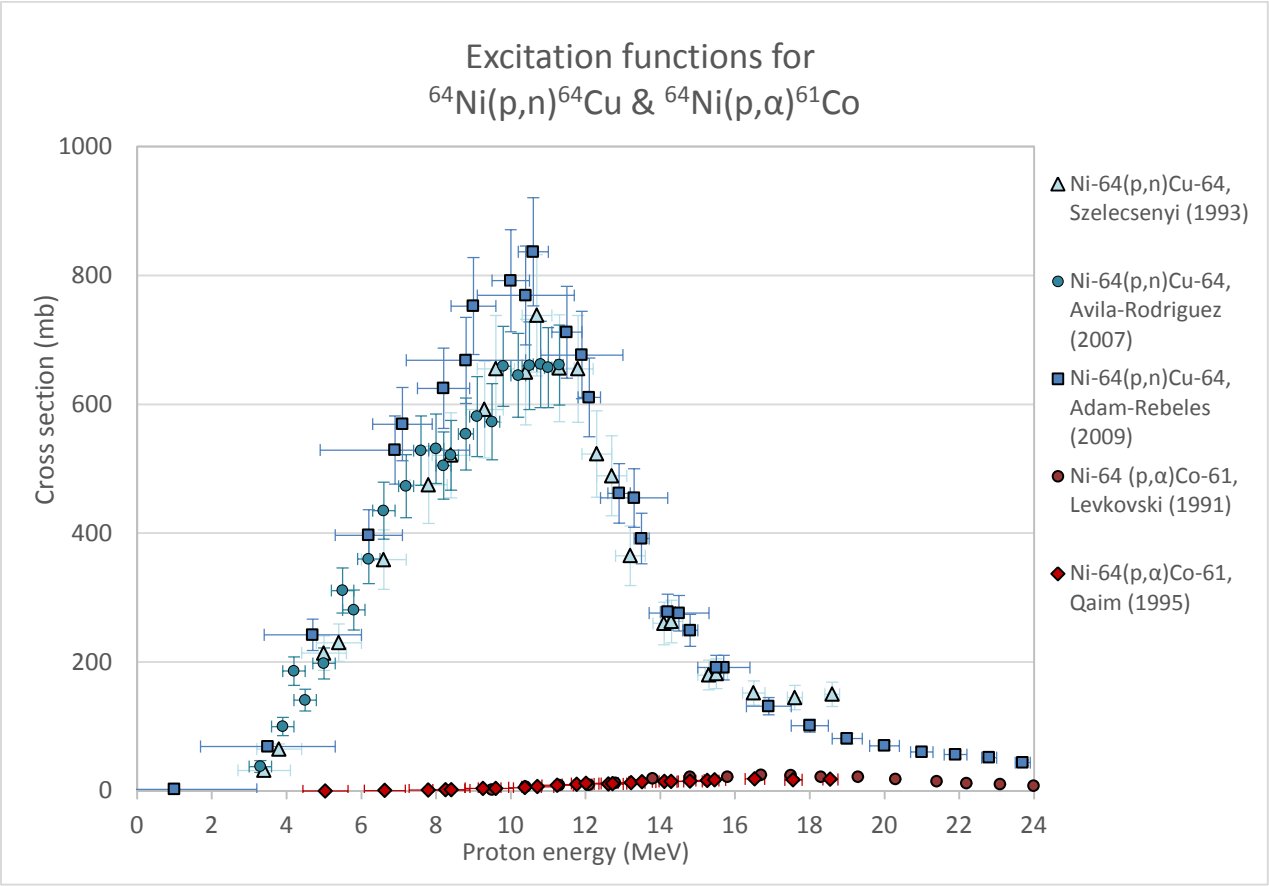

Figure 28: Excitation functions for the $^{64}Ni(p,n)^{64}Cu$ (blue) and $^{64}Ni(p,\alpha)^{61}Co$ (red) nuclear reactions showing their energy dependent cross sections and the potential for co-production of radionuclide contaminations. The experimental cross section data is collected from the EXFOR database [73] and published by [74], [101]–[104].

7.2 Chemical properties of copper

Cu^{2+} is a borderline hard/soft metal and favors borderline ligand donors, such as aliphatic and aromatic amines, but can also form complexes with harder or softer donors. [15] The different chemical properties of copper and nickel, and especially the tendency of copper to form negatively charged chloro-complexes have been utilized in the separation of the two elements. Cu^{2+} forms negatively charged cupric chloro-complexes, such as $CuCl_3^-$ and $CuCl_4^{2-}$, at increasing HCl concentration, as seen in Figure 29. [105] Nickel on the other hand is mostly present as Ni^{2+} or $NiCl^+$. [106] This difference makes anion exchange a suitable separation technique. As described in the previous section, the separation of ^{64}Cu from the co-produced ^{61}Co also needs to be considered. Cobalt likewise forms negatively charged anionic chloro-complexes in HCl, however, a higher HCl concentration is required in order to form $CoCl_3^-$ and $CoCl_4^{-2}$ [107], compared to $CuCl_3^-$ and $CuCl_4^{-2}$. This makes it possible to

separate these two elements by choosing an HCl concentration, where only the copper forms negatively charged chloro-complexes and not cobalt.

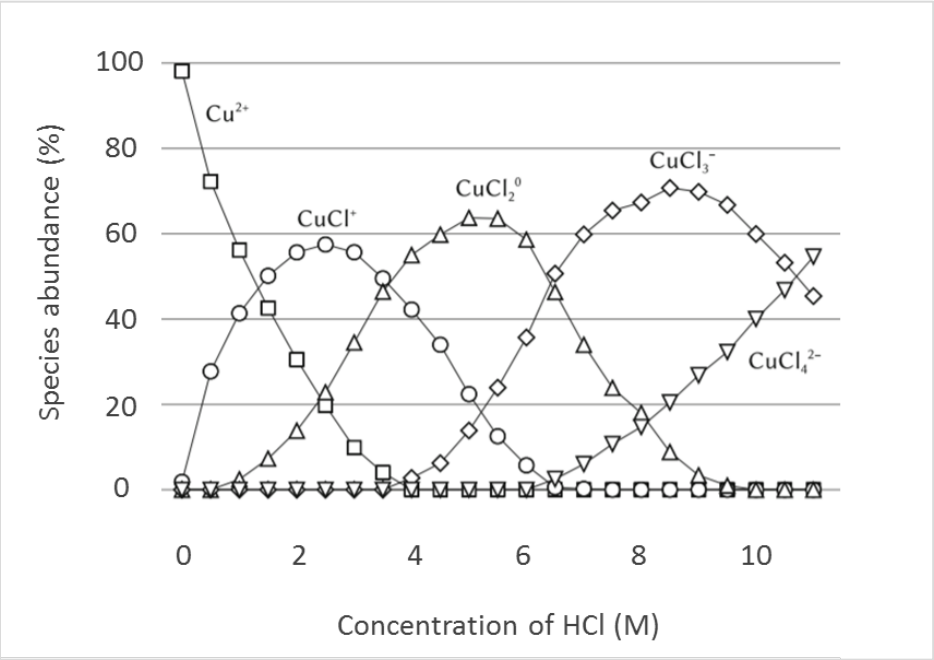

Figure 29: The species abundance of different copper(II) species (Cu^{2+}, $CuCl^{+}$, $CuCl_2$, $CuCl_3^{-}$, and $CuCl_4^{2-}$) from 0-12 M HCl. The figure was modified from [105].

7.3 Purification of ^{64}Cu

A common method to separate ^{64}Cu from cobalt and nickel is by anion exchange chromatography using AG 1-X8 resin. [101] Here, ^{64}Ni is eluted in 6 M HCl and can be reused for future use, ^{61}Co can be eluted in 5 M HCl, and ^{64}Cu is eluted in 1 or 0.1 M HCl. [44] LLE of copper has also been achieved with high extraction efficiency. Cyanex 923, which contains four trialkyl phosphine oxides including TOPO, has been applied for the extraction of copper from aqueous acid solutions. The highest extraction was obtained from 6 M HCl, where the neutral $CuCl_2$ species dominates the speciation diagram (Figure 29). [108], [109] It was seen from the LLE of zirconium with TOPO in section 6.3.2 that a complete phase separation between 6 M HCl and 0.1 M TOPO in heptane could be achieved. Therefore, this solvent system could be suitable for the LLE in flow of ^{64}Cu.

7.3.1 LLE of copper with trioctylphosphine oxide

The LLE of copper was performed with TOPO as extractant. The concentration of TOPO was varied and different diluents were tested to obtain a high extraction efficiency of copper from an aqueous phase also containing nickel (Table 8).

Table 8: The LLE in flow of copper with TOPO in toluene, hexane or heptane was performed with a PTFE/PP membrane with a pore size of 0.2 µm and a diaphragm with a thickness of 2 mil. The aqueous and organic phase, flow rates, and separation performance of the LLEs in flow of copper with TOPO are listed.

Aqueous phase	Organic phase	Aqueous flow rate (mL/min)	Organic flow rate (mL/min)	Separation performance
0.001 M $CuCl_2$ and $NiCl_2$ in 6 M HCl	0.4 M TOPO in toluene	0.1	0.1	Complete phase separation
		0.05	0.15	
		0.033	0.167	
0.001 M $CuCl_2$ and $NiCl_2$ in 6 M HCl	0.4 M TOPO in hexane	0.05	0.15	Complete phase separation
0.001 M $CuCl_2$ and $NiCl_2$ in 6 M HCl	0.1 M TOPO in hexane	0.05	0.15	Complete phase separation
60 ppm Cu, Ni, Co, Zn, Fe, and Ag in 6 M HCl	0.1 M TOPO in heptane	0.05	0.15	Complete phase separation
		0.25	0.75	

First, three different flow rate ratios (1:1, 1:3; and 1:5 (aq:org)) were tested with 0.4 M TOPO in toluene (Figure 30). It was seen that the extraction efficiency of copper increased when going from 1:1 to 1:3 (aq:org) flow rate ratio, while no increase was observed when increasing the volumetric phase ratio (P) further. The extraction of nickel was measured by ICP-OES. The extraction efficiency was -3.8 ± 2.9 % and it was therefore assumed that copper was extracted selective by TOPO in the presence of nickel.

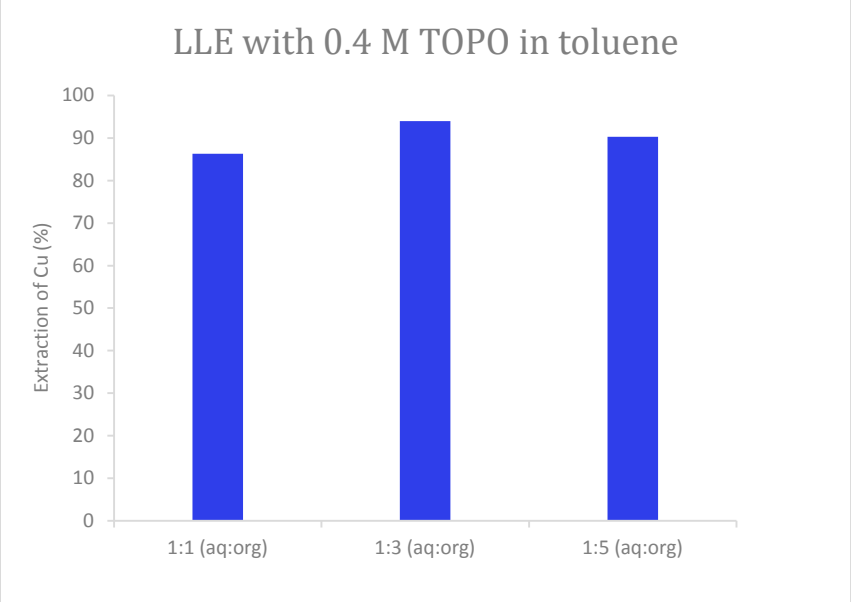

Figure 30: The extraction efficiencies from the LLE in flow of copper from 6 M HCl with 0.4 M TOPO in toluene. A flow rate ratio of 1:1, 1:3, and 1:5 (aq:org) were tested all with a total flow rate of 0.2 mL/min.

The concentration of TOPO in the organic phase was varied and different diluents were tested to find the minimum TOPO concentration to achieve high extraction efficiency, and thereby the most suitable diluent (Figure 31). The flow rate ratio for LLE in flow and the ratio between the volume of aqueous and organic phase for LLE in batch mode was 1:3 for all experiments shown in Figure 31. The diluent was then changed from toluene to hexane, still with a TOPO concentration of 0.4 M. The extraction efficiency of copper increased slightly when hexane was used as diluent. On the other hand, the extraction efficiency was reduced when the TOPO concentration was decreased to 0.1 M. However, over 90 % of copper was still extracted. There was no notable difference between hexane and heptane as diluent, and the LLE in flow and in batch mode performed equally well. The copper extraction efficiencies were 74 % and 26 % when the TOPO concentration was decreased further (0.05 and 0.01 M). Thus, it was found that the optimal conditions for the LLE of copper was 0.1 M TOPO in hexane or heptane with a flow rate ratio of 1:3 (aq:org). The nickel extraction efficiency at these conditions was -2.2 ± 0.7 % according to the ICP-OES analysis.

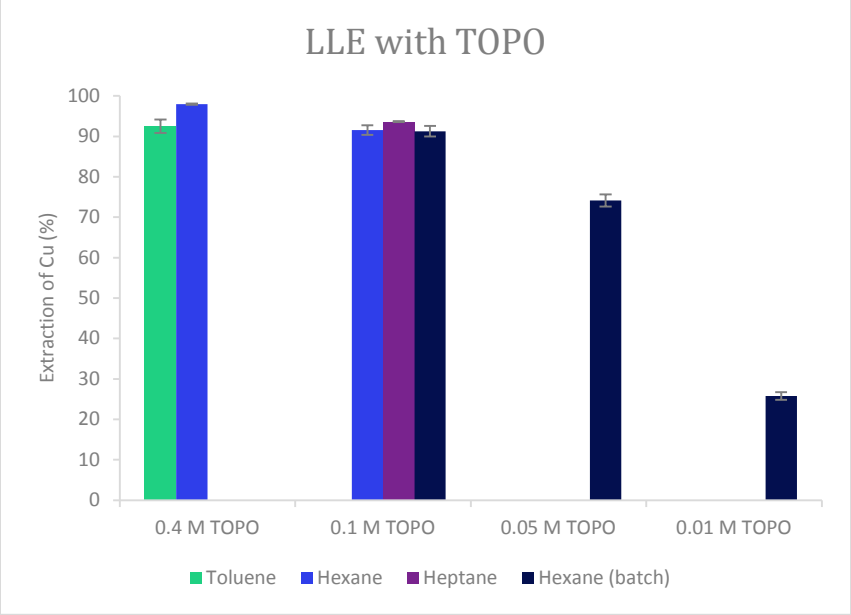

Figure 31: The LLE in flow and in batch mode of copper from 6 M HCl also containing nickel. The flow rate ratio in flow and volume ratio in batch mode were 1:3 (aq:org). The extraction efficiencies of copper with 0.4 M TOPO in toluene (green), 0.4 M or 0.1 M TOPO in hexane (blue), 0.1 M TOPO in heptane (purple), and 0.1 M, 0.05 M, and 0.01 M TOPO in hexane in batch mode (dark blue). The error bars represent the standard deviation of 2-5 samples measured with ICP-OES.

7.3.2 LLE of copper with ATSM

It was possible to extract copper with TOPO with high extraction efficiency (90 %) without extracting nickel. After the LLE, copper was expected to be coordinated to TOPO in the organic phase. However, the copper would need to be in a form, which could be suitable for the labeling of a potential radiopharmaceutical. One way would be to back-extract copper from the organic phase, using an aqueous phase with a lower HCl concentration (stripping). [109] Another approach would be to test, if it was possible to back-extract the copper to an aqueous phase containing a chelator or an unlabeled radiotracer. This approach could potentially facilitate a fast and simple labeling procedure. In section 2.4.1.1, the radiotracer ^{64}Cu-ATSM was described. The labeling of ATSM with ^{64}Cu can be performed at room temperature within short time at pH 5-6. [110] Thus, it was attempted to dissolve ATSM in sodium acetate buffer (pH 4.9) for the back-extraction and chelation of copper. However, the water solubility of ATSM was found to be relatively low, and ATSM was instead dissolved in dimethyl sulfoxide (DMSO). Fortunately, it was possible to separate DMSO and hexane with the membrane separator using the same setup as for the LLE of copper from 6 M HCl applying 0.1 M TOPO in hexane with the combination of a 0.2 µm pore sized PTFE/PP membrane and a 2 mil thick diaphragm (section 13.1.3.25). After the LLE, the organic phase after the LLE was collected and used for a second LLE, where 0.5 mM ATSM in DMSO was used as the other phase, and a flow rate ratio of 1:3 (hexane:DMSO) was applied for both LLE runs.

It was in our interest to evaluate whether Cu-ATSM was formed, which was not possible to determine with ICP-OES. The Cu-ATSM has previously been analyzed by UV-vis spectroscopy [111] and a calibration curve with Cu-ATSM was made, in order to quantify the concentration of Cu-ATSM in the DMSO phase after the second LLE. The DMSO phase after the second LLE was analyzed by UV-vis spectroscopy; however, as seen in Figure 32, the absorption spectrum was not consistent with the spectrum for Cu-ATSM. Additionally, the UV-vis absorption spectrum did not correspond to the spectrum for ATSM without copper. It was not expected that the absorption would be affected by TOPO in the hexane phase, due to the low solubility of TOPO in DMSO. However, it was suspected that HCl was released by the formation of Cu-ATSM, which might affect the absorption spectrum, although the addition of a base (KOH) to neutralize the HCl did not lead to the same absorption spectrum as for the Cu-ATSM reference material. Thus, it was not possible by UV-vis spectroscopy to verify, if or to which extent Cu-ATSM was formed during the second LLE. Another potential quantification method when performing the LLE with ^{64}Cu could be to develop an HPLC method. The amount of ^{64}Cu extracted to the DMSO phase could be measured with a dose calibrator and radio-HPLC could be used to evaluate, if ^{64}Cu-ATSM was formed by comparing the retention time with the nonradioactive Cu-ATSM reference. This, however, was not evaluated in this PhD study.

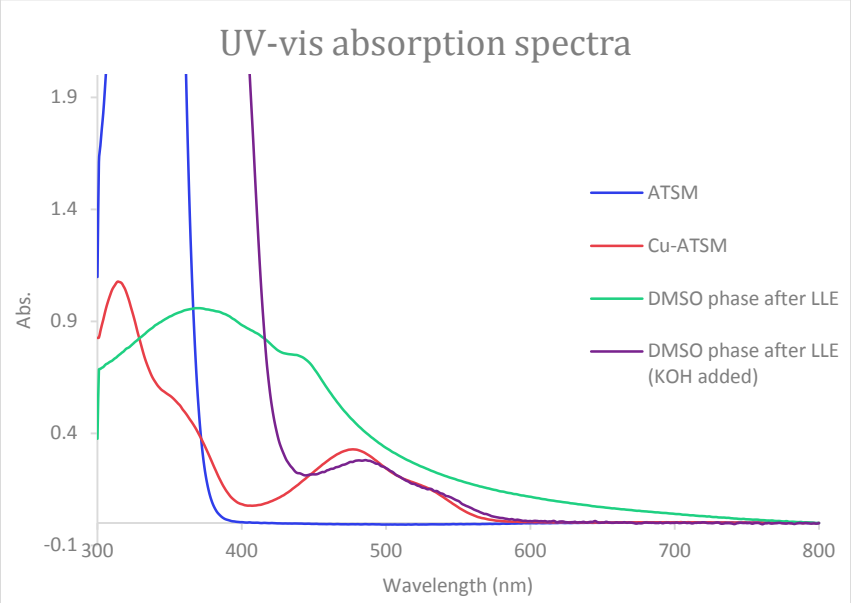

Figure 32: The UV-vis absorption spectrum for 0.5 mM ATSM (blue) and 0.05 mM Cu-ATSM in DMSO (red), the DMSO phase after the second LLE (green), and the DMSO phase after the second LLE where 0.1 M KOH was added (purple).

7.3.3 LLE of copper with DOTA

It was instead evaluated if the copper extracted to the hexane phase in the first LLE could be back extracted to an aqueous phase containing DOTA, which has been used as chelator for copper, as mentioned in section 2.4.1.1. DOTA is more water soluble than ATSM and it was possible to obtain a relative high concentration of DOTA (1.0 mM) in the aqueous phase used for the second LLE run. The second LLE was performed in batch mode with different concentrations of DOTA, including 0.1, 0.3, and 1 mM in the aqueous phase (Figure 33). The aqueous phase after the second LLE was analyzed by ICP-OES to quantify the amount of extracted copper. The extraction efficiency of copper increased up to 72 % with the higher DOTA concentration (1.0 mM DOTA) which corresponds to a 10 times higher concentration of DOTA than the concentration of copper. This concentration of DOTA was used for the further studies. The second LLE was performed in flow both at room temperature and at 55 °C by heating the mixing loop. It was expected that the chelation of copper by DOTA would be more efficient at higher temperature, but no difference between the extraction efficiency of copper at room temperature and at higher temperature was observed (Figure 33). It could not be verified by ICP-OES, if Cu-DOTA was formed, since the total copper concentration was measured with this analysis method. The formation of ^{64}Cu-DOTA might instead be possible to quantify with radio-TLC/HPLC, but it was not studied further.

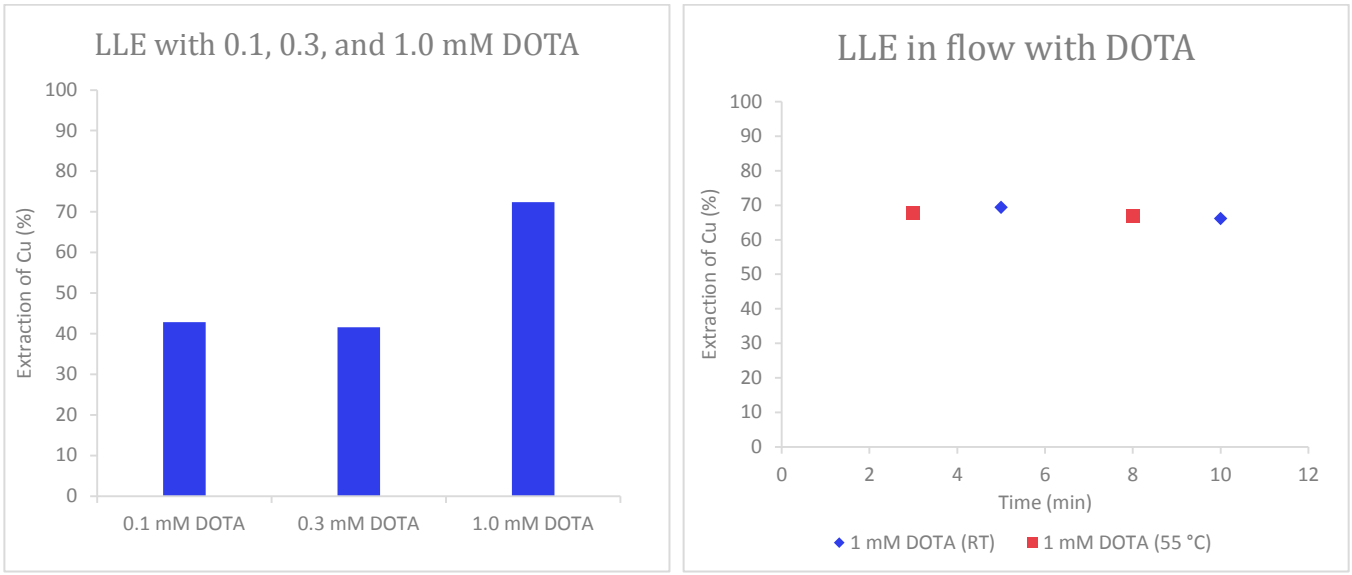

Figure 33: Left: The extraction efficiency of copper by a second LLE with 0.1, 0.3, and 1.0 mM DOTA in water and the organic phase from the first LLE with 0.1 M TOPO in hexane. A volumetric ratio of 3:1 (aq:org) was used for the LLEs. Right: The extraction efficiency of copper from the second LLE in flow with 1.0 mM DOTA in water at room temperature (blue) and at 55 °C (red). A flow rate ratio of 3:1 (aq:org) and total flow rate of 0.6 mL/min were applied.

7.3.4 LLE of ^{64}Cu with trioctylphosphine oxide

The LLE of ^{64}Cu was performed from 6 M HCl with 0.1 M TOPO in heptane. A flow rate ratio of 1:3 (aq:org) was applied and the extraction efficiency both at low (0.2 mL/min) and high (1 mL/min) total flow rates was tested. The residence time in the mixing loop was 2.5 minutes for the LLE with low total flow rate and 0.2 minutes for the LLE with high total flow rate. The extraction efficiencies were calculated by measuring the activity of ^{64}Cu in samples of the aqueous and organic phase after the LLE using a dose calibrator. The extraction efficiencies over time are shown in Figure 34. The extraction efficiency of ^{64}Cu at the high total flow rate was similar to the one observed for the LLE of nonradioactive copper, while the extraction of ^{64}Cu was decreased at the low total flow rate. Each test of the ^{64}Cu LLE in flow of was only performed once, so further experiments would need to be conducted to support the observations seen.

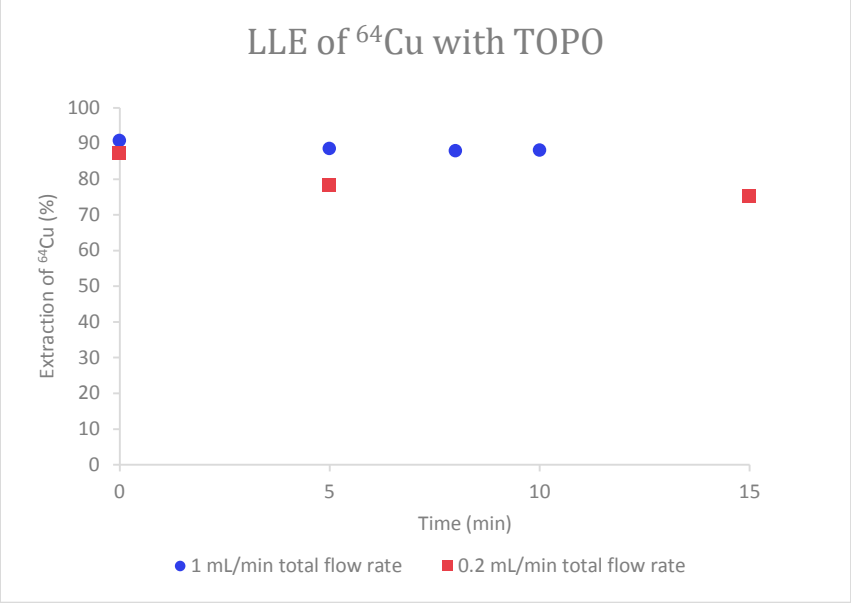

Figure 34: The extraction efficiency of ^{64}Cu over time from the LLE in flow from 6 M HCl with 0.1 M TOPO in heptane. A total flow rate of 1 mL/min and a residence time in the mixing loop of 0.2 minutes (blue circles) and a total flow rate of 0.2 mL/min and residence time of 2.5 minutes in the mixing loop (red squares) were tested.

The results from the extraction of ^{64}Cu were promising. However, it is known from the literature that TOPO can co-extract various metal ions [109] and additionally that different metal impurities are present from the production of ^{64}Cu. Common metal impurities are Ag, Fe, and Zn. [44] Furthermore, the co-produced ^{61}Co needs to be separated from ^{64}Cu. Thus, it was tested if TOPO extracted copper selectively in the presence of cobalt, iron, zinc, and silver. In Figure 35, the extraction efficiencies of each metal from 6 M HCl with 0.1 M TOPO in heptane can be seen. Cobalt, iron, and zinc were extracted with high extraction efficiencies, as observed for copper, and additionally 40 % of silver was extracted to the organic phase. Thus, it was not possible to separate

copper from cobalt, silver, iron, and zinc with TOPO as extractant under the applied conditions. The LLE was only performed with a 6 M HCl solution as aqueous phase, while the back-extraction (stripping) of copper with different HCl solutions was not studied. It might be possible to separate copper from the other metal ions, if copper can be selectively extracted or stripped at other HCl concentrations. The extraction efficiencies of various metal ions, including Cu(II), Fe(III), Co(II), and Zn(II), with cyanex 923 containing TOPO at different HCl concentrations have been studied by Gupta et al. In their study, it was observed that zinc was quantitatively extracted by cyanex 923 from 1-10 M HCl, while only around 5 % of copper was extracted at 1 M HCl. Thus, it might be possible to strip copper with 1 M HCl without stripping zinc. However, over 60 % of iron and no cobalt were extracted at 1 M HCl, which would probably result in 40 % of iron and all cobalt being stripped in 1 M HCl. [109] It might instead by possible to use a more selective extractant. This, however, was not explored further in this PhD study.

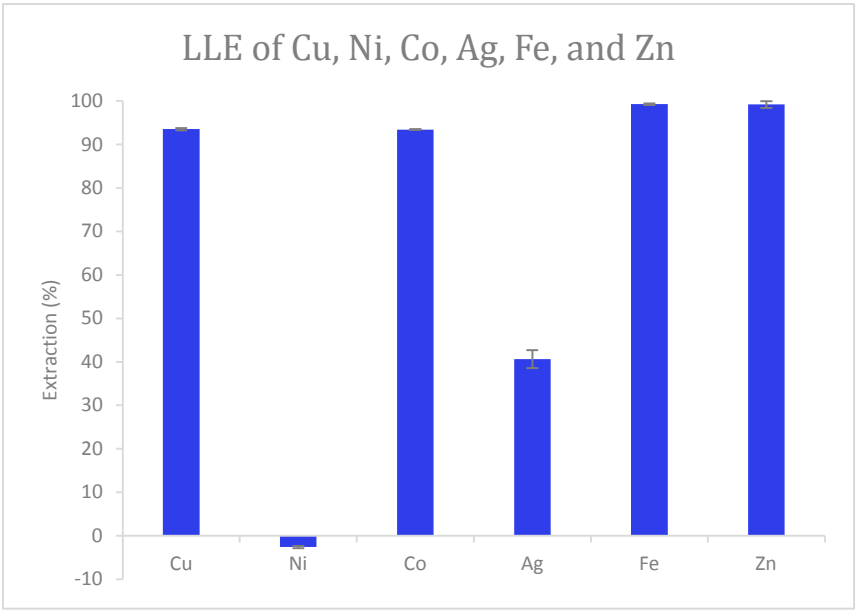

Figure 35: The extraction efficiencies from the LLE in flow of copper, nickel, cobalt, silver, iron, and zinc from 6 M HCl with 0.1 M TOPO in heptane. The error bars show the standard deviation of three samples analyzed by ICP-OES.

8 LLE of ^{68}Ga

^{68}Ga has a short half-life ($T_{½}$ = 68 min) and is therefore suitable for labeling peptides, antibody fragments, and small molecules, as described in section 2. ^{68}Ga is a commonly used PET radiometal and applied in one of the most studied PSMA tracers; ^{68}Ga-PSMA-11. Besides the application of ^{68}Ga in the diagnosis of prostate cancer, ^{68}Ga is also used for the imaging of neuroendocrine tumors by targeting the somatostatin receptors. [3] The LLE and phase separation in flow was applied to the extraction and separation of gallium from zinc. This study on the LLE of gallium from zinc led to a publication (*Separation of radiogallium from zinc using membrane-based liquid-liquid extraction in flow: experimental and COSMO-RS studies* [9]), which can be found in appendix B. In the paper, a COSMO-RS study has been conducted; however it is not included in this PhD thesis, since it was performed by Fedor Zhuravlev. The experimental LLE results are instead presented and interpreted in this chapter without a simulation study.

8.1 Production of ^{68}Ga

^{68}Ga can be obtained from a ^{68}Ge/^{68}Ga generator, where germanium-68 (^{68}Ge) is produced in a cyclotron by the ^{69}Ga(p,2n)^{68}Ge nuclear reaction and loaded on a resin. The half-life of ^{68}Ge is 271 days and decays to ^{68}Ga, making it possible to elute ^{68}Ga regularly. [3] The interest in cyclotron production of ^{68}Ga by the ^{68}Zn(p,n)^{68}Ga nuclear reaction has increased in recent years. This can most likely be explained by the supply limitation and price increase of the Good Manufacturing Practice (GMP) ^{68}Ge/^{68}Ga-generators. [45] A ^{68}Ge/^{68}Ga generator can be used for approximately 450 elutions or 12 months, whichever comes first. [112], [113] Furthermore, in some countries it is only allowed to obtain one patient dose per elution. This increases the demand for ^{68}Ge/^{68}Ga generators, which leads to a higher price and long waiting time (9-18 months). [45]

As seen in Figure 36, the maximum cross section for the ^{68}Zn(p,n)^{68}Ga nuclear reaction is obtained at a proton beam energy of 10-14 MeV. However, at a proton energy >12 MeV gallium-67 (^{67}Ga) ($T_{½}$ = 3.3 d) can be produced by the ^{68}Zn(p,2n)^{67}Ga nuclear reaction. It is therefore important to decrease the amount of co-produced ^{67}Ga by using a lower energy (Figure 36). Isotopically enriched ^{68}Zn is needed for the cyclotron production of ^{68}Ga in order to reduce the coproduction of other gallium radionuclides. However, impurities of zinc-66 (^{66}Zn) and zinc-67 (^{67}Zn) in the enriched ^{68}Zn will lead to the production of small amounts of gallium-66 (^{66}Ga) ($T_{½}$ = 9.5 h) and ^{67}Ga, through the ^{66}Zn(p,n)^{66}Ga and ^{67}Zn(p,n)^{67}Ga nuclear reactions, respectively. [45]

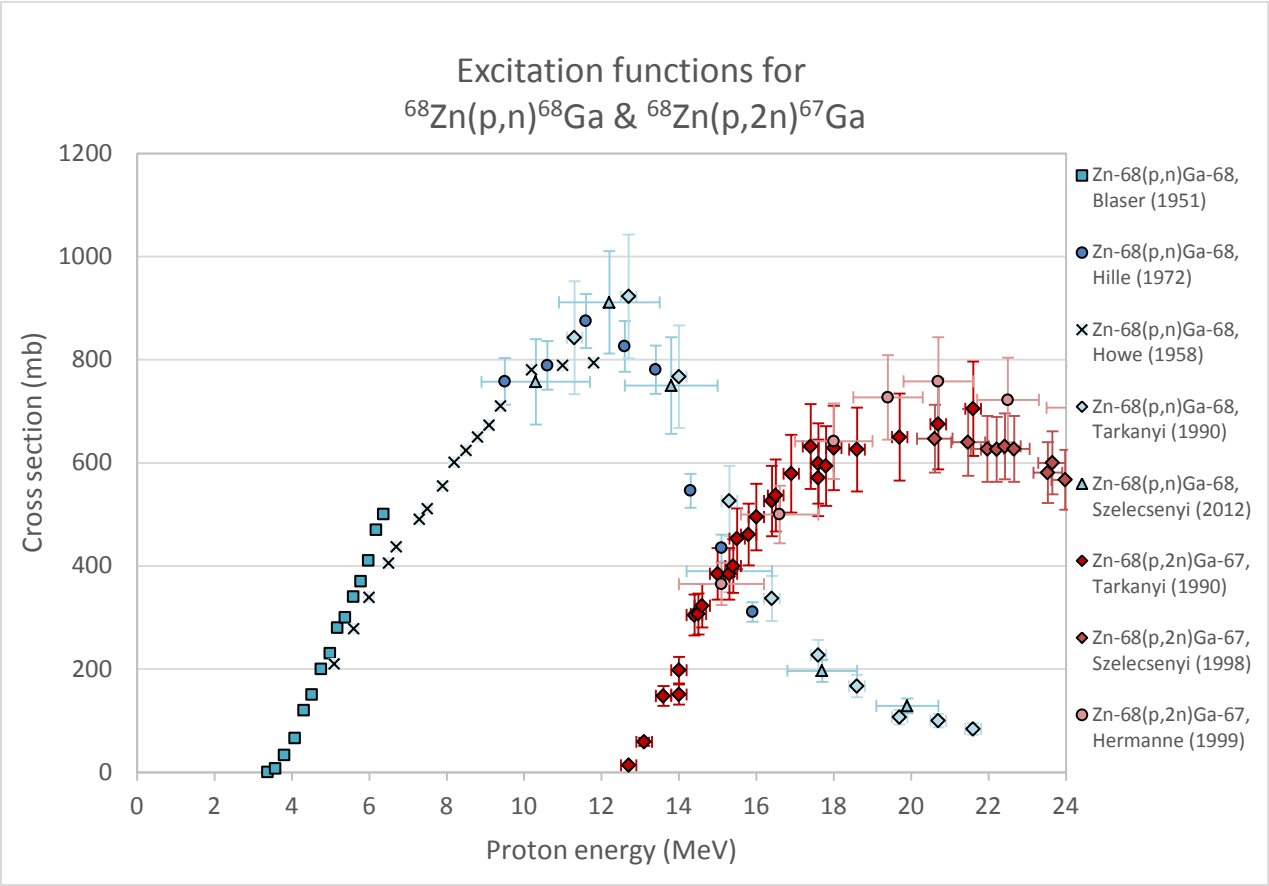

Figure 36: Excitation functions for the $^{68}Zn(p,n)^{68}Ga$ (blue) and $^{68}Zn(p,2n)^{67}Ga$ (red) nuclear reactions showing their energy dependent cross sections and the potential for co-production of radionuclide contaminations. The experimental cross section data is collected from the EXFOR database [73] and published by [114]–[120].

^{68}Ga can both be produced using a solid target or a liquid target. Solid targets can be obtained by applying zinc foils [121], electroplating the zinc onto a support material [122] or pressing ^{68}Zn powder [123], while a solution of $[^{68}Zn]ZnCl_2$ [124] or $[^{68}Zn]Zn(NO_3)_2$ [35], [125], [126] can be used for liquid targets. In recent years, the $[^{68}Zn]Zn(NO_3)_2$ targets have become more common, due to the gas formation associated with the $[^{68}Zn]ZnCl_2$ targets, leading to a higher pressure buildup during irradiation, and therefore sets a higher demand for the target body and foil properties. [45] Liquid targets are gaining popularity due to the simpler post-irradiation target handling. [35]

8.2 Chemical properties of ^{68}Ga

Gallium is a hard metal (HSAB theory) and gallium is in the +3 oxidation state in aqueous solution. Ga^{3+} and has a high tendency to form hydroxide species, where insoluble $Ga(OH)_3$ starts to form at pH above ~ 4. Free

hydrated gallium ($[Ga(H_2O)_6]^{3+}$) is stable under acidic conditions and radiolabeling with ^{68}Ga is therefore performed at low pH. [3]

8.3 Purification of ^{68}Ga

The produced ^{68}Ga is in most cases separated from the target solution using SPE with different types of resins. This can be done using cation exchange resin, e.g. AG 50W-X8 [122], [125], [127] or hydroxamate resin [123], [128]. Furthermore, a second purification step can be used to remove metal impurities or to obtain $[^{68}Ga]GaCl_3$ in a suitable HCl concentration. Here, resins, such as TK200 resin based on TOPO [128] or DGA resin based on tetra-n-octyldiglycolamide [127], can be applied. An equal purity of the ^{68}Ga, as for the generator produced ^{68}Ga [46], is required, and it should be obtained in a suitable solution for radiolabeling (not too high acid concentration and not too large volume). Recycling of the target material is also important due to the price of the enriched ^{68}Zn. [45] This can be done in a separate process after the production of ^{68}Ga [35], [126].

However, LLE techniques can also be applied for the purification of radionuclides of gallium. [129], [130] Furthermore, gallium has previously been separated from other metal ions in aqueous acidic solution by LLE using various extractants. One example is phosphine oxides, e.g. Cyanex 923, containing TOPO, which was applied for the LLE of ^{89}Zr and ^{64}Cu, described in section 6.3.2 and 7.3.1. It has been shown that gallium can be extracted almost quantitatively from aqueous solution containing 3-5 M HCl with Cyanex 923. It was expected that the extracted gallium species were neutral $GaCl_3$, which was solvated by 2 or 3 phosphine oxides. However, the extraction of zinc is also high from aqueous HCl solution in this concentration range, which was seen in the LLE of ^{64}Cu (section 7.3.4). [131], [132] TOPO would thus not be suitable for the separation of gallium and zinc. Ethers are another possible extractant group, which have been applied for the extraction of gallium with high efficiency from acidic aqueous solution. [133]–[136] In the case of gallium extraction into ethers, the extracted gallium specie was believed to be $HGaCl_4$. [133], [134], [137] The coordination number for gallium in this chloride complex is expected to be 4, which meant that $GaCl_4^-$ did not have coordinating water molecules, making it more hydrophobic. [138] At high HCl concentration, the main zinc species were most likely negatively charged, e.g. $ZnCl_3^-$ and $ZnCl_4^{2-}$, having a higher affinity for the aqueous phase. [139] Ethers were thus expected to have a selectivity for the extraction of gallium and were chosen for the LLE experiments in this study.

8.3.1 Design of ^{68}Ga LLE

In this study, the focus was on the separation of ^{68}Ga from a zinc salt solution by LLE, which might make it possible to reuse the zinc salt solution without any further purification. It was attempted to back-extract (strip) the extracted ^{68}Ga into 0.1 M HCl, as it would be a suitable form of ^{68}Ga for radiolabeling.

A $ZnCl_2$ solution in HCl was selected to simulate a liquid cyclotron target system, instead of $Zn(NO_3)_2$ in HNO_3 since the extraction of gallium with ethers have shown high extraction efficiency from aqueous HCl solutions. A relatively high $ZnCl_2$ concentration (5.6 M) was first chosen, because a high concentration was applied previously by Jensen and Clark. [124] When this system was tested for the LLE of gallium with ethers, phase separation challenges appeared and the use of a lower $ZnCl_2$ concentration (1 M) was thus also studied.

The ethers chosen for this study were both symmetric, such as diethyl ether (Et_2O), diisopropyl ether ($^{i}Pr_2O$), dibutyl ether (*n*-Bu_2O), and *n*-amyl ether (*n*-Am_2O), asymmetric, such as butyl methyl ether (*n*-BuOMe) and hexyl methyl ether (*n*-HexOMe), and cyclic, such as tetrahydropyran (THP). The structure of each of the ethers can be seen in Figure 37. A mixture of ^{66}Ga and ^{67}Ga and zinc-65 (^{65}Zn) ($T_{½}$ = 243.9 d) were used in order to evaluate the extraction efficiency of gallium and zinc in the LLE experiments. $^{66,67}Ga$ was applied instead of ^{68}Ga, but mainly ^{67}Ga was used to measure the gallium extraction, due to the longer half-life of this isotope. Natural zinc was used as cyclotron target material producing all three gallium isotopes by their individual $^{nat}Zn(p,n)^{66,67,68}Ga$ nuclear reactions. ^{65}Zn was produced from natural copper by the $^{nat}Cu(p,n)^{63,65}Zn$ nuclear reaction. Due to the relative long half-lives of ^{67}Ga and ^{65}Zn, decay corrections were not made for the samples for the calculation of the extraction efficiencies, since they were measured directly after each other. Nonradioactive gallium and zinc were not used for the quantification and calculation of extraction efficiency, since the high concentration of zinc needed in the experiments would necessitate considerable dilution of samples, if quantified by ICP-OES. This would place a relative high uncertainty on the sample preparation and the concentration of gallium would be very low. The access to relatively long-lived isotopes as ^{65}Zn and ^{67}Ga made it possible to work with low radioactivity for longer times.

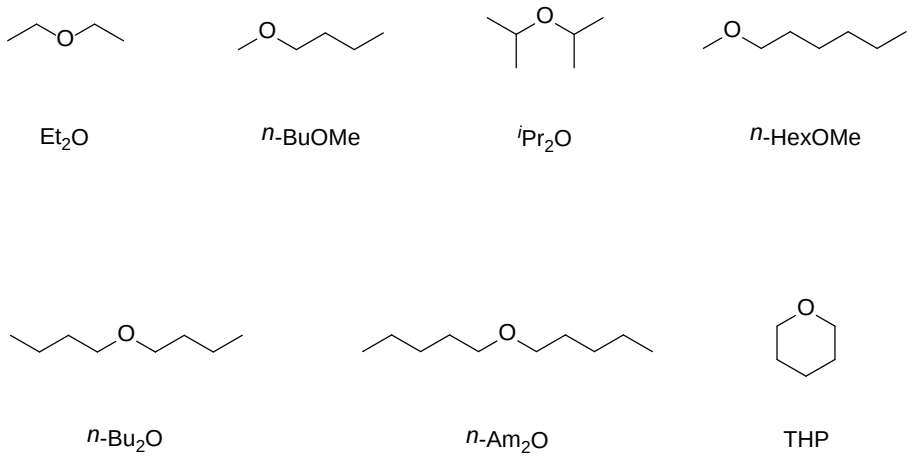

Figure 37: The chemical structure of the seven different ethers (Et_2O, *n*-BuOMe, $^{i}Pr_2O$, *n*-HexOMe, *n*-Bu_2O, *n*-Am_2O, and THP) can be seen.

8.3.2 Phase separation optimizations

From the study by Swift and by Brooks and Lloyd, it was seen that the extraction of gallium with Et_2O was highest from 6-8 M HCl. [134], [136] These conditions were thus attempted for the extraction of gallium from a 5.6 M $ZnCl_2$ in 6 M HCl solution. From the study by Irving and Rossotti, a change in the volume of the organic ether phase and the aqueous HCl phase was observed after mixing. The volume of the aqueous phase increased, while the volume of the organic phase decreased. The effect was more pronounced at higher HCl concentration. This resulted in a decrease in the concentration of HCl in the aqueous phase, which affected the extraction efficiency of gallium. The organic phase thus needed to be presaturated with the corresponding HCl concentration, before performing the LLE, to achieve a constant HCl concentration of the aqueous phase. [135], [136]

Et_2O was used for the first LLE experiments and was presaturated with the corresponding HCl solution in this case 6 M HCl, but when adding the presaturated Et_2O to the aqueous $ZnCl_2$ solution no phase separation could be observed, as the two phases were miscible. It was attempted to decrease the HCl concentration, but phase separation was first observed at an HCl concentration of 3.5 M HCl. At 3.5 M HCl, a notable difference in the volume of the aqueous and organic phase was seen (Figure 38). In this case, the volume of the organic phase was increased, suggesting a transfer of water or HCl from the aqueous phase. The opposite was observed by Swift, where a small increase in the volume of the aqueous phase was seen, when the LLE was performed without $ZnCl_2$ in the aqueous phase. This indicated that the high concentration of $ZnCl_2$ in our study affected the phase separation. The extraction of gallium to the ether phase increased with higher HCl concentration and up to 80 % of gallium was extracted from 3 M HCl (Figure 38). The extraction of zinc, however, was also increasing at higher HCl concentration. The high extraction of zinc was supposed to lead to an increased volume of the organic phase, especially if coordinating water molecules were extracted. It was expected that the formation of negatively charged zinc species, such as $ZnCl_3^-$ and $ZnCl_4^{2-}$ would increase with higher HCl concentration [139] leading to lower extraction of zinc, but the opposite was observed. The higher zinc extraction could be connected to the observed increased phase miscibility at higher HCl concentration, possibly caused by a lower interfacial tension, as also seen for the LLE of ^{45}Ti from 12 M HCl with 1-octanol, described in section 5.3.1.

Despite the decrease of the volume of the aqueous phase, a small migration of the ether to the aqueous phase could also be seen. Data from qNMR analysis, according to the method described by Pauli et al. [61], showed 2-4 % of Et_2O in the aqueous phase after the LLE from 0-3 M HCl.

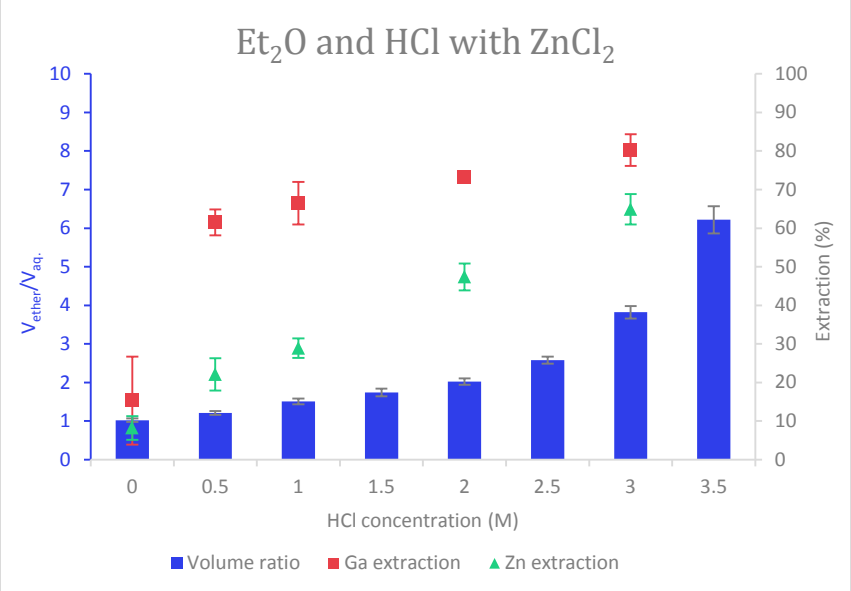

Figure 38: LLE in batch of gallium and zinc from 5.6 M $ZnCl_2$ in 0-3.5 M HCl with presaturated Et_2O. The volume ratio (volume of ether phase divided with the volume of the aqueous phase ($V_{ether}/V_{aq.}$)) (left y-axis), as a function of HCl concentration is shown as blue bars. The gallium extraction (red squares) and zinc extraction (green triangles) can be read on the right y-axis. The error bars represent the standard deviation of two experiments. The data are also shown in [9].

8.3.3 Effect of various diluents

The phase separation needed to be improved in order to evaluate, if the co-extraction of zinc could be avoided. In section 5.3.3 describing the LLE of titanium, anisole was added to guaiacol as a diluent, which increased the interfacial tension between concentrated HCl and the organic phase. The same concept was applied to the extraction of gallium with ethers. Different diluents were tested in order to find the most suitable diluent, to avoid partially miscibility between the aqueous and organic phase. Aromatic solvents, such as anisole, toluene, and TFT, an aliphatic solvent (heptane), and a chlorinated solvent (1,2-dichloroethane (DCE)) were tested as diluent. First, one of the diluents, in this case toluene, was added to the different ethers, which were mixed with the aqueous phase, containing 5.6 M $ZnCl_2$ in 6 M HCl until the volume of the aqueous phase was the same as before adding the ether. In this experiment, the ethers were not presaturated with HCl, since it was attempted to find a solvent system without phase migration, making it possible to avoid a presaturation step.

The required volume of toluene for each ether can be seen in Figure 39. A higher added amount of toluene was needed to the less hydrophobic ethers, such as THP, Et_2O, and *n*-BuOMe compared to *n*-Bu_2O and *n*-Am_2O. The amount of the various ethers in the aqueous phase, after the addition of toluene, was measured by qNMR. It was seen that the more hydrophilic ethers had a higher solubility in the aqueous phase than the more hydrophobic ethers even after the addition of toluene. THP had the highest solubility in the aqueous phase. Still, 10 % of THP

was dissolved in the aqueous phase after the addition of 5 mL toluene showing it to be difficult to obtain complete phase separation. THP was thus chosen as the ether in which the different diluents were evaluated. The same setup was applied, but now heptane, anisole, TFT, or DCE were added to THP, after the mixing with 5.6 M $ZnCl_2$ in 6 M HCl, until the volume of the aqueous phase was equal to the volume before the addition of the organic phase. The performance of anisole and DCE was similar to toluene, while an even higher amount of heptane was needed (Figure 39). TFT seemed to be most suitable, since only 2 mL was needed to obtain the apparent phase separation. However, the amount of THP in the aqueous phase after the addition of TFT was found to be high (around 15 %). The amount of THP in the aqueous phase was above 5 %, after the addition of all the diluents, except for DCE (2.6 %). However, the required volume of DCE was high (5 mL). Instead it was evaluated, if the solubility of THP in the aqueous phase could be reduced by decreasing the concentration of HCl in the aqueous phase. The phase separation study with the different diluents and THP was then repeated, but this time with 5.6 M $ZnCl_2$ in 3 M HCl. The volume of the diluents needed to obtain an apparent phase separation, was either the same as previously or slightly less, which indicated a better phase separation. A reduction in the amount of THP in the aqueous phase after the addition of the diluents to THP was also observed by qNMR (Figure 39). The amount of THP in the aqueous phase was below 5 %, when anisole, DCE, and TFT were applied as diluents. Due to the lower volume of TFT needed, this diluent was chosen for the further LLE studies. A ratio of 1/2 (v/v) ether/TFT was applied for all seven ethers to be able to compare the extraction efficiencies of gallium under the same conditions.

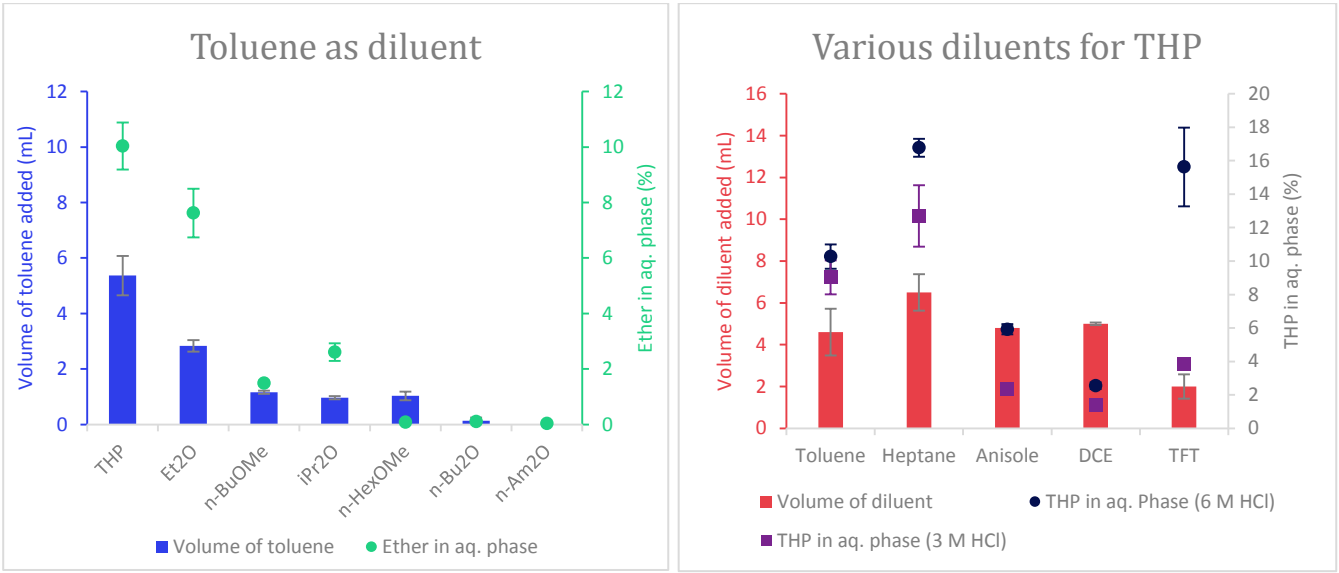

Figure 39: Phase separation studies with 5.6 M $ZnCl_2$ in 6 M HCl as aqueous phase. Left: The volume of toluene needed to regain the same volume of the aqueous phase as before adding the different ethers (THP, Et_2O, *n*-BuOMe, $^{i}Pr_2O$, *n*-HexOMe, *n*-Bu_2O,and *n*-Am_2O)

is shown as blue bars (left y-axis) and the amount of the ether in the aqueous phase after the addition of toluene is shown as green circles (right y-axis). Right: The volume of different diluents (toluene, heptane, anisole, DCE, and TFT) needed to obtain the same volume of the aqueous phase before adding THP, is shown as red bars (left y-axis) and the amount of THP in the aqueous phase after adding the diluents, is shown as dark blue circles (right y-axis). The same experiment was repeated with 5.6 M $ZnCl_2$ in 3 M HCl and the amount of THP in the aqueous phase can be seen as purple squares (right y-axis). The error bars are from the standard deviation of two experiments.

8.3.4 LLE of gallium from 5.6 M $ZnCl_2$ solution

8.3.4.1 LLE in batch

The extraction of gallium and zinc from 5.6 M $ZnCl_2$, both in 3 M HCl and 6 M HCl, with the different ethers/TFT 1/2 (v/v) were tested in batch LLE experiments in order to evaluate the effect of the HCl concentration as well as of the seven different ethers. The extraction efficiencies of gallium and zinc can be seen in Figure 40. In the figure, the ethers were listed after the number of carbon atoms in their structure, except THP, which was placed before Et_2O. It was expected that the gallium extraction would be higher for the more polar ethers, since an increased solubility of ion-association complexes have been seen, when more polar solvents were applied for LLE [140], which might also be seen with $HGaCl_4$. The size and steric hindrance of the ether was expected to have an effect on the extraction efficiency, since a coordination of the oxygen atom of the ethers to the gallium specie was anticipated. [134] The extraction of gallium was notably higher when extracted from 6 M HCl, compared to 3 M HCl, especially for the less polar ethers, such as *n*-HexOMe, *n*-Bu_2O, and *n*-Am_2O. The increased extraction of gallium was believed to be due to the increased formation of $HGaCl_4$ at higher HCl concentration.

The trend of the decreasing extraction efficiencies of gallium with increasing number of carbon atoms of the ether was broken by $^{i}Pr_2O$, where the extraction of gallium was higher than expected. This was more visible when the extraction was performed from 3 M HCl in the aqueous solution. It was assumed that the fact that $^{i}Pr_2O$ is branched, where the other ethers are linear, could be the reason for this observation. Therefore, even though $^{i}Pr_2O$ contains six carbon atoms, the steric hindrance might be less than, if a linear ether with same number of carbon atoms would be used for the extraction.

A small decrease of the zinc extraction was seen at the change from 6 M to 3 M HCl when $^{i}Pr_2O$ and *n*-BuOMe were used as extractant where the zinc extraction decreased from 5 % to 1 %. While the efficiency of the zinc extraction with the other ethers comparable at 3 M and 6 M HCl. Thus, it was expected that the zinc speciation was similar at 3 M and 6 M HCl, possibly due to the high (14.2 and 17.2 M) concentration of Cl^- [141] and was not as acid concentration dependent, as the extraction of gallium. The extracted zinc species were assumed to be

neutral, such as $ZnCl_2$, species and the observed different extraction efficiencies for the seven ethers was assumed to be due to the various solubility of these zinc species in the ethers.

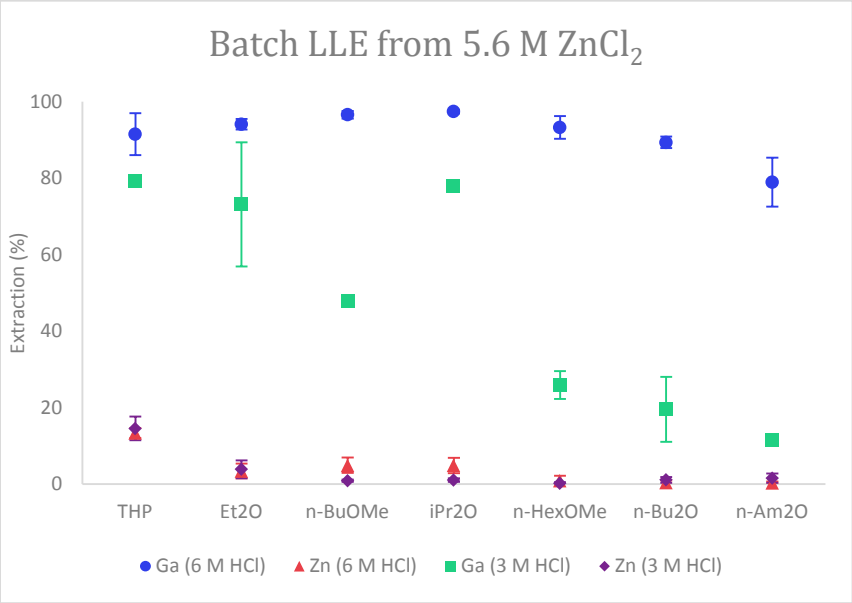

Figure 40: Batch LLE with the seven ethers (THP, Et_2O, *n*-BuOMe, $^{i}Pr_2O$, *n*-HexOMe, *n*-Bu_2O, and *n*-Am_2O) mixed with TFT 1/2 (v/v) from 5.6 M $ZnCl_2$ in 6 or 3 M HCl. The extraction efficiency of gallium (blue circles) and of zinc (red triangles) from the 6 M HCl zinc solution and the gallium (green squares) and zinc (purple diamonds) from the 3 M HCl zinc solution can be seen. The error bars are obtained from the standard deviation of two experiments. The data can also been found in [9].

8.3.4.2 Flow LLE

The extraction efficiency of gallium was acceptable for the more hydrophilic ethers, such as THP, Et_2O, *n*-BuOMe, and $^{i}Pr_2O$, and these were chosen for the translation into LLE in flow. First, the LLE from 5.6 M $ZnCl_2$ in 3 M HCl was tested, since the phase separation over the membrane was expected to be less challenging than with the $ZnCl_2$ solution in 6 M HCl. A complete phase separation between the four ethers (THP, Et_2O, *n*-BuOMe, and $^{i}Pr_2O$) mixed with TFT 1/2 (v/v) and 5.6 M $ZnCl_2$ in 3 M HCl was obtained using the same setup as for the LLE of ^{45}Ti, ^{89}Zr, and ^{64}Cu; a PTFE/PP membrane with a pore size of 0.2 µm and a diaphragm with a thickness of 2 mil. The flow rate ratio was 1:3 (aq:org), which corresponded to the volume ratio for the LLE batch experiments. The total flow rate was 1.0 mL/min and the residence time was 0.5 minutes. The extraction efficiencies of gallium and zinc, using THP, Et_2O, *n*-BuOMe, and $^{i}Pr_2O$ can be seen in Figure 41. The results were similar to the extraction efficiencies for the LLE batch experiments. However, a notably higher extraction of zinc with THP was observed. This could indicate that the phase separation was not completely successful, even though no breakthrough of the aqueous phase in the organic phase was observed. It was not investigated, if applying a different membrane with a smaller pore size or a thinner diaphragm, would reduce the extraction of

zinc, since it was not clear, if the high extraction of zinc was caused by uncomplete phase separation. The relative high solubility of THP in the aqueous phase (Figure 39) also indicated that THP would not be a suitable extractant. Instead, $^{i}Pr_2O$ was chosen as the most suitable ether for the purpose of extracting gallium from the zinc chloride solution at the applied conditions. The extraction of gallium was acceptable (76.3 ± 1.9 %) and the zinc extraction relatively low (1.8 ± 1.6 %). According to qNMR analyses, the amount of $^{i}Pr_2O$ in the aqueous phase after the LLE was also low (0.2 %) and it was possible to remove the traces of $^{i}Pr_2O$ from the aqueous phase by passing it through a C18 Sep Pak cartridge.

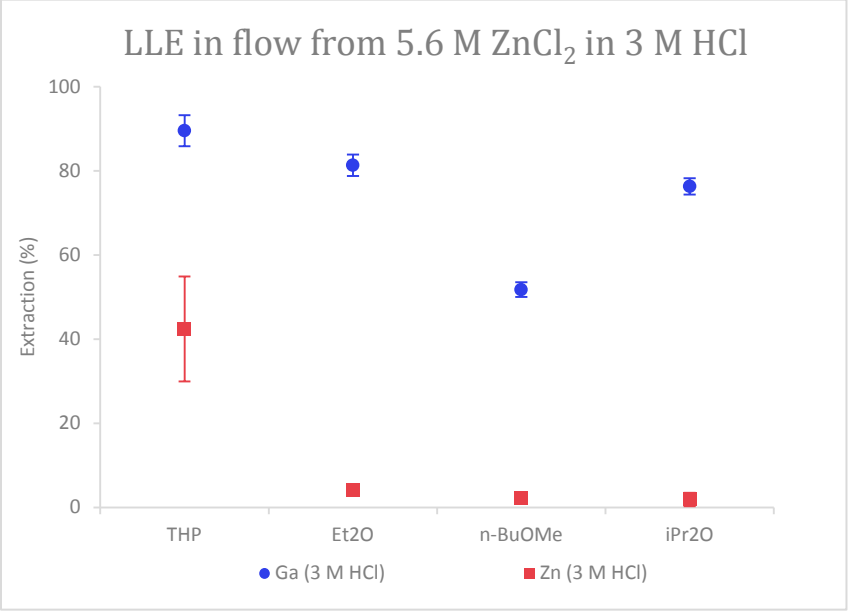

Figure 41: The LLE in flow from 5.6 M $ZnCl_2$ in 3 M HCl with THP, Et_2O, *n*-BuOMe, and $^{i}Pr_2O$ mixed with TFT 1/2 (v/v). A total flow rate of 1.0 mL/min and a flow rate ratio of 1:3 (aq:org) were applied. The extraction efficiency of gallium (blue circles) and of zinc (red squares) can be seen. The data can also be seen in [9].

The amount of extracted zinc was however still very high when taking the concentration of $ZnCl_2$ into account, where the zinc concentration in the organic phase would be approximately 35 mM (the concentration was diluted a factor of 3 due to the 1:3 (aq:org) volume ratio). It was thus tested if the extracted zinc in the $^{i}Pr_2O$ phase could be removed by a scrubbing step, where it was attempted to back-extract the zinc into an aqueous phase without back-extracting gallium. Aqueous phases with different HCl concentrations were tested and the scrubbing efficiencies using 0.5, 1, 6, and 8 M HCl can be seen in Figure 42. Zinc was efficiently extracted into the aqueous phase at all HCl concentrations tested, although it was necessary to use a high concentration of HCl to avoid gallium being extracted as well. The most suitable HCl concentration was 8 M, where above 97 % of zinc and only 4 % of gallium were extracted to the aqueous phase. The concentration of zinc in the organic phase was thereby reduced to 1 mM.

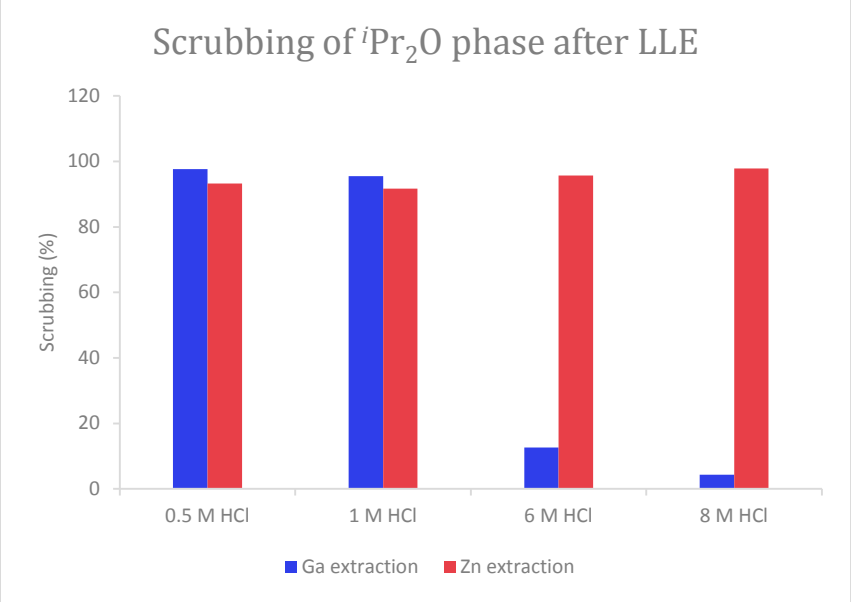

Figure 42: The scrubbing with 0.5, 1, 6, and 8 M HCl of the organic phase from the LLE of gallium with $^{i}Pr_2O$/TFT 1/2 (v/v) from 5.6 M $ZnCl_2$ in 3 M HCl. The amount of gallium (blue) and zinc (red) back-extracted to the aqueous phase is shown.

The extracted gallium could then be back-extracted into aqueous phase (stripping) using a low HCl concentration (0.1 M). The stripping was efficient (99 %), but no selectivity for gallium was observed in this step, as the remaining zinc in the organic phase was also stripped. Since a flow rate ratio of 1:3 (aq:org) was applied for the stripping, the concentration of zinc in the aqueous phase would be approximately 3 mM, which was still high compared to the low concentration of gallium. It might instead be possible to use a resin-based separation technique for the final purification of gallium. Additionally, the extraction of some common metal impurities, found in the cyclotron target solution (Fe, Cu, Co, and Mn) [126], were tested and it was found that Fe(III) was extracted, scrubbed, and stripped with similar efficiencies as gallium by $^{i}Pr_2O$/TFT 1/2 (v/v) (66 % extraction, 9 % scrubbing, and 98 % stripping), while only 0.04 % of Cu was extracted and no measurable extraction of Co, and Mn was seen. The scrubbing step was not optimized in regard to iron, it might therefore be possible to remove Fe(III), but it was expected to be challenging, due to the similar chemical properties of Fe(III) and Ga(III). [3] It is thus important to evaluate the amount of iron in the ^{68}Zn used for the cyclotron target material for the production of ^{68}Ga, as well as, other possible iron contamination sources, such as the HCl used to dissolve ^{68}Zn or the cyclotron target body and foils. [45]

The LLE in flow of gallium from 5.6 M $ZnCl_2$ in 6 M HCl with $^{i}Pr_2O$/TFT 1/2 (v/v) was tested to evaluate, if the phase separation could be achieved, using the membrane separation, since the extraction of gallium was notable higher when extracted from 6 M HCl (Figure 40). The same membrane and diaphragm as for the LLE from 5.6 M $ZnCl_2$ in 3 M HCl was applied. A complete phase separation, however, could not be obtained with this setup

at 6 M HCl. Breakthrough of the aqueous phase into the organic phase was observed. It was not attempted to obtain complete phase separation by changing the membrane and diaphragm in this study. Since the main phase separation challenge was expected to be due to the high concentration of $ZnCl_2$, it was instead chosen to decrease the $ZnCl_2$ concentration.

8.3.5 LLE of gallium from 1 M $ZnCl_2$ solution

The effect of $ZnCl_2$ on the extraction efficiency of gallium was not clear from the experiments, but it was noted that a higher extraction efficiency was obtained at a lower HCl concentration when the aqueous phase contained a high concentration of $ZnCl_2$, compared to the extraction from aqueous HCl solution without $ZnCl_2$. [133]–[136] The extraction of gallium from 2.2 M $ZnCl_2$ in 1 M HCl and 2.2 M $ZnCl_2$ in 6 M HCl with $^{i}Pr_2O$/TFT 1/2 (v/v) was determined from LLE in flow. The extraction efficiency of gallium from the 1 M HCl solution was 1.4 %, while 98.5 % of gallium was extracted from the 6 M HCl solution. The extraction of zinc was in both cases low (0.2% and 0.1 %, respectively). It was thus assumed that $ZnCl_2$ mainly improved the extraction efficiency of gallium at high concentrations and a lower HCl concentration. A relatively high HCl concentration was thus necessary in order to obtain a high extraction of gallium, when a lower $ZnCl_2$ concentration was used. The extraction of gallium from 1 M $ZnCl_2$ in 6 M HCl was chosen for the further experiments. The LLE with all seven ethers, mentioned in section 8.3.1, was studied both in batch mode and in flow. The LLE in flow was possible with the same setup as for the LLE with high $ZnCl_2$ concentration (section 8.3.4.2). The extraction efficiencies of gallium and zinc can be seen in Figure 43.

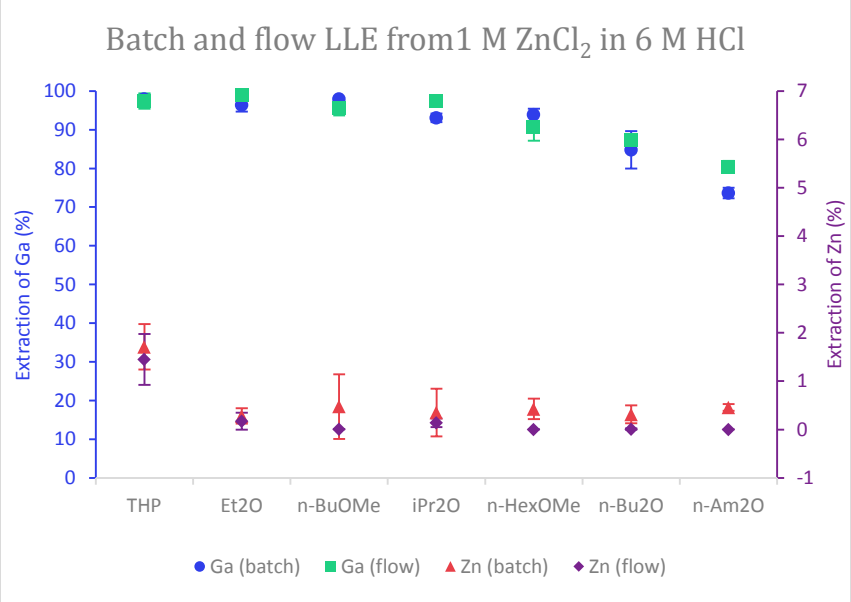

Figure 43: LLE of gallium from 1 M $ZnCl_2$ in 6 M HCl with the seven different ethers (THP, Et_2O, *n*-BuOMe, $^{i}Pr_2O$, *n*-HexOMe, *n*-Bu_2O, and *n*-Am_2O) mixed with TFT 1/2 (v/v). The LLEs were performed in batch and in flow and all experiments were performed

twice. The error bars represents the standard deviation of the two experiments. The gallium extraction (left y-axis) in batch (blue circles) and in flow (green squares) and the zinc extraction (right y-axis) in batch (red triangles) and in flow (purple diamonds) can be seen. The data can also be found in [9].

The extraction efficiency of gallium was similar to the data obtained from the LLE of gallium from 5.6 M $ZnCl_2$ in 6 M HCl and gallium extraction efficiencies above 90 % could be obtained with five of the ethers (THP, Et_2O, *n*-BuOMe, $^{i}Pr_2O$, and *n*-HexOMe). The extraction of zinc was on the other hand decreased, especially for the more polar ethers, such as THP, Et_2O, *n*-BuOMe, and $^{i}Pr_2O$. This reduction might be due to the lower $ZnCl_2$ concentration and the higher Cl^-/Zn^{2+} ratio. The coordination number for zinc in aqueous solution can vary, and it has been seen that the coordination number decreases from 6 to 4 with increasing $ZnCl_2$ concentration. The concentration of the counter ion, in this case Cl^-, also affects the coordination number. [142] For the 5.6 M $ZnCl_2$ in both 3 M HCl and 6 M HCl a coordination number of 4 was expected and the ratio between Zn^{2+} and Cl^- was 1:2.5 and 1:3, respectively. The zinc species were both suspected to have coordinating Cl^- and water molecules at this condition. [142], [143] Similarly, 1 M $ZnCl_2$ in aqueous solution have been shown to have a coordination number of 6, although at lower Zn^{2+}/Cl^- ratios the coordination number decreases to 4. The Zn^{2+}/Cl^- ratio in 1 M $ZnCl_2$ in 6 M HCl was 1:8 and the zinc species were supposed to be $ZnCl_4^{2-}$ without water in the coordination sphere. [142] The zinc species in the 5.6 M $ZnCl_2$ solutions were assumed to be more extractable due to the less negatively charge when partly coordinated by water molecules. The zinc extraction was in general lower when the LLE was performed in flow compared to the batch mode, as seen in Figure 43. This could be due to the manual phase separation of the LLE experiments performed in batch. A small amount of aqueous phase in the organic phase would affect the calculated extraction efficiencies, due to the very low concentration of zinc in the organic phase. From the LLE data obtained in Figure 43, *n*-BuOMe appeared as the most suitable extractant for gallium. The gallium extraction efficiency was above 95 % and the zinc extraction efficiency below 0.01 % in flow. The zinc concentration in the organic phase was 26 µM. The scrubbing step was not tested for this LLE, but if similar efficiency was expected as for the scrubbing of the organic phase from the LLE from 5.6 M $ZnCl_2$ in 3 M HCl with $^{i}Pr_2O$/TFT 1/2 (v/v), the zinc concentration could be decreased to 0.8 µM in the organic phase, corresponding to 2 µM in the 0.1 M HCl solution used for the stripping of gallium. This concentration corresponded to 0.13 µg/mL zinc with a scrubbing step and around 5 µg/mL without a scrubbing step. This was an acceptable level, since the content of zinc should be below 10 µg/GBq according to the European Pharmacopoeia monograph no. 2464. [46]

High extraction efficiencies of gallium could be obtained with the LLE in flow using the ethers. The extraction was more efficient and selective when a 1 M $ZnCl_2$ in 6 M HCl solution was used, compared to the extraction from 5.6 M $ZnCl_2$ in 3 M HCl. Relatively polar ethers, such as Et_2O, $^{i}Pr_2O$, and *n*-BuOMe, were the most

suitable ethers, since high extraction efficiency of gallium was obtained and low co-extraction of zinc took place. The extraction of gallium with THP was similarly high, but the co-extraction of zinc was also relatively high. The back-extraction (stripping) of gallium was almost quantitative when using 0.1 M HCl and a scrubbing with 8 M HCl was also possible. The most optimal conditions for the LLE of gallium from a $ZnCl_2$ solution was *n*-BuOMe/TFT 1/2 (v/v) as organic phase and a 1 M $ZnCl_2$ in 6 M HCl solution. In the introduction to section 8, it was mentioned that it might be possible to reuse the $ZnCl_2$ solution directly for a new production. This still needs to be evaluated further, as the composition and concentration of $ZnCl_2$ and HCl in the solution might change, when irradiated in a cyclotron and during the separation, which would affect the next extraction of gallium. It was expected that the final gallium solution in 0.1 M HCl could be used for the labeling of a radiotracer, but this was not verified in this PhD study.

9 Summary – Separation of radiometals by LLE in flow

The separations of four different radiometals (^{45}Ti, ^{89}Zr, ^{64}Cu, and ^{68}Ga) from their cyclotron target material (scandium, yttrium, nickel, and zinc) were performed by LLE in flow with the membrane-based separation technique. It was possible to find solvent systems where the radiometal was selectively extracted from its cyclotron target material and the two phases could be separated by the membrane-based separation.

Solvent systems, which resulted in an extraction efficiency over 85 % was found for the LLE of ^{45}Ti, ^{64}Cu, and ^{68}Ga (^{67}Ga). The LLE of zirconium would need to be optimized further to obtain a higher extraction efficiency. A lack of selectivity for copper with TOPO was seen, when it was attempted to separate ^{64}Cu from metal impurities, such as iron, cobalt, zinc, and silver but this was not possible with the chosen extractant. The LLE of gallium with ethers was not selective in regards to iron, which also needed to be considered. It would furthermore be interesting to evaluate radiolabeling of a tracer with the purified radiometals. This was only tested for ^{45}Ti where the formation of [^{45}Ti](salan)Ti(dipic) was performed directly in the organic phase after the LLE.

The membrane-based separation and LLE in flow could be applied for the separation of radiometals, although various challenges should be addressed in a potential further development of the system. As mentioned in section 5.3.3, it is important to ensure that the amount of organic solvents in the final product is below the limits specified by the European Pharmacopoeia no. 50400. [88], [89] It is also necessary to evaluate, if the amount of the cyclotron target materials and other metal impurities are at an acceptable low concentration in the final product. Especially since the extraction efficiencies of the respective cyclotron target materials (scandium, yttrium, and copper) calculated by ICP-OES, resulted in negative values, which indicated an uncertainty on these measurements.

The actual LLE in flow of the radiometals could be performed relatively fast (within 20 minutes with an aqueous volume of 3-5 mL and aqueous flow rate of 0.25 mL/min). The time needed for the preparation of the setup and cleaning of the system should also be taken into account, although most setup steps could be prepared in advance, without radiation exposure. After the LLE, stripping of the radiometal from the organic phase might be applied, which would require the same amount of time as for the first LLE. It should be noted that in this study the setup for the LLE and membrane separation in flow was performed manually; therefore the filling of the syringes and system priming was not automated. These steps would need to be automated, if the LLE in flow was performed in larger scale with higher radioactivity. It is also necessary to ensure that the phase separation is

complete, which was done by visual evaluation in this study. This would not be possible, when high amount of radioactivity would be applied and a detector might instead be connected.

Finally, it should be evaluated for each individual radiometal and application, if the purification by LLE is more suitable than other separation methods, e.g. SPE. For the purification of ^{45}Ti, the LLE method could be an alternative approach, due to the challenges with SPE purification (section 5.3). In the case of ^{89}Zr and ^{64}Cu, the LLE method would need to be optimized further concerning the efficiency and selectivity, respectively, in order to be an alternative to the already applied SPE purification methods (section 6.3 and 7.3). For the separation of ^{68}Ga, the aim was to apply the LLE technique in order to test if this method could make it possible to reuse the cyclotron target solution directly. The selectivity between ^{68}Ga and zinc might however not be high enough, if high concentrations of $ZnCl_2$ are applied and it might thus be possible to combine LLE and SPE methods.

Chapter 3

[^{45}Ti]Ti-CAS-PSMA – development of a PSMA-targeted ^{45}Ti-labeled radiotracer

10 Application of ^{45}Ti for PET

As described in section 5.1, the positron emitting ^{45}Ti has a suitable physical half-life (3.1 hours) and can be produced from natural scandium with a 16-18 MeV cyclotron, which makes it a promising radiometal for PET. However, the high oxophilicity of titanium complicates the application of ^{45}Ti for PET. The challenging aqueous chemistry also complicates the purification and recovery of ^{45}Ti from the cyclotron target material, although the developed LLE method appeared to be a suitable method to separate ^{45}Ti from scandium, as described in section 5.3.4. With this method tested and optimized, the production of a ^{45}Ti-labeled targeting vector was initiated.

A few studies with ^{45}Ti for PET have been performed. These include the chelation of ^{45}Ti with citrate, diethylenetriaminepenta acetic acid, human albumin serum, and ascorbic acid. [62], [64], [66], [70] Vavere et al. and Price et al. have studied the biodistribution of ^{45}Ti-transferrin. [67]–[69] Furthermore, nanoparticles have been labeled with ^{45}Ti. [63] The ^{45}Ti-labeling of specific targeting vectors, however, has not been studied and as mentioned in section 2.4.1.1 and 5.2, the chelation of titanium is challenging due to the hydrolysis of titanium complexes in aqueous environment.

The application of titanium for different types of anti-cancer compounds has been evaluated and developments have been made to increase their hydrolytic stability and cytotoxicity. Diamino bis(phenolato) complexes are one type of anti-cancer compounds (Figure 44). The cytotoxicity and the hydrolysis rate of different diamino bis(phenolato)Ti(O^iPr)$_2$ complexes have been analyzed, showing that the properties of the complex can be improved by changing the substituents. [144]–[148] The use of a second chelator together with diamino bis(phenolato) ligands (referred to as salan) have been studied and the use of dipic (Figure 44) showed improved hydrolytic stability, compared to the complex with alkoxo-ligands. [149], [150]

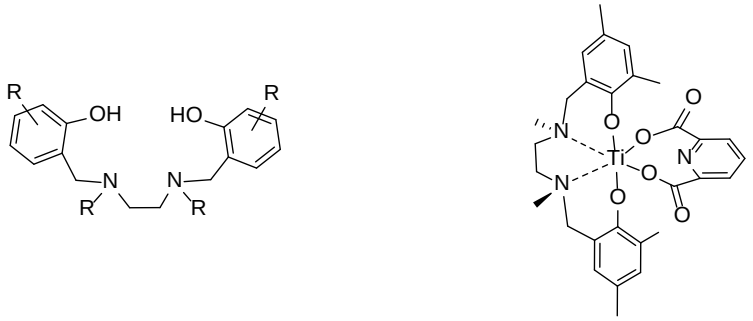

Diamino bis(phenolato) ligand (salan)Ti(dipic)

Figure 44: Structure of a diamino bis(phenolato) (left) and of the (salan)Ti(dipic) complex.

A ^{45}Ti complex with salan and dipic as ligands has previously been synthesized in this laboratory and evaluated *in vivo* to study the properties of (salan)Ti(dipic) as an anticancer agent. However, the circulation time and tumor uptake of [^{45}Ti](salan)Ti(dipic) was low, while the complex was metabolized relatively fast in the liver. It was expected that increasing the hydrophilicity of the complex might improve the tumor uptake. [65]

In this study, it was attempted to attach a targeting vector to one of the ligands of [^{45}Ti](salan)Ti(dipic) and to increase the hydrophilicity. Studies have showed that the dipic chelator can be modified with methoxy or hydroxymethyl groups at the 4-position without negative effect on the cytotoxicity, which makes it possible to further improve the properties of this type of titanium(IV) complexes. [150] Thus, it was attempted to attach the targeting vector to dipic.

A PSMA targeting vector was chosen due to the rapidly growing interest and development of PET tracers for the diagnosis of prostate cancer using small-molecule PSMA targeting vectors. [7] This development can also be seen in Figure 2 in section 1.3, where an increase in the number of publications regarding ^{68}Ga for PET was seen after 2012, which might be attributed to the introduction of ^{68}Ga-PSMA-11. It is important to clarify that PSMA is the biological target and not part of the radiotracer, e.g. ^{68}Ga-PSMA-11 does not contain PSMA, but is instead a ligand, which binds to PSMA. The promising results with ^{68}Ga-labeled PSMA targeting vectors have led us to an interest in developing a ^{45}Ti-based PSMA-targeted radiotracer.

10.1 Prostate cancer detection with PSMA-targeted small molecules

Prostate cancer is one of the most widespread cancer types among men. The imaging-based detection of prostate cancer can be performed by CT or MRI scan or with ^{99m}Tc-methylene diphosphonate bone scan, which is not specific for prostate cancer and the detection of small volumes of disease with these techniques are not efficient. [7] Thus, the detection of prostate cancer with other medical imaging methods is desirable. Small-molecule PET radiotracers as ^{11}C-choline, which is a substrate for the synthesis of cell membrane [151] and ^{18}F-FACBC,

which is a modified amino acid that is transported by upregulated channels in prostate cancer cells [152] have been approved by the FDA (Food and Drug Administration) for prostate cancer imaging. However, to improve the detection of prostate cancer the development of other PET radiotracers is ongoing. [7]

PSMA is a favorable target for small-molecule radiotracers in the detection of prostate cancer. It is a transmembrane protein consisting of 750-amino-acids. [153] In almost all cases of prostate cancer there will be a PSMA expression, which is 100-1000 times higher than the expression by normal tissue. A correlation between PSMA expression and the aggressiveness of the tumor has also been seen. Furthermore, a high tumor-to-background image can be achieved with radiotracers, since PSMA ligands are trapped in the cell due to internalization after the ligand binding. [7], [154]

PSMA is in the class of α-linked acidic dipeptidases (NAALADases) and can catalyze the formation of glutamate and *N*-acetyl-aspartate (NAA) from the hydrolysis of *N*-acetyl-apartyl-glutamate (NAAG). The development of small molecules which bind to PSMA have been based on different types of scaffolds, but they often include glutamate or similar molecules. The scaffold can have the structure as a substrate for PSMA and will then consist of amide or urea derivatives. The scaffold can also be phosphorus-based as phosphinate and phosphonates or thiol derivatives, which represents transition states of the NAALADase substrates (Figure 45).

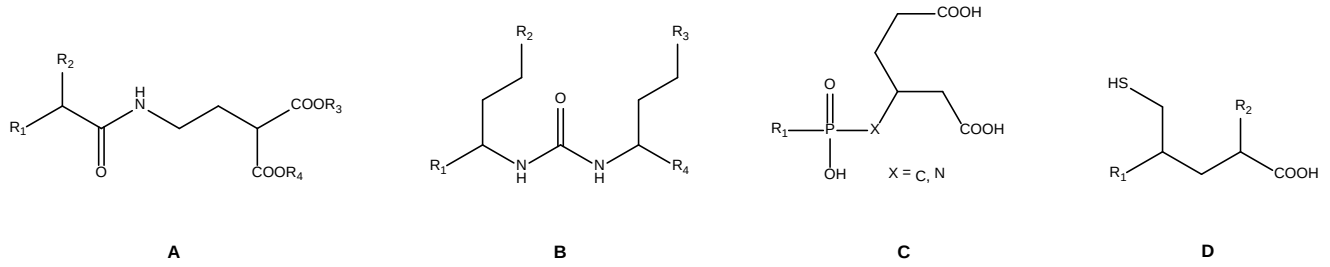

Figure 45: The general structure of substrates for NAALADase (A and B) and transition states of substrates (C and D). Amide- (A), urea- (B), phosphorus- (C), and thiol-based (D) derivatives.

The phosphorus-based PSMA ligands were first developed and high affinity for PSMA was obtained, but the polarity of the compounds was too high for good membrane permeability and bioavailability. This could be improved by producing thiol-based ligand, but these compounds were found to be unstable and having too low selectivity. [155] The following urea-based ligands showed improved properties. The first urea-based ligands consisted of two glutamate moieties connected by a urea-bond, but were further developed to glutamate-urea-lysine (Glu-urea-Lys), where the ε-amino group of lysine can be used to attach different groups. [155]

The structure of some promising urea-based PSMA-targeted radiotracers can be seen in Figure 46. The labeling of urea-based PSMA-targeted radiotracers with radiometals has primarily been done using ^{68}Ga. The lysine

moiety of Glu-urea-Lys has been modified with spacers attaching chelators to the PSMA binding motif making it possible to chelate ^{68}Ga. The beneficial and convenient radionuclide production from the ^{68}Ge/^{68}Ga generator and labeling made the study of ^{68}Ga-labeled small-molecule PSMA-targeted radiotracers widespread. ^{68}Ga-PSMA-11 shows encouraging properties for prostate cancer detection. The properties might be ascribed to the HBED-CC chelator, which makes the radiotracer slightly hydrophobic. [7] PSMA-617, which is a modification of PSMA-11, contains DOTA instead of HBED-CC as chelator making it possible to chelate therapeutic radiometals, such as ^{177}Lu, and can therefore be used for theranostic application with ^{68}Ga/^{177}Lu-PSMA-617. Furthermore, ^{68}Ga-PSMA-617 shows a lower inhibition constant (K_i) compared to ^{68}Ga-PSMA-11 (2.3±2.9 nM and 12.0±2.8 nM, respectively), but also slower pharmacokinetics, which can be challenging due to the short half-life of ^{68}Ga. [30] The promising results obtained with the ^{68}Ga-labeled PSMA-targeted radiotracers are expected to lead to an increased number of PSMA-PET scans. Thus, the production of ^{18}F-labeled radiotracers as ^{18}F-DCFPyL and ^{18}F-PSMA-1007 was started since large scale production of ^{18}F is possible at most hospital cyclotron sites. ^{18}F-DCFPyL and ^{18}F-PSMA-1007 have an aromatic moiety, which is expected to interact with a hydrophobic pocket close to the binding site of PSMA and both radiotracers have high tumor uptake and good imaging characteristics. [156]

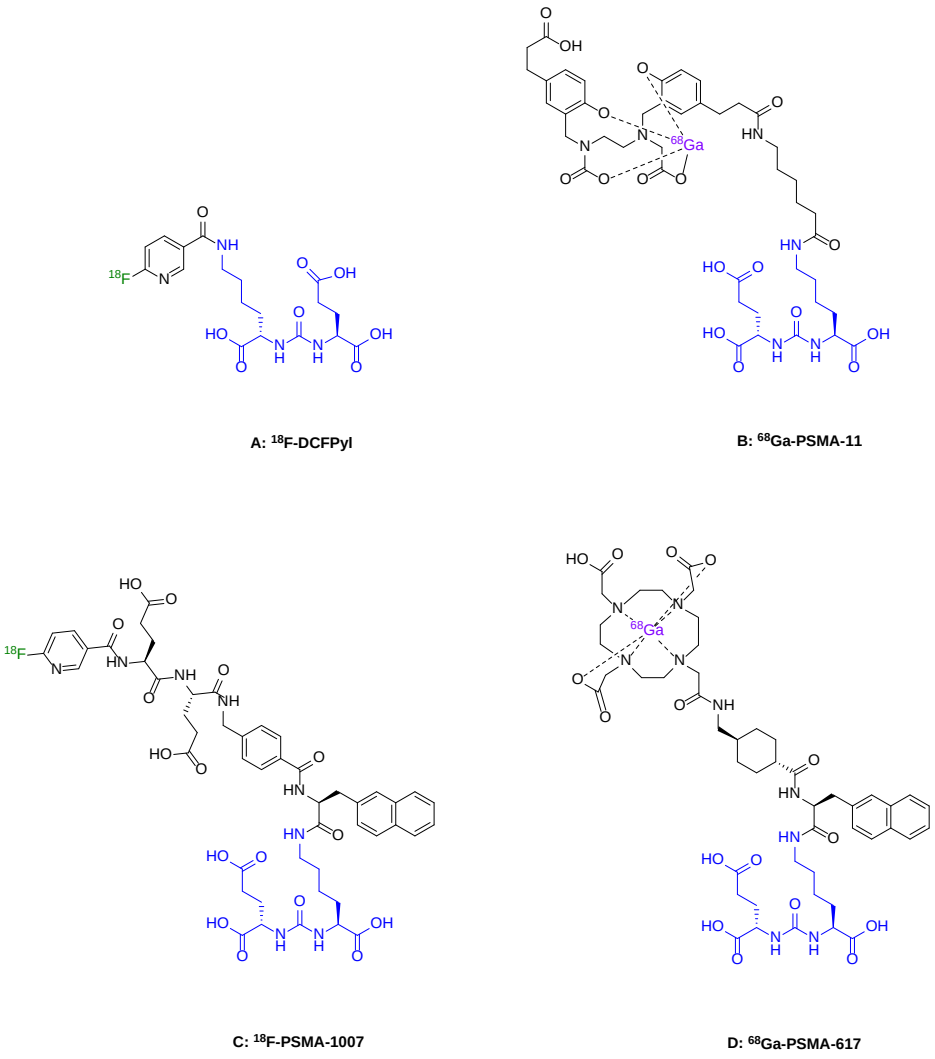

Figure 46: The structure of two ^{18}F-labeled (^{18}F-DCFPyl and ^{18}F-PSMA-1007) and two ^{68}Ga-labeled (^{68}Ga-PSMA-11 and ^{68}Ga-PSMA-617) small-molecule urea-based PSMA ligands. The Glu-urea-Lys moieties are marked with blue color.

The availability limitations of ^{68}Ga from the ^{68}Ge/^{68}Ga generator and the relative high β^+ end-point energy of ^{68}Ga (Table 1), support the interest in developing PSMA-targeted radiotracers with other radionuclides. When this development of a ^{45}Ti-labeled PSMA-targeted radiotracer was started, only preliminary results with ^{18}F-labeled PSMA-targeted radiotracers, such as ^{18}F-DCFPyl and ^{18}F-PSMA-1007, were obtained. [157], [158] The further study of ^{18}F-PSMA-targeted radiotracers showed promising results and the optimal physical properties and well-developed production method of ^{18}F makes it difficult to compete with ^{18}F-labeled PSMA-targeted radiotracers. However, the use of a radiometal as ^{45}Ti has the advantage of late-stage radiolabeling using a chelator, while ^{18}F needs to be introduced by a covalent bond. Furthermore, ^{45}Ti has a longer half-life than ^{18}F.

Additionally, the radiolabeling with ^{45}Ti and its uses for PET application have not been widely explored making it relevant to investigate the possibility of developing a ^{45}Ti-labeled PSMA-targeted radiotracer.

10.2 Design and synthesis of [^{45}Ti]Ti-CAS-PSMA: a prospective radiotracer

Due to the favorable prostate cancer imaging properties of ^{68}Ga-PSMA-11, ^{68}Ga-PSMA-617, ^{18}F-DCFPyL, and ^{18}F-PSMA-1007, a Glu-urea-Lys-based PSMA ligand with a ^{45}Ti-chelating moiety was synthesized and characterized. The structure can be seen in Figure 47. Two chelators, salan and chelidamic acid (Figure 47, red), were used for the chelation of ^{45}Ti, since the combination of salan and dipic has shown improved hydrolytic stability. The coordination of ^{45}Ti was expected to be similar to the one found from the crystal structure of (salan)Ti(dipic) by Immel et al. [149] Furthermore, the structure of salan is comparable to HBED, which is similar to the HBED-CC, applied as the chelator in PSMA-11 (Figure 46). A spacer (Figure 47, green), which was relatively short and simple to synthesize, was added to the hydroxy group of chelidamic acid. The spacer had an isothiocyanate group, which ensured a fast and efficient bond formation with the primary amine of the lysine moiety via a thiourea bond. The chelator and the spacer were used to attach ^{45}Ti to the Glu-urea-Lys PSMA binding motif (Figure 47, blue). This compound is referred to as [^{45}Ti]Ti-CAS-PSMA.

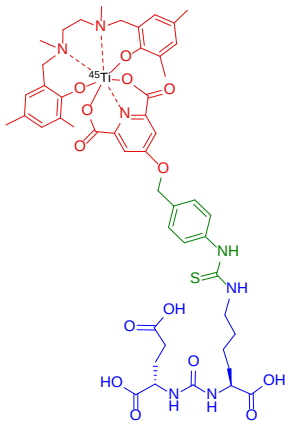

Figure 47: The structure of a ^{45}Ti-labeled urea-based PSMA ligand. Salan and chelidamic acid (red) were used as chelator and a spacer (green) was applied to attach the ^{45}Ti-chelating moiety to the PSMA binding motif, Glu-urea-Lys (blue).

10.2.1 Synthesis of CA-PSMA

The synthesis of the Glu-urea-Lys-based PSMA ligand (referred to as CA-PSMA) can be seen in Figure 48. First, the carboxylic acids of chelidamic acid were protected by forming the ethyl esters as described by Rizeq and Georgiades [159]. In an attempt to increase the reactivity of the hydroxy group of **1**, for the following ether synthesis with **3**, the thallium salt of **1** was formed subsequently (**2**) by a reaction of thallium(I) ethoxide with **1**. Compound **3** was synthesized from *p*-tolyl isothiocyanate, which was the main component of the spacer, by

bromination at the benzylic position, as described by Wang et al. [160] Compound **4** was formed by the ether synthesis of **2** and **3**, but also some unidentified impurities were formed. In an alternative one-pot approach, cesium carbonate was used as a base to deprotonate the hydroxy group of **1** for the ether synthesis with **3**. This reduced the number of synthesis steps towards CA-PSMA. Some unreacted **1** was seen when using an equimolar solution of **1** and **3**, while no remaining **3** could be seen by TLC and NMR. It was expected that a fraction of **3** might have decomposed or formed a by-product. The reaction was repeated with 2 equivalents of **3** and no remaining **1** was seen after the reaction time (2 h). The same was seen when reducing the amount to 1.5 equivalents of **3**. Unfortunately, a small amount of impurities, which were not identified, were also formed under these conditions. Furthermore, the excess of **3** needed to be removed. The separation and purification of **4** was challenging due to the similar polarity of the two impurities and the product. Different eluent systems for column chromatography were tested, but it was still challenging to isolate the product. However, the second approach was still found more efficient and thus used for the further synthesis.

The Glu-urea-Lys part of CA-PSMA was synthesized following the method described by Maresca et al. [161] The *tert*-butyl protected glutamic acid and the benzyloxy carbamate (Cbz) and *tert*-butyl protected lysine are used. Triphosgene was used to form the isocyanate intermediate in the presence of *N*,*N*-diisopropylethylamine (DIPEA) from the amine of glutamic acid, forming a urea-bond with the amine of lysine. The Cbz group was removed by hydrogenation, which led to the formation of compound **6**. The primary amine of lysine could now be attached to the spacer through the thiourea bond formation with the isothiocyanate group of **4**, leading to compound **7**. The coupling was fast and without any side-reactions. However, the product was in some cases purified using column chromatography, if a small excess of one of the starting materials was added. Compound **7** is the fully protected analog of the final CA-PSMA ligand.

Different orders of the removal of the protecting groups were tested. In the first approach, the removal of the *tert*-butyl groups was successfully done using trifluoroacetic acid (TFA) in dichloromethane (DCM) (compound **8**). The ethyl esters were then removed by hydrolysis using NaOH in water (CA-PSMA). For the second approach, the ethyl esters were first hydrolyzed with LiOH in tetrahydrofuran (THF)/water (compound **9**), followed by removal of the *tert*-butyl groups with TFA in DCM (CA-PSMA). The second approach seemed more suitable for the synthesis of CA-PSMA. A higher concentration of base (6 equiv. vs. 2.2 equiv.) was needed if the hydrolysis of the ethyl esters was the final step and the sodium salt of CA-PSMA was formed as in the first approach. By removing the *tert*-butyl groups as the final step, all carboxylic acids of CA-PSMA were expected to be protonated and a high solubility in DMSO was seen, which is compatible with the further synthesis of Ti-CAS-PSMA. In summary, the synthesis of CA-PSMA was performed in 8 steps, where the longest linear sequence was 6 steps with an overall yield of 28 %. The purification of compound **4** was

challenging and the yield of the synthesis of compound **5** was low, which resulted in a decreased overall yield. The coupling between **4** and **5** and the following deprotection steps were, however, efficient and led to the final product.

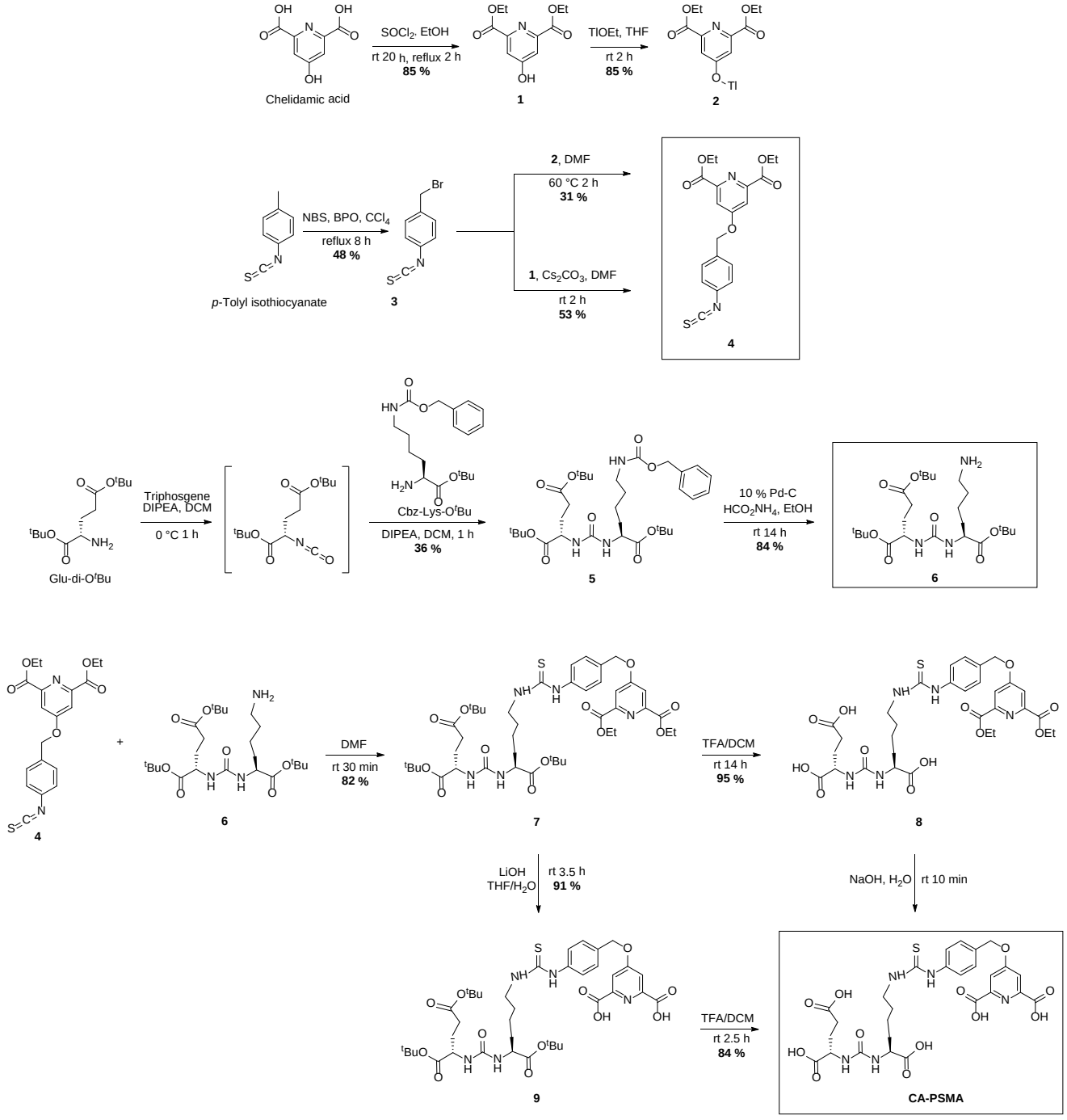

Figure 48: The synthesis route of the Glu-urea-Lys-based PSMA ligand with a Ti-chelating moiety (CA-PSMA). (rt: room temperature, NBS: *N*-bromosuccinimide, BPO: benzoyl peroxide)

10.2.2 Chelation of titanium and formation of Ti-CAS-PSMA

The formation of the nonradioactive Ti-CAS-PSMA complex is performed by the routes presented in Figure 49. The synthesis of (salan)Ti(O^iPr)$_2$ (compound **10**) has been described previously by Chmura et al. [162] The first attempt to form Ti-CAS-PSMA was by dissolving (salan)Ti(O^iPr)$_2$ (**10**) in pyridine and adding CA-PSMA, which was synthesized by the first deprotection approach. This was not possible, since the CA-PSMA was insoluble in pyridine. Pyridine was chosen as solvent since it can quench residual HCl from the purification of ^{45}Ti and has previous been applied as solvent for the radiolabeling with ^{45}Ti. [65], [81]

In the next attempt, the synthesis of the *tert*-butyl-protected titanium-complex **11**, using compound **9** as chelator was performed. Thereby, a possible interference from the carboxylic acids of the glutamate moiety on the titanium complexation could be avoided. The complex could be formed in pyridine and was purified and analyzed by NMR. Next, the *tert*-butyl groups were removed with TFA in DCM. The treatment with TFA seemed to decompose the complex partially and only a small amount of Ti-CAS-PSMA was formed. Furthermore, it would be more convenient to avoid a deprotection step, when forming the radioactive [^{45}Ti]Ti-CAS-PSMA due to the relative short half-life of ^{45}Ti.

An attempt using CA-PSMA, which was synthesized using the second deprotection approach, was studied. This time CA-PSMA and (salan)Ti(O^iPr)$_2$ were dissolved in DMSO and Ti-CAS-PSMA was formed within 15 minutes at 60 °C. The formed Ti-CAS-PSMA still needed to be purified, which was possible with preparative TLC/HPLC. This approach was found suitable for the formation of [^{45}Ti]Ti-CAS-PSMA. Thus, the conditions for the radiolabeling were tested, where nonradioactive $TiCl_4$ was used as titanium-source. Titanium was extracted with guaiacol/anisole 9/1 (v/v) from 12 M HCl, as described in section 5.3.3. Salan and CA-PSMA were dissolved in DMSO and added to the organic Ti-containing guaiacol/anisole phase and the purified Ti-CAS-PSMA could be obtained by preparative HPLC. Hence, the method was expected to be suitable for the radiolabeling with ^{45}Ti.

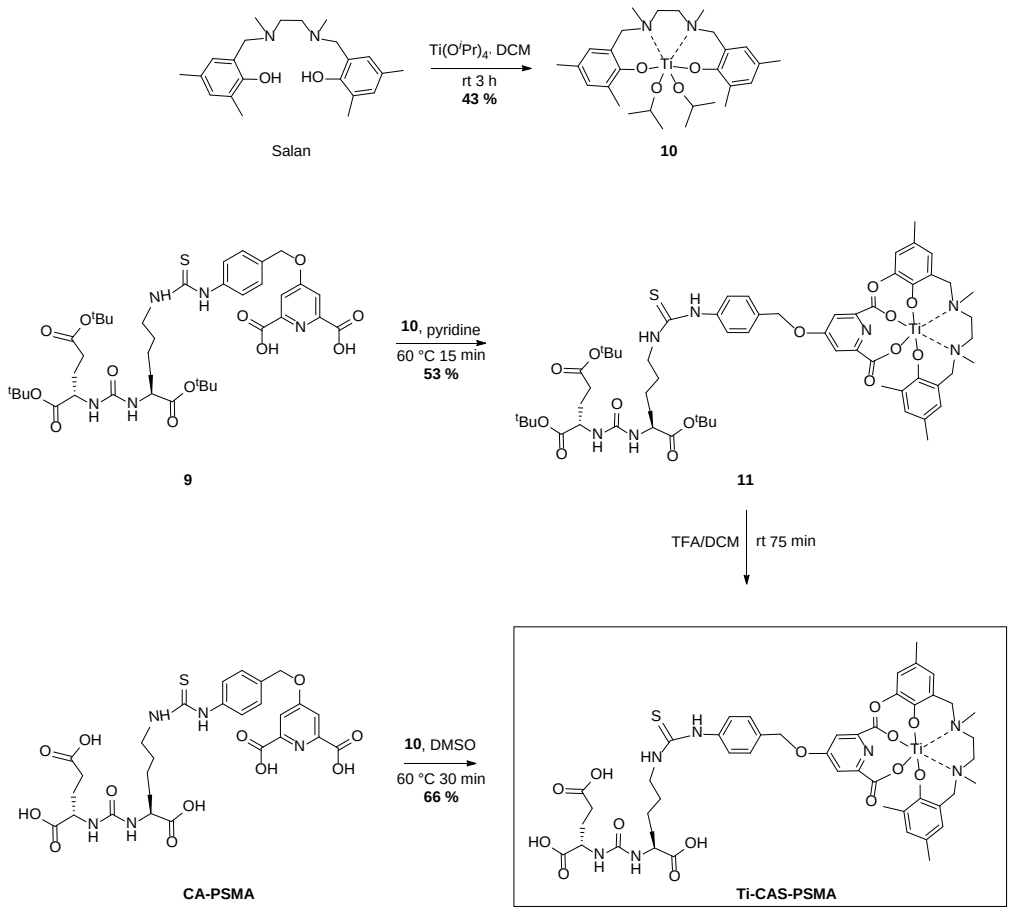

Figure 49: The synthesis route of the nonradioactive Ti-complex (Ti-CAS-PSMA).

10.2.3 Production and purification of ^{45}Ti

^{45}Ti was produced from natural scandium foil with two different thicknesses (250 µm and 127 µm). The experimental saturation yield and the percentage ratio of the theoretical saturation yield for the two different thicknesses, as well as the masses of scandium foil applied, can be seen in Table 9. The experimental values were calculated from the ^{45}Ti radioactivity at the end of bombardment (EOB), the proton beam current, and irradiation time. The theoretical values were calculated from the cross section data of the ^{45}Sc(p,n)^{45}Ti nuclear reaction found in the EXFOR database (Figure 14) and the stopping power calculated using SRIM (Stopping and Range of Ions in Matter) software. From the results in Table 9, it could be seen that the experimental saturation yield was decreasing when lowering the mass of the thick scandium foil (250 µm). This was due to the reduction of the size (area) of scandium foil, which increased the risk of not hitting the scandium foil with the entire beam profile. Thus, a decreased mass of scandium foil could be used with the thinner foil. The reason for reducing the mass of scandium foil was to facilitate the following purification by LLE separation, and decreasing the amount

of nonradioactive titanium impurity introduced by the foil. Thus, another way to lower the mass of scandium foil to around 30 mg was achieved by using a thinner scandium foil (127 µm), and thereby not critically reducing the size (area) of the scandium foil.

Table 9: The experimental saturation yields and percentages of the theoretical yield for the $^{45}Sc(p,n)^{45}Ti$ nuclear reaction using two different thicknesses and different masses of scandium foil.

	Mass of scandium foil (mg)	Experimental saturation yield (MBq/µA)	Ratio of theoretical saturation yield (%)
Thick (250 µm) scandium foil	56-80	1837 ± 24	82 ± 1
	46-52	1461 ± 336	65 ± 15
	31-43	1198 ± 393	53 ± 17
Thin (127 µm) scandium foil	33	847 ± 223	76 ± 20
	22-25	653 ± 250	59 ± 22

As described in section 5.3.3, the guaiacol/anisole 9/1 (v/v) mixture was found to be most suitable for the LLE of titanium. The same method was used to obtain ^{45}Ti for the radiolabeling of the synthesized CA-PSMA ligand. The extraction was performed both with the membrane separator but also with LLE in batch. From the optimizations in section 5.3.3, it could be seen that the extraction was improved by using a ratio of 1:3 of the aqueous and organic phase. This ratio was first applied, but later it became clear that the large volume of organic phase after the LLE was inconvenient for the further isolation of [^{45}Ti]Ti-CAS-PSMA.

Both guaiacol and anisole have a high boiling point, 205 °C and 154 °C respectively, so it would be challenging to evaporate the solvents. Additionally, the amount of concentrated HCl used for dissolving the scandium foil after irradiation could not be reduced, since the concentration of HCl decreases when dissolving scandium due to the formation of $ScCl_3$ and H_2. The extraction of titanium is less efficient when the HCl concentration is below 11 M (section 5). As described above, the mass of scandium foil was reduced by applying thinner scandium foil (127 µm) and it was tested, if a decreased amount of organic phase could be applied for the LLE. The average extraction of ^{45}Ti at three different aqueous-to-organic ratios can be seen in Table 10. It should be noted that different masses of scandium foil and volumes of HCl were used, which result in different HCl concentration and amount of scandium per volume of HCl. These conditions also influence the extraction efficiency. The lowest amount of scandium which was used was 22 mg scandium foil and the lowest volume of 12 M HCl used to dissolve the foil was 3 mL. This gave a final HCl concentration of 11.7 M. When using a ratio of 1:1.33 (aq:org) a ^{45}Ti extraction of 77 % was achieved. This was close to the average extraction when using a ratio of

1:3 (aq:org) and resulted only in 4 mL organic phase instead of 9 mL. These conditions were acceptable for the further radiolabeling and no further optimizations were made.

Table 10: The average ^{45}Ti extraction at different aqueous to organic ratios is listed. The mass of scandium foil, the concentration of HCl after dissolving the scandium foil and the mass of scandium per HCl volume are listed as a range.

Sc foil (mg)	Concentration of HCl after dissolving foil (M)	Sc/HCl (mg/mL)	Aq:org ratio	Average extraction %
42-80	10.9-12.0	2.6-18.7	1:3	77.7 ± 10.8
22-36	11.4-11.7	7.3-12.0	1:1.33	68.0 ± 6.5
31-57	11.2-12.0	2.3-14.3	1:1	59.0 ± 5.8

10.2.4 Radiolabeling optimizations

For the synthesis of [^{45}Ti]Ti-CAS-PSMA, ^{45}Ti was introduced probably as a guaiacol complex ([^{45}Ti]TiCl$_2$(guaiacolato)$_2$) from the LLE step before the radiolabeling. Salan and CA-PSMA were added to the ^{45}Ti-containing organic phase from the LLE leading to the final [^{45}Ti]Ti-CAS-PSMA complex (Figure 50).

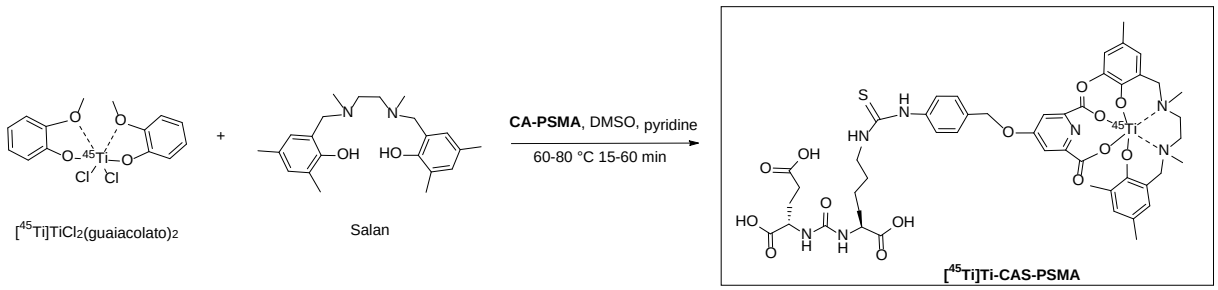

Figure 50: The radiolabeling with ^{45}Ti forming [^{45}Ti]Ti-CAS-PSMA. ^{45}Ti is assumed to be chelated by guaiacol from the LLE step.

As shown in Table 11, various conditions for the radiolabeling were tested to improve the radiolabeling yield. The LLE conditions were varied with different aqueous-to-organic phase ratios, as described in section 10.2.3. The radiolabeling was performed at either 60 or 80 °C, where salan dissolved in DMSO, was added first and the reaction mixture was stirred for 5 minutes before CA-PSMA, dissolved in DMSO, was added. Different volumes of the organic phase from the ^{45}Ti LLE were applied for the radiolabeling. In some experiments pyridine was added to the radiolabeling solution.

Table 11: The tested radiolabeling conditions: solvent volume, temperature, LLE method and ratio between aqueous and organic phase, volume of organic phase, amount and concentration of salan and CA-PSMA and the mixing time.

No.	Solvent	Temperature (°C)	LLE method (aq:org)	Volume of organic phase (mL)	Salan (mg)	CA-PSMA (mg)	Concentration of salan and CA-Glu-urea-Lys (mM)	Time (m)
1	DMSO (0.6 mL)	60	Flow (1:3)	0.5	8	15	20.7	30
2	DMSO (1mL)	60	Batch (1:3)	0.5	8	15	15.2	80
				0.5	16	30	30.4	
3	DMSO (1 mL)	60	Batch (1:3)	0.5	8	15	15.2	60
				2			7.6	80
4	DMSO (1 mL)	80	Batch (1:3)	0.5	8	15	15.2	60
	DMSO (4 mL)			2			2.0	
5	DMSO (1 mL)	80	Batch (1:3)	0.5	8	15	15.2	60
				1			11.4	
	DMSO (2 mL)		Batch (1:1)	0.5	16	30	18.2	
				1			15.2	
6	DMSO (1.6 mL) Pyridine (0.8 mL)	80	Batch (1:1)	2	8	15	5.2	60
					4	7.5	2.6	
7	DMSO (1.6 mL) Pyridine (0.8 mL)	80	Batch (1:1)	2	8	15	5.2	15
	DMSO (0.6 mL) Pyridine (0.2 mL)			1	4	7.5	6.3	60
8	DMSO (1.6 mL) Pyridine (0.8 mL)	80	Batch (1:1)	4	8	15	3.6	60

9	DMSO (1.6 mL) Pyridine (0.8 mL)	80	Batch (1:1.33)	4	8	15	3.6	15

The radiolabeling with ^{45}Ti was initially performed at 60 °C followed by radio-TLC analysis (Table 11, entry 1). It was not possible to conclude, if and to which extent [^{45}Ti]Ti-CAS-PSMA was formed by the radio-TLC, since the radiolabeling solution contained high boiling point solvents, which were difficult to dry on the TLC-plate, leading to tailing of the compounds. An example of this can be seen in Figure 51. The R_f value of the reference Ti-CAS-PSMA was 0.31, and it was therefore assumed that 18 % of [^{45}Ti]Ti-CAS-PSMA was formed, since the area of the peak at a R_f value of 0.28 (Figure 51, blue) was 18 %. However, this was slightly unclear due to overlapping peaks.

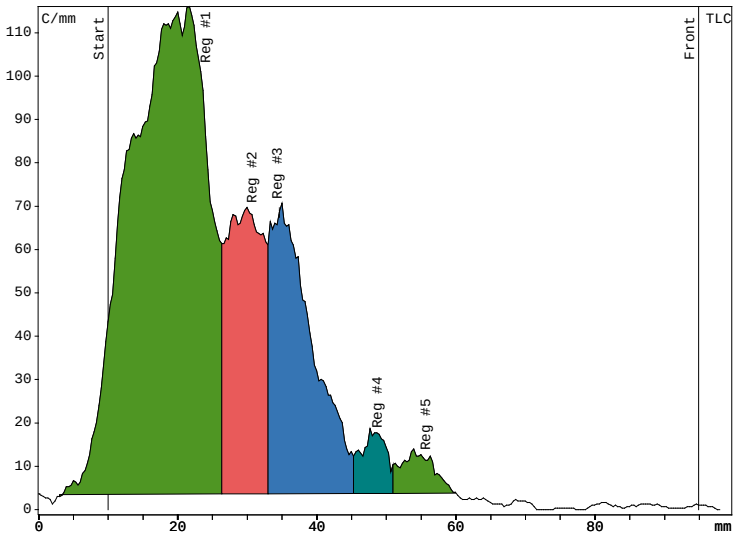

R_f	Area (%)
0.102	53.96
0.239	15.06
0.286	17.59
0.451	2.20
0.537	1.95

Figure 51: Radio-TLC chromatogram with R_f values and area percentages from the radiolabeling at 60 °C after 30 minutes (Table 11 entry 1). It was assumed that the peak at a R_f value of 0.28 (blue) corresponded to [^{45}Ti]Ti-CAS-PSMA, since the R_f value of Ti-CAS-PSMA was 0.31.

Instead, the following radiolabeling experiments were followed over time by radio-HPLC, where the retention time of the radio-signal was compared to the UV-signal of the reference Ti-CAS-PSMA. The retention time of Ti-CAS-PSMA was 7.7 minutes with the applied gradient. The UV-signal at 270 nm and 420 nm can be seen in Figure 52. The radio-detector connected to the HPLC was placed after the UV-detector, delaying the peak from [^{45}Ti]Ti-CAS-PSMA compared to the UV-signal.

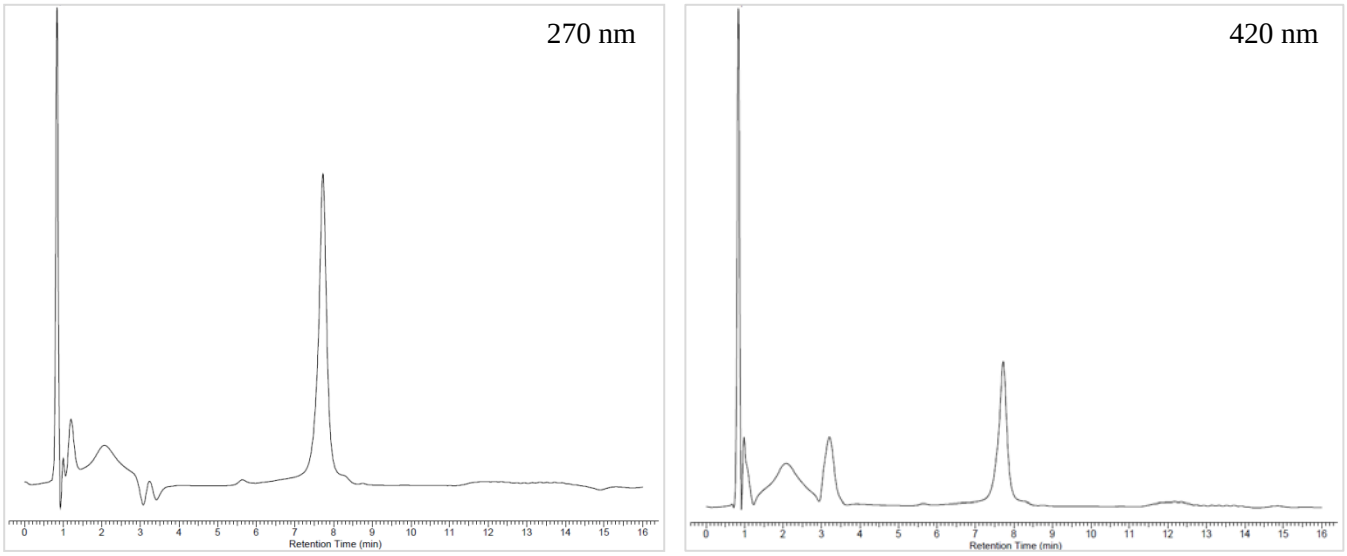

Figure 52: The HPLC chromatogram of Ti-CAS-PSMA, where the left chromatogram is the UV-signal at 270 nm and the right the UV-signal at 420 nm. The retention time of Ti-CAS-PSMA was 7.7 minutes.

In the first radiolabeling experiments small volumes of the organic phase from the LLE were used and the labeling was performed at 60 °C (Table 11, entry 2-3). Here, 0.5 mL organic phase was mixed with salan and CA-PSMA (15 mM). Within 60 minutes approximately 50 % of ^{45}Ti was chelated as [^{45}Ti]Ti-CAS-PSMA, which can be seen from the HPLC chromatogram in Figure 53. The peak with a retention time of 8.0 minutes was expected to arise from [^{45}Ti]Ti-CAS-PSMA, while the peak at the beginning might be ^{45}Ti chelated by guaiacol.

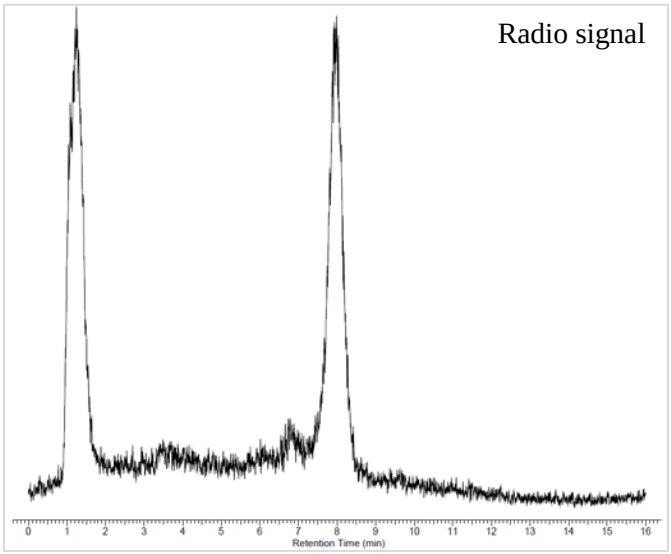

Figure 53: The radio signal of a HPLC chromatogram of a sample from the radiolabeling solution after 60 minutes at 60 °C can be seen. The retention time of the expected [^{45}Ti]Ti-CAS-PSMA peak was 8.0 minutes and the area of the peak corresponded to 47 % of the total area.

In order to improve the radiolabeling, the concentration of salan and CA-PSMA was doubled, but this did not lead to higher radiolabeling yield. The radiolabeling yield over time can be seen in Figure 54. The radiolabeling with a lower concentration (7.6 mM) was tested by increasing the volume of the organic phase from the LLE to 2 mL. Unfortunately, this resulted in no radiolabeling.

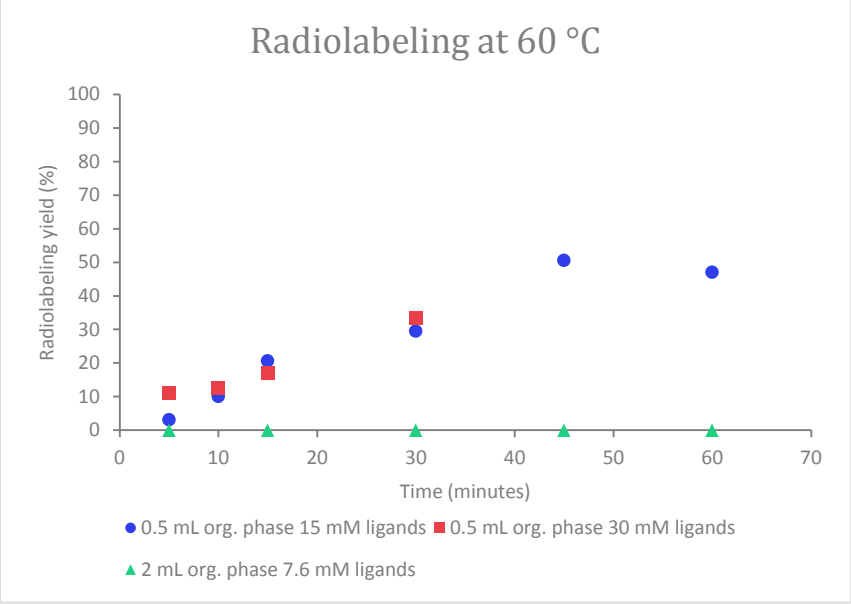

Figure 54: The radiolabeling yield at different time points at 60 °C analyzed by radio-HPLC. Blue circles: 0.5 mL organic phase with 15 mM salan and CA-PSMA (Table 11 Entry 2-3), red squares: 0.5 mL organic phase with 30 mM salan and CA-PSMA (Table 11 Entry 2), green triangles: 2 mL organic phase with 7.6 mM salan and CA-PSMA (Table 11, Entry 3).

The temperature was increased to evaluate if a higher radiolabeling yield could be obtained. The previous radiolabeling experiments with 0.5 mL and 1 mL organic phase from the LLE were tested at 80 °C (Table 11, entry 4-5). Now, up to 90 % of ^{45}Ti formed [^{45}Ti]Ti-CAS-PSMA after 60 minutes, and already after 15 minutes a high radiolabeling of 80 % was achieved (Figure 55). The radiolabeling with 2 mL of organic phase with a lower concentration of salan and CA-PSMA (2.0 mM), still did not lead to any radiolabeling.

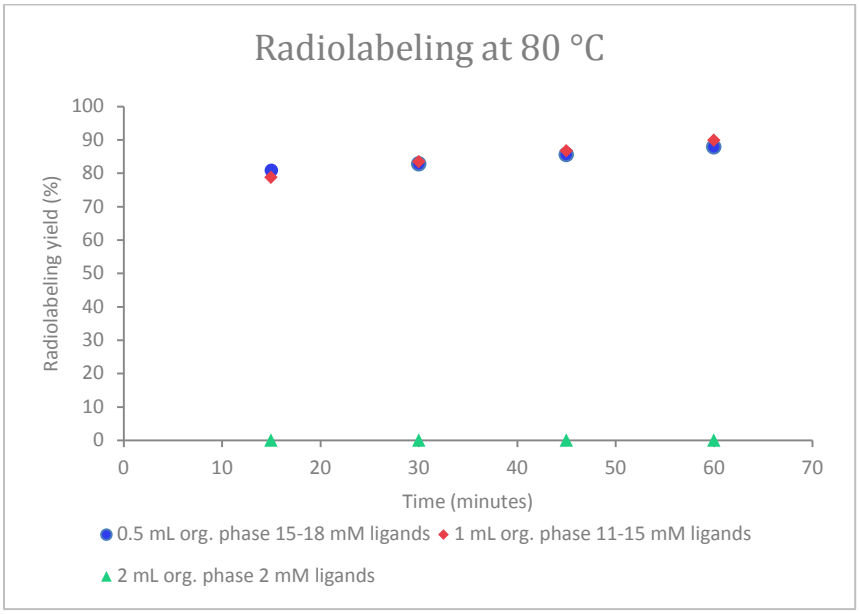

Figure 55: The radiolabeling yield at different time points at 80 °C analyzed by radio-HPLC. Blue circles: 0.5 mL organic phase with 15-18 mM salan and CA-PSMA (Table 11 Entry 4-5), red diamonds: 1 mL organic phase with 11-15 mM salan and CA-PSMA (Table 11 Entry 5), green triangles: 2 mL organic phase with 2 mM salan and CA-PSMA (Table 11 Entry 4).

It was suspected that a small amount of HCl could be dissolved in guaiacol/anisole, when the organic phase is mixed with the concentrated HCl solution during the LLE. The acid could thereby protonate the ligands and reduce the chelation of ^{45}Ti, which could explain why no [^{45}Ti]Ti-CAS-PSMA was formed at lower ligand concentration. In order to test this, pyridine was added as a base to the organic phase after the LLE and before the addition of salan and CA-PSMA (Table 11, entry 6-10). Now, 85 % of ^{45}Ti was found as [^{45}Ti]Ti-CAS-PSMA already after 5 minutes (Figure 56 and Figure 57). In the final optimization step, the concentration of salan and CA-PSMA was decreased to 2.6-5.7 mM and different volumes of organic phase were used. The volume of pyridine was also decreased from 20 % of the total volume to 12.5 %. The radiolabeling yield was also high with the lower concentration of salan and CA-PSMA and with the total amount of organic phase after LLE (4 mL). The conditions were not optimized further, so the same concentrations and volumes were used for the following radiolabeling experiments. A reaction time of 15 minutes was found to be sufficient and an aqueous-to-organic phase ratio for the LLE at 1:1.33 was used (Table 11, Entry 9).

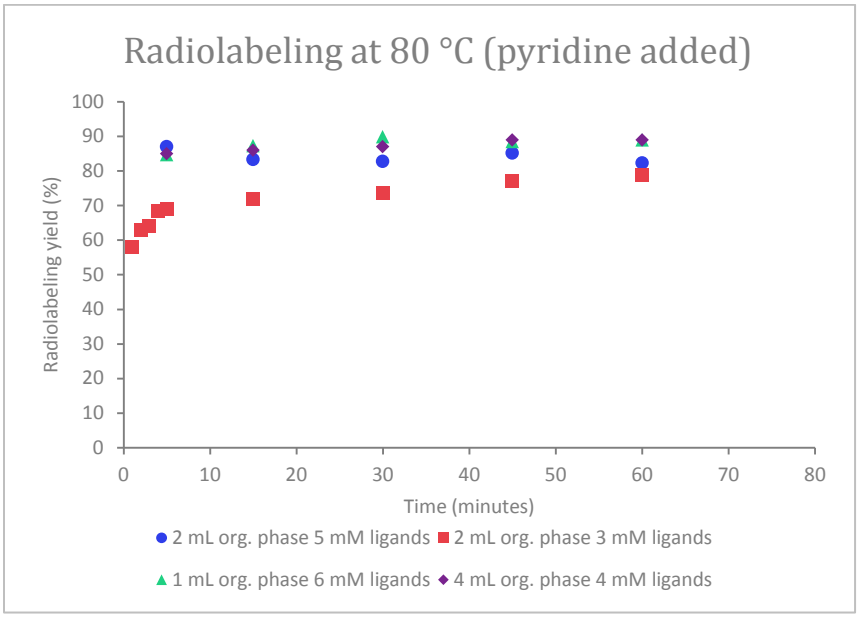

Figure 56: The radiolabeling yield at 80 °C with the addition of pyridine, analyzed at different time points by radio-HPLC. Blue circles: 2 mL organic phase with 5 mM salan and CA-PSMA (Table 11**,** Entry 6-7), red squares: 2 mL organic phase with 3 mM salan and CA-PSMA (Table 11 Entry 6), green triangles: 1 mL organic phase with 5 mM salan and CA-PSMA (Table 11**,** Entry 7), purple diamonds: 4 mL organic phase with 4 mM salan and CA-PSMA (Table 11**,** Entry 8).

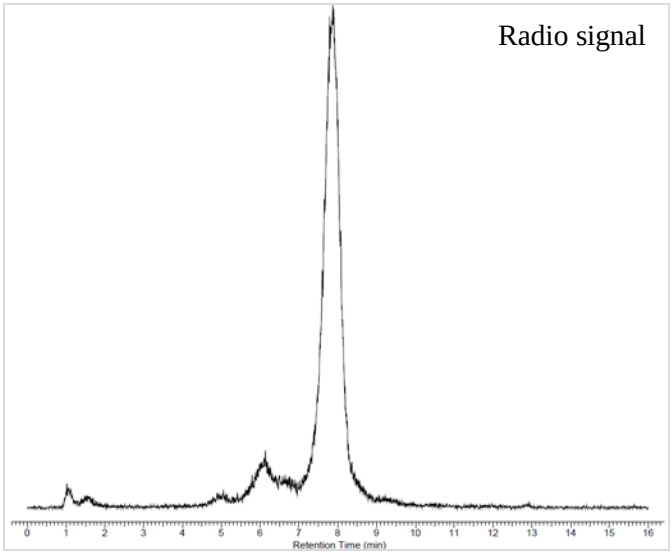

Figure 57: The radio-HPLC chromatogram of a sample from the radiolabeling solution containing 0.2 mL pyridine and 6.3 mM salan and CA-PSMA after 5 minutes at 80 °C. The retention time of the main peak, expected to be [^{45}Ti]Ti-CAS-PSMA was 7.9 minutes and the area of the peak corresponds to 85 % of the total peak area.

10.2.5 Purification of [^{45}Ti]Ti-CAS-PSMA

The next step after the radiolabeling was the purification of [^{45}Ti]Ti-CAS-PSMA. The product needed to be separated from the excess salan and CA-PSMA, but also from [^{45}Ti]Ti-impurities. Furthermore, the [^{45}Ti]Ti-CAS-PSMA was in a large volume (6 mL) of high boiling point solvents after the radiolabeling, which was not compatible with the formulation of the radiotracer product. In order to remove the solvents, it was attempted to trap [^{45}Ti]Ti-CAS-PSMA on different types of cartridges, followed by elution in a more suitable solvent e.g. methanol or water. An overview of the different cartridges evaluated can be seen in Table 12. The radiolabeling solution was either loaded directly on the cartridge or diluted with toluene before. The best adsorption to the cartridge was obtained by using an alumina N cartridge. A polar eluent was needed in order to elute the product from this cartridge and it was only possible applying 60 % with 1-butanol (BuOH)/H_2O/acetic acid (AcOH) (4/1/1). The volume needed was also relative high (6 mL). A similar problem was seen when using the silica cartridges. Only a small percentage of the product was trapped on C18 cartridges, which was expected to be due to the large volume of relatively polar solvents. On the QMA cartridges, it was only a small amount of the product that was adsorbed, since the product was washed out with water. Consequently, as no optimal cartridge was found, preparative HPLC was used to purify the [^{45}Ti]Ti-CAS-PSMA directly after the radiolabeling.

Table 12: The different cartridges, which were evaluated in the separation of the [^{45}Ti]Ti-CAS-PSMA from the radiolabeling reaction mixture. The solutions used for loading the reaction mixture on the cartridge and the percentage trapped on the cartridge can be seen. The solvent used for washing the cartridge and eluting the [^{45}Ti]Ti-CAS-PSMA are listed and the percentage of the [^{45}Ti]Ti-CAS-PSMA removed by the washing and elution and the total recovery percentage have been calculated. ACN: acetonitrile, DCM: dichloromethane

Cartridge	Loading	Wash	Elute	Recovery
Silica plus	Diluted with toluene (1:2) 40 %	Toluene 3 %	MeOH/H_2O 1/1 (v/v) (22 mL) 78 %	30 %
Alumina N	Diluted with toluene (1:2) 98 %	DCM 1 %	BuOH/H_2O/AcOH (4/1/1) (6mL) 61 %	60 %
C18 plus	Diluted with toluene (1:2) 7 %	Toluene 23 %	ACN/H_2O 6/4 (v/v) 1 %	0.2 %
QMA (CO_3^{2-})	Not diluted 82 %	Water 35 %	-	-

Given the disappointing results with the cartridge purification, we turned to preparative HPLC. The purification with preparative HPLC was first tested with the nonradioactive Ti-CAS-PSMA. The product was eluted as three different peaks (Figure 58), but when analyzing the individual product from the three different peaks on an analytical HPLC, they all had the same retention time. A peak was seen after the two first product peaks. A fraction containing this peak was analyzed with analytical HPLC and the compound was expected to be anisole, since the retention time of the peak (3.7 minutes) was similar to the one for the HPLC chromatogram of anisole (Figure 59). It was tested if the addition of an acid (HCl in dioxane) before loading on the preparative HPLC could result in one peak, if the three peaks were a result of different degrees of deprotonation. But still three peaks were seen. The product from the three peaks were combined and dried and analyzed by NMR. It was consistent with the structure of Ti-CAS-PSMA. Afterwards, the product was dissolved in DMSO and reloaded on the preparative HPLC again. Now, only one product peak was seen (Figure 58), but an increase in UV intensity of the baseline was additionally observed before and after the peak, which might be due to an artifact. However, this was not further examined. It was expected that the three product peaks were due to the large volume of the relatively polar organic solvents injected affecting the interaction with the C18 column.

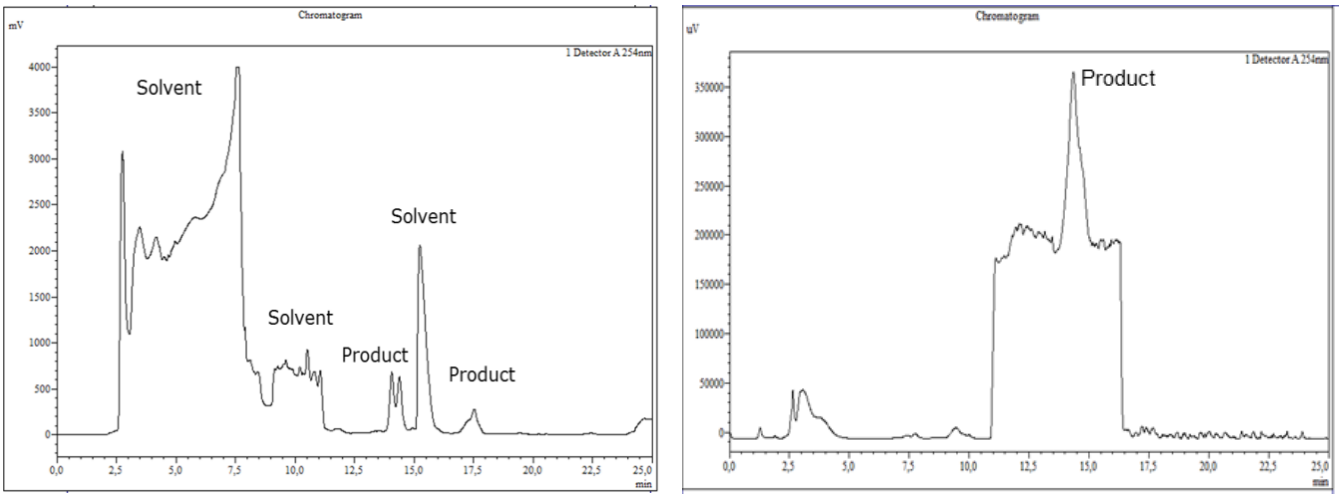

Figure 58: Left: Preparative HPLC chromatogram with UV signal at 254 nm of the test-labeling with nonradioactive Ti-CAS-PSMA. Right: Preparative HPLC chromatogram with UV signal at 254 nm of the product from the three product peaks in the left chromatogram, where the product was dried, dissolved in DMSO and then injected on preparative HPLC.

Next, the purification of [^{45}Ti]Ti-CAS-PSMA using preparative HPLC was tested. The fractions collected from HPLC were analyzed by measuring the radioactivity with a dose calibrator to quantify the amount of ^{45}Ti and by analytical HPLC, in order to identify the fractions containing the pure [^{45}Ti]Ti-CAS-PSMA. The radio signal was used to see if other [^{45}Ti]Ti-compounds were present, while the UV signal was used to evaluate if the guaiacol/anisole and the free CA-PSMA and salan were separated from [^{45}Ti]Ti-CAS-PSMA. The

chromatograms at 270 nm for salan, CA-PSMA, pyridine, guaiacol, anisole, and DMSO can be seen in Figure 59. The HPLC gradient was optimized to improve the amount of pure [^{45}Ti]Ti-CAS-PSMA that could be collected, but it was still not possible to separate all of the product from impurities, since some fractions contained the product and small amount of [^{45}Ti]Ti-impurities or anisole. HPLC chromatograms before and after the purification with preparative HPLC can be seen in Figure 60. The large solvent peaks before the purification has been removed, which can be seen from the UV-signal at 270 nm and the ^{45}Ti-impurities were also removed, which can be seen by the radio-signal.

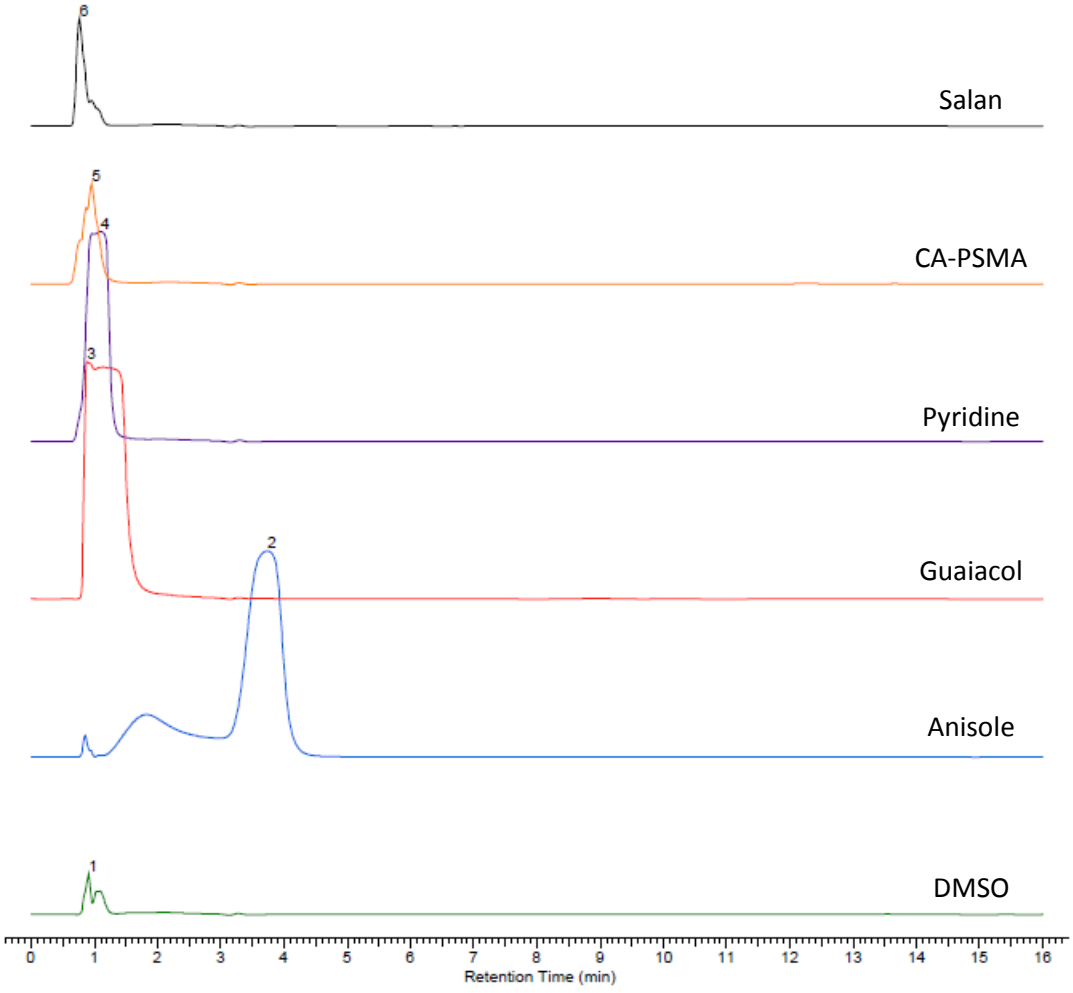

Figure 59: The analytical HPLC chromatograms at 270 nm for salan (black, no. 6), CA-PSMA (orange, no. 5), pyridine (purple, no. 4), guaiacol (red, no. 3), anisole (blue, no. 2), and DMSO (green, no. 1).

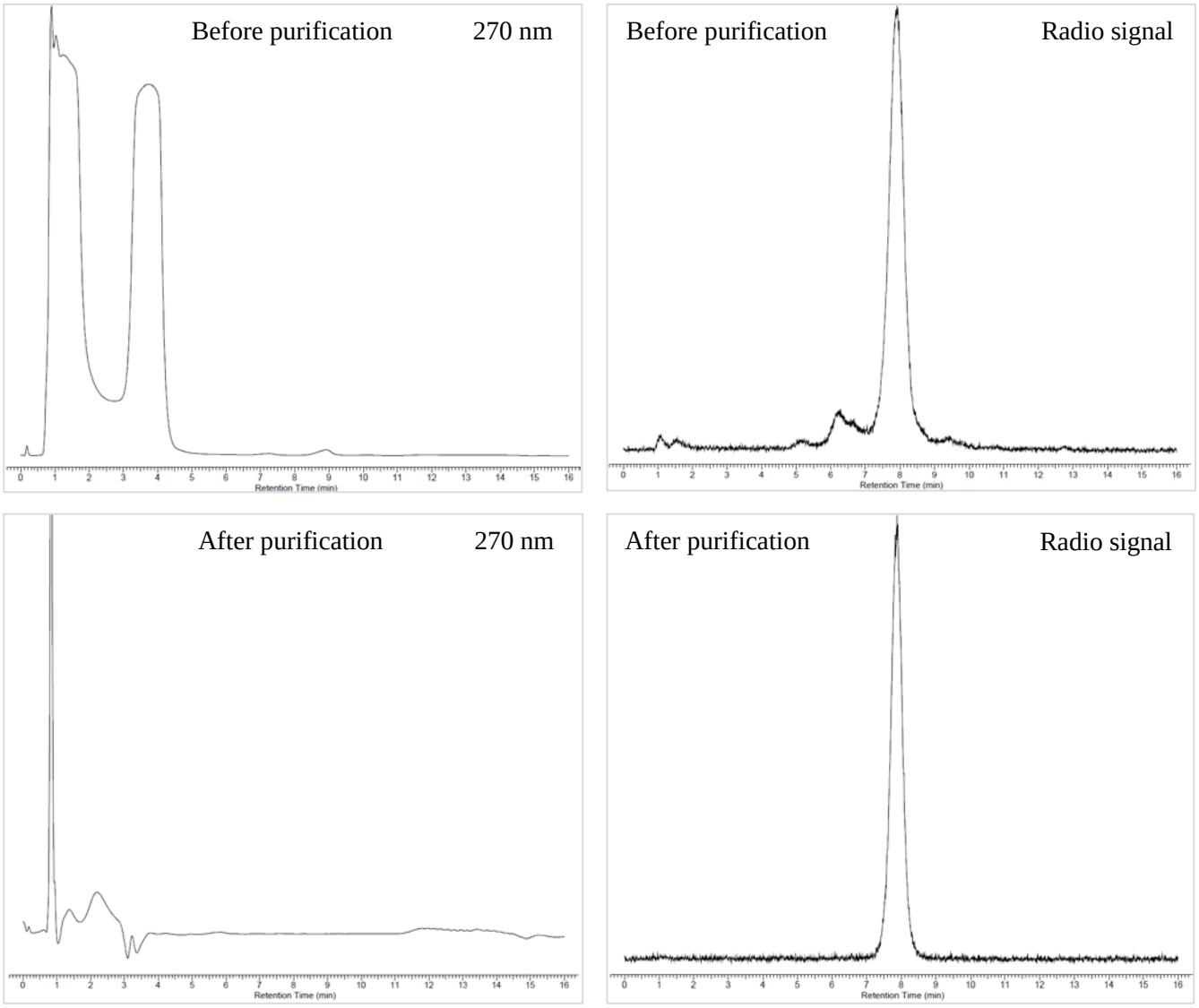

Figure 60: HPLC chromatograms (both UV-signal and radio-signal) before and after the purification of [^{45}Ti]Ti-CAS-PSMA by preparative HPLC. Top left: The UV-signal at 270 nm before purification, top right: The radio-signal before purification, lower left: The UV-signal at 270 nm after purification, lower right: The radio-signal after purification.

[^{45}Ti]Ti-CAS-PSMA was in a relative large volume (20-40 mL) of ACN/H_2O after preparative HPLC, the product was therefore concentrated on a C18 cartridge and then eluted in a small volume (1.5 mL) of EtOH/H_2O. In this step, 86.3±7.1 % of [^{45}Ti]Ti-CAS-PSMA could be recovered. The main loss of the product was on the cartridge. The [^{45}Ti]Ti-CAS-PSMA could be concentrated further by evaporating the EtOH/H_2O down to 50-100 µL under argon flow. The final product formulation of [^{45}Ti]Ti-CAS-PSMA was obtained by adding PBS (phosphate-buffered saline) buffer or HEPES (4-(2-hydroxyethyl)-1-piperazineethanesulfonic acid) buffer to the small amount of EtOH/H_2O.

The radiochemical yield (RCY) at the end of synthesis and purification (EOS) of [^{45}Ti]Ti-CAS-PSMA was 13.0 ± 5.6% decay corrected (d.c.) and 5.1 ± 2.3 % non-decay corrected (n.d.c.). The main reasons for the low RCY were found in the separation of ^{45}Ti by LLE, where 20-40 % of the total ^{45}Ti was left in the aqueous phase after LLE, and in the purification of [^{45}Ti]Ti-CAS-PSMA by preparative HPLC, in which 20-50 % of the purified [^{45}Ti]Ti-CAS-PSMA had a radiochemical purity (RCP) of 100%.

10.3 Analyses of [^{45}Ti]Ti-CAS-PSMA

10.3.1.1 Radiochemical and radionuclidic purity

The RCP of the final formulation of [^{45}Ti]Ti-CAS-PSMA in PBS buffer was 96±3 % for the latest experiments, which were conducted as described in Table 11, entry 9, purified by preparative HPLC, and concentrated using a C18 cartridge.

The radionuclidic purity was determined using a germanium detector measuring the gamma spectrum of the final [^{45}Ti]Ti-CAS-PSMA formulation. The radionuclidic purity was 100 % and the three most abundant gamma lines (511.0, 719.6, and 1408.1 keV) for ^{45}Ti were found. A peak at 74 keV was seen, which is ascribed to X-rays from the lead shielding around the germanium detector when hit by gamma radiation from the sample. A peak at 609 keV and one at 1460 keV were seen, which correspond to gamma lines from bismuth-214 and potassium-40, respectively. These radionuclides were not present in the [^{45}Ti]Ti-CAS-PSMA sample, but the radiation from these radioisotopes was from the background radiation in the laboratory.

10.3.1.2 Molar activity and metal content

The molar activity was calculated from the amount of the nonradioactive Ti-CAS-PSMA, which could be quantified from the UV-signal from the HPLC and calculated from a HPLC standard curve with known concentrations of Ti-CAS-PSMA. ICP-OES was also applied to measure the amount of titanium, since only titanium present as Ti-CAS-PSMA that could be measured by HPLC. However, the amount of titanium measured in the ICP-OES samples of [^{45}Ti]Ti-CAS-PSMA diluted in 1 % HCl was below the amount of titanium found in a 1 % HCl reference samples and the calculated molar activity is thus higher than the listed value. The molar activity of [^{45}Ti]Ti-CAS-PSMA in the eluate from the C18 cartridge purification is listed in Table 13. The molar activity was significant lower, when the thick (250 µm) scandium foil was used compared to the thin (127 µm) scandium foil. ICP-OES was only used to calculate the molar activity of [^{45}Ti]Ti-CAS-PSMA formed with ^{45}Ti produced from the thin scandium foil.

Table 13: The molar activity of [^{45}Ti]Ti-CAS-PSMA in the eluate from the final concentration step on the C18 cartridge. The values were obtained by measuring the concentration of Ti-CAS-PSMA from a HPLC standard curve or by measuring the concentration of titanium

by ICP-OES. The molar activities of [^{45}Ti]Ti-CAS-PSMA containing ^{45}Ti produced from thick (250 µm) and thin (127 µm) scandium foil are listed. The values are an average of four measurements.

	Molar activity (GBq/µmol) (HPLC)	Molar activity (GBq/µmol) (ICP-OES)
Thick (250 µm) Sc foil (31-36 mg Sc foil)	0.49 ± 0.15	-
Thin (127 µm) scandium foil (22-33 mg Sc foil)	110 ± 59	> 107

The thick (250 µm) and thin (127 µm) scandium foils were analyzed by ICP-OES to calculate the amount of titanium in the foils. A significant difference in the amount of titanium was found. The thick foil contained 0.13±0.002 % (w/w) titanium, while the thin foil only contained 0.003 ± 0.002 % (w/w) titanium. The amount of titanium, scandium, iron, zinc, silver, and copper in the final [^{45}Ti]Ti-CAS-PSMA product (eluate from C18 cartridge) using the thin scandium foil in the ^{45}Ti production was also analyzed by ICP-OES. The amount of the six different metals in the eluate can be seen in Table 14. The amount of titanium, scandium, silver, and zinc in the samples were below the amount of these metals in a reference samples containing 1 % HCl. Relative high amounts of iron was seen, while only low concentrations of copper was present.

Table 14: The amount of titanium, scandium, silver, copper, iron, and zinc in the final eluate of [^{45}Ti]Ti-CAS-PSMA calculated from ICP-OES measurements. The amount of titanium, scandium, silver, and zinc in the samples were below the amount of these metals in a reference sample containing 1 % HCl, not shown.

m Ti (µg)	m Sc (µg)	m Ag (µg)	m Cu (µg)	m Fe (µg)	m Zn (µg)
< 0.2	< 8.3	< 0.05	0.2 ± 0.1	2.0 ± 2.1	< 5.0

10.3.1.3 Lipophilicity

The lipophilicity of [^{45}Ti]Ti-CAS-PSMA was determined by measuring the octanol/water partition coefficient (log P). A log P value of 0.99 ± 0.27 was found by measuring the activity in the aqueous and in the organic phase after mixing (2 min). This value was significantly higher than the partition coefficient of the four PSMA-targeted radiotracers shown in Figure 46 in section 10.1. The log P values of ^{18}F-DCFPyl (log P: -3.4) and ^{18}F-PSMA-1007 (log P: -1.6) have been measured by Robu et al. and the values for ^{68}Ga-PSMA-11 (log P: -4.8) and ^{68}Ga-PSMA-617 (log P: -4.3) have been determined by Umbricht et al. [163], [164] The more lipophilic character of [^{45}Ti]Ti-CAS-PSMA might still be acceptable due to the characteristics of PSMA, which is a transmembrane protein, as mentioned in section 10.1.

10.4 Stability studies

The stability of [^{45}Ti]Ti-CAS-PSMA in H_2O/EtOH 1/9 (v/v) (eluate from C18 cartridge) and in 9/1 (v/v), in PBS buffer, and in HEPES buffer was analyzed by HPLC after 0, 1, 2, 3, and 4 hours at room temperature (Figure 61). The stability in both 9/1 and 1/9 (v/v) EtOH/H_2O was constant in the analyzed time period. Although, the RCP of [^{45}Ti]Ti-CAS-PSMA in H_2O/EtOH 9/1 (v/v) seems to be higher than for the 1/9 ratio. However, the sample in H_2O/EtOH 9/1 (v/v) was diluted from the other sample, so it might be due to dilution, which made the detection of small amounts of impurities more difficult and their peak could disappear in the baseline of the HPLC chromatogram. The challenge of detecting small peaks might also be the reason why an increased RCP of [^{45}Ti]Ti-CAS-PSMA was seen in HEPES and PBS buffer over time, since the area of the peaks decreased over time as ^{45}Ti decays. Another possibility for the observed increased RCP, could be the formation of insoluble ^{45}Ti-compounds or/and ^{45}Ti-compounds, which did not elute from the HPLC C18-column. Thus, the following stability studies were then analyzed by radio-TLC, where compounds with no affinity for the mobile phase can be seen on the baseline.

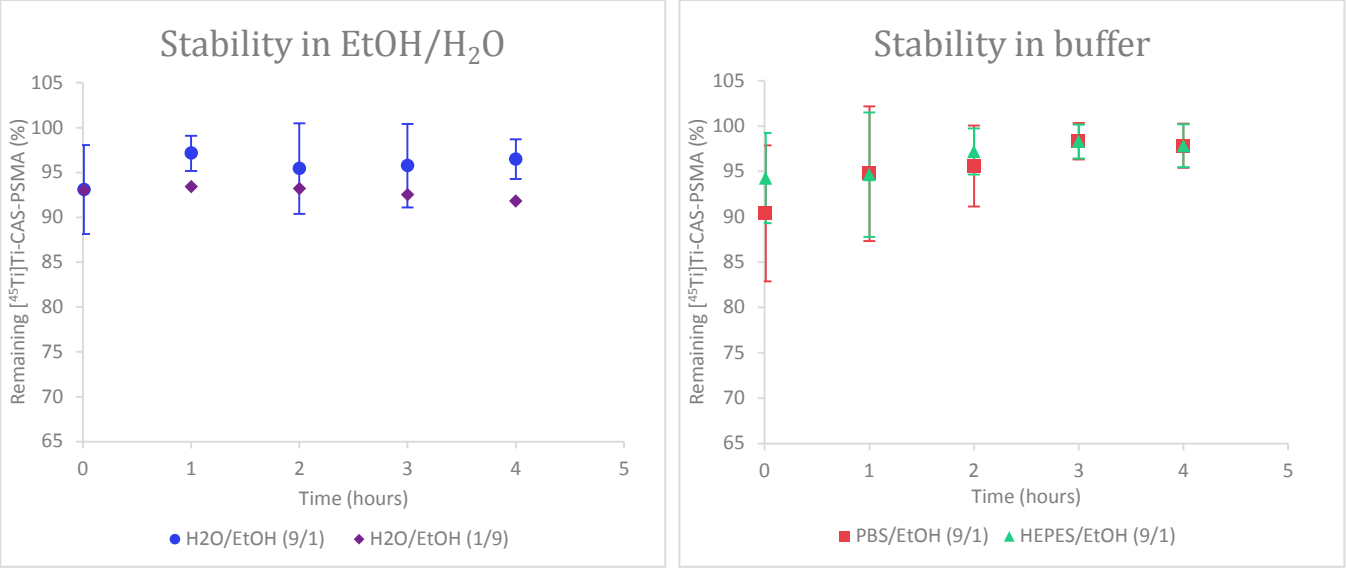

Figure 61: The stability of [^{45}Ti]Ti-CAS-PSMA in H_2O/EtOH (9/1 (blue) and 1/9 (purple)) (left) and in PBS buffer/EtOH 9/1 (v/v) (red), and in HEPES buffer/EtOH 9/1 (v/v) (green) (right). The error bars for the stability in H_2O/EtOH 9/1 (v/v), PBS/EtOH 9/1 (v/v), and HEPES/EtOH 9/1 (v/v) show the standard deviation of three measurements, while the stability in H_2O/EtOH 1/9 (v/v) was measured only once.

The stability of [^{45}Ti]Ti-CAS-PSMA in mouse serum was measured by mixing the final formulation of [^{45}Ti]Ti-CAS-PSMA in PBS buffer with mouse serum 1/1 (v/v) and incubating at 37 °C. The final formulation was either obtained by evaporating the C18 cartridge eluate with [^{45}Ti]Ti-CAS-PSMA down to 50-100 µL and adding PBS

buffer or by diluting a sample of the eluate with PBS buffer. The stability was followed by radio-TLC with C18 TLC plates and ACN/H_2O 7/3 (v/v) as eluent, comparing the R_f value to the one of the nonradioactive Ti-CAS-PSMA and the stability observed in the PBS buffer samples were analyzed as well. The stability over 4 hours can be seen in Figure 62. The percentage of [^{45}Ti]Ti-CAS-PSMA compared to the amount of other ^{45}Ti-compounds is decreasing over time. The stability in mouse serum/PBS buffer 1/1 (v/v) seemed to be higher than the stability in PBS buffer. The percentage of [^{45}Ti]Ti-CAS-PSMA was decreased to 33-48 % after 4 hours in PBS buffer, while only to 80 % in mouse serum/PBS buffer. The ^{45}Ti-compound that formed over time had an R_f value of 0, so it had low affinity for the TLC eluent. The formed ^{45}Ti-compound might be $Ti(OH)_4$, if the chelation of ^{45}Ti by salan and CA-PSMA is not stable towards hydrolysis.

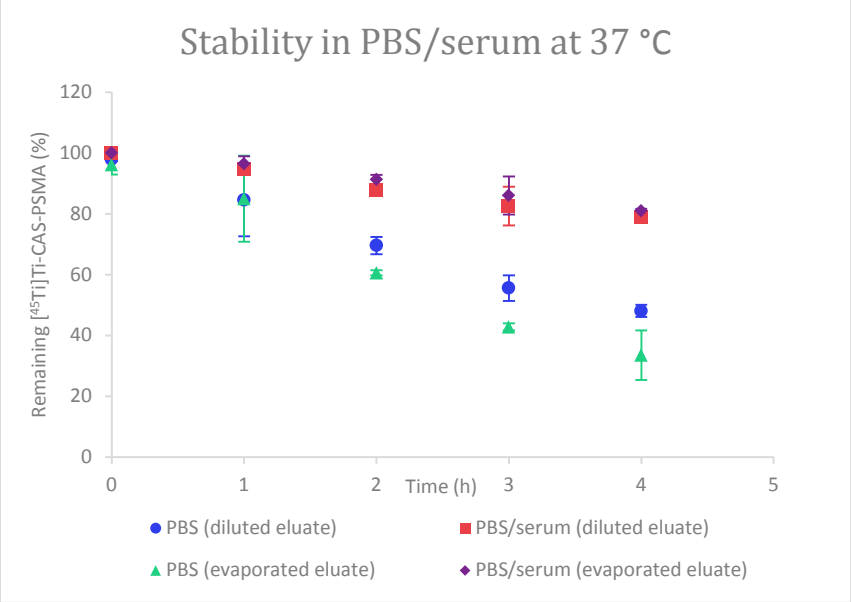

Figure 62: The stability of [^{45}Ti]Ti-CAS-PSMA in PBS buffer and in mouse serum/PBS buffer 1/1 (v/v) at 37 °C. The amount of [^{45}Ti]Ti-CAS-PSMA was determined by radio-TLC where the R_f value was compared to the one for Ti-CAS-PSMA.

When mixed with the mouse serum, the concentration of the PBS buffer was diluted by half, which might be the reason for the increased stability in mouse serum. In order to study if the salts in the buffer might affect the stability, the stability of [^{45}Ti]Ti-CAS-PSMA in a sample with PBS buffer diluted with water 1/1 (v/v) was studied at 37 °C (Figure 63). The stability in this sample was found to be similar to the stability in PBS buffer; therefore, the lower salt concentration was not expected to be the reason for the higher stability in mouse serum. Instead, it could be the lower amount of water, which might decrease the hydrolysis rate. A slightly higher stability was seen in the PBS buffer sample containing [^{45}Ti]Ti-CAS-PSMA from the diluted eluate compared to the sample containing [^{45}Ti]Ti-CAS-PSMA from the evaporated eluate. This might be due to a higher concentration of ethanol in the diluted eluate. The effect of ethanol was tested by following the stability of

[^{45}Ti]Ti-CAS-PSMA in PBS buffer/ethanol 1/1 (v/v) at 37 °C. An increased stability could be seen (Figure 63). The percentage of [^{45}Ti]Ti-CAS-PSMA was 78 % after 4 hours which was similar to the amount in mouse serum/PBS buffer. Thus, it was expected that the decomposition of [^{45}Ti]Ti-CAS-PSMA was due to the water in the samples. The stability in mouse serum without any PBS buffer was comparable with the stability in mouse serum/PBS buffer 1/1 (v/v) (Figure 63).

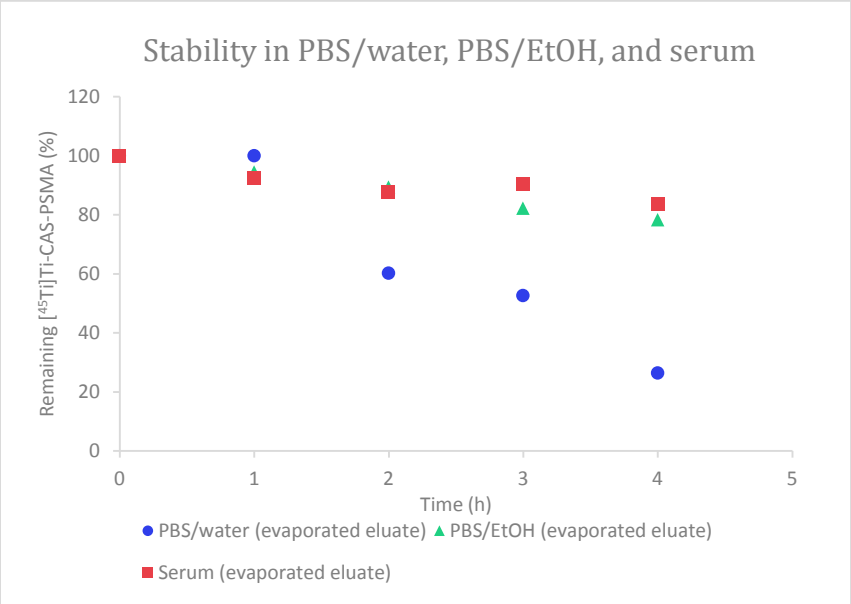

Figure 63: The stability at 37 °C of [^{45}Ti]Ti-CAS-PSMA in PBS buffer diluted with water (blue) or ethanol (green) (1/1) and in serum without PBS buffer (red). The percentage of [^{45}Ti]Ti-CAS-PSMA was measured with radio-TLC.

The stability in HEPES buffer and mouse serum/HEPES buffer 1/1 (v/v) was also tested to determine if a higher stability could be obtained in this buffer. However, similar results were seen as with PBS buffer (Figure 64). Since no decomposition of [^{45}Ti]Ti-CAS-PSMA was seen in PBS buffer at room temperature when using radio-HPLC as analysis method (Figure 61), the stability of [^{45}Ti]Ti-CAS-PSMA in PBS buffer and in mouse serum/PBS buffer 1/1 (v/v) at room temperature was tested with radio-TLC. The decomposition of [^{45}Ti]Ti-CAS-PSMA could be seen with radio-TLC. The decomposition rate was slower than at 37 °C, so at room temperature, 70 % of [^{45}Ti]Ti-CAS-PSMA was present after 4 hours in PBS buffer and 93 % was present in mouse serum/PBS buffer 1/1 (v/v) (Figure 64).

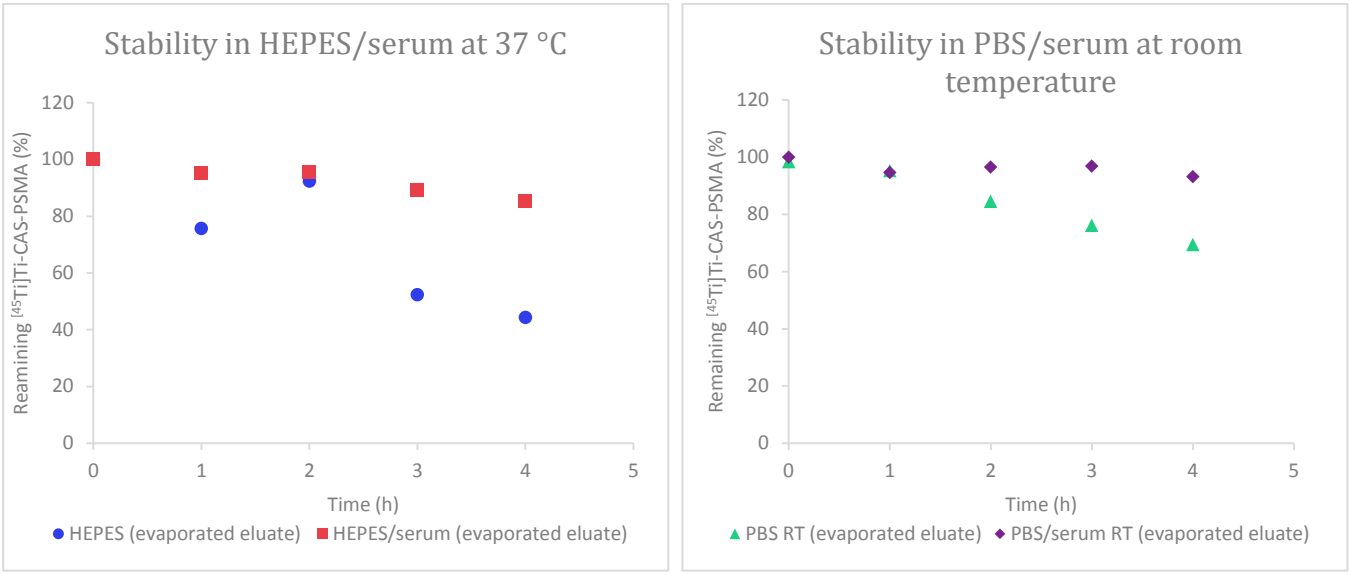

Figure 64: The stability of [^{45}Ti]Ti-CAS-PSMA followed by radio-TLC. Left: The stability in HEPES buffer (blue circles) and in mouse serum/HEPES buffer 1/1 (v/v) (red squares) at 37 °C. Right: The stability in PBS buffer (green triangles) and mouse serum/PBS buffer 1/1 (v/v) (purple diamonds) at room temperature.

The stability of (salan)Ti(dipic) has been studied by Grützke et al. Here, the decomposition of (salan)Ti(dipic) in THF/phosphate buffer at 37 °C (pH 6.8) was measured by UV-vis spectroscopy and the measured half-life was 150 hours. [150] With a half-life of 150 hours, still 98 % of (salan)Ti(dipic) would be present after 4 hours, which was considerable higher than the 78 % of [^{45}Ti]Ti-CAS-PSMA present after 4 hours in PBS buffer/ethanol 1/1 (v/v) at 37 °C. The use of CA-PSMA as chelator instead of dipic might have affected the stability. The size of CA-PSMA was larger than the size of dipic, which might affect the chelation of titanium. However, the stabilities of (salan)Ti(dipic) and of [^{45}Ti]Ti-CAS-PSMA were not tested under the same conditions (solvent and buffer and analysis method), so the difference could also be due to other effects. However, due to reasonable serum stability and acceptable log P value, [^{45}Ti]Ti-CAS-PSMA was evaluated *in vivo* next.

10.5 *In vivo* study in mice

The *in vivo* distribution of the [^{45}Ti]Ti-CAS-PSMA in the PSMA-positive tumor-bearing mice was studied. The study was conducted with 4 mice all receiving the same batch of [^{45}Ti]Ti-CAS-PSMA (Table 15).

Table 15: The time between EOS of [^{45}Ti]Ti-CAS-PSMA and injection, the injected activity, and the scans performed on the four mice are listed.

Mouse no.	Time between EOS and injection (h)	Activity injected (MBq)	Scan type
1	4	1.4	Dynamic 0-75 min.

2	5.5	1.0	Static 4 h after injection
3	6	0.8	Static 1 and 4 h after injection
4	7.5	0.5	

The PET images of the mice are shown in Figure 65. From the PET scans, a high radioactivity accumulation could be seen in the gallbladder and intestines. However, no visible tracer uptake in the tumor, located at the left shoulder of each mouse, could be observed. The molar activity of the tracer was assumed to be at an acceptable level (14-30 GBq/µmol depending at the injection time) therefore the absence of tumor binding was not expected to be due to occupation of binding sites by the nonradioactive Ti-CAS-PSMA in the sample.

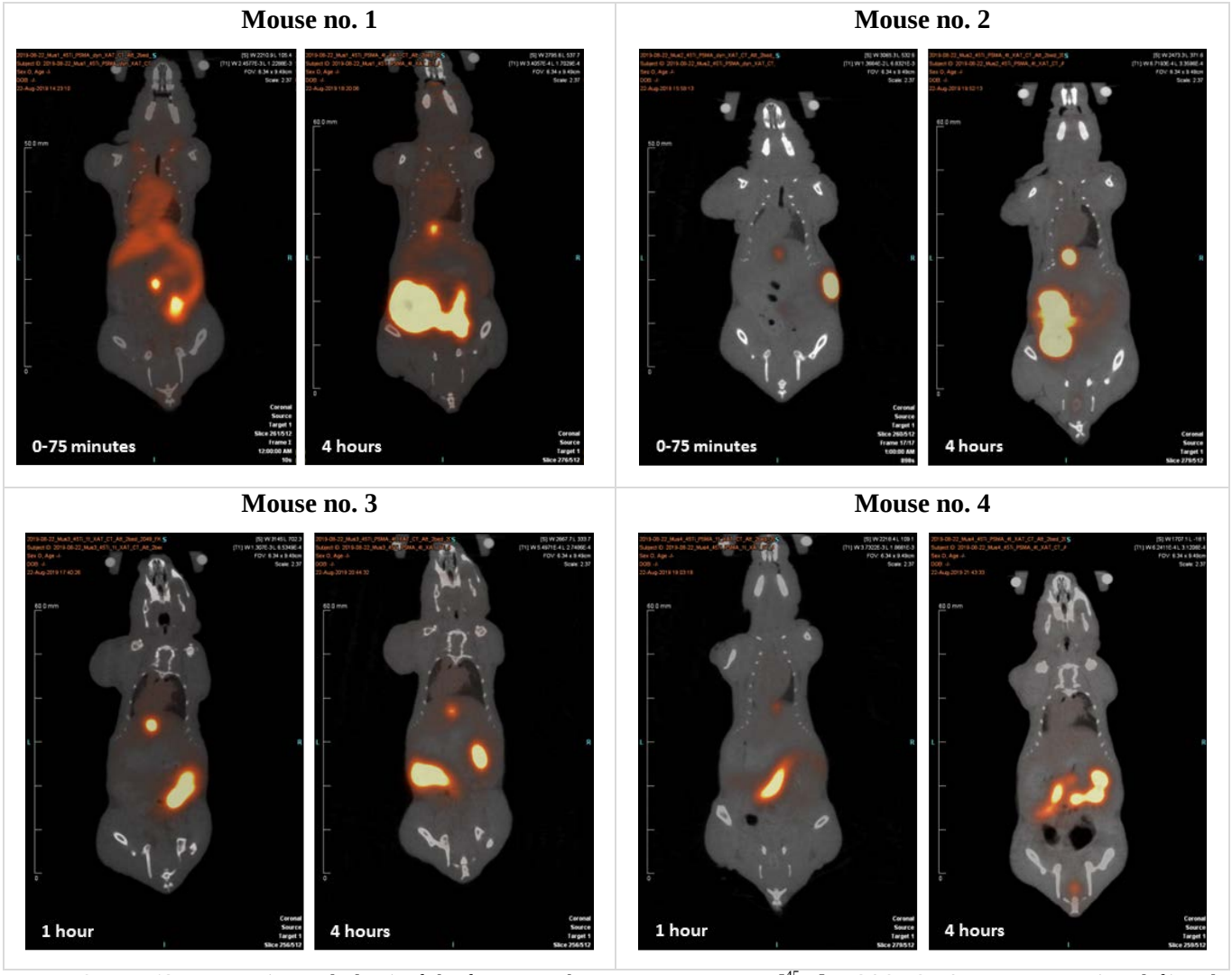

Figure 65: PET/CT images (coronal plane) of the four tumor-bearing mice receiving [^{45}Ti]Ti-CAS-PSMA. Mouse no. 1 (top, left) and mouse no. 2 (top, right) were scanned 0-75 minutes and four hours post injection (p.i.). Mouse no. 3 (bottom, left) and mouse no. 4 (bottom, right) were scanned one hour and four hours p.i.

The *ex vivo* biodistribution for all four mice was analyzed and the injected dose per gram tissue (%ID/g) of the different organs analyzed, can be seen in Figure 66. From these measurements, a low amount of radioactivity (1.1 ± 0.1 %) was also observed in the tumor tissue, however, this amount was not notable higher than for the other organs. A relative high amount of radioactivity was found in the blood (4.0 ± 0.6 % ID/g) and in the liver (3.4 ± 0.3 % ID/g). The highest accumulation per weight of organ was seen in the gallbladder (92.7 ± 40.5 % ID/g); however, a relative large variation between the different mice was seen for this organ. The gallbladder of mouse no. 1 was not analyzed, as the high radioactivity in the gallbladder first was noticed after the µPET scan of this mouse. The mass of the gallbladder was low (6-7 mg) and the large variety might be caused by the uncertainty on the mass. The gallbladder is also fragile and some of the bile might be lost during the transfer to the glass for the *ex vivo* measurement. The measurement of the gallbladder of the last mouse was notable lower than for the two previous mice. Here only 16.6 % ID/g was seen. Additionally, this could also be seen on the PET scan four hours p.i. for mouse no. 4 (Figure 65). A radioactivity accumulation in the gallbladder of mouse no. 4 was seen on the µPET scan 1 hour p.i., though less clearly than for the other mice. However, the amount of radioactivity injected was relatively low for mouse no. 4 (Table 15) and the [^{45}Ti]Ti-CAS-PSMA tracer was administered 7.5 hours EOS.

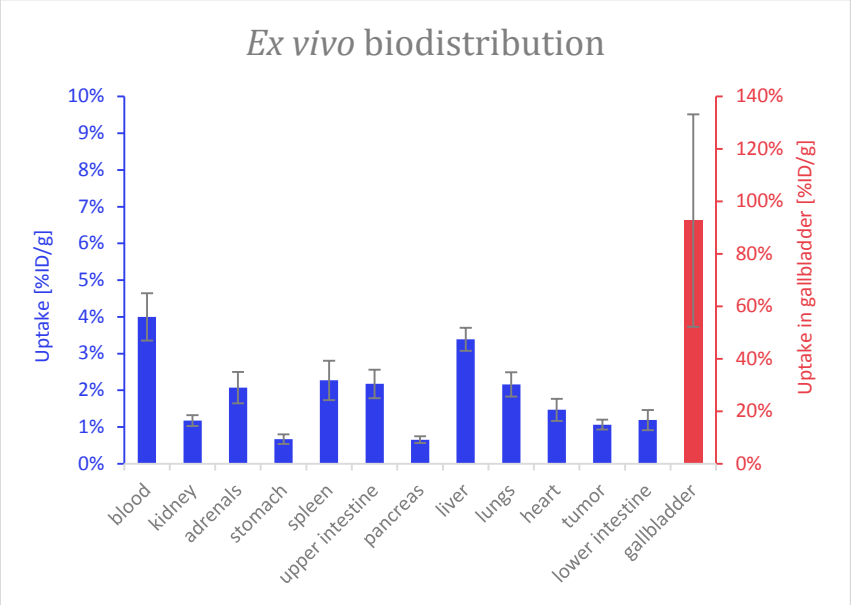

Figure 66: The *ex vivo* organ biodistribution data shown as uptake of ^{45}Ti in percentage of injected dose per weight of tissue. The uptake in the gallbladder (red) can be read off on the right y-axis. The values were an average for the four mice and the error bars represent the standard deviation.

The stability of [^{45}Ti]Ti-CAS-PSMA in PBS buffer was not studied for more than 4 hours. If the decrease of the amount of [^{45}Ti]Ti-CAS-PSMA in PBS buffer at room temperature was expected to be linear only approximately

40 % of ^{45}Ti would be remaining as [^{45}Ti]Ti-CAS-PSMA (calculated from the data from the stability in PBS buffer at room temperature in Figure 64) after 7.5 hours. However, it would be necessary to conduct the stability study for 7.5 hours to verify this. The time of tracer injection for mouse no. 2 and 3 were also outside the time range tested for the stability of [^{45}Ti]Ti-CAS-PSMA in PBS buffer. At these time points it was expected that 50-60 % of ^{45}Ti injected was [^{45}Ti]Ti-CAS-PSMA according to the estimation from the data in Figure 64.

The *ex vivo* biodistribution and the PET images of the four mice indicated that [^{45}Ti]Ti-CAS-PSMA was metabolized and/or excreted through the hepatobiliary system; first being transferred from the blood to the liver, where it was released to the gallbladder and further to the intestines.

[^{45}Ti]Ti-CAS-PSMA was expected to be relative stable while in the blood *in vivo* since the stability in serum *in vitro* was acceptable, but it was not analyzed. A possible way to evaluate the *in vivo* stability of [^{45}Ti]Ti-CAS-PSMA would be to analyze blood samples and the organs for radiometabolites post-mortem at different time points either by radio-TLC or radio-HPLC. Although, if other ^{45}Ti-compounds than [^{45}Ti]Ti-CAS-PSMA were present, it would still be challenging to determine if these ^{45}Ti-compounds were metabolites, transchelated ^{45}Ti products, or products of the hydrolysis of the ^{45}Ti-complex using this method. Transchelation and hydrolysis of the complex would take place if the chelation of ^{45}Ti by salan and chelidamic acid was not stable *in vivo*. The stability of the chelation of ^{45}Ti can be evaluated *in vitro* by transchelation and transmetallation analysis, employing plasma proteins and competing chelating metals, respectively, which could give an indication on the [^{45}Ti]Ti-CAS-PSMA chelation stability *in vivo*. The study performed at our laboratory of the *in vivo* distribution of [^{45}Ti](salan)Ti(dipic) showed a similar biodistribution and a short circulation time of [^{45}Ti](salan)Ti(dipic). In this study, blood samples showed that the compound was relative stable in the blood, but the analysis of the liver and gallbladder showed almost no remaining [^{45}Ti](salan)Ti(dipic) in these organs. [65] From this study it was expected that the chelating part of [^{45}Ti]Ti-CAS-PSMA would also be metabolized or the chelation of ^{45}Ti would be unstable in the liver.

In addition to the poor *in vivo* stability of the tracer, the affinity of [^{45}Ti]Ti-CAS-PSMA towards PSMA also seemed to be reduced. In mouse no. 1, which received 1.4 MBq [^{45}Ti]Ti-CAS-PSMA at four hours p.i. and scanned at 0-75 minutes p.i., no accumulation was seen at the tumor region during the circulation and excretion of the tracer (Figure 65). A possible loss of affinity could be due to modifications that affect the target binding of the Glu-urea-Lys binding moiety. The spacer might be too short so the chelating part of [^{45}Ti]Ti-CAS-PSMA interrupted the binding between Glu-urea-Lys and PSMA. It could also be possible that [^{45}Ti]Ti-CAS-PSMA was too lipophilic and thus was not able to interact with PSMA before being excreted. The binding affinity of [^{45}Ti]Ti-CAS-PSMA could be evaluated in an *in vitro* binding assay with PC3+ cells, analyzing the binding and

blocking of the tracer employing the nonradioactive Ti-CAS-PSMA. Additionally, the measured binding affinity could be compared to e.g. ^{68}Ga-PSMA-11.

For the further development of a ^{45}Ti-labeled PSMA-targeted radiotracer most likely both the *in vivo* stability and the binding affinity of the compound should be improved and evaluated. A different chelator could be incorporated in the tracer or salan could be modified or exchanged. A different spacer might be applied to increase the distance between the Glu-urea-Lys moiety and the chelator. The modification could also be a way to decrease the lipophilicity of the compound.

11 Summary – Synthesis and evaluation of [^{45}Ti]Ti-CAS-PSMA

A Glu-urea-Lys-based radiotracer with a titanium chelating moiety was synthesized and the radiolabeling of the tracer could be performed with ^{45}Ti purified and separated from its cyclotron target material by the LLE method established in section 5.3.4. The identity of the radiotracer, [^{45}Ti]Ti-CAS-PSMA was evaluated by radio-HPLC by comparing the retention time to the one for the nonradioactive Ti-CAS-PSMA. The radiolabeling was performed in high boiling point solvents and the purification of [^{45}Ti]Ti-CAS-PSMA was challenging and consequently the final RCY was low (13.0 ± 5.6% (d.c.) and 5.1 ± 2.3 % (n.d.c.)). [^{45}Ti]Ti-CAS-PSMA could however be obtained in high RCP which made it possible to analyze the lipophilicity and stability of the radiotracer. The lipophilicity of [^{45}Ti]Ti-CAS-PSMA was first thought to be acceptable (log P: 0.99±0.27), but other PSMA-targeting radiotracer as ^{68}Ga-PSMA-11 (log P: -4.8 [164]) and ^{18}F-PSMA-1007 (log P: -3.4 [163]) are more hydrophilic. The stability in mouse serum was found to be acceptable for 4 hours, where 80 % of the total activity was expected to be [^{45}Ti]Ti-CAS-PSMA. The stability was lower in PBS buffer, which was expected to be due to an increased hydrolysis of the ^{45}Ti complex. The *in vivo* distribution of [^{45}Ti]Ti-CAS-PSMA was tested in four PSMA-positive tumor-bearing mice. The µPET imaging and *ex vivo* biodistribution were performed in order to evaluate if [^{45}Ti]Ti-CAS-PSMA would localize and bind to PSMA in the tumor region, but no notable tumor uptake was observed. The reason for this could be a loss of affinity if the Glu-urea-Lys binding motif was affected by the chosen spacer and chelating moiety. Another possibility could be the relative high lipophilicity. Furthermore, the chelation of ^{45}Ti might not have been stable *in vivo*. Modifications of [^{45}Ti]Ti-CAS-PSMA would be necessary e.g. by changing the spacer or the chelating moiety in order to further evaluate if a ^{45}Ti-labeled PSMA-targeted radiotracer can be obtained. However, this study displayed the possibility of developing a ^{45}Ti-labeled radiotracer with high RCP and with acceptable serum stability. Additionally, the LLE method described in section 5.3.4 could be applied to obtain ^{45}Ti for the radiolabeling of the radiotracer.

12 Conclusion and perspectives

In this study, a new technique for the separation of radiometals from their cyclotron target material and the application of a novel radiotracer for PET were evaluated with the purpose of improving the utilization of radiometal-based radiopharmaceuticals for PET.

The separation of four different positron emitting radiometals (^{45}Ti, ^{89}Zr, ^{64}Cu, and ^{68}Ga) from their cyclotron target material was studied in order to obtain the radiometal in high purity suitable for the production of radiopharmaceuticals. The separations were performed and optimized by liquid-liquid extraction (LLE) in flow by applying a membrane-based separation technique. The advantage of this technique is the possibility of a fast and simple separation method which can be automatized. This can further enable an LLE method with low radiation exposure to the personnel producing radiopharmaceuticals.

Solvent systems capable of separating the respective radiometals from the cyclotron target materials and with successful phase separation in flow were established. ^{45}Ti was separated from scandium in 12 M HCl, where above 84.8 ± 2.4 % of ^{45}Ti was extracted into an organic phase consisting of guaiacol/anisole 9/1 (v/v) with no measurable extraction of scandium. ^{89}Zr could be separated from yttrium in 12 M HCl also with guaiacol/anisole 9/1 (v/v) with 53.7 ± 3.9 % extraction efficiency and no measurable yttrium extraction was observed. The separation of ^{64}Cu from nickel was obtained with trioctylphosphine oxide as extractant. Here 86.1 ± 5.5 % of ^{64}Cu was extracted to the organic phase and no measurable extraction of nickel was detected. The LLE of ^{68}Ga from a simulated liquid target system containing 1-5.6 M $ZnCl_2$ in 3-6 M HCl was explored. At the optimal conditions, 95.7 ± 2.0 % ^{68}Ga and $5 \cdot 10^{-3} \pm 3 \cdot 10^{-3}$ % zinc were extracted with *n*-butyl methyl ether/trifluorotoluene 1/2 (v/v). It was possible to back-extract ^{68}Ga into an aqueous phase containing 0.1 M HCl which was expected to be suitable for the labeling of a radiotracer. The next steps in the further development of the method for large scale production of radiometals would be to fully automatize the process. Furthermore, the co-extraction of metal impurities and traces of organic solvents in the final product should be evaluated and decreased.

The main goal in this study was to increase the availability and utilization of PET radiometals, especially of ^{45}Ti which has suitable properties for PET application, but it has not been widely applied to PET, possibly due to its challenging aqueous chemistry. The studied LLE method might improve the availability of ^{45}Ti and thereby promote the further development of ^{45}Ti-based radiopharmaceuticals. In this study, a novel radiotracer with a titanium chelating moiety was synthesized and radiolabeled with ^{45}Ti purified by the LLE technique. The radiotracer ([^{45}Ti]Ti-CAS-PSMA) contained glutamate-urea-lysine as binding motif targeting the prostate-

specific membrane antigen (PSMA) for the detection of prostate cancer. The *in vivo* distribution of [^{45}Ti]Ti-CAS-PSMA was analyzed by µPET imaging of four PSMA-positive tumor-bearing mice, but no visible tumor uptake of [^{45}Ti]Ti-CAS-PSMA was observed. The further development of a ^{45}Ti-labeled PSMA-targeted radiotracer would include modifications of the chemical structure to decrease the lipophilicity and increase the distance between the binding motif and the chelating part of the molecule. Furthermore, an improvement of the titanium chelation could also be explored.

In summary, the LLE and phase separation in flow could be applied for the separation of ^{45}Ti, ^{89}Zr, ^{64}Cu, and ^{68}Ga from their respective cyclotron target material. It should be evaluated for the specific radiometal if the LLE method is preferable compared to other separation techniques. A ^{45}Ti-labeled radiotracer was synthesized and evaluated by µPET imaging. The radiotracer showed no affinity for its biological target, PSMA, and further developments are necessary. Despite the low tumor uptake, the synthesis of a ^{45}Ti-labeled radiotracer displayed the possibility of applying the established LLE method to purify ^{45}Ti followed by radiolabeling, purification and evaluation of the radiotracer.

13 Experimental

13.1 LLE of radiometals

13.1.1 Materials

Guaiacol, Anisole (99 %), 1-octanol (99 %), α,α,α-trifluorotoluene (99 %), 1,1,1,3,3,3-hexafluoro-2-propanol (99 %), diethyl ether (99.0 %), acetone (99.5 %), *n*-butyl methyl ether (99 %), tetrahydropyran (anhydrous, 99 %), toluene, 1,2-dichloroethane (99 %), perfluoro(methylcyclohexane) (90 %), chloroform-d (99.8 atom % D), methanol-d_4 (99.8 atom % D), deuterium oxide (99.9 % atom % D), hydrochloric acid (37 %), sulfuric acid (95.0-98.0 %), titanium(IV) chloride solution (0.09 M in 20 % HCl), pyridine-2,6-dicarboxylic acid (dipic) (98 %), pyridine (anhydrous, 99.8 %), octane (98 %), 1,2-decanediol (98 %), 2,3-naphtalene diol (98 %), perfluoro-*1H,1H,2H,2H*-1-octanol (97 %), multi-element standard solution 1 for ICP (TraceCert in 10 % HNO_3), citric acid (99.5 %), zinc chloride (97 %), iron(III) chloride (97 %), zinc foil (250 µm, 99.9 % trace metal basis), copper foil (500 µm, 99.98 % trace metal basis), trioctylphosphine oxide (98.5 %), copper(II) chloride (99 %), nickel(II) chloride (98 %), zirconium(IV) chloride (99.5 %), yttrium(III) chloride (99.99 %), Cu-ATSM (98 %), 1-iodoperfluorodecane (96 %), allyltributylstannane (97 %), benzoyl peroxide, *N*-methylmorpholine-*N*-oxide (97 %), osmium tetroxide (99.8 %), nitric acid (65 %), TLC plates (silica gel on TLC Al foil), 10 mL and 25 mL Hamilton glass syringes, silica gel (high purity, pore size 60 Å, 230-400 mesh particle size) were purchased from Sigma Aldrich. Dibutyl ether (99 %), diisopropyl ether (99 %), hydrochloric acid (30 %, SupraPure) and DMSO (99 %) from Merck, hydrochloric acid (37 %, trace metal basis) from Honeywell and DOTA from Macrocyclics were applied. Hexyl methyl ether (98 %) and *n*-amyl ether (98 %) were purchased from abcr GmbH. Heptane (99.7 %), ethyl acetate (99.9 %), hexane (97 %), 15 mL plastic centrifuge tubes with screw caps (SuperClear), and aluminum foil (500 µm, 99.9 %) were purchased from VWR.

Scandium foil (250 µm and 127 µm, 99.9 % pure, rare earth analysis), scandium(III) chloride (anhydrous, 99.9 %), yttrium foil (640 µm, 99.5 %) were purchased from Alfa Aesar and nickel-64 (99.6 % isotope enriched) was purchased from Campro Scientific. Customized ICP standards were obtained from Inorganic ventures (Sc and Ti, Zr and Y, Cu and Ni, and Ag, Fe, Co, and Zn (100 ppm of each metal in 5 % HCl)). TK200 resin was purchased from Triskem. The membrane separator was purchased from Zaiput Flow Technologies

Pall PTFE membranes, PFA diaphragms from McMaster Carr. and PFA tubing (1/16” OD, 0.03” ID and 1/8″ OD, 1/16″ ID) from Idex Health and science were purchased. Static mixers (PTFE, 10 element, 1.7 cm length, placed inside a piece of 1/8” OD, 1/16” ID PFA tubing) were purchased from Stamixco.

Salan [165] and (salan)Ti(dipic) [149] were synthesized by Fedor Zhuravlev following procedure described previously. ^{54}Mn and ^{60}Co were provided by Prof. Xiaolin Hou.

13.1.2 Instruments

NMR spectra were recorded with an Agilent 400 MR spectrometer operating at 400.445 MHz (^{1}H). The radiometals were produced with a GE 16.5 MeV PETtrace cyclotron. The radioactivity was measured with a CRC-55tR, CII Capintec, Inc. dose calibrator or with a Princeton Gammatech LGC 5 or a Ortec GMX 35195-P germanium detector. ICP-OES measurements were performed with a Thermo Scientific iCAP 6000 Series ICP Optical Emission Spectrometer or an ICP-AES, Agilent 5100 Dual View. UV-vis absorption spectra were recorded with a UV-3101PC Shimadzu spectrophotometer. For the batch LLEs an IKA ROCKER 3D digital shaker was applied for the mixing and an eppendorf 5702 centrifuge was used to separate the phases. KDS 100 Legacy Syringe pumps or Harvard Apparatus PHD 2000 Programmable and Infusion syringe pumps were applied for the LLEs in flow. For radio-TLC, a Raytest MiniGita TLC scanner was applied. A Hitachi Chromaster equipped with a Carrol & Ramsey 105-S radio-detector and a Hitachi 5430 double diode array detector with a Phenomenex Luna 3 µ C18 (2) column was applied for HPLC.

13.1.3 Methods

13.1.3.1 LLE of titanium

13.1.3.2 Production of ^{45}Ti

30-60 mg 250 µm thick scandium foil was irradiated for 5-15 minutes at 10-20 µA with a GE 16.5 MeV PETtrace cyclotron. A 500 µm thick aluminum foil was placed in front of the scandium foil to degrade the proton beam energy from 16 MeV to approximately 13 MeV in order to reduce the coproduction of ^{44}Ti by the ^{45}Sc(p,2n)^{44}Ti nuclear reaction. [81] The scandium foil was dissolved in 3 mL 12 M HCl or 6 M HCl, filtered and centrifuged, and diluted with 10-20 mL 12 M or 6 M HCl.

13.1.3.3 Batch LLE of ^{45}Ti with 1-octanol, 1,2-decanediol, and DHN

1 mL of the dissolved irradiated scandium foil containing 2-4 MBq of ^{45}Ti in concentrated HCl was transferred to a falcon tube. 1 mL 1-octanol was added to the falcon tube as organic phase. The tube was shaken for 2 minutes and then centrifuged for 2 minutes. The two phases were separated with a syringe and the activity of each phase was measured with a dose calibrator. 1 mL 1-octanol was added to the aqueous phase in the falcon tube and the phases were again shaken for 2 minutes. The tube was centrifuged for 2 minutes and the phases were separated and the activity of each phase was measured. This was repeated once more, where 1 mL 1-octanol was added to the aqueous phase.

This procedure was repeated with 0.1 M 1,2-decanediol in 1-ocantol and 0.1 M DHN in 1-octanol as organic phase.

The procedure was repeated using 1 mL dissolved irradiated scandium foil containing 2-3 MBq ^{45}Ti in 6 M HCl as aqueous phase.

The extraction efficiency of ^{45}Ti was calculated from the activity in the aqueous (A_{aq}) and in the organic phase (A_{org}) (equation (14)).

$$E\% = \frac{A_{org}}{A_{aq} + A_{org}} \cdot 100\ \% \tag{14}$$

The LLE of titanium from 8, 10, and 12 M HCl with 1-octanol or 10 mM 1,2-decanediol in 1-octanol was analyzed by preparing 1 mM $TiCl_4$ in 8, 10, and 12 M HCl and mixing 1 mL of each of the aqueous phases with 1 mL of one of the organic phases. The phases were mixed for 2 minutes, separated and analyzed by UV-vis spectroscopy.

13.1.3.4 Batch LLE of ^{45}Ti with fluorinated compounds

The synthesis of the fluorinated compound is described in the following section and an overview of the synthesis can be seen in Figure 20. The LLE of ^{45}Ti with Rf_{10}-diol was performed using the same procedure as in section 13.1.3.3. 0.05 M Rf_{10}-diol in TFT/hexafluoroisopropanol (1/1) was used as organic phase. The extraction from concentrated HCl was tested. The LLE with Rf_6-ol was performed by mixing 0.5 mL Rf_6-ol with 0.5 mL 0.01 M $TiCl_4$ and 0.01 M $ScCl_3$ in 12 M HCl for 2 minutes and let the phases separate. The aqueous phase before and after the LLE was analyzed by ICP-OES.

*Synthesis of 3-(4,4,5,5,6,6,7,7,8,8,9,9,10,10,11,11,12,12,13,13,13-henicosafluorodecyl)-propene **(1)***

1.21 g (1.9 mmol) 1-iodoperfluorodecane was dissolved in 1.5 mL TFT in a 10 mL round-bottom flask. 0.96 g (2.9 mmol) allyltributylstannane was added to the flask and the solution was heated to 95°C under argon flow. 26 mg (0.11 mg) BPO in 0.5 mL trifluorotoluene was added dropwise and the mixture was stirred at 95°C for 3 h. The solvent was removed under reduced pressure and now two phases could be seen. 2 mL perfluoro(methylcyclohexane) was added and the mixture was centrifuged. The two phases were separated and the fluorous phase was passed through a SPE tube with dry silica. The product was eluted in 2 mL perfluoro(methylcyclohexane). The product was obtained as a white solid (0.69 g, 66 % yield). ^{1}H NMR ($CDCl_3$) δ 5.79 (m, 1H), 5.33 (m, 2H), 2.84 (m, 2H) . ^{19}F NMR ($CDCl_3$) δ -80.76, -113.30, -121.79, -122.75, -123.11, -126.15 ppm.

*Synthesis of 3-(4,4,5,5,6,6,7,7,8,8,9,9,10,10,11,11,12,12,13,13,13-henicosafluorodecyl)-propane diol (**Rf_{10}-diol**)*

The compound was synthesized following a procedure described by Wang et al. [166]

Acetone/water/pyridine (2.5mL/0.25mL/0.062mL) was added to a 10 mL round-bottom flask. 0.14 g (1.2 mmol) NMO and 0.4 g (0.7 mmol) **1** were then added. The mixture was cooled in an ice bath. 2.7 mg (11 µmol) OsO_4 in 70µL water was added to the mixture dropwise and the mixture was stirred at 0°C for 1 h. The mixture was then heated to 50 °C overnight and the reaction was followed by TLC using hexane/ethyl acetate (50/1) as eluent. The mixture contained still starting material, so 50 mg (0.4mmol) NMO and 2 mg (8 µmol) OsO_4 were added at 0 °C. The mixture was stirred at 50°C for 26 hours. 1.5 mL 20% sodium metabisulfite ($Na_2S_2O_5$) was added dropwise whereby a gel was formed. The gel was centrifuged and the liquid was washed twice with ethyl acetate and the organic phase was collected. The solid was dissolved in ethyl acetate and combined with the organic phase. The organic phase was dried over Na_2SO_4, filtered and the solvent removed under reduced pressure. The crude product was purified with column chromatography using hexane/ethyl acetate (4/3) as eluent. The product was obtained as a white solid (0.2 g, 46% yield). ^{1}H NMR (methanol-d_4) δ 3.92 (m, 1H), 3.43-3.31 (m, 2H), 2.40-2.24 (m, 1H), 2.17-2.00 (m, 1H) ppm. ^{19}F NMR (methanol-d_4) δ -82.24, -113.55, -114.31, -122.66, -123.56, -124.54, -127.18 ppm.

13.1.3.5 Setup for LLE in flow

The LLE and phase separation in flow was performed with a Zaiput membrane-based separator with a polyfluoroalkoxy alkane (PFA) diaphragm for pressure control. The setup can be seen in Figure 13. The aqueous and organic phase were loaded in two respective syringes and pumped by two syringe pumps. The two phases passed through PFA tubing into a PEEK tee. The phases were mixed by passing through tubing containing two 10-element static mixers. Hereafter, steady slug flow was developed and the phases were mixed further by passing through various lengths of PFA mixing tubing. Then, the mixed phases entered the separator, where the organic phase permeated the hydrophobic membrane and the aqueous phase was retained. The aqueous phase was collected from the retentate outlet, while the organic phase was collected from the permeate outlet. Different diaphragm thicknesses, membranes, flow rates and length of mixing tubing were tested in order to achieve complete phase separation and obtain high extraction efficiency.

13.1.3.6 LLE in flow of titanium with 1-ocatnol

The LLE in flow with 1-octanol was performed with nonradioactive titanium, so a solution of 0.01 M $TiCl_4$ and 0.01 M $ScCl_3$ in 12 M HCl or in 10 M HCl was used as aqueous phase. The organic phase was 1-octanol, 10 mM DHN in 1-octanol, 10 or 70 % hexane in 1-octanol or 10 % octane in 1-octanol. An aqueous flow rate of 0.5

mL/min and an organic flow rate of 0.5 mL/min were used for the experiments. Five different membranes were tested. The membranes were made of different materials (PTFE, PVDF, PEEK, and PTFE/PP) and had different pore sizes (0.1, 0.2, and 0.5 µm). Three different diaphragm thicknesses (1, 2, and 5 mil) were tested as well. The experiments and the separation performance of each LLE are outlined in Table 3.

13.1.3.7 LLE in flow of titanium with Rf_6-ol

The LLE in flow using Rf_6-ol was performed with 0.01 M $TiCl_4$ and 0.01 M $ScCl_3$ in 12 M HCl as aqueous phase. An aqueous flow rate of 0.1 mL/min and organic flow rate of 0.1 mL/min were applied. PTFE membranes with either 0.5 µm or 0.2 µm pore size were used. Three different diaphragm thicknesses (1, 2, and 5 mil) were used. The experiment can be seen in Table 4.

13.1.3.8 LLE in flow of titanium with guaiacol/anisole

0.01 M $TiCl_4$ and 0.01 M $ScCl_3$ in 12 M HCl was used as aqueous phase for the LLE in flow using guaiacol/anisole. Different guaiacol/anisole ratios were prepared and used as the organic phase for the LLE. PTFE membranes with different pore sizes (0.05, 0.2, and 0.5 µm) and different diaphragm thicknesses (1, 2, and 5 mil) were applied to separate the aqueous and organic phase. In some cases, the membrane was washed with heptane before the LLE, which improved the phase separation. Different aqueous and organic flow rates were studied, so that the ratio between the aqueous and organic phase was varied. The separation performance for the experiments and the details for each experiment are shown in Table 5. Samples of the aqueous phase before and after the LLE were analyzed by ICP-OES, when complete phase separation was obtained. The volume of the aqueous and organic phase after the LLE was measured with 0.01 M $TiCl_4$ in 12 M HCl as aqueous phase and guaiacol/anisole 9/1 (v/v) as organic phase. A PTFE/PP membrane (0.2 µm pore size) and a 2 mil thick diaphragm were applied. A total flow rate of 1.0 mL/min, flow rate ratio of 1:3 (aq:org) and a 54 cm mixing loop were used. The volume of each of the two phases was measured after 14-20 minutes in graduated cylinders.

13.1.3.9 LLE in flow of titanium with guaiacol/anisole at various residence times

The titanium extraction efficiency at different residence times through the tubing was tested. Different lengths of tubing were used (10, 25, 54, 108, and 216 cm), which resulted in different residence times (0.2, 0.6, 1.2, 2.5, and 4.9 minutes). Guaiacol/anisole (9/1) was used as organic phase and 0.01 M $TiCl_4$ and 0.01 M $ScCl_3$ in 12 M HCl was the aqueous phase for the experiments. A PTFE/PP membrane with a 0.2 µm pore sizes, a diaphragm with a thickness of 2 mil, an aqueous flow rate of 0.05 mL/min and organic flow rate of 0.15 mL/min were applied.

13.1.3.10 LLE in flow of ^{45}Ti with guaiacol/anisole

^{45}Ti and scandium dissolved in 12 M HCl was used as aqueous phase and guaiacol/anisole 9/1 (v/v) was used as organic phase. A flow rate ratio of 1:3 (aq:org) and a total flow rate of 0.2 mL/min or 1.0 mL/min were used. The length of the mixing loop was 10 cm when a total flow rate of 0.2 mL/min was used and a 48 cm long mixing loop was used for the LLE with a total flow rate of 1 mL/min. Samples from the aqueous and from the organic phase were analyzed by measuring the activity of ^{45}Ti with a dose calibrator. The amount of scandium was measured in the aqueous phase before and after the LLE by ICP-OES.

13.1.3.11 Formation of [^{45}Ti](salan)Ti(dipic)

60 mg (0.36 mmol) dipic and 120 mg (0.34 mmol) salan were dissolved in 2 mL pyridine and added to 7.5 mL of the organic phase from the LLE (guaiacol/anisole 9/1 (v/v)).The mixture was stirred at 60 °C for 15 minutes. The formation of [^{45}Ti](salan)Ti(dipic) was analyzed by radio-HPLC and radio-TLC and the retention time and R_f value were compared to nonradioactive (salan)Ti(dipic). A Merck Hitachi Elite Lachrom HPLC was used which has a Carrol & Ramsey 105-S radio-detector and a Hitachi L-2450 diode array detector. The UV-signal at 420 nm was recorded. The column was a Phenomenex Luna 3µ C18(2) (100 Å, 100 mm x 2.00 mm) column and a flow rate of 0.5 mL/min was applied. The eluents were (A) 0.1 % TFA in Milli-Q water and (B) 0.1 % TFA in ACN. For radio-TLC, ethyl acetate/chloroform 1/1 (v/v) was used as eluent. The TLC plate was analyzed with a Raytest MniGina TLC scanner.

13.1.3.12 Quantification of titanium and scandium by ICP-OES

The concentration of titanium and scandium in the aqueous phase before and after LLE was measured by ICP-OES using an Agilent 5100 Dual View ICP-OES. Calibration standards were prepared with a concentration of 22.2, 18, 15, 10, and 5 ppm titanium and scandium with the same concentration of HCl and H_2SO_4 as the samples. The samples were prepared by diluting 0.35 mL of the sample up to 5 mL with 10 % (v/v) H_2SO_4 and digest the sample at 160 °C for 6 hours. 2.7 mL of the digested sample was diluted up to 10 mL to obtain a total acid concentration of 5 % (v/v). The extraction efficiency of titanium and scandium were calculated by equation (15), where $c_{aq,before\ LLE}$ is the concentration of titanium or scandium in the aqueous phase before the LLE and $c_{aq,after\ LLE}$ is the concentration of titanium or scandium in the aqueous phase after the LLE.

$$E\% = \frac{c_{aq,before\ LLE} - c_{aq,afterLLE}}{c_{aq,before\ LLE}} \cdot 100\ \% \qquad (15)$$

13.1.3.13 Quantification of titanium by UV-vis spectroscopy

The amount of titanium in the organic phase after LLE was calculated by using UV-vis spectroscopy with a (salan)Ti(dipic) calibration curve. The samples were prepared in pyridine and the concentrations of (salan)Ti(dipic) were $1 \cdot 10^{-4}$, $8 \cdot 10^{-5}$, $5 \cdot 10^{-5}$, $2 \cdot 10^{-5}$, and $1 \cdot 10^{-5}$ M. The samples were measured at 405 nm. Salan and dipic were added to diluted samples of the organic phase from the LLE and heated to 60 °C for 45 minutes and then analyzed by UV-vis spectroscopy. The extraction efficiency was calculated from the concentration of titanium in the aqueous phase before the LLE ($c_{aq,\ before\ LLE}$) and the concentration of titanium in the organic phase after the LLE ($c_{org,\ after\ LLE}$) (equation (16)).

$$E\% = \frac{c_{org,after\ LLE}}{c_{aq,before\ LLE}} \cdot 100\ \% \tag{16}$$

13.1.3.14 LLE of zirconium

13.1.3.15 Production of ^{89}Zr

^{89}Zr was produced from natural yttrium foil by the ^{nat}Y(p,n)^{89}Zr nuclear reaction. 189 mg yttrium foil (0.64 mm thick, 99.5 %) was irradiated for 30 minutes at 15 µA on a GE 16.5 MeV PETtrace cyclotron. A 500 µm thick aluminum foil was used to degrade the proton energy to approximately 13 MeV. The irradiated yttrium foil was dissolved in 3 mL 12 M HCl, filtered and centrifuged. The solution was diluted with 10 mL 12 M HCl.

13.1.3.16 LLE in flow of zirconium with guaiacol/anisole

The LLE in flow of zirconium was performed with 0.01 M $ZrCl_4$ and 0.01 M YCl_3 in 12 M, 10 M, or 7 M HCl as aqueous phase and guaiacol/anisole 9/1 (v/v) as organic phase. A PTFE/PP membrane with a 0.2 µm pore size and a diaphragm with a thickness of 2 mil were applied for all experiments. Different flow rate ratios (1:3 and 1:5 (aq:org)) and total flow rates (0.2 mL/min or 1 mL/min) were tested. The residence time was also varied by using different lengths of tubing for the mixing loop. A list of the LLEs in flow of zirconium can be seen in Table 6.

13.1.3.17 LLE in batch of zirconium with trioctylphosphine oxide

0.001 M $ZrCl_4$ and 0.001 M YCl_3 in 6 M, 8 M, or 10 M HCl was used as aqueous phase and 0.1 M TOPO in heptane was used as organic phase. 0.5 mL of the aqueous phase was mixed with 1.5 mL of the organic phase. The two phases were mixed for 2 minutes, the phases separated by gravity, and the two phases were separated. Samples of the aqueous phase before and after the LLE were analyzed by ICP-OES following the procedure

described in section 13.1.3.20. The extraction efficiencies of zirconium and yttrium were calculated from equation (15).

13.1.3.18 LLE in flow of zirconium with trioctylphosphine oxide

The LLE in flow of zirconium was also tested with 0.1 M TOPO in heptane as organic phase. 0.01 M or 0.001 M $ZrCl_4$ and YCl_3 in 12 M HCl was used as aqueous phase. A 0.2 µm pore sized PTFE/PP membrane and a diaphragm with a thickness of 2 mil were used for all LLEs. A total flow rate of 0.2 mL/min and a residence time in the mixing loop of 2.5 minutes were applied. The flow rate ratio was 1:3 or 1:5 (aq:org). The LLEs of zirconium in flow with TOPO as extractant are listed in Table 7.

13.1.3.19 LLE in flow of ^{89}Zr with guaiacol/anisole

10 MBq/mL ^{89}Zr in 12 M HCl containing dissolved yttrium foil was used as aqueous phase for the LLE in flow. Guaiacol/anisole 9/1 (v/v) was used as organic phase. A flow rate ratio of 1:5 (aq:org) was applied. The total flow rate was 0.2 mL/min with a mixing loop of 108 cm or 1 mL/min with a mixing loop of 47 cm. The extraction efficiency was calculated by measuring the activity of ^{89}Zr with a dose calibrator in samples from the aqueous and organic phase (equation (14)).

13.1.3.20 Quantification of zirconium and yttrium by ICP-OES

ICP-OES was used to analyze the concentration of zirconium and yttrium in the aqueous phase before and after the LLE. The samples were prepared by diluting 0.5 mL of the sample up to 10 mL to reach an HCl concentration of 5 % (v/v). The concentration of the calibration standards were 5, 10, 20, 30, and 50 ppm in 5 % (v/v) HCl. The extraction efficiency was calculated with equation (15).

13.1.3.21 LLE of copper

13.1.3.22 Production of ^{64}Cu

^{64}Cu was obtained from the medical production at the Hevesy Laboratory. ^{64}Ni was electroplated on a silver disk and the target was irradiated with a proton beam from a GE 16.5 MeV PETtrace cyclotron. A 1000 µm thick aluminum foil was placed in front to degrade the proton beam energy to approximately 9 MeV. The current was 20 µA. The target was dissolved in 30 % HCl and ^{64}Cu was purified over Dowex 1x8 chloride form (200-400 mesh) resin. Nickel was eluted with 6 M HCl, cobalt was then eluted with 5 M HCl, and finally ^{64}Cu was eluted in 1 M HCl.

13.1.3.23 LLE in batch of copper with trioctylphosphine oxide

0.1 M, 0.05 M, or 0.01 M TOPO in hexane was used as organic phase. 1.5 mL of each of the three solutions was mixed with 0.5 mL 0.001 M $CuCl_2$ and 0.001 M $NiCl_2$ in 6 M HCl. The two phases were mixed for 2 minutes, the phases separated by gravity and the phases were separated. The aqueous phase before and after the LLE was analyzed by ICP-OES (Section 13.1.3.28).

13.1.3.24 LLE in flow of copper with trioctylphosphine oxide

The LLE in flow of copper was performed with a PTFE/PP membrane with a 0.2 µm pore size and a diaphragm with a thickness of 2 mil (same setup as described in section 13.1.3.5). Different concentrations of TOPO and diluents were applied. The aqueous phase was 6 M HCl containing 0.001 M $CuCl_2$ and $NiCl_2$. For one LLE in flow the aqueous phase contained 60 ppm Cu, Ni, Co, Zn, Fe, and Ag from an ICP standard solution. Different flow rate ratios (1:1, 1:3, and 1:5 (aq:org)) were tested and a total flow rate of 0.2 mL/min or 1 mL/min was applied. The residence time in the mixing loop was 2.5 minutes. The LLEs in flow of copper with TOPO can be seen in Table 8. Samples of the aqueous phase before and after the LLEs were analyzed by ICP-OES (Section 13.1.3.28).

13.1.3.25 Second LLE in flow of copper with ATSM

The organic phase from the LLE of copper in flow with 0.1 M TOPO in hexane was collected for 1 hour (9 mL) and used for a second LLE, where 0.5 mM ATSM in DMSO was used as the second phase. A flow rate ratio of 1:3 (hexane:DMSO) and a total flow rate of 0.6 mL/min were applied. A PTFE/PP membrane with a pore size of 0.2 µm and a diaphragm with a thickness of 2 mil were used to achieve complete phase separation between the two phases. Samples from the DMSO phase were collected and analyzed by UV-vis spectroscopy (section 13.1.3.29). The second LLE was repeated in batch mode where the hexane phase containing 0.1 M TOPO and the extracted copper from the first LLE was mixed with 0.05 M ATSM and 0.1 M KOH in DMSO/water 1/1 (v/v). The phases were mixed and then separated. The DMSO phase was analyzed by UV-vis spectroscopy.

13.1.3.26 Second LLE of copper with DOTA

The second LLE of copper with DOTA was first performed in batch mode. 0.1, 0.3, and 1.0 mM DOTA in water were prepared. 2.7 mL of each of the three solutions were mixed with 0.9 mL of the organic phase from the first LLE with 0.1 M TOPO in hexane. The two phases were mixed and the phases separated. The samples of the aqueous phase were analyzed by ICP-OES (section 13.1.3.28) and the extraction efficiencies were calculated by equation (17), where $c_{aq,\ after\ second\ LLE}$ is the concentration of copper and nickel in the aqueous phase after the second LLE, $c_{aq,\ before\ first\ LLE}$ is the initial concentration of copper and nickel in the feed for the first LLE, and $c_{aq,\ after\ first\ LLE}$ is the concentration of copper and nickel in the aqueous phase after the first LLE with 0.1 M TOPO in

hexane. The second LLE was performed in flow where 1.0 mM DOTA in water was used as aqueous phase and the organic phase from the first LLE with 0.1 M TOPO in heptane was used as organic phase. A flow rate ratio of 3:1 (aq:org), a total flow rate of 0.6 mL/min, and a residence time in the mixing loop of 2.3 minutes were applied. A diaphragm with a 2 mil thickness and a PTFE/PP membrane with a pore size of 0.2 µm were used and complete phase separation was obtained. The LLE was repeated where the mixing loop (3 m) was heated to 55 °C. Samples of the aqueous phase were analyzed by ICP-OES.

$$E\% = \frac{9 \cdot c_{aq,after\ second\ LLE}}{c_{aq,before\ first\ LLE} - c_{aq,after\ first\ LLE}} \cdot 100\ \% \quad (17)$$

13.1.3.27 LLE in flow of ^{64}Cu with trioctylphosphine oxide

1-3 MBq/mL ^{64}Cu in 6 M HCl and 0.1 M TOPO in heptane were used as aqueous and organic phase, respectively, for the LLE in flow. A PTFE/PP membrane with a 0.2 µm pore size and a diaphragm with a thickness of 2 mil were applied as for the LLE of nonradioactive copper. A flow rate ratio of 1:3 (aq:org) was applied and the total flow rate was 0.2 mL/min or 1 ml/min. The residence time in the mixing loop was 2.5 minutes for the LLE with low flow rate and 0.2 minutes for the LLE with a high flow rate. Samples of the organic and aqueous phase after the LLE were analyzed by measuring the activity of ^{64}Cu with a dose calibrator. The extraction efficiency was calculated with equation (14).

13.1.3.28 Quantification of copper and nickel by ICP-OES

The concentration of copper and nickel in the aqueous phase before and after LLE was analyzed by ICP-OES. Calibration standards were prepared with a concentration of 0.5, 1, 2, 3, and 5 ppm Cu and Ni in 5 % (v/v) HCl. The samples of the aqueous phase were prepared by diluting 0.5 mL of the sample up to 10 mL to reach a final HCl concentration of 5 % (v/v). The samples containing Cu, Ni, Co, Zn, Fe, and Ag and calibration standards were prepared the same way. The samples from the second extraction with DOTA were also diluted by taking 2 mL of the sample and adding 0.5 mL 12 M HCl and diluting up to 10 mL. The extraction efficiencies were calculated with equation (15).

13.1.3.29 Quantification of copper by UV-vis spectroscopy

Calibration samples with 0.05, 0.1, 0.2, and 0.4 mM Cu-ATSM in DMSO were prepared and the absorption spectrum from 300-800 nm was recorded by UV-vis spectroscopy. The absorption spectrum for 0.5 mM ATSM was also recorded. The DMSO phase after the second LLE with ATSM in DMSO and after the LLE with ATSM in DMSO also containing KOH (section 13.1.3.25) were also measured from 300-800 nm.

13.1.3.30 LLE of gallium

The following experimental section for the LLE of gallium can also be found in [9].

13.1.3.31 Production of ^{66,67,68}Ga and ^{65}Zn

The radiometals were produced by the ^{nat}Zn(p,n)^{66,67,68}Ga and the ^{nat}Cu(p,n)^{63,65}Zn nuclear reactions on a GE 16.5 MeV PETtrace cyclotron. A 250 µm thick zinc foil (750-831 mg) and a 500 µm thick copper foil (301-341 mg) were stacked and irradiated at 10 µA for 120-160 minutes. The irradiated zinc foil was dissolved in 3 mL 12 M HCl after 18-24 hours containing mainly ^{67}Ga (approximately 50 MBq at EOB). The HCl concentration was adjusted to 3 M or 6 M. 10-50 µL of the solution was added per mL to a 5.6 M or 1 M $ZnCl_2$ in 3 M or 6 M HCl stock solution to obtain 100-300 kBq/mL of ^{67}Ga. The irradiated copper foil (5-10 MBq ^{65}Zn at EOB) was dissolved in 1.7 mL concentrated HNO_3 at 60 °C 18-24 hours after EOB. The solution was evaporated to dryness under argon flow at 150 °C. The solid was dissolved in 2.5 mL 1 M HCl and loaded on 3 g TK200 resin. The copper was removed by washing the resin with 14 mL 1 M HCl. ^{65}Zn was eluted in 25 mL water collected in fractions of 2-3 mL. The fractions containing a high amount of ^{65}Zn were evaporated to dryness and ^{65}Zn was dissolved in 2 mL 3 M HCl. 10-50 µL of the solution was added per mL to the $ZnCl_2$ stock solution also containing ^{67}Ga. The stock solutions with ^{65}Zn and ^{67}Ga were used as aqueous phase for the LLE experiments.

13.1.3.32 Quantification of ^{65}Zn and ^{67}Ga by gamma spectroscopy

The extraction efficiencies of gallium and zinc were calculated by equation (14) by measuring the activity of ^{65}Zn and ^{67}Ga in the aqueous and organic phase after the LLE by gamma spectroscopy. ^{65}Zn was quantified by its gamma lines at 511.0 (annihilation) and 1115.5 keV and ^{67}Ga by its gamma lines at 93.3, 184.6, 209.0, 300.2, and 393.5 keV. The germanium detector was calibrated with barium-133 and europium-152 certified samples.

13.1.3.33 Phase separation study with Et_2O and 5.6 M $ZnCl_2$ in HCl

Solutions of 5.6 M $ZnCl_2$ in 0, 0.5, 1, 1.5, 2, 2.5, 3, 3.5, and 4 M HCl were prepared. 3 mL of each solution was added to nine different centrifuge tubes. 3 mL of Et_2O (presaturated with the corresponding HCl concentration) was added to each tube. The tubes were mixed for 30 minutes and centrifuged afterwards. The level of the aqueous and organic phase in each tube was marked with a pen on the centrifuge tube. The tubes were then emptied and dried. The volumes of the phases were measured by adding water to the marks on the tubes and weighing the amount of water and calculating the volume from the density of water. The LLE of gallium and zinc was measured under the same conditions. 1.3 mL of 5.6 M $ZnCl_2$ in 0.05, 0.6, 1, 2, and 3 M HCl also containing ^{65}Zn and ^{67}Ga were added to five different centrifuge tubes. 1.3 mL of presaturated Et_2O was added to each tube. The phases were mixed for 30 minutes and the tubes were centrifuged. The phases were separated and

the activity of zinc and gallium in the aqueous and organic phases were measured by gamma spectroscopy (section 13.1.3.32).

13.1.3.34 Diluent study

6 M and 3 M HCl prepared from concentrated HCl in deuterium oxide (D_2O) were prepared and $ZnCl_2$ was added to reach a concentration of 5.6 M $ZnCl_2$. 1.3 mL of 5.6 M $ZnCl_2$ in 6 M HCl was added to each of seven centrifuge tubes. The level of this solution in the tubes was marked with a pen. 1 mL of THP, Et_2O, *n*-BuOMe, $^{i}Pr_2O$, *n*-HexOMe, *n*-Bu_2O, and *n*-Am_2O were added to their respective centrifuge tube. The phases were mixed for one minute and some phases were partly or completely miscible. Toluene was added as diluent until the volume of the aqueous phase was the same as before the addition of the ether, which could be seen by comparing to the mark on the tubes.

1.3 mL of 5.6 M $ZnCl_2$ in 6 M HCl was added to four different centrifuge tubes. 1 mL of THP was added to each of the four tubes. Anisole, DCE, TFT, and heptane were added to their respective tubes until the volume of the aqueous phase was the same as before adding THP. This study with THP was repeated but with 5.6 M $ZnCl_2$ in 3 M HCl. The phases were separated and the aqueous phase was analyzed by qNMR to evaluate the amount of diluent and ether in the aqueous phase. 0.7 mL of each aqueous phase was added to NMR tubes and 15-20 mg of citric acid was added to each sample. The amount of diluent and ether was calculated by the following equation (18), where n_{IC} and n_t are the number of protons of the peak used for quantification for the internal calibrant (IC) and the target analyte (t), respectively. Int_{IC} and Int_t are the integral of the peak used for quantification for IC and for t. MW_{IC} and MW_t are the molecular weight of IC and t. P_{IC} is the purity of IC and m_s the mass of the sample. [61]

$$P\ (\%) = \frac{n_{IC} \cdot Int_t \cdot MW_t \cdot m_{IC}}{n_t \cdot Int_{IC} \cdot MW_{IC} \cdot m_s} \cdot P_{IC} \tag{18}$$

13.1.3.35 LLE in batch of gallium with ethers

5.6 M $ZnCl_2$ in 3 M or 6 M HCl or 1 M $ZnCl_2$ in 6 M HCl also containing ^{65}Zn and ^{67}Ga were used as aqueous phase. The seven ethers (THP, Et_2O, *n*-BuOMe, $^{i}Pr_2O$, *n*-HexOMe, *n*-Bu_2O, and *n*-Am_2O) mixed with TFT 1/2 (v/v) were the organic phases for the LLE in batch. The aqueous and the organic phase were mixed in a volume ratio of 1:3 (aq:org) in a centrifuge tube and mixed for 30 minutes. The tubes were centrifuged and the phases separated manually. The amount of ^{65}Zn and ^{67}Ga in the aqueous and organic phase was measured by gamma spectroscopy (section 13.1.3.32). For the scrubbing, 0.5, 1, 6, or 8 M HCl were added to the organic phase after the LLE (1:3 (aq:org)). The phases were mixed for 10 minutes. The phases were separated after centrifugation

and the amount of ^{65}Zn and ^{67}Ga in each phase was measured by gamma spectroscopy. For the stripping of ^{67}Ga, 0.1 M HCl was added to the organic phase after the LLE (1:1 (aq:org)).The phases were mixed for 10 minutes, centrifuged and the phases separated. The amount of ^{65}Zn and ^{67}Ga in each phase was measured by gamma spectroscopy and the stripping efficiency was calculated as the amount of ^{65}Zn or ^{67}Ga in the aqueous phase divided by the total amount of ^{65}Zn or ^{67}Ga. The LLE from 5.6 M $ZnCl_2$ in 3 M HCl with the different ethers mixed with TFT 1/2 (v/v) was repeated where ^{54}Mn and ^{60}Co were added to the aqueous phase before the LLE. The extraction of Mn and Co was measured by gamma spectroscopy.

13.1.3.36 LLE in flow of gallium with ethers

The LLE in flow was performed as described in section 13.1.3.5 with a PTFE/PP membrane (0.2 µm pore size) and a diaphragm with a thickness of 2 mil. A flow rate ratio of 1:3 (aq:org) and a total flow rate of 1.0 mL/min were applied for the LLEs in flow. The residence time in the mixing loop was 0.5 minutes. The aqueous phase was 5.6 M $ZnCl_2$ in 3 M HCl with ^{65}Zn and ^{67}Ga and the organic phase was THP, Et_2O, *n*-BuOMe, or $^{i}Pr_2O$ mixed with TFT 1/2 (v/v). Complete phase separation was obtained, but when changing to 5.6 M $ZnCl_2$ in 6 M HCl and $^{i}Pr_2O$/TFT 1/2 (v/v) breakthrough was seen. The aqueous phase after the LLE with $^{i}Pr_2O$/TFT 1/2 (v/v) was analyzed by qNMR as described in section 13.1.3.34. The aqueous phase was also passed through a C18 Sep Pak cartridge and then analyzed by qNMR. Complete phase separation was obtained with 1 M $ZnCl_2$ in 6 M HCl with ^{65}Zn and ^{67}Ga as aqueous phase and the seven ethers (THP, Et_2O, *n*-BuOMe, $^{i}Pr_2O$, *n*-HexOMe, *n*-Bu_2O, and *n*-Am_2O) mixed with TFT 1/2 (v/v) as organic phase. Scrubbing of the organic phase after the LLE was performed with 8 M HCl and a flow rate ratio of 3:1 (aq:org) and total flow rate of 1.0 mL/min. Stripping of gallium from the organic phase was performed with 0.1 M HCl and a flow rate ratio of 1:3 (aq:org) and total flow rate of 1.0 mL/min.

The LLE in flow from 5.6 M $ZnCl_2$ in 3 M HCl with $^{i}Pr_2O$/TFT 1/2 (v/v) was repeated with 7 MBq ^{64}Cu in the aqueous phase. The extraction of copper was measured by gamma spectroscopy. The same LLE was repeated with 9 mM $FeCl_3$ in the aqueous phase. The organic phase after the LLE was used for the scrubbing with 8 M HCl, followed by stripping with 0.1 M HCl. The extraction, scrubbing and stripping of iron was measured by ICP-OES by diluting 82.5 µL of samples from the aqueous phase up to 100 mL (10 mL for the scrubbing samples) with 1 % v/v HCl. The iron concentration in the aqueous phase before and after the LLE was measured and the extraction efficiency was calculated by equation (15), while the scrubbing and stripping was calculated by dividing the iron concentration in the scrubbing or stripping solution with the concentration in the organic phase before the scrubbing and stripping.

13.2 Development of [^{45}Ti]Ti-CAS-PSMA

The syntheses of the CA-PSMA ligand and the Ti-CAS-PSMA complex are described in this section. The syntheses required access to a well-equipped chemistry laboratory; especially NMR spectroscopy was essential to evaluate the structure of the synthesized compounds. The NMR spectra of the compounds, which have not been published previously, can be found in appendix C. The production of ^{45}Ti, which necessitated local access to cyclotron facilities, and the optimizations of the radiolabeling and the purification of [^{45}Ti]Ti-CAS-PSMA are included in this section. Lastly, analyses of [^{45}Ti]Ti-CAS-PSMA together with stability studies and an *in vivo* evaluation of the compound are described.

13.2.1 Materials

The materials applied for the production and purification of ^{45}Ti can be found in section 13.1.1.

Sodium hydroxide (98-100.5 %), benzoyl peroxide, hydrogen chloride solution (4.0 M in dioxane), 1-butanol (99.4 %), diethyl ether (99.0 %), mouse serum, 1-octanol (99 %), tetrahydrofuran (99.0 %), titanium isopropoxide (97 %), thionyl chloride (97 %), dimethyl sulfoxide-d_6 (99.5 atom % D), chloroform-d (99.8 atom % D), palladium on carbon (10 wt. % loading, matrix activated carbon support), pyridine-d_5 (99.5 atom % D), *N*,*N*-dimethylformamide (anhydrous, 99.8 %), triphosgene (98 %), pyridine (anhydrous, 99.8 %), DIPEA (99 %), cesium carbonate (99 %), *N*-bromosuccinimide (99 %), trifluoroacetic acid (99 %), trifluoroacetic acid-d (99 atom % D), ammonium formate (97 %), celite S, dichloromethane-d_2 (99.9 atom % D), acetone (99.5 %), sodium carbonate, and preparative TLC plates (silica gel, glass support) were purchased from Sigma Aldrich. Sodium chloride (99.5 %), acetic acid, and ethanol (anhydrous) were purchased from Fluka and sodium hydrogen sulfate ($NaHSO_4$) (99.0 %) was purchased from BDH Chemicals. Methanol (LiChroSolv), DMSO (99 %), and TLC plates (silica gel and silica gel 60 RP-18, F_{254}) from Merck and heptane (99.7 %), *n*-hexane (97 %), chloroform (99.2 %), dichloromethane (100 %), ethyl acetate (99.9 %), acetonitrile (99.9 % gradient grade for liquid chromatography) and toluene (HiPER Chromanorm) from VWR were used. Glutamic acid di-*t*-butyl ester hydrochloride (98 %), O^{t}Bu-Lys-Cbz · HCl (97 %), *p*-Tolyl isothiocyanate (97 %), carbon tetrachloride (99 %), chelidamic acid monohydrate (95 %), lithium hydroxide (anhydrous, 95 %), and thallium(I) ethoxide (95 %) were purchased from abcr GmbH. Formic acid was purchased from Bie & Berntsen A-S. Various cartridges (alumina N, C18 plus, QMA, silica plus) were purchased from Waters and from ABX (QMA preconditioned with CO_3^{2-}).

13.2.2 Instruments

The details for the NMR spectrometer, analytical HPLC, cyclotron, germanium detector, TLC scanner, ICP spectrometer, centrifuge, syringe pumps, and dose calibrator are listed in section 13.1.2.

A Shimadzu LC-MS system consisting of a CBM-20A communications bus module, a SPD-20A UV-vis detector, a FRC-10A fraction collector, a LC-20AP preparative liquid chromatograph, a FCV-200AL Prep Quaternary Valve, and an LC-MS-2020 was applied for preparative HPLC and Mass spectrometry (MS). A Shim-pack GIST 5 µm C18, 20x250mm column was used. For radio-TLC, a Perkin Elmer Cyclone Plus imager and a Wolf Trimline LED illuminator were applied. A Siemens INVEON multimodality scanner in a docked mode (Siemens pre-clinical solutions, Knoxville, TN, US) was applied.

13.2.3 Methods

13.2.3.1 Synthesis of CA-PSMA

The synthesis route for CA-PSMA can be seen in Figure 48.

*13.2.3.2 Synthesis of diethyl-4-hydroxypyridine-2,6-dicarboxylate (**1**)*

Compound **1** was synthesized following the method as described previously. [159]

50 mL anhydrous EtOH was added to a round-bottom flask in an ice bath under a flow of argon. 12.6 mL (173 mmol) thionyl chloride was added. Afterwards, 5.03g (27 mmol) chelidamic acid was added in small portions as solid and the mixture was stirred at 0 °C for 5 min. The mixture was stirred at room temperature for 20 h. The mixture was then heated to reflux for 2h. The solvent was removed under reduced pressure and a yellow oil was obtained. The flask with the crude product was placed in an ice bath and 50mL water was added. The mixture was neutralized with 5 mL 10% aqueous Na_2CO_3 and 5 mL 50% aqueous EtOH. The precipitate was filtered and dried under reduced pressure. The product was obtained as a white solid (5.49 g, 23mmol, 85% yield). ^{1}H NMR (400 MHz, ACN-d_3) δ 7.65 (s, 2H), 4.39 (q, *J*=7.1 Hz, 4H), 1.37 (t, *J*=7.1 Hz, 6H).

*13.2.3.3 Synthesis of thallium(I) 2,6-bis(ethoxycarbonyl)pyridine-4-olate (**2**)*

1mL TlOEt (3.69 g, 15 mmol) was collected with a syringe. 3.53 g (15 mmol) of **1** and 25 mL distilled THF were added to a 100 mL round-bottom flask and stirred. The TlOEt was mixed with 4 mL distilled THF and this mixture was added dropwise to the reaction mixture in the flask. The flask was evacuated and the reaction mixture was stirred for 2 h at room temperature. White precipitate was formed. The mixture was transferred to a falcon tube and centrifuged. The liquid was decanted and the solid was re-suspended in THF and centrifuged again. This was repeated three times. The solid was dried and 5.5 g (12.6 mmol, 85% yield) of **2** was obtained. ^{1}H NMR (DMSO-d_6) δ 6.86 (s, 2H), 4.27 (q, 4H), 1.30 (t, 6H) ppm.

*13.2.3.4 Synthesis of 1-(bromomethyl)-4-isothiocyanatobenzene (**3**)*

Compound **3** was synthesized as described previously. [160]

2.6 g (17.5 mmol) *p*-Tolyl isothiocyanate was dissolved in 40 mL CCl_4 in a 100 mL round-bottom flask. 3.2 g (18 mmol) NBS was added followed by a small amount of BPO. The mixture was stirred at reflux (90 °C) for 8 hours. The reaction was followed by TLC with hexane as eluent until full conversion. The mixture was cooled to room temperature, filtered and the solvent evaporated. The crude product was recrystallized in MeOH (80 °C) and the product was obtained as pale yellow needle-like crystals (1.9 g (48 %)). ^{1}H NMR (400 MHz, DMSO-d_6) δ 7.52 (d, *J*=8.6 Hz, 2H), 7.42 (d, *J*=8.6 Hz, 2H), 4.72 (s, 2H). ^{13}C NMR (100 MHz, acetone-d_6) δ 141.1, 141.1, 139.0, 131.6, 126.9, 33.2.

*13.2.3.5 Synthesis of diethyl 4-((4-isothiocyanatobenzyl)oxy)pyridine-2,6-dicarboxylate (**4**) from compound **1***

All starting materials and reagents were dried under vacuum. 1.0 g (4.2 mmol, 1 equiv.) **1** was dissolved in 70 mL dry *N*,*N*-dimethylformamide (DMF) in a round-bottom flask. 2.7 g (8.3 mmol, 2 equiv.) Cs_2CO_3 was added. The mixture was stirred for 30 minutes at room temperature. 1.42 g (6.2 mmol, 1.5 equiv.) of **3** was dissolved in 6 mL dry DMF and added dropwise. The mixture was stirred for 2 hours at room temperature. 0.5 mL of the reaction mixture was taken out and the solvent evaporated. The sample was analyzed by NMR to see if any remaining CAEE was left. The reaction mixture was then filtered and DMF was removed. The crude product was dissolved in DCM and filtered, and dried. The product was isolated as a white solid (0.85 g (53 %)) by column chromatography with chloroform/ethyl acetate 9/1 (v/v). ^{1}H NMR (400 MHz, DMSO-d_6) δ 7.81 (s, 2H), 7.57 (d, *J*=8.6 Hz, 2H), 7.49 (d, *J*=8.6 Hz, 2H), 5.39 (s, 2H), 4.37 (q, *J*=7.1 Hz, 4H), 1.33 (t, *J*=7.1 Hz, 6H). ^{13}C NMR (100 MHz, DMSO-d_6) δ 166.0, 164.1, 149.7, 135.5, 133.6, 129.8, 129.3, 126.2, 114.4, 69.3, 61.7, 14.1.

*13.2.3.6 Synthesis of diethyl 4-((4-isothiocyanatobenzyl)oxy)pyridine-2,6-dicarboxylate (**4**) from compound **2***

0.12 g (0.27 mmol) of **2** and 0.06 g (0.27 mmol) of **3** were mixed in 4 mL dry DMF. The reaction mixture was heated to 60 °C and stirred for 2 hours. The reaction was followed by TLC with chloroform/ethyl acetate 9/1 (v/v) as eluent. The reaction mixture was centrifuged and the supernatant was collected, the solvent evaporated and the crude product was dried. Preparative TLC with chloroform/ethyl acetate 9/1 (v/v) as eluent was used to obtain compound **4** (32 mg (31 %)). Identical NMR spectra were obtained as for the previous synthesis of compound **4**.

*13.2.3.7 Synthesis of (S)-2-[3((S)-(5-Benzyloxycarbonylamino)-1-tert-butoxycarbonylpentylureido] pentanedioic acid Di-tert-butyl Ester (**5**)*

The method described by Maresca et. al was used for the synthesis of compound **5**. [161]

1.24 g (4.2 mmol) triphosgene was dissolved in 20 mL dry DCM at 0 °C. 4.22 g (11 mmol) O^{t}Bu-Lys-Cbz · HCl and 4.3 mL (24 mmol) DIPEA in 20 mL dry DCM was added dropwise over 1 hour. A solution of 3.35 g (11 mol) OtBu$_2$-Glu · HCl and 4.3 mL (24 mmol) DIPEA in 20 mL dry DCM was added in one portion. The mixture was stirred for 1 hour. The solvent was evaporated and the crude product was dissolved in 60 mL ethyl acetate and washed twice with 80 mL 2 M $NaHSO_4$. The organic phase was then washed with brine and dried over Na_2SO_4. Na_2SO_4 was removed by filtration and the crude product was dried. The product (2.47 g (36%)) was obtained by column chromatography with hexane/ethyl acetate 2/1 (v/v) as eluent. ^{1}H NMR (400 MHz, $CDCl_3$) δ 7.32 (m, 5H), 5.24-5.12 (m, 3H), 5.09 (d, *J*=5.8 Hz, 2H), 4.37-4.28 (m, 2H), 3.22-3.12 (m, 2H), 2.36-2.20 (m, 2H), 2.10-2.00 (m, 1H), 1.88-1.71 (m, 2H), 1.66-1.56 (m, 1H), 1.54-1.47 (m, 2H), 1.46-1.41 (m, 27H), 1.40-1.30 (m, 2H). ^{13}C NMR (100 MHz, $CDCl_3$) δ 172.6, 172.5, 172.4, 157.0, 156.7, 136.8, 128.6, 128.2, 128.2, 82.3, 81.9, 80.7, 66.7, 53.4, 53.1, 40.8, 32.7, 31.7, 29.5, 28.5, 28.2, 28.1, 22.4.

The product was also synthesized by first adding OtBu$_2$-Glu · HCl dropwise to the triphosgene solution and then adding O^{t}Bu-Lys-Cbz · HCl in one portion afterwards.

*13.2.3.8 Synthesis of (S)-di-tert-butyl 2-(3-((S)-6-amino-1-tert-butoxy-1-oxohexane-2-yl)ureido) pentanedioate (**6**)*

The deprotection was performed as described previously by Maresca et. al. [161]

0.63 g (1.0 mmol) ammonium formate was suspended in 10 ml EtOH. 0.62 g (1 mmol) of **5** was dissolved in 10 mL EtOH and added to the suspension. 67 mg 10% Pd-C was added and the mixture was stirred at room temperature overnight. The mixture was filtered through a celite pad and the solvent was removed under reduced pressure. Remaining ammonium formate was removed by dissolving the crude product in 50 mL DCM and washing with 50 mL 1 M Na_2CO_3 aqueous solution. The organic phase was then washed with brine and dried over Na_2SO_4. The solvent was removed under reduced pressure and the product was obtained (0.41 g (84 %)). ^{1}H NMR (400 MHz, $CDCl_3$) δ 6.41-6.20 (m, 2H), 4.36-4.26 (m, 2H), 3.07-2.92 (m, 2H), 2.34-2.89 (m, 2H), 2.12-2.01 (m, 1H), 1.89-1.61 (m, 5H), 1.55-1.38 (m, 28H), 1.28-1.23 (m, 1H). ^{13}C NMR (100 MHz, DMSO-d_6) δ 172.3, 172.0, 171.5, 157.3, 80.5, 80.3, 79.8, 53.1, 52.2, 38.6, 31.3, 30.9, 27.8, 27.7, 27.6, 22.1.

*13.2.3.9 Synthesis of diethyl 4-((4-(3-((S)-6-(tert-butoxy)-5-(3-((S)-1,5-di-tert-butoxy-1,5-dioxopentan-2-yl)ureido)-6-oxohexyl)thioureido)benzyl)oxy)pyridine-2,6-dicarboxylate (**7**)*

0.75 (19 mmol) of **4** was dissolved in 20 mL dry DMF and transferred to a round-bottom flask. 0.95 g (19 mmol) **6** was dissolved in 20 mL dry DMF and added dropwise to the flask. The mixture was stirred at room temperature for 30 minutes. The solvent was evaporated and the product dried under reduced pressure. The

product was purified by column chromatography with hexane/ethyl acetate 1/2 (v/v) and 1.36 g (82 %) of **7** was obtained. ^{1}H NMR (400 MHz, DMSO-d_6) δ 7.81 (s, 2H), 7.44 (m, 4H), 6.28 (m, 2H), 5.31 (s, 2H), 4.38 (q, *J*=7.1 Hz, 4H), 4.07-3.96 (m, 2H), 3.46 (m, 2H), 2.29-2.15 (m, 2H), 1.91-1.82 (m, 1H), 1.71-1.50 (m, 5H), 1.40-1.37 (m, 28H), 1.34 (t, *J*=7.1Hz, 6H), 1.36-1.29 (m, 1H). ^{13}C NMR (100 MHz, DMSO-d_6) δ 180.3, 172.2, 171.9, 171.4, 166.1, 164.1, 157.1, 149.7, 139.5, 130.8, 128.6, 122.7, 114.3, 80.6, 80.3, 79.7, 70.0, 61.6, 53.1, 52.1, 43.6, 31.8, 28.1, 27.7, 27.6, 22.5, 14.1.

*13.2.3.10 Synthesis of (((S)-5-(3-(4-(((2,6-bis(ethoxycarbonyl)pyridin-4-yl)oxy)methyl)phenyl) thioureido)-1-carboxy-pentyl)carbamoyl)-L-glutamic acid (**8**)*

0.21 g (0.24 mmol) of **7** was mixed with 4 mL TFA/DCM (1/1) and stirred at room temperature overnight. The product was precipitated by adding the reaction mixture to 35 mL cold diethyl ether. The mixture was centrifuged and the precipitate was washed three times with cold diethyl ether. The product was obtained as a white solid (0.16 g (95 %)). ^{1}H NMR (400 MHz, DMSO-d_6) δ 7.81 (s, 2H), 7.44 (m, 4H), 6.33 (m, 2H), 5.31 (s, 2H), 4.37 (q, *J*=7.1 Hz, 4H), 4.13-4.04 (m, 2H), 3.44 (m, 2H), 2.32-2.17 (m, 2H), 1.96-1.88 (m, 1H), 1.75-1.64 (m, 2H), 1.60-1.50 (m, 3H), 1.34 (t, *J*=7.1 Hz, 6H), 1.36-1.28 (m, 2H). ^{13}C NMR (100 MHz, DMSO-d_6) δ 180.2, 174.6, 174.3, 173.8, 166.2, 164.2, 157.3, 149.7, 139.5, 128.7, 122.8, 116.5, 114.4, 70.1, 61.7, 52.4, 51.7, 43.8, 31.9, 29.9, 28.3, 27.6, 22.8, 15.2, 14.2. MS (*m/z*): $[M+Na]^+$ calcd for $C_{31}H_{39}N_5O_{12}S$, 728.7; found, 728.5.

*13.2.3.11 Synthesis of 4-((4-(3-((S)-6-(tert-butoxy)-5-(3-((S)-1,5-di-tert-butoxy-1,5-dioxopentan-2-yl)ureido)-6-oxohexyl)thioureido)benzyl)oxy)pyridine-2,6-dicarboxylic acid (**9**)*

0.25 g (0.29 mmol) of **7** was dissolved in 7 mL THF and 14 mg (0.58 mmol, 2.2 equiv.) LiOH in 3 mL water was added. The mixture was stirred for 3.5 hours at room temperature. The reaction was followed by TLC with BuOH/AcOH/H_2O (8/1/1) as eluent. The solvent was removed under reduced pressure and the product was obtained as the lithium salt (0.22 g (91 %)) without further purification. ^{1}H NMR (400 MHz, DMSO-d_6) δ 7.60 (d, *J*=8.0 Hz, 2H), 7.55 (s, 2H), 7.36 (d, *J*=8.4 Hz 2H), 6.40 (m, 2H), 5.20 (s, 2H), 4.00 (m, 2H), 3.46 (m, 2H), 2.30-2.14 (m, 2H), 1.90-1.81 (m, 1H), 1.71-1.50 (m, 5H), 1.40-1.36 (m, 27H), 1.36-1.27 (m, 2H). ^{13}C NMR (100 MHz, DMSO-d_6) δ 180.4, 172.3, 171.9, 171.5, 167.6, 166.2, 157.2, 156.4, 140.0, 128.0, 122.5, 110.0, 80.6, 80.3, 79.7, 69.2, 53.2, 52.2, 43.5, 31.8, 30.9, 30.4, 28.2, 27.7, 27.7, 22.7.

*13.2.3.12 Synthesis of 4-((4-(3-((S)-5-carboxy-5-(3-((S)-1,3-dicarboxypropyl)ureido)pentyl)thio-ureido)benzyl)oxy)pyridine-2,6-dicarboxylic acid (**CA-PSMA**)*

Method 1: Synthesis from compound **8**

34 mg (0.86 mmol, 6 equiv.) NaOH was dissolved in 2 mL water and 0.1 g (0.14 mmol) of **8** was added. The mixture was shaken until the compound was dissolved. The pH was adjusted to pH 4 with 0.1 M HCl and the solvent was evaporated. The product was not purified. ^{1}H NMR (400 MHz, D_2O) δ 7.74 (s, 2H), 7.50 (d, *J*=7.9 Hz, 2H), 7.26 (d, *J*=7.9 Hz, 2H), 5.36 (s, 2H), 3.95 (m, 2H), 3.48 (m, 2H), 2.23-2.16 (m, 2H), 1.99-1.90 (m, 1H), 1.83-1.74 (m, 2H), 1.67-1.49 (m, 3H), 1.38-1.28 (m, 2H).

Method 2: Synthesis from compound **9**

0.20 g (0.24 mmol) of **9** was mixed with 6 mL TFA/DCM 1/1 (v/v) and stirred at room temperature for 2.5 hours. The product was precipitated in 30 mL cold diethyl ether and washed three times with cold diethyl ether. The product was dried and the product was obtained as a white solid (0.13 g (84 %)). ^{1}H NMR (400 MHz, DMSO-d_6) δ 7.74 (s, 2H), 7.48 (d, *J*=8.7 Hz, 2H), 7.41 (d, *J*=8.5 Hz, 2H), 6.36 (m, 2H), 5.32 (s, 2H), 4.08 (m, 2H), 3.44 (m, 2H), 2.29-2.19 (m, 2H), 1.96-1.87 (m, 1H), 1.76-1.64 (m, 2H), 1.60-1.50 (m, 3H), 1.38-1.28 (m, 2H). ^{13}C NMR (100 MHz, DMSO-d_6) δ 180 (weak signal), 174.5, 174.2, 173.7, 170.1, 167.4, 164.5, 157.3, 150.3, 139.4, 128.6, 122.6, 113.2, 70.2, 52.2, 51.6, 43.7, 31.9, 29.9, 28.2, 27.5, 22.8.

13.2.3.13 Synthesis of Ti-CAS-PSMA

The synthesis route of Ti-CAS-PSMA can be seen in Figure 49.

*13.2.3.14 Synthesis of (6,6'-((ethane-1,2-diylbis(methylazanediyl))bis(methylene))bis(2,4-dimethyl-phenol))Ti(O^iPr)$_2$ ((salan)Ti(O^iPr)$_2$ (**10**))*

Compound **10** was synthesized by following a similar method as described previously by Chmura et al. [162]

0.44 g (1.5 mmol) titanium isopropoxide was transferred to a round-bottom flask under argon flow and dissolved in 12 mL dry DCM. 0.54 g (1.5 mmol) salan was dissolved in 3 mL dry DCM and added to the round-bottom flask. The mixture was stirred for 3 hours at room temperature. The solvent was evaporated and the crude product was recrystallized in heptane. The product was obtained as yellow crystals (0.33 g (43 %)). ^{1}H NMR (400 MHz, $CDCl_3$) δ 6.89 (d, *J*=1.5 Hz, 2H), 6.61 (d, *J*=1.5 Hz, 2 H), 5.17 (sept., *J*=6.1 Hz, 2H), 4.69 (d, *J*=13.3 Hz, 2H), 3.05 (d, *J*=13.3 Hz, 2H), 3.04 (d, *J*=9.4 Hz, 2H), 2.41 (s, 6H), 2.24 (s, 6H), 2.22 (s, 6H), 1.73 (d, *J*=9.5 Hz, 2H), 1.28 (d, *J*=6.1 Hz, 6H), 1.20 (d, *J*=6.1 Hz, 6H).

*13.2.3.15 Formation of **Ti-CAS-PSMA***

Method 1: Synthesis from compound **9**

*Synthesis of ^{t}Bu-protected Ti-CAS-PSMA (**11**)*

0.24 g (0.29 mmol) of **9** and 0.15 g (0.29 mmol) (salan)Ti(^{i}OPr)$_2$ (**10**) were dissolved in 4 mL dry pyridine in a round-bottom flask. The reaction mixture was stirred at 60 °C for 15 min. The color changed from yellow to red. The solvent was evaporated and the product was dissolved in toluene and dried. The product was purified by column chromatography with MeOH/$CHCl_3$ (1/99 to 2/98) as eluent. The product (**11**) was obtained as a red solid (0.19 g (53 %)). ^{1}H NMR (400 MHz, pyridine-d_5) δ 7.82-7.78 (m, 4H), 7.53 (d, *J*=8.2 Hz, 2H), 7.17 (d, *J*=8.4 Hz, 1H), 7.13 (d, *J*=8.4 Hz, 1H), 6.82 (s, 2H), 6.70 (s, 2H), 5.44 (d, *J*=13.8 Hz, 2H), 5.21 (s, 2H), 4.88 (m, 1H), 4.74 (m, 1H), 3.92 (m, 2H), 3.22 (d, *J*=8.9 Hz, 2H), 3.14 (d, *J*=14.1 Hz, 2H), 2.72 (s, 6H), 2.60-2.55 (m, 2H), 2.41-2.32 (m, 1H), 2.23 (s, 6H), 2.18-2.13 (m, 1H), 2.11 (s, 6H), 2.00 (d, *J*=9.8 Hz, 2H), 1.97-1.90 (m, 1H), 1.82-1.74 (m, 3H), 1.67-1.56 (m, 2H), 1.51-1.38 (m, 27H). ^{13}C NMR (100 MHz, pyridine-d_5) δ 182.8, 173.7, 173.4, 172.7, 171.3, 169.3, 159.1, 157.1, 152.6, 131.8, 131.4, 130.8, 130.0, 128.8, 128.3, 125.2, 123.4, 112.0, 81.6, 81.4, 80.5, 72.2, 64.1, 54.8, 54.1, 47.0, 33.4, 32.5, 29.6, 29.3, 28.5, 28.3, 23.9, 21.1, 16.4.

*Synthesis of Ti-CAS-PSMA from **11***

30 mg (0.025 mmol) of **11** was dissolved in 0.8 mL DCM-d_2/TFA-d 1/1 (v/v) and followed by NMR for 75 min. The product was not further purified.

Method 2: Synthesis from **CA-PSMA**

20 mg (0.04 mmol) (salan)Ti(^{i}OPr)$_2$ and 25 mg (0.04 mmol) of **CA-PSMA** were dissolved in 1.5 mL DMSO. The reaction mixture was heated to 60 °C and stirred for 30 minutes. The product was precipitated in diethyl ether and washed twice with diethyl ether. 20 mg of the crude product was purified by preparative TLC (C18 plates) using ACN/H_2O 1/1 (v/v) as eluent. The product was collected from the plate, dried and dissolved in DMSO. The product was precipitated in diethyl ether and dried a second time (13 mg (66 %)). ^{1}H NMR (400 MHz, DMSO-d_6) δ 7.69 (s, 2H), 7.45 (m, 4H), 6.78 (s, 2H), 6.76 (s, 2H), 6.33 (m, 2H), 5.47 (d, *J*=11.7 Hz, 1H), 5.42 (d, *J*=11.7 Hz, 1H), 4.92 (d, *J*=13.7 Hz, 2H), 4.08 (m, 2H), 3.44 (m, 2H), 3.32 (d, *J*=13.8 Hz, 2H), 3.12 (d, *J*=8.8 Hz, 2H), 2.6 (s, 6H), 2.3 (d, *J*=8.9 Hz, 2H), 2.27-2.20 (m, 2H), 2.15 (s, 6H), 1.95-1.87 (m, 1H), 1.83 (s, 6H), 1.75-1.64 (m, 2H), 1.58-1.49 (m, 3H), 1.35-1.28 (m, 2H). ^{13}C NMR (100 MHz, DMSO-d_6) δ 180.2, 174.6, 174.3, 173.8, 170.6, 167.9, 157.3, 155.5, 150.9, 139.7, 135.5, 130.2, 129.6, 128.9, 127.9, 127.2, 123.8, 122.8, 111.4, 71.4, 53.1, 52.3, 51.7, 45.9, 31.9, 30.0, 28.2, 27.6, 22.8, 20.3, 15.4. MS (*m/z*): $[M+H]^+$ calcd for $C_{49}H_{59}N_7O_{14}S$, 1050.96; found, 1050.

Method 3: Test of radiolabeling conditions

2 mL 0.01 M (0.02 mmol) $TiCl_4$ in 12 M HCl was mixed with 2 mL guaiacol/anisole 9/1 (v/v) for 10 minutes. The mixture was centrifuged and the two phases were separated with a pipette. 0.4 mL pyridine was added to 1 mL of the organic phase. Then, 4 mg (0.01 mmol) salan in 0.4 mL DMSO was added and the mixture was stirred at 80 °C for 5 minutes. 7.5 mg (0.01 mmol) of **CA-PSMA** in 0.4 mL DMSO was added and the reaction mixture was stirred for 30 minutes. The product was purified using preparative HPLC (section 13.2.3.16). The fractions were analyzed by analytical HPLC (section 13.2.3.16) and the fractions containing the product were collected and the solvent was evaporated. The product was dried and analyzed by NMR, which gave identical spectra to **Ti-CAS-PSMA** synthesized by method 2.

13.2.3.16 HPLC method

For analytical HPLC, the Merck Hitachi Elite Lachrom with a Carrol & Ramsey 105-S radio-detector and a Hitachi L-2450 diode array detector was used. The UV-signal at 270 and 420 nm was recorded. A Phenomenex Luna 3µ C18(2) (100 Å, 100 mm x 2.00 mm) column and a flow rate of 0.5 mL/min was applied. The eluents were (A) 0.1 % TFA in Milli-Q water and (B) 0.1 % TFA in ACN.

A Shimadzu LC-MS system with a Shim-pack GIST 5 µm C18 (20 mm x 250 mm) column was applied for preparative HPLC. A flow of 15 mL/min was applied and a total run time of 42 minutes. The eluents were (A) 0.1 % formic acid in Milli-Q water and (B) ACN. Fractions of 3 mL were collected automatic with a fraction collector. The fractions were analyzed by measuring the radioactivity with a dose calibrator and by analytical HPLC.

13.2.3.17 Production of ^{45}Ti and formation of [^{45}Ti]Ti-CAS-PSMA

13.2.3.18 Production and purification of ^{45}Ti

^{45}Ti was produced from 250 µm or 127 µm thick scandium foil by the ^{45}Sc(p,n)^{45}Ti nuclear reaction using a 16 MeV GE PETtrace cyclotron. A 500 µm thick aluminum foil was used to degrader the beam energy to approximately 13 MeV. The mass of the scandium foil used in the target was between 22-80 mg. The scandium foil was irradiated for 10-30 min at 15-20 µA and was dissolved in 3-6 mL 12 M HCl after irradiation. The solution was filtered and centrifuged. ^{45}Ti was separated from scandium by LLE with guaiacol/anisole 9/1 (v/v) either by the membrane-based separation method as described in section 5.3.4 and described in [8] where an organic flow rate of 0.75 mL/min and aqueous flow rate of 0.25 mL/min were used or in batch mode, where the two phases where mixed for 10 minutes, centrifuged, and separated with a pipette. The ratio between the organic and aqueous phase was varied in batch mode to obtain a higher concentration of ^{45}Ti. The different LLE methods can be seen in Table 11. Most LLEs were done in batch mode since relative low radioactivity was used.

13.2.3.19 Formation of [^{45}Ti]Ti-CAS-PSMA

The ^{45}Ti-labeling was performed by mixing the organic phase (guaiacol/anisole) containing ^{45}Ti from the LLE with salan dissolved in DMSO at 60 °C or 80 °C for 5 minutes. Then, CA-PSMA dissolved in DMSO was added to the reaction mixture and stirred at 60 °C or 80 °C for 15-80 minutes. The radiolabeling was followed by analytical HPLC. Different conditions (solvent volume, temperature, ligand concentration, and mixing time) were studied in order to improve the radiolabeling. These conditions can be seen in Table 11. The formation of [^{45}Ti]Ti-CAS-PSMA was followed by radio-HPLC, where the retention time of the radio-peak was compared to the UV-signal of Ti-CAS-PSMA. The most optimal tested conditions can be seen in entry 9 in Table 11 and these conditions were used for the further experiments.

13.2.3.20 Purification of [^{45}Ti]Ti-CAS-PSMA

In order to separate and purify the formed [^{45}Ti]Ti-CAS-PSMA, different methods were tested. First, it was attempted to trap the product on a cartridge to separate the product from the guaiacol/anisole/DMSO solution. The radiolabeling solution was diluted with toluene (1:1) and loaded on a silica plus or an alumina N cartridge. The cartridge was washed with toluene and the product was eluted with 20-50 % H_2O in MeOH or BuOH/H_2O/AcOH (4/1/1). It was also attempted to trap the product on a C18 plus cartridge (washed with EtOH and water before) and elute the product with ACN/H_2O 6/4 (v/v). The radiolabeling solution was also loaded on a QMA cartridge preconditioned with carbonate solution and washed with water. The cartridge was washed with water and DMSO.

A different approach was to inject the radiolabeling solution directly on a preparative HPLC (C18 column) (see section 13.2.3.16). The fractions were analyzed by measuring the activity with a dose calibrator and evaluating the radiochemical identity by analytical radio-HPLC. The fractions containing the product were collected and diluted with H_2O (1:1). This solution was passed through a C18 plus cartridge (washed with EtOH and H_2O before). The cartridge was washed with H_2O and the product was eluted in 1.5 mL EtOH/H_2O 9/1 (v/v). The solution was dried down to 50-100 µL under argon flow and was diluted with PBS or HEPES buffer (pH 7.5). This method was suitable for the purification of [^{45}Ti]Ti-CAS-PSMA and was used for the further experiments.

13.2.3.21 Analyses and stability studies of [^{45}Ti]Ti-CAS-PSMA

The RCP and radionuclidic purity were determined to evaluate the presence of other radioactive compounds or nuclides. The molar activity and the content of other possible metals were calculated to evaluate the interference from the nonradioactive Ti-CAS-PSMA or from other metals and the octanol/water partition coefficient of [^{45}Ti]Ti-CAS-PSMA was measured to evaluate the lipophilicity. Lastly, the stability of [^{45}Ti]Ti-CAS-PSMA in

buffer and in mouse serum was studied to evaluate if the compound was stable for an acceptable time period (3-6 hours).

13.2.3.22 Radiochemical purity of [^{45}Ti]Ti-CAS-PSMA

The RCP of the final product was analyzed by radio-HPLC (same method as described in section 13.2.3.16) and radio-TLC using C18 TLC plates and ACN/H_2O 7/3 (v/v) as eluent and measuring the TLC plate with a Raytest MiniGita TLC scanner. The HPLC or TLC radio-peak expected to arise from the [^{45}Ti]Ti-CAS-PSMA was identified by comparing the retention time or R_f value to the one of the nonradioactive Ti-CAS-PSMA. The RCP was calculated by dividing the area of the [^{45}Ti]Ti-CAS-PSMA peak with the total peak area.

13.2.3.23 Radionuclidic purity of [^{45}Ti]Ti-CAS-PSMA

The radionuclidic purity was measured by gamma spectroscopy using a Germanium detector, which was calibrated with barium-133 and europium-152 sources. The samples were containing approximately 3 MBq ^{45}Ti and were measured in a distance of 1 meter for 0.3-3 hours. ^{45}Ti was identified from the three gamma lines with highest intensity (511.0 keV (169.6 %), 719.6 keV (0.154 %), and 1408.1 keV (0.085 %) [17]). The radionuclidic purity was calculated by dividing the activity of ^{45}Ti with the total activity of the sample.

13.2.3.24 Metal content and molar activity of the final formulation of [^{45}Ti]Ti-CAS-PSMA

The amount of metals (Ti (323.4 nm), Sc (357.2 nm), Fe (239.5, 240.4, 259.8 nm), Ag (328.0 nm), Cu (224.7 nm), and Zn (202.5, 206.2, 213.8 nm)) in the final product was analyzed by ICP-OES at the listed wavelengths, where 50 µL of the [^{45}Ti]Ti-CAS-PSMA in the final eluate solution (EtOH/H_2O 9/1 (v/v)) was diluted to 10 mL with 1 % HCl. The concentrations of metals were calculated from a standard curve of samples with known concentrations. The molar activity was calculated from the amount of titanium found by ICP-OES or from the concentration of Ti-CAS-PSMA calculated from the UV-signal of the product seen on the analytical HPLC from a standard curve.

13.2.3.25 Partition coefficient of [^{45}Ti]Ti-CAS-PSMA

The lipophilicity of the product was determined by measuring the octanol/water partition coefficient. 0.5 mL of the eluate with the product was evaporated to dryness and 1 mL water and 1 mL octanol were added. The two phases were mixed for 2 minutes and subsequently separated. 0.5 mL of each phase was taken out and the activity of each phase was measured with a dose calibrator. The partition coefficient was found by dividing the activity in the octanol phase ($A_{45Ti,octanol}$) with the activity in the aqueous phase ($A_{45Ti,water}$) and the log P value was calculated by equation (19).

$$\log P = \log\left(\frac{A_{^{45}Ti,octanol}}{A_{^{45}Ti,water}}\right) \quad (19)$$

13.2.3.26 Stability studies

The stability of [^{45}Ti]Ti-CAS-PSMA was analyzed in the eluate from the C18 cartridge (EtOH/H_2O 9/1 (v/v)) and by diluting the eluate with water (pH 7), PBS buffer (pH 7.5) or HEPES buffer (pH 7.5) to 10 % EtOH. The samples were analyzed by HPLC after 0, 1, 2, 3, and 4 hours using the same HPLC method as described previously. The stability in mouse serum was tested by diluting the eluate from the C18 cartridge with PBS or HEPES buffer (1/9) or by evaporating the eluate down to 50-100 µL and diluting with PBS or HEPES buffer. Mouse serum was used since the *in vivo* evaluation of [^{45}Ti]Ti-CAS-PSMA will be performed in a mouse model. The solutions were then mixed with mouse serum 1/1 (v/v). The samples were incubated at 37 °C, and analyzed by radio-TLC after 0, 1, 2, 3, and 4 hours using C18 TLC plates and ACN/H_2O 7/3 (v/v) as eluent. The stability in PBS and HEPES buffer at 37 °C and at room temperature was also followed as a comparison to the serum samples. Furthermore, the stability of [^{45}Ti]Ti-CAS-PSMA in serum without buffer, in PBS/EtOH 1/1 (v/v) and PBS/H_2O 1/1 (v/v) at 37 °C was tested. The nonradioactive Ti-CAS-PSMA was used as a TLC reference and the plates were analyzed using a Perkin Elmer Cyclone Plus imager.

13.2.3.27 In vivo studies

The *in vivo* studies were performed at Odense University Hospital. The animal experiment license number was 2016-15-0201-01027.

Four male Balb/c nude mice (Janvier) received an injection with 5 million PC3+ cells at the left shoulder. The tumors were allowed to grow for 24 days. The tumor sizes were between 7x6 to 9x9.5 mm and the mice weighed 25-27 g two days before the µPET scanning. A CT scan of 15 minutes was performed prior to each PET scan. A Siemens INVEON multimodality scanner was applied for the scans. The mice were anesthetized with a mixture of 1.5-2 % isoflurane and 100 % oxygen during injection of the radiotracer and during the scans, where the mice were placed feet first in a prone position on a heated PET/CT animal bed. Each mouse received 0.5-1.4 MBq of [^{45}Ti]Ti-CAS-PSMA in PBS buffer containing 10 % EtOH administered intravenously through the tail vein. The first mouse received the [^{45}Ti]Ti-CAS-PSMA tracer four hours EOS, while the fourth mouse received the tracer 7.5 hours EOS. The two first mice were scanned by dynamic acquisition from 0-75 minutes followed by 20 minutes static scan four hours p.i. The two last mice received a 15 minutes static scan 1 hour p.i., followed by a 20 minutes static scan four hours p.i. (Table 15). After the last scanning, the mice were euthanatized by cervical dislocation and dissected. The organs were collected and weighed separately. The amount of ^{45}Ti in the organs was measured with a gamma well counter.

14 References

[1] *A Guide to Clinical PET in Oncology: Improving Clinical Management of Cancer Patients*. Vienna: International Atomic Energy Agency, 2008.

[2] M. A. Haidekker, *Medical Imaging Technology*. Springer, 2013.

[3] T. I. Kostelnik and C. Orvig, "Radioactive Main Group and Rare Earth Metals for Imaging and Therapy," *Chem. Rev.*, vol. 119, pp. 902–956, 2019.

[4] P. Martini *et al.*, "Perspectives on the use of liquid extraction for radioisotope purification," *Molecules*, vol. 24, p. 334, 2019.

[5] A. Adamo, P. L. Heider, N. Weeranoppanant, and K. F. Jensen, "Membrane-based, liquid-liquid separator with integrated pressure control," *Ind. Eng. Chem. Res.*, vol. 52, pp. 10802–10808, 2013.

[6] K. M. Buettner and A. M. Valentine, "Bioinorganic Chemistry of Titanium," *Chem. Rev.*, vol. 112, pp. 1863–1881, 2012.

[7] S. P. Rowe, M. A. Gorin, and M. G. Pomper, "Imaging of Prostate-Specific Membrane Antigen with Small-Molecule PET Radiotracers: From the Bench to Advanced Clinical Applications," *Annu. Rev. Med.*, vol. 70, no. 1, pp. 461–477, 2019.

[8] K. S. Pedersen, J. Imbrogno, J. Fonslet, M. Lusardi, K. F. Jensen, and F. Zhuravlev, "Liquid–liquid extraction in flow of the radioisotope titanium-45 for positron emission tomography applications," *React. Chem. Eng.*, vol. 3, pp. 898–904, 2018.

[9] K. S. Pedersen, K. M. Nielsen, J. Fonslet, M. Jensen, and F. Zhuravlev, "Separation of Radiogallium from Zinc Using Membrane-Based Liquid-Liquid Extraction in Flow: Experimental and COSMO-RS Studies," *Solvent Extr. Ion Exch.*, vol. 37, no. 5, pp. 376–391, 2019.

[10] F. Zhuravlev, K. S. Pedersen, J. Fonslet, J. M. Imbrogno, A. Adamo, and K. F. Jensen, "A method for continuous separation of radiometals for positron emission tomography," EP2019/071156, 2019.

[11] S. R. Cherry, J. A. Sorenson, and M. E. Phelps, "Positron Emission Tomography," in *Physics in nuclear medicine*, Elsevier/Saunders, 2012, pp. 307–343.

[12] J. J. Vaquero and P. Kinahan, "Positron Emission Tomography: Current Challenges and Opportunities for

Technological Advances in Clinical and Preclinical Imaging Systems," *Annu. Rev. Biomed. Eng.*, vol. 17, no. 1, pp. 385–414, 2015.

[13] M. Brandt, J. Cardinale, M. L. Aulsebrook, G. Gasser, and T. L. Mindt, "An overview of PET radiochemistry, Part 2: Radiometals," *J. Nucl. Med.*, vol. 59, no. 10, pp. 1500–1506, 2018.

[14] D. Brasse and A. Nonat, "Radiometals: Towards a new success story in nuclear imaging?," *Dalt. Trans.*, vol. 44, no. 11, pp. 4845–4858, 2015.

[15] E. Boros and A. B. Packard, "Radioactive Transition Metals for Imaging and Therapy," *Chem. Rev.*, vol. 119, pp. 870–901, 2019.

[16] M. J. Welch, R. Laforest, and J. S. Lewis, "Production of Non-standard PET Radionuclides and the Application of Radiopharmaceuticals Labeled with these Nuclides," in *PET Chemistry The Driving Force in Molecular Imaging*, P. A. Schubiger, L. Lehmann, and M. Friebe, Eds. Springer, 2007, pp. 159–182.

[17] "NuDat 2.7, National Laboratory National Nuclear Data Center Brookhaven." [Online]. Available: https://www.nndc.bnl.gov/nudat2/. [Accessed: 03-Jul-2019].

[18] P. W. Miller, N. J. Long, R. Vilar, and A. D. Gee, "Synthesis of 11C, 18F, 15O, and 13N radiolabels for positron emission tomography," *Angew. Chemie - Int. Ed.*, vol. 47, pp. 8998–9033, 2008.

[19] J. Notni and H.-J. Wester, "Re-thinking the role of radiometal isotopes: Towards a future concept for theranostic radiopharmaceuticals," *J. Label. Compd. Radiopharm.*, vol. 61, pp. 141–153, 2018.

[20] M. Eder *et al.*, "68Ga-complex lipophilicity and the targeting property of a urea-based PSMA inhibitor for PET imaging," *Bioconjug. Chem.*, vol. 23, no. 4, pp. 688–697, 2012.

[21] M. Hofmann *et al.*, "Biokinetics and imaging with the somatostatin receptor PET radioligand 68Ga-DOTATOC: Preliminary data," *Eur. J. Nucl. Med.*, vol. 28, no. 12, pp. 1751–1757, 2001.

[22] A. Haug *et al.*, "Intraindividual comparison of 68Ga-DOTA-TATE and 18F-DOPA PET in patients with well-differentiated metastatic neuroendocrine tumours," *Eur. J. Nucl. Med. Mol. Imaging*, vol. 36, no. 5, pp. 765–770, 2009.

[23] A. Afshar-Oromieh *et al.*, "PET imaging with a [68Ga]gallium-labelled PSMA ligand for the diagnosis of prostate cancer: biodistribution in humans and first evaluation of tumour lesions," *Eur. J. Nucl. Med. Mol. Imaging*, vol. 40, pp. 486–495, 2013.

[24] A. Afshar-Oromieh, U. Haberkorn, M. Eder, M. Eisenhut, and C. M. Zechmann, "[68Ga]Gallium-labelled PSMA ligand as superior PET tracer for the diagnosis of prostate cancer: Comparison with 18F-FECH," *Eur. J. Nucl. Med. Mol. Imaging*, vol. 39, no. 6, pp. 1085–1086, 2012.

[25] S. Heskamp, R. Raavé, O. Boerman, M. Rijpkema, V. Goncalves, and F. Denat, "89Zr-Immuno-Positron Emission Tomography in Oncology: State-of-the-Art 89Zr Radiochemistry," *Bioconjug. Chem.*, vol. 28, no. 9, pp. 2211–2223, 2017.

[26] H. Wan, "An Overall Comparison of Small Molecules and Large Biologics in ADME Testing," *ADMET DMPK*, vol. 4, pp. 1–22, 2016.

[27] Y. A. Haggag, A. A. Donia, M. A. Osman, and S. A. El-Gizawy, "Peptides as Drug Candidates: Limitations and Recent Development Perspectives," *Biomed. J. Sci. Tech. Res.*, vol. 8, no. 4, pp. 6659–6662, 2018.

[28] A. Bachmair, D. Finley, and A. Varshavsky, "In Vivo Half-Life of a Protein Is a Function of Its Amino-Terminal Residue," *Science.*, vol. 234, no. 4773, pp. 179–186, 1986.

[29] A. L. Nelson, "Antibody fragments Hope and hype," *MAbs*, vol. 2, pp. 77–83, 2010.

[30] A. Afshar-Oromieh *et al.*, "The theranostic PSMA ligand PSMA-617 in the diagnosis of prostate cancer by PET/CT: Biodistribution in humans, radiation dosimetry, and first evaluation of tumor lesions," *J. Nucl. Med.*, vol. 56, no. 11, pp. 1697–1705, 2015.

[31] C. Cullinane *et al.*, "Comparing the therapeutic efficacy of 67Cu-SARTATE and 177Lu-DOTA-octreotate in a neuroendocrine tumor model," *J. Nucl. Med.*, vol. 59, no. supplement 1, p. 315, May 2018.

[32] International Atomic Energy Agency, *Cyclotron Produced Radionuclides: Principles and Practice*. Vienna, 2008.

[33] TRIUMF, "Isotope Production | TRIUMF : Canada's particle accelerator centre." [Online]. Available: https://www.triumf.ca/isotope-production. [Accessed: 25-Oct-2019].

[34] C. S. Cutler, H. M. Hennkens, N. Sisay, S. Huclier-Markai, and S. S. Jurisson, "Radiometals for Combined Imaging and Therapy," *Chem. Rev.*, vol. 113, no. 2, pp. 858–883, 2013.

[35] V. H. Alves, S. J. C. do Carmo, F. Alves, and A. J. Abrunhosa, "Automated Purification of Radiometals Produced by Liquid Targets," *Instruments*, vol. 2, p. 17, 2018.

[36] H. M. R. Moreira, “Cyclotron Production of 68Ga using a 68Zn-based liquid target,” University of Coimbra, 2013.

[37] A. Robin and J. L. Rosa, “Corrosion behavior of niobium, tantalum and their alloys in hot hydrochloric and phosphoric acid solutions,” *Int. J. Refract. Met. Hard Mater.*, vol. 18, no. 1, pp. 13–21, 2000.

[38] A. Boschi, P. Martini, V. Costa, A. Pagnoni, and L. Uccelli, “Interdisciplinary tasks in the cyclotron production of radiometals for medical applications. The case of 47Sc as example,” *Molecules*, vol. 24, p. 444, 2019.

[39] A. Dash and R. Chakravarty, “Radionuclide generators: the prospect of availing PET radiotracers to meet current clinical needs and future research demands,” *Am. J. Nucl. Med. Mol. Imaging*, vol. 9, no. 1, pp. 30–66, 2019.

[40] J. S. Fritz and D. T. Gjerde, *Ion Chromatography*, 4th ed., vol. 6, no. 1. Weinheim: WILEY-VCH Verlag GmbH & Co. KGaA, 2009.

[41] J. S. Fritz, “Early milestones in the development of ion-exchange chromatography: A personal account,” *J. Chromatogr. A*, vol. 1039, pp. 3–12, 2004.

[42] C. K. Vyas, J. H. Park, and S. D. Yang, “Application of Extraction Chromatographic Techniques for Separation and Purification of Radiometals 44/47Sc and 64/67Cu,” *J. Radiopharm. Mol. Probes*, vol. 2, no. 2, pp. 84–95, 2016.

[43] V. S. Kislik, “Chemistry of Metal Solvent Extraction,” in *Solvent Extraction*, 1st ed., Oxford, UK: Elsevier, 2012, pp. 113–156.

[44] International Atomic Energy Agency, “Cyclotron Produced Radionuclides: Emerging Positron Emitters for Medical Applications: 64Cu and 124I,” Vienna, 2016.

[45] International Atomic Energy Agency, *Gallium-68 Cyclotron Production*. Vienna: IAEA, 2019.

[46] “Gallium (68Ga) chloride solution for radiolabeling,” in *European Pharmacopoeia 9.0*, Council of Europe, 2013, pp. 1148–1149.

[47] R. D. Shannon, “Revised Effective Ionic Radii and Systematic Studies of Interatomic Distances in Halides and Chaleogenides,” *Acta Crystallogr.*, vol. A 32, pp. 751–767, 1976.

[48] A. E. Martell, R. J. Motekaitis, E. T. Clarke, R. Delgado, Y. Sun, and R. Ma, “Stability constants of metal complexes of macrocylic ligands with pendant donor groups,” *Supramol. Chem.*, vol. 6, pp. 353–363, 1996.

[49] C. F. Ramogida and C. Orvig, “Tumour targeting with radiometals for diagnosis and therapy,” *Chem. Commun.*, vol. 49, no. 42, pp. 4720–4739, 2013.

[50] A. L. Vavere and J. S. Lewis, “Cu-ATSM: A radiopharmaceutical for the PET imaging of hypoxia,” *Dalt. Trans.*, pp. 4893–4902, 2007.

[51] C. A. Boswell *et al.*, “Comparative in Vivo Stability of Copper-64-Labeled Cross-Bridged and Conventional Tetraazamacrocyclic Complexes,” *J. Med. Chem.*, vol. 47, no. 6, pp. 1465–1474, 2004.

[52] D. J. Vugts *et al.*, “Comparison of the octadentate bifunctional chelator DFO*-pPhe-NCS and the clinically used hexadentate bifunctional chelator DFO-pPhe-NCS for 89Zr-immuno-PET,” *Eur. J. Nucl. Med. Mol. Imaging*, vol. 44, no. 2, pp. 286–295, 2017.

[53] K. E. Jones, K. L. Batchler, C. Zalouk, and A. M. Valentine, “Ti(IV) and the Siderophore Desferrioxamine B: A Tight Complex Has Biological and Environmental Implications,” *Inorg. Chem.*, vol. 56, no. 3, pp. 1264–1272, 2017.

[54] B. M. Zeglis, J. L. Houghton, M. J. Evans, N. Viola-Villegas, and J. S. Lewis, “Underscoring the influence of inorganic chemistry on nuclear imaging with radiometals,” *Inorg. Chem.*, vol. 53, no. 4, pp. 1880–1899, 2014.

[55] E. W. Price and C. Orvig, “Matching chelators to radiometals for radiopharmaceuticals,” *Chem. Soc. Rev.*, vol. 43, no. 1, pp. 260–290, 2014.

[56] V. M. Nurchi, G. Crisponi, T. Pivetta, M. Donatoni, and M. Remelli, “Potentiometric, spectrophotometric and calorimetric study on iron(III) and copper(II) complexes with 1,2-dimethyl-3-hydroxy-4-pyridinone,” *J. Inorg. Biochem.*, vol. 102, no. 4, pp. 684–692, 2008.

[57] D. S. Abou, T. Ku, and P. M. Smith-Jones, “In vivo biodistribution and accumulation of 89Zr in mice,” *Nucl. Med. Biol.*, vol. 38, no. 5, pp. 675–681, 2011.

[58] G. A. Bailey *et al.*, “H2azapa: A versatile acyclic multifunctional chelator for 67Ga, 64Cu, 111In, and 177Lu,” *Inorg. Chem.*, vol. 51, no. 22, pp. 12575–12589, 2012.

[59] S. Z. Lever, K. H. Fan, and J. R. Lever, “Tactics for preclinical validation of receptor-binding radiotracers,” *Nucl. Med. Biol.*, vol. 44, pp. 4–30, 2017.

[60] X. Hou and B. T. Jones, “Inductively Coupled Plasma/Optical Emission Spectroscometry,” *Encyclopedia of Analytical Chemistry*. John Wiley & Sons, Inc., pp. 9468–9485, 2000.

[61] G. F. Pauli *et al.*, “Importance of purity evaluation and the potential of quantitative 1H NMR as a purity assay,” *J. Med. Chem.*, vol. 57, no. 22, pp. 9220–9231, 2014.

[62] J. C. Merrill, R. M. Lambrecht, and A. P. Wolf, “Cyclotron Isotopes and Radiopharmaceuticals - XXIV. Titanium-45,” *Int. J. Appl. Radiat. Isot.*, vol. 29, no. 2, pp. 116–117, 1978.

[63] F. Chen, H. F. Valdovinos, R. Hernandez, S. Goel, T. E. Barnhart, and W. Cai, “Intrinsic radiolabeling of Titanium-45 using mesoporous silica nanoparticles,” *Acta Pharmacol. Sin.*, vol. 38, no. 6, pp. 907–913, 2017.

[64] M. Kawamura *et al.*, “Metabolism of 45Ti-labeled compounds: Effect of ascorbic acid,” *Journal of Labelled Compounds and Radiopharmaceuticals*, vol. 23, no. 10–12. pp. 1360–1362, 1986.

[65] G. W. Severin, C. H. Nielsen, A. I. Jensen, J. Fonslet, A. Kjær, and F. Zhuravlev, “Bringing Radiotracing to Titanium-Based Antineoplastics: Solid Phase Radiosynthesis, PET and ex Vivo Evaluation of Antitumor Agent [45 Ti](salan)Ti(dipic),” *J. Med. Chem.*, vol. 58, pp. 7591–7595, 2015.

[66] K. Ishiwata *et al.*, “Potential radiopharmaceuticals labeled with titanium-45,” *Int. J. Radiat. Appl. Instrumentation. Part A*, vol. 42, no. 8, pp. 707–712, 1991.

[67] A. L. Vavere and M. J. Welch, “Preparation, Biodistribution, and Small Animal PET of 45Ti-Transferrin,” *J. Nucl. Med.*, vol. 46, pp. 683–690, 2005.

[68] R. I. Price *et al.*, “Titanium-45 as a Candidate for PET Imaging: Production, Processing & Applications,” in *15th International Workshop on Targetry and Target Chemistry*, 2015.

[69] A. L. Vavere, L. A. Jones, T. J. McCarthy, D. J. Rowland, and M. J. Welch, “Preparation, biodistribution, and microPET Imaging of 45Ti-transferrin,” *J. Label. Compd. Radiopharm.*, vol. 44, no. S1, pp. S793–S795, 2001.

[70] K. Ishiwata *et al.*, “Preparation of 45Ti-labeled compounds and their medical application,” *J. Label. Compd. Radiopharm.*, vol. 19, no. 11–12, pp. 1539–1541, 1982.

[71] P. Costa, L. Metello, F. Alves, and M. Duarte Naia, “Cyclotron Production of Unconventional Radionuclides for PET Imaging: the Example of Titanium-45 and Its Applications,” *Instruments*, vol. 2, p. 8, 2018.

[72] L. Daraban, R. Adam Rebeles, A. Hermanne, F. Tarkanyi, and S. Takacs, “Study of the excitation functions for 43K, 43,44,44mSc and 44Ti by proton irradiation on 45Sc up to 37 MeV,” *Nucl. Instruments Methods Phys. Res. Sect. B*, vol. 267, no. 5, pp. 755–759, 2009.

[73] International Atomic Energy Agency, “EXFOR: Experimental Nuclear Reaction Data.” [Online]. Available: https://www-nds.iaea.org/exfor/. [Accessed: 31-Oct-2019].

[74] V. Levkovskij, *Act. Cs. by Protons and Alphas*. Moscow, 1991.

[75] A. J. Howard, H. B. Jensen, M. Rios, W. A. Fowler, and B. A. Zimmerman, “Mearuement and theoretical analysis of some reaction rates of interest in silicon burning,” *Astrophys. J.*, vol. 188, pp. 131–139, 1974.

[76] J. W. Meadows, R. M. Diamond, and R. A. Sharp, “Excitation functions and yield ratios for the isomeric pairs Br80,80m, Co58,58m, and Sc44,44m formed in (p,pn) reactions,” *Phys. Rev.*, vol. 102, no. 1, pp. 190–195, 1956.

[77] V. Kislik, “Competetive complexation/solvation theory of solvent extraction. II. Solvent extraction of metals by acidic extractants,” *Sep. Sci. Technol.*, vol. 37, no. 11, pp. 2623–2657, 2002.

[78] K. J. Fisher, “Scandium and Yttrium,” in *Comprehensive Coordination Chemistry II*, vol. 4, Elsevier Ltd, 2004, pp. 1–29.

[79] S. Kuhn, I. Spahn, B. Scholten, and H. H. Coenen, “Positron and γ-ray intensities in the decay of 45Ti,” *Radiochim. Acta*, vol. 103, no. 6, pp. 403–409, 2015.

[80] K. Gagnon, G. W. Severin, T. E. Barnhart, J. W. Engle, H. F. Valdovinos, and R. J. Nickles, “45Ti extraction using hydroxamate resin,” *AIP Conf. Proc.*, vol. 1509, pp. 211–214, 2012.

[81] G. W. Severin, J. Fonslet, and F. Zhuravlev, “Hydrolytically Stable Titanium-45,” in *15th International Workshop on Targetry and Target Chemistry*, 2014.

[82] Y. G. Sevastianov, “Method of Radioisotope Isolation from Cyclotron Targets,” *J. Radioanal. Chem.*, vol. 21, pp. 247–257, 1974.

[83] J. Siikanen *et al.*, “Production, separation and labeling of 45Ti,” *J. Nucl. Med.*, vol. 54, no. supplement 2, p. 1095, May 2013.

[84] V. Kislik and A. Eyal, “Acidity dependence of Ti(IV) extraction: A critical analysis,” *Solvent Extr. Ion Exch.*, vol. 11, no. 2, pp. 259–283, 1993.

[85] VICI AG International, “Chemical Resistance of PEEK & Polymers,” 2019. [Online]. Available: https://www.vici-jour.com/support/resistance.php. [Accessed: 20-Sep-2009].

[86] K. Nakashima, T. Maruyama, F. Kubota, and M. Goto, “Metal Extraction from Water and Organic Solvents into Fluorous Solvents by Fluorinated β-Diketone and Its Application to the Colorimetric Analysis of Metal Ions,” *Anal. Sci.*, vol. 25, no. 1, pp. 77–82, 2009.

[87] P. Sobota *et al.*, “Syntheses, structure, and reactivity of chiral titanium compounds: Procatalysts for olefin polymerization,” *Chem. - A Eur. J.*, vol. 7, no. 5, pp. 951–958, 2001.

[88] Committee for Human Medicinal Products, “ICH guideline Q3C (R5) on impurities: Guideline for Residual Solvents,” *Int. Conf. Harmon. Tech. Requir. Regist. Pharm. Hum. Use*, pp. 1–35, 2018.

[89] “5.4. Residual Solvents: Limiting Residual Solvent Levels in Active Substances, Excipients and Medicinal Products,” in *European Pharmacopoeia 7.0*, 2008, pp. 583–590.

[90] S. A. Kandil, B. Scholten, Z. A. Saleh, A. M. Youssef, S. M. Qaim, and H. H. Coenen, “A comparative study on the separation of radiozirconium via ion-exchange and solvent extraction techniques, with particular reference to the production of 88Zr and 89Zr in proton induced reactions on yttrium,” *J. Radioanal. Nucl. Chem.*, vol. 274, no. 1, pp. 45–52, 2007.

[91] G. M. Dias *et al.*, “89Zr for antibody labeling and in vivo studies – A comparison between liquid and solid target production,” *Nucl. Med. Biol.*, vol. 58, pp. 1–7, 2018.

[92] M. K. Pandey, A. Bansal, H. P. Engelbrecht, J. F. Byrne, A. B. Packard, and T. R. DeGrado, “Improved production and processing of 89Zr using a solution target,” *Nucl. Med. Biol.*, vol. 43, pp. 97–100, 2016.

[93] M. G. Mustafa, H. I. West, H. O’Brien, R. G. Lanier, M. Benhamou, and T. Tamura, “Measurements and a direct-reaction plus-Hauser-Feshbach analysis of 89Y(p,n)89Zr, 89Y(p,2n)88Zr, and 89Y(p,pn)88Y reactions up to 40 MeV,” *Phys. Rev. C*, vol. 38, no. 4, pp. 1624–1637, 1988.

[94] M. U. Khandaker, K. Kim, M. W. Lee, K. S. Kim, G. Kim, and N. Otuka, “Investigations of 89Y(p,x)

86,88,89gZr, 86m+g,87g,87m,88gY, 85gSr, and 84gRb nuclear processes up to 42 MeV," *Nucl. Instruments Methods Phys. Res. Sect. B*, vol. 271, pp. 72–81, 2012.

[95] Z. Wenrong, S. Qingbiao, L. Hanlin, and Y. Weixiang, "Investigation of Y-89(p, n)Zr-89, Y-89(p, 2n)Zr-88 and Y-89(p, pn)Y-88 reactions up to 22 MeV," *Chinese J. Nucl. Phys.*, vol. 14, no. 1, pp. 7–14, 1992.

[96] L. Poriel, A. Favre-Réguillon, S. Pellet-Rostaing, and M. Lemaire, "Zirconium and hafnium separation, part 1. Liquid/liquid extraction in hydrochloric acid aqueous solution with aliquat 336," *Sep. Sci. Technol.*, vol. 41, no. 9, pp. 1927–1940, 2006.

[97] J. P. Holland, Y. Sheh, and J. S. Lewis, "Standardized methods for the production of high specific-activity zirconium-89," *Nucl. Med. Biol.*, vol. 36, no. 7, pp. 729–739, 2009.

[98] A. G. Kazakov, R. A. Aliev, V. S. Ostapenko, A. B. Priselkova, and S. N. Kalmykov, "Separation of 89Zr from irradiated yttrium targets by extraction chromatography," *J. Radioanal. Nucl. Chem.*, vol. 317, no. 1, pp. 605–611, 2018.

[99] T. Sato, "The extraction of zirconium(IV) from aqueous acid solutions by trioctylphosphine oxide," *Solvent Extr. Ion Exch.*, vol. 1, no. 2, pp. 251–261, 1983.

[100] C. S. Kedari, T. Coll, A. Fortuny, and A. Sastre, "Third Phase Formation in the Solvent Extraction System Ir(IV)— Cyanex 923," *Solvent Extr. Ion Exch.*, vol. 23, pp. 545–559, 2005.

[101] M. A. Avila-Rodriguez, J. A. Nye, and R. J. Nickles, "Simultaneous production of high specific activity 64Cu and 61Co with 11.4 MeV protons on enriched 64Ni nuclei," *Appl. Radiat. Isot.*, vol. 65, no. 10, pp. 1115–1120, 2007.

[102] F. Szelecsényi, G. Blessing, and S. M. Qaim, "Excitation functions of proton induced nuclear reactions on enriched 61Ni and 64Ni: possibility of production of no-carrier-added 61Cu and 64Cu at a small cyclotron," *Appl. Radiat. Isot.*, vol. 44, no. 3, pp. 575–580, 1993.

[103] R. Adam Rebeles, P. Van den Winkel, A. Hermanne, and F. Tárkányi, "New measurement and evaluation of the excitation function of 64Ni(p,n) reaction for the production of 64Cu," *Nucl. Instruments Methods Phys. Res. Sect. B*, vol. 267, no. 3, pp. 457–461, 2009.

[104] S. M. Qaim, M. Uhl, F. Rösch, and F. Szelecsényi, "Excitation functions of (p, α) reactions on Ni64, Kr78, and Sr86," *Phys. Rev. C*, vol. 52, no. 2, pp. 733–739, 1995.

[105] M. Uchikoshi, “Determination of the Distribution of Cupric-Chloro Complexes in Hydrochloric Acid Solutions at 298 K,” *J. Solution Chem.*, vol. 46, pp. 704–719, 2017.

[106] M.-S. Lee and S.-H. Nam, “Solvent extraction of Ni(II) from strong hydrochloric acid solution by Alamine336,” *Bull. Korean Chem. Soc.*, vol. 32, no. 1, pp. 113–116, 2011.

[107] M. Uchikoshi, “Determination of the Distribution of Cobalt-Chloro Complexes in Hydrochloric Acid Solutions at 298 K,” *J. Solution Chem.*, vol. 47, no. 12, pp. 2021–2038, 2018.

[108] N. B. Devi and S. Mishra, “Liquid-liquid extraction of copper(II) from chloride media by Cyanex 923 in kerosene,” *J. South. African Inst. Min. Metall.*, vol. 112, pp. 859–864, 2012.

[109] B. Gupta, A. Deep, P. Malik, and S. N. Tandon, “Extraction and separation of some 3d transition metal ions using Cyanex 923,” *Solvent Extr. Ion Exch.*, vol. 20, no. 1, pp. 81–96, 2002.

[110] Y. Fujibayashi *et al.*, “Comparative Studies of Cu-64-ATSM and C-11-Acetate in an Acute Myocardial Infarction Model: Ex Vivo Imaging of Hypoxia in Rats,” *Nucl. Med. Biol.*, vol. 26, pp. 117–121, 1999.

[111] J. P. Holland *et al.*, “Functionalized bis(thiosemicarbazonato) complexes of zinc and copper: Synthetic platforms toward site-specific radiopharmaceuticals,” *Inorg. Chem.*, vol. 46, no. 2, pp. 465–485, 2007.

[112] Eckert & Ziegler Product specification sheet, “GalliaPharm® 68Ge/68Ga Generator Radionuclide Generator Description,” 2017.

[113] Galli Eo Product specification sheet, “68Ge/68Ga generator: Positron-emtiting isotope generator for diagnosis imaging, produced under GMP conditions,” 2019.

[114] J.-P. Blaser, F. Boehm, P. Marmier, and D. C. Peaslee, “Fonctions d’excitation de la réaction,” *Helv. Phys. Acta*, vol. 24, p. 3, 1951.

[115] M. Hille, “Exctiation functions of (p,n) and (α, n) reactions on Ni, Cu and Zn,” *Nucl. Phys. A*, vol. 198, pp. 625–640, 1972.

[116] H. A. Howe, “(p,n) Cross Sections of Copper and Zinc,” *Phys. Rev.*, vol. 109, no. 6, pp. 2083–2085, 1958.

[117] F. Tárkányi, F. Szelecsényi, Z. Kovács, and S. Sudár, “Excitation Functions of Proton Induced Nuclear Reactions on Enriched 66Zn, 67Zn and 68Zn: Production of 67Ga and 66Ga,” *Radiochim. Acta*, vol. 50,

no. 1–2, pp. 19–26, 1990.

[118] F. Szelecsényi, Z. Kovács, K. Nagatsu, K. Fukumura, K. Suzuki, and K. Mukai, “Investigation of direct production of 68Ga with low energy multiparticle accelerator,” *Radiochim. Acta*, vol. 100, no. 1, pp. 5–11, 2012.

[119] F. Szelecsényi, T. E. Boothe, S. Takács, F. Tárkányi, and E. Tavano, “Evaluated cross section and thick target yield data bases of Zn + p processes for practical applications,” *Appl. Radiat. Isot.*, vol. 49, no. 8, pp. 1005–1032, 1998.

[120] A. Hermanne, F. Szelecsényi, M. Sonck, S. Takács, F. Tárkányi, and P. Van Den Winkel, “New cross section data on 68Zn(p, 2n)67Ga and natZn(p, xn)67Ga nuclear reactions for the development of a reference data base,” *J. Radioanal. Nucl. Chem.*, vol. 240, no. 2, pp. 623–630, 1999.

[121] A. A. Abbasi and B. Easwaramoorthy, “Method and system for producting gallium-68 radioisotope by solid targeting in a cyclotron,” WO 2016/197084 Al, 2016.

[122] J. W. Engle *et al.*, “Very high specific activity 66/68Ga from zinc targets for PET,” *Appl. Radiat. Isot.*, vol. 70, no. 8, pp. 1792–1796, 2012.

[123] A. Alnahwi, S. Tremblay, S. Ait-mohand, J.-F. Beaudoin, and B. Guerin, “Large-scale routine production of 68Ga using 68Zn-pressed target.,” *J. Nucl. Med.*, vol. 60, no. supplement 1, p. 634, 2019.

[124] M. Jensen and J. Clark, “Direct production of Ga-68 from proton bombardment of concentrated aqueous solutions of [Zn-68] Zinc Chloride,” in *The 13th International Workshop on Targetry and Target Chemistry Proceedings*, 2011, pp. 288–292.

[125] M. K. Pandey, J. F. Byrne, H. Jiang, A. B. Packard, and T. R. Degrado, “Cyclotron production of 68Ga via the 68Zn(p,n)68Ga reaction in aqueous solution,” *Am J Nucl Med Mol Imaging*, vol. 4, no. 4, pp. 303–310, 2014.

[126] S. Riga *et al.*, “Production of Ga-68 with a General Electric PETtrace cyclotron by liquid target,” *Phys. Medica*, vol. 55, pp. 116–126, 2018.

[127] E. Oehlke *et al.*, “Production of Y-86 and other radiometals for research purposes using a solution target system,” *Nucl. Med. Biol.*, vol. 42, no. 11, pp. 842–849, 2015.

[128] M. Nair, S. Happel, T. Eriksson, M. K. Pandey, T. R. DeGrado, and K. Gagnon, “Cyclotron production

and automated new 2-column processing of [68Ga]GaCl3," *J. Nucl. Med. Mol. imaging*, vol. 44, no. 2, p. S275, 2017.

[129] Ö. Ugur *et al.*, "Ga-66 labeled somatostatin analogue DOTA-DPhe1-Tyr3-octreotide as a potential agent for positron emission tomography imaging and receptor mediated internal radiotherapy of somatostatin receptor positive tumors," *Nucl. Med. Biol.*, vol. 29, no. 2, pp. 147–157, 2002.

[130] L. C. Brown, "Chemical Processing of Cyclotron-Produced 67Ga," *Int. J. Appl. Radiat. Isot.*, vol. 22, pp. 710–713, 1971.

[131] B. Gupta, N. Mudhar, Z. Begum I, and I. Singh, "Extraction and recovery of Ga(III) from waste material using Cyanex 923," *Hydrometallurgy*, vol. 87, pp. 18–26, 2007.

[132] I. M. Ahmed, Y. A. El-Nadi, and N. E. El-Hefny, "Extraction of gallium(III) from hydrochloric acid by Cyanex 923 and Cyanex 925," *Hydrometallurgy*, vol. 131–132, pp. 24–28, 2013.

[133] N. H. Nachtrieb and R. E. Fryxell, "The Extraction of Gallium Chloride by Isopropyl Ether," *J. Am. Chem. Soc.*, vol. 71, no. 12, pp. 4035–4039, 1949.

[134] R. R. Brooks and P. J. Lloyd, "Influence of Molecular Structure on the Liquid/Liquid Extraction of the Chloro-Complexes of Gallium and Indium with Aliphatic Ethers," *Nature*, vol. 189, no. 4762, pp. 375–376, 1961.

[135] H. M. Irving and F. J. C. Rossotti, "The solvent extraction of Group IIIB metal halides," *Analyst*, vol. 77, pp. 801–812, 1952.

[136] E. H. Swift, "A new method for the separation of gallium from other elements," *J. Am. Chem. Soc.*, vol. 46, pp. 2375–2381, 1924.

[137] I. Mihaylov and P. A. Distin, "Gallium solvent extraction in hydrometallurgy: An overview," *Hydrometallurgy*, vol. 28, no. 1, pp. 13–27, 1992.

[138] S. Katsuta, M. Okai, Y. Yoshimoto, and Y. Kudo, "Extraction of gallium(III) from hydrochloric acid solutions by trioctylammonium-based mixed ionic liquids," *Anal. Sci.*, vol. 28, no. 10, pp. 1009–1012, 2012.

[139] V. Gallardo, R. Navarro, I. Saucedo, M. Ávila, and E. Guibal, "Zinc(II) extraction from hydrochloric acid solutions using amberlite XAD-7 impregnated with cyphos IL 101 (tetradecyl(trihexyl)phosphonium

chloride),” *Sep. Sci. Technol.*, vol. 43, pp. 2434–2459, 2008.

[140] N. Dallali, M. Ghanbari, Y. Yamini, B. Fateh, and Y. K. Agrawal, “Liquid-liquid extraction of ultra trace amounts of technetium produced by 100Mo(p, 2n)99mTc nuclear reaction in cyclotron,” *Indian J. Chem. - Sect. A Inorganic, Phys. Theor. Anal. Chem.*, vol. 46, no. 10, pp. 1615–1617, 2007.

[141] T. Sato and T. Kato, “The stability constants of the chloro complexes of copper(II) and zinc(II) determined by tri-n-octylamine extraction,” *J. Inorg. Nucl. Chem.*, vol. 39, no. 7, pp. 1205–1208, 1977.

[142] P. D’Angelo, A. Zitolo, F. Ceccacci, R. Caminiti, and G. Aquilanti, “Structural characterization of zinc(II) chloride in aqueous solution and in the protic ionic liquid ethyl ammonium nitrate by x-ray absorption spectroscopy,” *J. Chem. Phys.*, vol. 135, no. 15, pp. 1–7, 2011.

[143] D. L. Wertz and J. R. Bell, “Solute species and equilibria in concentrated zinc chloride/hydrochloric acid solutions,” *J. Inorg. Nucl. Chem.*, vol. 35, pp. 861–868, 1973.

[144] E. Y. Tshuva and D. Peri, “Modern cytotoxic titanium(IV) complexes; Insights on the enigmatic involvement of hydrolysis,” *Coord. Chem. Rev.*, vol. 253, no. 15–16, pp. 2098–2115, 2009.

[145] M. Shavit, D. Peri, C. M. Manna, J. S. Alexander, and E. Y. Tshuva, “Active cytotoxic reagents based on non-metallocene non-diketonato well-defined C2-symmetrical titanium complexes of tetradentate bis(phenolato) ligands,” *J. Am. Chem. Soc.*, vol. 129, no. 40, pp. 12098–12099, 2007.

[146] D. Peri, S. Meker, C. M. Manna, and E. Y. Tshuva, “Different ortho and para electronic effects on hydrolysis and cytotoxicity of diamino bis(Phenolato) ‘Salan’ Ti(IV) complexes,” *Inorg. Chem.*, vol. 50, no. 3, pp. 1030–1038, 2011.

[147] S. Meker, C. M. Manna, D. Peri, and E. Y. Tshuva, “Major impact of N-methylation on cytotoxicity and hydrolysis of salan Ti(IV) complexes: Sterics and electronics are intertwined,” *Dalt. Trans.*, vol. 40, no. 38, pp. 9802–9809, 2011.

[148] H. Glasner and E. Y. Tshuva, “C1-symmetrical titanium(IV) complexes of salan ligands with differently substituted aromatic rings: Enhanced cytotoxic activity,” *Inorg. Chem.*, vol. 53, no. 6, pp. 3170–3176, 2014.

[149] T. A. Immel, M. Grützke, A. K. Späte, U. Groth, P. Öhlschläger, and T. Huhn, “Synthesis and X-ray structure analysis of a heptacoordinate titanium(IV)-bis-chelate with enhanced in vivo antitumor

efficacy," *Chem. Commun.*, vol. 48, no. 46, pp. 5790–5792, 2012.

[150] M. Grützke, T. Zhao, T. A. Immel, and T. Huhn, "Heptacoordinate Heteroleptic Salan (ONNO) and Thiosalan (OSSO) Titanium(IV) Complexes: Investigation of Stability and Cytotoxicity," *Inorg. Chem.*, vol. 54, no. 14, pp. 6697–6706, 2015.

[151] R. C. Murphy, A. Kawashima, and P. J. Peller, "The utility of 11C-choline PET/CT for imaging prostate cancer: A pictorial guide," *Am. J. Roentgenol.*, vol. 196, no. 6, pp. 1390–1398, 2011.

[152] Z. A. Glaser and S. Rais-Bahrami, "Fluciclovine positron emission tomography in the setting of biochemical recurrence following local therapy of prostate cancer," *Transl. Androl. Urol.*, vol. 7, no. 5, pp. 824–830, 2018.

[153] E. Witkowska-Patena, A. Mazurek, and M. Dziuk, "68Ga-PSMA PET/CT imaging in recurrent prostate cancer: Where are we now?," *Cent. Eur. J. Urol.*, vol. 70, no. 1, pp. 37–43, 2017.

[154] J. D. Evans *et al.*, "Prostate cancer–specific PET radiotracers: A review on the clinical utility in recurrent disease," *Pract. Radiat. Oncol.*, vol. 8, no. 1, pp. 28–39, 2018.

[155] A. E. Machulkin *et al.*, "Small-molecule PSMA ligands. Current state, SAR and perspectives," *J. Drug Target.*, vol. 24, no. 8, pp. 679–693, 2016.

[156] F. L. Giesel *et al.*, "Intraindividual comparison of 18F-PSMA-1007 and 18F-DCFPyL PET/CT in the prospective evaluation of patients with newly diagnosed prostate carcinoma: A pilot study," *J. Nucl. Med.*, vol. 59, no. 7, pp. 1076–1080, 2018.

[157] Z. Szabo *et al.*, "Initial Evaluation of [18F]DCFPyL for Prostate-Specific Membrane Antigen (PSMA)-Targeted PET Imaging of Prostate Cancer," *Mol Imaging Biol.*, vol. 17, no. 4, pp. 565–574, 2015.

[158] J. Cardinale *et al.*, "Preclinical evaluation of 18F-PSMA-1007, a new prostate-specific membrane antigen ligand for prostate cancer imaging," *J. Nucl. Med.*, vol. 58, no. 3, pp. 425–431, 2017.

[159] N. Rizeq and S. N. Georgiades, "Linear and Branched Pyridyl – Oxazole Oligomers: Synthesis and Circular Dichroism Detectable Effect on c-Myc G-Quadruplex Helicity," *Eur. J. Org. Chem.*, pp. 122–131, 2016.

[160] N. Wang, A. Kähkönen, T. Ääritalo, P. Damlin, J. Kankare, and C. Kvarnström, "Polyviologen synthesis by self-assembly assisted grafting," *RSC Adv.*, vol. 5, no. 122, pp. 101232–101240, 2015.

[161] K. P. Maresca *et al.*, "A Series of Halogenated Heterodimeric Inhibitors of Prostate Specific Membrane Antigen (PSMA) as Radiolabeled Probes for Targeting Prostate Cancer," *J. Med. Chem.*, vol. 52, pp. 347–357, 2009.

[162] A. J. Chmura *et al.*, "Group 4 Complexes with Aminebisphenolate Ligands and Their Application for the Ring Opening Polymerization of Cyclic Esters," *Macromolecules*, vol. 39, pp. 7250–7257, 2006.

[163] S. Robu *et al.*, "Synthesis and preclinical evaluation of novel 18F-labeled Glu-urea-Glu-based PSMA inhibitors for prostate cancer imaging: a comparison with 18F-DCFPyl and 18F-PSMA-1007," *EJNMMI Res.*, vol. 8, no. 30, pp. 1–11, 2018.

[164] C. A. Umbricht *et al.*, "44Sc-PSMA-617 for radiotheragnostics in tandem with 177Lu-PSMA-617 — preclinical investigations in comparison with 68Ga-PSMA-11 and 68Ga-PSMA-617," *EJNMMI Res.*, vol. 7, no. 9, pp. 1–10, 2017.

[165] E. Y. Tshuva, I. Goldberg, and M. Kol, "Isospecific living polymerization of 1-hexene by a readily available nonmetallocene C2-symmetrical zirconium catalyst," *J. Am. Chem. Soc.*, vol. 122, no. 43, pp. 10706–10707, 2000.

[166] C. Wang, W. Meng, Y. Huang, and F. Qing, "The synthesis and application of fluorous boronates without perfluorinated solvents," *J. Fluor. Chem.*, vol. 126, pp. 996–1001, 2005.

Appendix A

"Liquid–liquid extraction in flow of the radioisotope titanium-45 for positron emission tomography applications"

Kristina Søborg Pedersen, Joseph Imbrogno, Jesper Fonslet, Marcella Lusardi, Klavs F. Jensen and Fedor Zhuravlev

Reaction Chemistry & Engineering, vol. 3, pp. 898-904, 2018

Reaction Chemistry & Engineering

PAPER

View Article Online
View Journal | View Issue

Cite this: *React. Chem. Eng.*, 2018, **3**, 898

Liquid–liquid extraction in flow of the radioisotope titanium-45 for positron emission tomography applications†

Kristina Søborg Pedersen,‡[ab] Joseph Imbrogno, ‡[b] Jesper Fonslet,[a] Marcella Lusardi,[c] Klavs F. Jensen *[bc] and Fedor Zhuravlev *[a]

Received 17th August 2018,
Accepted 26th September 2018

DOI: 10.1039/c8re00175h

rsc.li/reaction-engineering

A continuous liquid–liquid extraction of ^{nat}Ti and its PET radioisotope ^{45}Ti into an organic phase from 12 M HCl is described. The extraction is completely selective with respect to Sc, which is commonly used as a cyclotron target for ^{45}Ti production. A membrane-based separator with integrated pressure control allowed for efficient, reproducible, and robust aqueous/organic phase separation in flow. Optimization studies established a guaiacol–anisole 9/1 (v/v) mixture and a flow rate ratio of 1/3 (aq. to org.), with a residence time of 13.7 s as the optimal extraction conditions. 90.3 ± 1.1% of ^{nat}Ti was consistently extracted from a 0.01 M solution of $^{nat}TiCl_4$ and $ScCl_3$, while 84.8 ± 2.4% of ^{45}Ti was extracted from 0.03–0.13 M $ScCl_3$ containing picomolar amounts of the ^{45}Ti radionuclide, without extracting any Sc from either system. The organic phase can be directly used for ^{45}Ti-radiolabelling as demonstrated by the efficient radiosynthesis of the ^{45}Ti-radiolabeled antineoplastic [^{45}Ti](salan)Ti(dipic). This development opens a pathway to achieve continuous and efficient ^{45}Ti recovery and processing using an automated micro or millifluidics setup.

1 Introduction

Over the past several decades positron emission tomography (PET) has become a medical modality providing the best diagnostic options for cancer available today.[1] PET radiopharmaceuticals based on radiometals are gaining increasing popularity due to their ability to probe biological processes occurring on timescales from hours to days.[2] Convenient chelation chemistry and ready availability *via* the ^{68}Ge generator currently make the ^{68}Ga radiometal the most popular choice for radiolabelling of peptides and antibody fragments.[3] ^{45}Ti is emerging as a promising PET radiometal due to its 85.7% positron branch, negligible secondary radiation, and facile production.[4] The 3 hour half-life of ^{45}Ti compares favorably to that of ^{68}Ga (68 min) and can allow for longer transport distances. Furthermore, the sharper PET images of ^{45}Ti due to its lower β^+ endpoint energy (1.04 MeV for ^{45}Ti *vs.* 1.90 MeV for ^{68}Ga) can be especially advantageous for a small-animal PET. A number of small molecule ^{45}Ti compounds were previously synthesized and used for PET imaging[5–7] and radiotracing.[8] Our research efforts are directed towards increasing the adoption of ^{45}Ti PET by developing efficient ^{45}Ti recovery procedures and water-compatible chelation chemistry.

The bombardment of naturally monoisotopic scandium with low energy protons from a medical cyclotron *via* the ^{nat}Sc(p,n)^{45}Ti nuclear reaction is an attractive ^{45}Ti production route.[9–11] Recovery of a radiometal is the first post-production step, which for a highly hydrolyzable metal such as Ti is critical. Currently, the solid phase extraction from acidic solutions onto a cation or anion-exchange resin is the predominant way to separate ^{45}Ti from its Sc matrix. We and others previously used PEG-functionalized diol,[8] cation-exchange[5–7] and hydroxamate[12] resins. With the recent advances and availability of automation, there is a strong drive to implement advanced chemical separation techniques compatible with micro and millifluidics.

One of these techniques is liquid–liquid extraction (LLE). In recent years, LLE in micro-scale flow has received increasing attention.[13] Continuous extraction has been successfully demonstrated in rectangular microreactors,[14] three-phase microfluidic chips,[15] and porous capillary,[16] and capillary membrane-based devices.[17] In the area of radiopharmaceutical production and research, LLE is still underdeveloped

[a] *Technical University of Denmark, Center for Nuclear Technologies, Frederiksborgvej 399, Building 202, 4000 Roskilde, Denmark. E-mail: fezh@dtu.dk; Fax: +45 4677 5347; Tel: +45 46775337*
[b] *Department of Chemical Engineering, Massachusetts Institute of Technology, Cambridge, MA, 02139, USA. E-mail: kfjensen@mit.edu*
[c] *Department of Materials Science and Engineering, Massachusetts Institute of Technology, Cambridge, MA, 02139, USA*

† Electronic supplementary information (ESI) available: Separator material optimization and solvent selection. See DOI: 10.1039/c8re00175h

‡ K. S. P. and J. I. contributed equally to this work.

since up until now LLE was primarily performed manually, resulting in significant radiation exposure to personnel. Due to recent developments in flow chemistry, LLE can now be carried out continuously by exploiting the high mass transfer of slug flow followed by complete phase separation utilizing the wettability of polymer membranes.[18] This system has been used for multi-stage counter-current LLE of small organics and solvents,[19] solvent exchange and purification during continuous pharmaceutical synthesis,[20,21] and quantum dot purification.[22] In this work, LLE followed by a single stage of membrane-based phase separation was utilized to purify both non-radioactive and radioactive Ti from a Sc metal continuously. This process does not require any manual operation after the initial setup and therefore is highly applicable to radioactive systems, like the one described here.

The membrane separators used herein have been published for various applications, but are briefly described here.[18,19,22] The membrane separator module consists of two main components: a polymer microfiltration (MF) membrane and a thin plastic diaphragm (Fig. 1).

The diaphragm, a thin, chemically compatible perfluoroalkoxy alkane (PFA) polymer, acts to modulate the pressure between the aqueous and organic sides of the membrane. Various diaphragm thicknesses allow one to control the pressure the diaphragm exerts on the system, known as P_{dia}. The upper and lower bounds for operating this system while achieving complete phase separation correspond to the capillary, P_{cap}, and permeation pressures, P_{perm}, respectively. A more accurate model for the upper and lower pressure bounds that accounts for the pore size distribution and the tortuosity has been recently published.[23]

The interfacial tension between the two phases is also critically important since it cannot be varied without chemical additives or changing the solvents. It is essential to stay within the operating range of the system; otherwise incomplete phase separation will occur. The capillary and permeation pressures are only the theoretical upper and lower limits, respectively, of the system; therefore it is important to note that the actual operating range where complete separation will occur usually exists in a smaller region when using a real system. Therefore, after the radioisotope of interest is selectively extracted into one of the phases (organic or aqueous), the membrane separator will completely separate the two phases, and the radioisotope-enriched phase can be used directly for downstream radiolabelling. By combining two or more membrane separators, multiple LLEs can be easily carried out in series, such as extraction into the organic phase and back-extraction into the aqueous phase.

In this contribution, we describe the use of a single membrane separator for the facile purification of the radioisotope ^{45}Ti in flow directly after production with a total system residence time of less than 1 min and a residence time of ≤15 s for the LLE mixing step. To demonstrate that the extracted ^{45}Ti can be used directly for radiolabelling after the LLE in flow, we performed a radiosynthesis of [^{45}Ti](salan)Ti(dipic), an anti-tumour compound previously used for ^{45}Ti-radiotracing.[8]

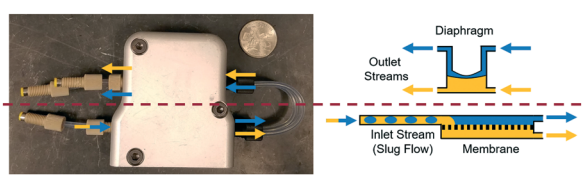

Fig. 1 Schematic diagram showing the flow paths of the membrane separator alongside a photograph of an actual separator. The aqueous phase is shown in blue (retained phase) and the organic phase is shown in yellow (permeated phase). A U.S. quarter is shown for scale.

2 Experimental

2.1 Materials

Guaiacol, anisole (99%), 1-octanol (99%), titanium(IV) chloride (neat), titanium(IV) chloride solution (0.09 M in 20% HCl), hydrochloric acid (37%), sulfuric acid (95.0–98.0%), pyridine-2,6-dicarboxylic acid (dipic) (98%), 1,2-decandiol (98%), 2,3-napthalene diol (98%), α,α,α-trifluorotoluene (99%), 1,1,1,3,3,3-hexafluoropropanol (99%), and 1*H*,1*H*,2*H*,2*H*-perfluoro-1-octanol were purchased from Sigma Aldrich and used without further purification. TLC plates (Silica gel on TLC Al foil) were also purchased from Sigma Aldrich. Scandium(III) chloride (anhydrous, 99.9%) and scandium foil (250 μm, 99.9% pure, rare earth analysis) were purchased from Alfa Aesar. Custom Ti and Sc ICP standards were purchased from Inorganic Ventures (100 ppm of each metal in 5% HCl solution). Salan[24] and (salan)Ti(dipic)[25] were synthesized according to literature procedures. The membrane separator module was similar to those manufactured by Zaiput Flow Technologies. Pall PTFE membranes were used for all experiments (47 mm diameter, 0.1/0.2/0.5 μm pore size, polypropylene (PP) support for the 0.1/0.2 μm pore sizes). PFA diaphragms (0.001″/0.002″/0.005″ (0.0254/0.0508/0.1270 mm)) were purchased from McMaster Carr. All PFA tubing (1/16″ OD, 0.03″ ID) was purchased from Idex Health and Science. PTFE static mixers were purchased from Stamixco. 15 mL plastic centrifuge tubes with screw caps were purchased from VWR.

2.2 Instrumentation

The solutions for the continuous membrane-based separation were pumped using either a KDS 100 Legacy syringe (radioactive experiments) or Harvard Apparatus PHD 2000 Programmable and Infusion syringe pumps (non-radioactive experiments). The NMR spectra were obtained using an Agilent 400 MR operating at 400.445 MHz (^{1}H). The radioactivities were measured on a CRC-55tR, CII Capintec, Inc. dose calibrator. Radio-TLC was performed with a Raytest MiniGita TLC scanner using chloroform/ethyl acetate (1/1, v/v) as the mobile phase. The HPLC and radio-HPLC analyses were performed on a Hitachi Chromaster equipped with a Carrol & Ramsey 105-S radio-detector and a Hitachi 5430 double diode array

detector. Column: Phenomenex Luna 3 μ C18(2) (100 Å, 100 mm × 2.00 mm). Flow: 0.5 mL min^{-1}. Eluents: (A) 0.1% (v/v) CF_3COOH in Milli-Q water and (B) 0.1% (v/v) CF_3COOH in CH_3CN. The radiochemical identity of [^{45}Ti](salan)Ti(dipic) was established by comparing its retention time with that of its natural abundance isotopomer. The radiochemical conversion (RCC) was determined by radio-HPLC or radio-TLC and calculated as: RCC = ($Area_{product}$/Total Area) × 100%.

The extent of extraction (extraction % in Fig. 4 and 5) was determined relative to the concentration of titanium initially present in the aqueous phase (100%*$[Ti]_{(org)}/[Ti]_{(aq)}$) using inductively coupled plasma atomic emission spectroscopy (ICP-AES, Agilent 5100 Dual View) of the aqueous phase. Samples of the aqueous phase were collected before the LLE and after 5, 15, 30, and 45 minutes of LLE. 0.35 mL of each sample was mixed with 0.5 mL H_2SO_4, diluted up to 5 mL with Milli-Q water and then digested for 6 hours at 160 °C. 2.7 mL of the digested sample was diluted up to 10 mL with Milli-Q water to reach a total acid concentration of 5% (v/v). Calibration standards (Inorganic Ventures) were prepared to match the sample matrix with concentrations of 22.2, 18, 15, 10, and 5 ppm Ti and Sc and run prior to every set of samples. The samples were analyzed in radial view at a viewing height of 8 mm. Because organic solutions are not directly amenable to ICP analysis, the extraction to the organic phase was calculated from the concentration of Ti and Sc in the aqueous phase ($C^{Ti,Sc}$) before and after the LLE by $E = ((C^{Ti,Sc}_{beforeLLE} - C^{Ti,Sc}_{afterLLE})/C^{Ti,Sc}_{beforeLLE}) \times 100\%$.

2.3 Radiochemistry

^{45}Ti was produced by 10–20 μA proton irradiation of 30–60 mg of scandium foil, for 5–15 min using a GE PETtrace cyclotron. To minimize coproduction of ^{44}Ti (half-life = 60.0 years), a 500 μm thick aluminium foil was used to degrade the incidental 16 MeV beam to approximately 13 MeV. The ^{45}Ti-loaded foils were dissolved in 3 mL 12 M HCl, and the reaction mixture was filtered through a glass frit and further diluted with 12 M HCl to a total of 10–20 mL. The radioisotope ^{45}Ti was extracted from the HCl solution into the organic phase using either shaking/spinning (batch) or slug flow (continuous) procedures. The organic phase was separated and mixed with a 0.06 M solution of salan and dipic in pyridine. The solution was stirred at 60 °C for 15 min to complete the formation of [^{45}Ti](salan)Ti(dipic) and then analyzed.

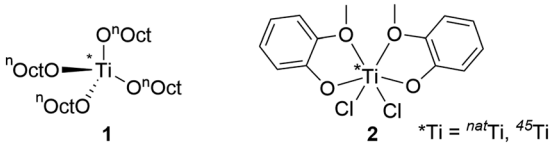

Fig. 3 The putative Ti species extracted in 1-octanol (**1**) and guaiacol (**2**).

2.4 Batch LLE and separation

For the non-radioactive study, 0.5 mL of 0.01 M $TiCl_4$ and 0.01 M $ScCl_3$ in 37% HCl was mixed with 1.5 mL of guaiacol/anisole, 9/1 (v/v), and shaken for 2 minutes in a centrifuge tube. The phases were allowed to separate by gravity. The concentration of Ti and Sc in the aqueous phase before and after the LLE was measured by ICP-AES.

For the ^{45}Ti study, a centrifuge tube was filled with 2 mL of the solution of ^{45}Ti (10–50 MBq) in 37% HCl and 2 mL of the organic phase. The mixture was shaken vigorously, spun for 15 minutes, and centrifuged at 4000 rpm to separate the phases. Then, the radioactivity in each phase was measured.

2.5 Continuous membrane-based LLE and separation

The LLE and phase separation in flow were performed using a membrane-based separator with a PFA diaphragm for integrated pressure control (with this design, the transmembrane pressure is intrinsically linked with the back-pressure applied by the diaphragm). A flow schematic of the experimental setup is shown (Fig. 2). The two phases passed through the PFA tubing (1/16″ OD, 0.03″ ID) and were mixed in a PEEK tee, followed by two 10 element PTFE static mixers (3.4 cm total length, placed inside a short length of 1/8″ OD, 1/16″ ID PFA tubing) and various lengths of PFA mixing tubing, which

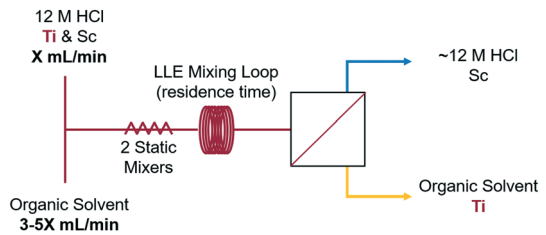

Fig. 2 Schematic of the setup used for continuous phase separation. The aqueous and the organic phases were combined through a tee and mixed using two static mixers and mixing tubing. The aqueous phase was retained by the membrane, while the organic phase permeated through the membrane. Ti was selectively extracted from Sc into the organic phase.

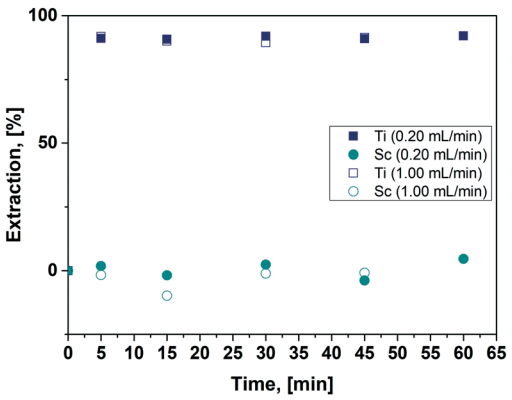

Fig. 4 Extraction performance over time for a total flow rate of 0.20 mL min^{-1} (solid symbols) and for a five-fold scale-up at 1.00 mL min^{-1} (open symbols). These data show the ability for a facile scale-up of the system.

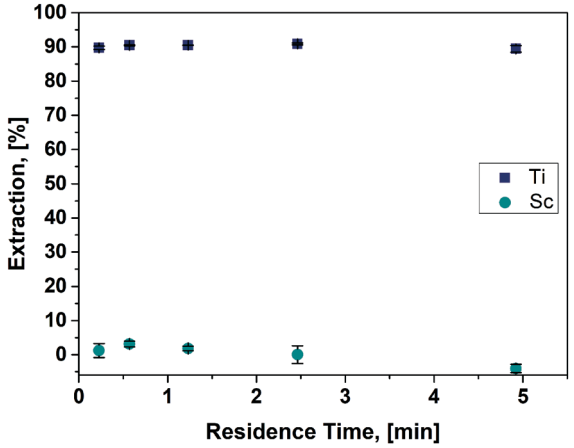

Fig. 5 Extraction performance for various different residence times (time for LLE in the mixing loop in Fig. 2). The maximum Ti extraction (90%) was achieved for all residence times, down to the shortest residence time of 13.7 s.

were used to control the residence time of the LLE. After the static mixers, a steady slug flow developed and passed through the LLE mixing loop and finally into the membrane separator, where the organic phase permeated the membrane while the aqueous phase was retained. Different diaphragm thicknesses, membranes, and flow rates were tuned to achieve complete separation of the aqueous and organic phases.

3 Results and discussion

3.1 LLE in batch mode: preliminary experiments

Several practical considerations merit emphasis at the outset. In radiochemistry, ^{45}Ti is obtained as a strongly acidic solution after digestion of the cyclotron-irradiated Sc foil in concentrated HCl. High acidity is necessary because when $[H^+] <$ 11 M the titanium speciation diagram becomes populated by titanyl species,[26] unusable for radiolabelling. Such a high acidity limits the choice of extractants and diluents to non-basic compounds. The oxophilicity of titanium further narrows it down to O-donors, such as alcohols, diols, and phenols, and certain organic acids. Finally, high acid concentration increases the phase miscibility and lowers the interfacial tension, making the phase separation potentially more complicated.[26] Our preliminary screening experiments were performed in batch using gravity separation and were inspired by a report claiming that ^{45}Ti can be extracted from aqueous HCl into 1-octanol, presumably as [^{45}Ti]Ti *n*-octyloxide [1] (Fig. 3).[27]

We observed little extraction when a solution of ^{45}Ti in 20% HCl was used (Table 1, entry 1). Using 37% HCl (12 M) significantly improved the extraction. A 0.1 M 1,2-decanediol solution used as the co-extractant in 1-octanol gave only a slight improvement compared to neat 1-octanol. 2,3-Naphthalene diol, reported to extract Ti at pH = 4,[28] showed a similarly modest performance (Table 1, entries 3 and 4). During these batch extractions, we noticed a significant increase in the volume of the 1-octanol phase suggestive of conc. HCl migrating into the organic phase. In an attempt to improve the phase separation we turned to perfluorinated extractants.[29] Disappointingly, the fluorous analog of 1-octanol, $CF_3(CF_2)_5CH_2CH_2OH$ formed an emulsion. A 0.05 M solution of $C_{10}F_{21}CH_2CH(OH)CH_2OH$ in trifluorotoluene/hexafluoropropanol (1/1, v/v) failed to extract any ^{45}Ti (Table 1, entry 5). Previously, it was reported that guaiacol (*o*-methoxyphenol) easily forms a moisture-sensitive but isolable complex *cis*-[$TiCl_2(\eta^2$-guaiacolato$)_2$] with titanium tetrachloride.[30] Gratifyingly, using neat guaiacol as an extractant, we were able to extract 75% of titanium-45 into the organic phase, presumably as [2] (Fig. 3). Next, we translated the batch experiments into fully continuous flow experiments.

Table 1 Liquid–liquid batch extraction of ^{45}Ti from cyclotron-irradiated Sc foil digested in 37% HCl, except entry 1.[a] EE is the extraction efficiency, EE = 100% × $A_{(org)}/A_{(org+aq)}$, where $A_{(org)}$ and $A_{(org+aq)}$ is the activity of ^{45}Ti in the organic and organic + aqueous layers, correspondingly, as measured using a radiation detector

Entry	Extraction system (organic phase)	EE (%)
1	1-Octanol, neat[a]	4
2	1-Octanol, neat	47
3	1,2-Decanediol, 0.1 M in 1-octanol	54
4	2,3-Naphthalene diol, 0.1 M in 1-octanol	52
5	$C_{10}F_{21}CH_2CH(OH)CH_2OH$[b]	<0.1
6	Guaiacol, neat	75

[a] 20% HCl. [b] Trifluorotoluene/hexafluoropropanol (1/1, v/v).

3.2 LLE of ^{nat}Ti in flow: system optimization

In order to find the optimum extraction conditions, the diaphragm thickness, membrane pore size, organic phase composition, flow rate ratios, and residence times were varied. Once the optimal materials and conditions were determined, a study was conducted to determine the shortest residence time, thereby minimizing the dead volume and overall processing time, while still maintaining high extraction. The residence time was varied by varying the length of the mixing tubing after the static mixers while maintaining a constant flow rate. All systems were operated for 60 min each and samples were collected every 15 min.

Complete separation requires both the diaphragm thickness and membrane pore size to be chosen so that P_{dia} lies between the P_{cap} and P_{perm} pressures. In general, low interfacial tension mixtures often require smaller pore size membranes and thinner diaphragms. In these experiments, polytetrafluoroethylene (PTFE) membranes were tested using the following pore sizes 0.1, 0.2, and 0.5 μm. Three different diaphragm film thicknesses were also tested: 0.001″, 0.002″, and 0.005″ (0.025 mm, 0.051 mm, and 0.127 mm).

Since guaiacol had shown the most selective and highest extraction efficiency for Ti over Sc in the batch experiments, it was chosen as the most viable candidate for carrying out

the extraction *via* continuous processing. A solution of 0.01 M $TiCl_4$ and 0.01 M $ScCl_3$ in 37% HCl was extracted in guaiacol using the membrane separator. Occasional retention and/or breakthrough of the aqueous into the organic phase was observed with a 0.2 μm PTFE/PP membrane, a 0.002″ diaphragm thickness, and a 0.2 mL min^{-1} total flow rate. The situation was remedied by adding various amounts of anisole, which is structurally similar to guaiacol but acts to increase the interfacial tension. The COSMO-RS calculations[31] showed that the interfacial tension is expected to increase linearly with the increase in the volume fraction of anisole (Fig. S1, see the ESI†). These organic mixtures were used to extract Ti, (0.01 M) from 37% HCl at a total flow rate of 0.20 mL min^{-1} and aqueous to organic flow rate ratios of 1/5, 1/3, and 1/1 (v/v). The corresponding flow rates and extraction performance are shown in Table S1, see the ESI.† To determine the scalability of the process, the total flow rate was then increased five-fold. Therefore, a total flow rate of 1.00 mL min^{-1} was used, while maintaining the same flow rate ratios and residence times.

The separation results for both 1-octanol and 1/1 guaiacol/anisole using different membranes and diaphragm thicknesses are shown in Table S2, see the ESI.† Although the guaiacol/anisole mixture performed much better than 1-octanol, its extraction efficiency was not high enough. Therefore, the ratio of guaiacol to anisole was varied as well, as summarized in Table 2. After an optimal system was developed, the residence time of mixing was varied to minimize the dead volume and decrease the total amount of time spent in the system. This was achieved by increasing or decreasing the length of the PTFE tubing used for mixing. The following lengths were tested with their corresponding residence times at 0.20 mL min^{-1}: 10 cm (13.7 s), 25 cm (34.2 s), 54 cm (73.9 s), 108 cm (147.8 s), and 216 cm (295.6 s).

3.3 Optimization of continuous LLE and phase separation in flow using non-radioactive metals

Due to the harsh nature of both the aqueous and organic solvents used for this extraction, both the membrane and diaphragm had to be extremely stable. Therefore, PTFE membranes were used for all experiments described herein. Since the 0.2 μm membrane and 0.002″ diaphragm was the only combination that led to complete phase separation, it was used for all of the optimization experiments.

The composition of the organic phase needed to both selectively extract only Ti and have a high enough interfacial tension with the HCl phase so that complete separation could be achieved. It was determined that extraction directly correlated with the guaiacol concentration, that is a higher guaiacol concentration led to higher extraction up to a maximum Ti extraction of 90% with 90% guaiacol. Guaiacol concentrations above 90% led to incomplete phase separation. A summary of the phase separation performance using various organic phase compositions is shown in Table 2.

In addition to the composition of the organic phase, the relative ratios of aqueous to organic flow rates were also varied. When comparing the relative flow rate ratios of 1/1, 1/3, and 1/5 (v/v) (aq. to org.), it was determined that 1/1 gave the lowest extraction. A ratio of 1/3 gave a higher extraction, but 1/5 did not yield a further increase in performance (see Table S1, ESI†). All ratios where the aqueous flow rate was higher led to lower extraction efficiency. Therefore, the flow rate ratio of 1/3 was chosen as to avoid using excess solvent.

In order to determine the scalability and stability of the extraction, the total flow rates were scaled five-fold to a total flow rate of 1.00 mL min^{-1}, while maintaining the same flow rate ratios and residence times. The extraction performance was identical to the original scale, and the maximum extraction of 90% was still achieved at 90% guaiacol and a flow rate ratio of 1/3 (Fig. 4).

The total production time is a critical parameter in this system since radioactive Ti is continuously undergoing decay back to Sc ($t_{1/2}$ = 3 hours). Therefore, the shortest residence time is desirable. Residence times of the mixing tubing were varied from 13.7 s up to ~5 min. The extraction efficiency was the same for all residence times. Therefore the shortest residence time was the most optimal (Fig. 5). This performance is due to the enhanced uniform mixing imparted by t-mixing, helical static mixing, and segmented flow, which allows for the equilibrium stage to be reached quickly. Overall, an organic phase consisting of 90% guaiacol and 10% anisole, total flow rates of 0.20 or 1.00 mL min^{-1}, an aqueous to organic flow rate ratio of 1/3, and a residence time of 13.7 s led to the highest and most efficient extraction resulting in 90.3 ± 1.1% extraction of Ti. No scandium extraction (within the experimental error) was detected.

Table 2 Phase separation performance for different guaiacol to anisole ratios in the organic phase using different aqueous to organic flow rate ratios

Org. phase guaiacol/anisole (v/v)	Aq. flow rate [mL min^{-1}]	Org. flow rate [mL min^{-1}]	Performance [–]
Aqueous phase: 37% HCl (12 M) 0.2 μm PTFE membrane and 0.002″ diaphragm thickness			
10/90	0.10	0.10	Complete sep.
75/25	0.05	0.15	Complete sep.
	0.10	0.10	
	0.10	0.30	
	0.25	0.75	
90/10	0.03	0.17	Complete sep.
	0.05	0.15	
	0.25	0.75	
95/05	0.10	0.10	Retention/breakthrough

3.4 LLE of ^{45}Ti in flow and radiosynthesis of [^{45}Ti](salan)Ti(dipic)

With the extraction conditions optimized for ^{nat}Ti, we turned to the radioactive isotopomer, ^{45}Ti. While the concentration of Sc was comparable in both non-radioactive and radioactive cases (0.01 M *vs.* 0.03–0.13 M correspondingly) the concentration of the radiometal in the Sc-

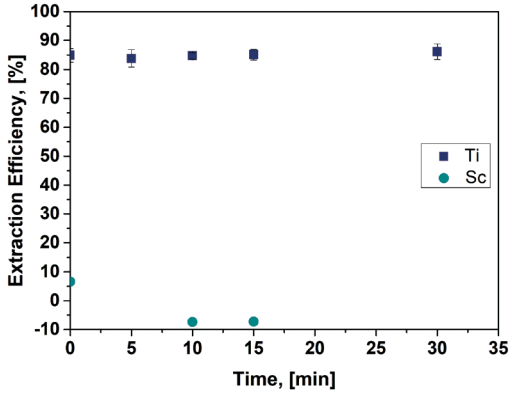

Fig. 6 Continuous LLE of ^{45}Ti at a flow rate ratio of 1/3 (aq. to org.) with a 90% guaiacol, 10% anisole mixture. ^{45}Ti extraction efficiency calculated from the radioactivity measurements and Sc extraction calculated by ICP-AES.

containing matrix solution was lower than that of its natural abundance isotopomer by 10 orders of magnitude, ranging from 1 to 10 picomoles. At these concentrations, even the trace levels of impurities or water could potentially lead to a side-reaction or hydrolysis and as a consequence, change the extraction efficiencies of ^{45}Ti. To our delight, the LLE of ^{45}Ti in flow using a 90% guaiacol 10% anisole mixture and a flow rate ratio of 1/3 (aq. to org.), with a residence time of 13.7 s showed that the extraction efficiency of ^{45}Ti was consistent with that of ^{nat}Ti (84.8 ± 2.4% and 90.3 ± 1.1%, correspondingly), (Fig. 6). The ICP-AES analysis of the aqueous phase before and after the LLE confirmed that no Sc was extracted into the organic phase.

Finally, to examine if the extracted solution of ^{45}Ti can be directly used for radiolabelling, we attempted to synthesise [^{45}Ti](salan)Ti(dipic) [3], a Ti-antineoplastic, previously used for animal ^{45}Ti-PET and *ex vivo* radiotracing.[8]

To that end, the organic phase after the continuous LLE of ^{45}Ti was collected and reacted with an equimolar solution of salan and 2,6-pyridinedicarboxylic acid (dipic) in pyridine at 60 °C (Scheme 1). An essentially complete (98.7%) conversion to the desired product [3] was observed within 15 min as evidenced by radio-TLC (red peak for the product [3] and only traces of unreacted [2], green peak), proving the high quality and reactivity of the extracted ^{45}Ti (Fig. 7, inset). HPLC/radio-HPLC further confirmed the identity of the product [3], matching its retention time to that of the independently synthesized non-radioactive [^{nat}Ti](salan)Ti(dipic) determined by HPLC equipped with a UV-detector (Fig. 7).

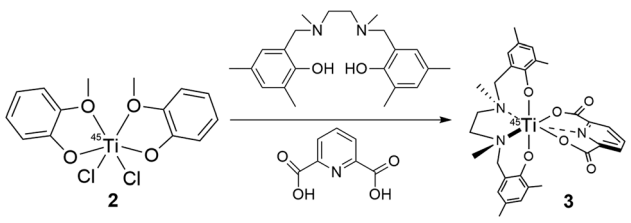

Scheme 1 Radiosynthesis of [^{45}Ti](salan)Ti(dipic) from ^{45}Ti extracted in the organic phase directly after LLE in flow.

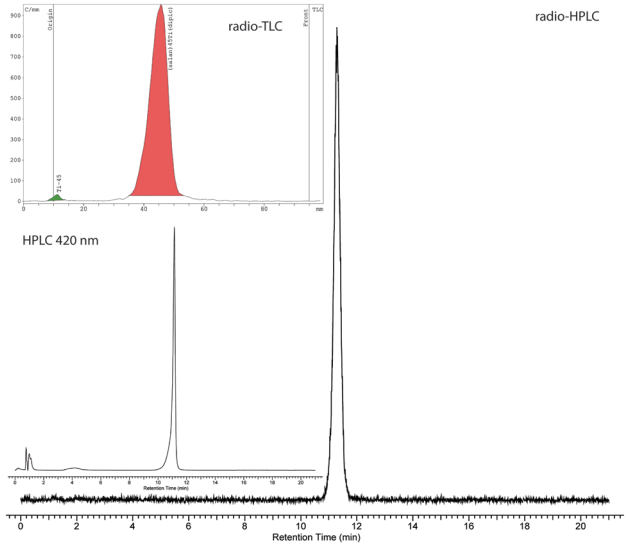

Fig. 7 Radio-HPLC results of [^{45}Ti](salan)Ti(dipic), retention time= 11.3 min. Bottom: HPLC results of (salan)Ti(dipic) at 420 nm, retention time= 11.2 min, insert: Radio-TLC results of [^{45}Ti](salan)Ti(dipic) **3**, R_f = 0.49, red peak, and **2**, baseline, green peak.

Conclusions

We have reported the selective liquid–liquid extraction of ^{nat}Ti and its PET radioisotope (^{45}Ti) into an organic phase from a solution containing various amounts of Sc in 37% (12 M) HCl. A membrane-based separator with integrated pressure control allowed for continuous aqueous/organic phase separation in flow. Optimization studies established a 90% guaiacol 10% anisole mixture and a flow rate ratio of 1/3 (aq. to org.), with a residence time of 13.7 s as the optimal extraction conditions. 90.3% ± 1.1 of ^{nat}Ti was consistently extracted from a 0.01 M solution of $TiCl_4$ and $ScCl_3$, while 84.8 ± 2.4% of ^{45}Ti was extracted from 0.03–0.13 M $ScCl_3$ containing picomolar amounts of the ^{45}Ti radionuclide. As a process, the LLE in flow of ^{45}Ti was reproducible and robust. Additionally, the throughput demonstrated in this work would be capable of meeting the demand in a hospital or industrial setting. The organic phase can be directly used for ^{45}Ti-radiolabelling as demonstrated by the efficient radiosynthesis of [^{45}Ti](salan)Ti(dipic) resulting in a 98.7% conversion.

Conflicts of interest

There are no conflicts to declare.

Acknowledgements

K. S. P. is grateful for the financial support by the Danish Agency for Science, Technology and Innovation.

Notes and references

1 R. Huang, M. Wang, Y. Zhu, P. Conti and K. Chen, *Curr. Top. Med. Chem.*, 2015, **15**, 795–819.
2 D. Brasse and A. Nonat, *Dalton Trans.*, 2015, **44**, 4845–4858.
3 I. Velikyan, *Molecules*, 2015, **20**, 12913–12943.
4 S. Kuhn, I. Spahn, B. Scholten and H. H. Coenen, *Radiochim. Acta*, 2015, **103**, 403–409.
5 K. Ishiwata, T. Ido, M. Monma, M. Murakami, H. Fukuda, M. Kameyama, K. Yamada, S. Endo, S. Yoshioka, T. Sato and T. Matsuzawa, *Appl. Radiat. Isot.*, 1991, **42**, 707–712.
6 A. L. Vāvere, R. Laforest and M. J. Welch, *Nucl. Med. Biol.*, 2005, **32**, 117–122.
7 A. L. Vāvere and M. J. Welch, *J. Nucl. Med.*, 2005, **46**, 683–690.
8 G. W. Severin, C. H. Nielsen, A. I. Jensen, J. Fonslet, A. Kjær and F. Zhuravlev, *J. Med. Chem.*, 2015, **58**, 7591–7595.
9 J. C. Merrill, R. M. Lambrecht and A. P. Wolf, *Int. J. Appl. Radiat. Isot.*, 1978, **29**, 115–116.
10 M. Sadeghi, M. Enferadi and H. Nadi, *Radiochemistry*, 2011, **53**, 411.
11 Y. Fazaeli, M. Aboudzadeh, K. Aardaneh, T. Kakavand, F. Bayat and K. Yousefi, *Nucl. Technol. Radiat. Prot.*, 2014, **29**, 28–33.
12 K. Gagnon, G. W. Severin, T. E. Barnhart, J. W. Engle, H. F. Valdovinos and R. J. Nickles, in *AIP Conference Proceedings*, AIP, 2012, vol. 1509, pp. 211–214.
13 K. Wang and G. Luo, *Chem. Eng. Sci.*, 2017, **169**, 18–33.
14 D. M. Fries, T. Voitl and P. R. von Rohr, *Chem. Eng. Technol.*, 2008, **31**, 1182–1187.
15 K. K. R. Tetala, J. W. Swarts, B. Chen, A. E. M. Janssen and T. A. van Beek, *Lab Chip*, 2009, **9**, 2085–2092.
16 T. W. Phillips, J. H. Bannock and J. C. deMello, *Lab Chip*, 2015, **15**, 2960–2967.
17 H. Breisig, M. Schmidt, H. Wolff, A. Jupke and M. Wessling, *Chem. Eng. J.*, 2017, **307**, 143–149.
18 A. Adamo, P. L. Heider, N. Weeranoppanant and K. F. Jensen, *Ind. Eng. Chem. Res.*, 2013, **52**, 10802–10808.
19 N. Weeranoppanant, A. Adamo, G. Saparbaiuly, E. Rose, C. Fleury, B. Schenkel and K. F. Jensen, *Ind. Eng. Chem. Res.*, 2017, **56**, 4095–4103.
20 A. Adamo, R. L. Beingessner, M. Behnam, J. Chen, T. F. Jamison, K. F. Jensen, J.-C. M. Monbaliu, A. S. Myerson, E. M. Revalor, D. R. Snead, T. Stelzer, N. Weeranoppanant, S. Y. Wong and P. Zhang, *Science*, 2016, **352**, 61–67.
21 J. Imbrogno, L. Rogers, D. A. Thomas and K. F. Jensen, *Chem. Commun.*, 2018, **54**, 70–73.
22 Y. Shen, N. Weeranoppanant, L. Xie, Y. Chen, M. R. Lusardi, J. Imbrogno, M. G. Bawendi and K. F. Jensen, *Nanoscale*, 2017, **9**, 7703–7707.
23 L. Yang, N. Weeranoppanant and K. F. Jensen, *Ind. Eng. Chem. Res.*, 2017, **56**, 12184–12191.
24 E. Y. Tshuva, I. Goldberg and M. Kol, *J. Am. Chem. Soc.*, 2000, **122**, 10706–10707.
25 T. A. Immel, M. Grutzke, A.-K. Spate, U. Groth, P. Ohlschlager and T. Huhn, *Chem. Commun.*, 2012, **48**, 5790–5792.
26 V. Kislik and A. Eyal, *Solvent Extr. Ion Exch.*, 1993, **11**, 259–283.
27 J. Siikanen, *J. Nucl. Med.*, 2013, **54**, 1095.
28 R. Mondal and P. Tarafder, *Microchim. Acta*, 2004, **148**, 327–333.
29 E. de Wolf, G. van Koten and B.-J. Deelman, *Chem. Soc. Rev.*, 1999, **28**, 37–41.
30 P. Sobota, K. Przybylak, J. Utko, L. Jerzykiewicz, A. Pombeiro, M. da Silva and K. Szczegot, *Chem. – Eur. J.*, 2001, **7**, 951–958.
31 M. P. Andersson, M. V. Bennetzen, A. Klamt and S. L. S. Stipp, *J. Chem. Theory Comput.*, 2014, **10**, 3401–3408.

Appendix B

"Separation of Radiogallium from Zinc Using Membrane-Based Liquid-Liquid Extraction in Flow: Experimental and COSMO-RS Studies"

Kristina Søborg Pedersen, Karin Michaelsen Nielsen, Jesper Fonslet, Mikael Jensen and Fedor Zhuravlev

Solvent Extraction and Ion Exchange, vol. 37, no. 5, pp. 376-391, 2019

SOLVENT EXTRACTION AND ION EXCHANGE
2019, VOL. 37, NO. 5, 376–391
https://doi.org/10.1080/07366299.2019.1646982

Taylor & Francis
Taylor & Francis Group

Separation of Radiogallium from Zinc Using Membrane-Based Liquid-Liquid Extraction in Flow: Experimental and COSMO-RS Studies

Kristina Søborg Pedersen[a], Karin Michaelsen Nielsen[a], Jesper Fonslet[a,b], Mikael Jensen[a], and Fedor Zhuravlev[a]

[a]Hevesy Laboratory, Center for Nuclear Technologies, Technical University of Denmark, Roskilde, Denmark; [b]Minerva Imaging ApS, Copenhagen N, Denmark

ABSTRACT

A switch from batch to continuous manufacturing of gallium-68 (^{68}Ga) and ^{68}Ga-labeled pharmaceuticals can be advantageous, as it recycles isotopically-enriched zinc-68 (^{68}Zn), removes pre- and post-irradiation target manipulations, and provides scalability via dose-on-demand production. Herein we report efficient extraction of radiogallium (^{66,67,68}Ga = *Ga) from $ZnCl_2$/HCl solutions in batch and in flow using a membrane-based liquid-liquid separator. From 5.6 M $ZnCl_2$/3 M HCl, a 1/2 (v/v) diisopropyl ether ($^{i}Pr_2O$)/trifluorotoluene (TFT) solvent extracts 76.3 ± 1.9% of *Ga and 1.9 ± 1.6% of Zn in flow using a single pass through. From 1 M $ZnCl_2$/6 M HCl, a 1/2 (v/v) *n*-butyl methyl ether (*n*-BuOMe)/TFT solvent extracts 95.7 ± 2.0% of *Ga and 0.005 ± 0.003% of Zn in flow. TFT plays a key role in controlling the interfacial tension between the aqueous and the organic phases, ensuring clean membrane-based separation. The process did not extract Cu, Mn, and Co but did extract Fe. Using $HGaCl_4$ and $ZnCl_2$ as the extractable species, the COSMO-RS theory predicts the solvation-driven extraction of Ga and Zn with a mean unsigned error of prediction of 4.0% and 3.4% respectively.

KEYWORDS

Gallium-68; gallium-67; liquid-liquid extraction in flow; COSMO-RS

Introduction

Radiogallium (^{66,67,68}Ga = *Ga) has a long and notable history in nuclear medicine. For years, gallium-67 (^{67}Ga, $t_{1/2}$ = 78 h) scintigraphy has been a linchpin of molecular imaging of cancer,[1] including non-Hodgkin's lymphoma, Hodgkin's disease,[2] as well as various infections.[3] The advancement of positron emission tomography (PET) and FDA's approval of [^{68}Ga]Ga-DOTA-TATE (Netspot®) moved gallium-68 (^{68}Ga, $t_{1/2}$ = 68 min) to the forefront of neuroendocrine tumor diagnostics.[4] In recent years [^{68}Ga]Ga-HBED-PSMA-11, a ^{68}Ga-labeled PSMA (prostate-specific membrane antigen) ligand emerged as the gold standard for prostate cancer diagnostics, driving a high adoption rate of ^{68}Ga in clinics.[5] The easy chelation chemistry and convenience of ^{68}Ge/^{68}Ga-generators further contribute to ^{68}Ga popularity in clinical and pre-clinical settings.[6] Meeting the growing demand for ^{68}Ga is a challenge, as it is mostly supplied by the gallium generators which suffer from high prices, long lead time, quality inconsistencies, and limited shelf life.[7] An alternative method of ^{68}Ga production is the irradiation of ^{68}Zn using a cyclotron.[8] Since many PET-centers have their own cyclotrons, this is potentially a convenient means of in-house production of ^{68}Ga-tracers. However, the cyclotron production of ^{68}Ga in solid targets from ^{68}Zn

CONTACT Fedor Zhuravlev fezh@dtu.dk Center for Nuclear Technologies, Technical University of Denmark, Frederiksborgvej 399, Building 202, 4000 Roskilde, Denmark

Color versions of one or more of the figures in the article can be found online at www.tandfonline.com/lsei.

and its subsequent separation require either installation of expensive automated solid target systems or requires a series of manual pre- and post-irradiation target handlings. Recently, the production of ^{68}Ga in liquid targets from enriched ^{68}Zn salt solutions has been described, using either [^{68}Zn]$ZnCl_2$ [9,10] or [^{68}Zn]$Zn(NO_3)_2$.[11–13] Compared to the solid target production, the solution target approach leads to lower radionuclide yields but has an advantage of being more amenable to automation. Currently, all ^{68}Ga made in cyclotron solution targets is produced in batch mode; the desired radionuclide is subsequently purified from the ^{68}Zn salt solution by solid-phase extraction (SPE) using commercial radiosynthesis modules, without directly recycling the ^{68}Zn. If recycling of isotopically enriched ^{68}Zn target material is desired, reprocessing needs to be performed in a separate step.

At the outset, we recognized that the cyclotron production of radiogallium in a solution target is compatible with fluidic chemistry. By coupling a liquid target-based radionuclide production step with a liquid-liquid extraction (LLE) and a phase separation step one can conceivably construct a closed-loop system for continuous manufacturing of ^{68}Ga (Figure 1).

This provides an opportunity to continuously recycle isotopically-enriched ^{68}Zn. We have recently described an efficient LLE in flow of radioisotope titanium-45 (^{45}Ti), where we used a static mixer and a membrane separator with integrated pressure control[14] to extract the ^{45}Ti radionuclide into the organic phase and separate it from the 12 M HCl feed containing scandium-45.[15] By implementing a similar technique here, one can envision a continuous production of ^{68}Ga on the cyclotron through the ^{68}Zn(p,n)^{68}Ga nuclear reaction using a liquid target with a ^{68}Zn salt solution (Figure 1). After irradiation, the aqueous target solution is combined with the organic extractant, and before entering a membrane separator, the aqueous and organic phases are thoroughly mixed via static mixers and a slug flow developing in the mixing tubing, further facilitating the liquid-liquid extraction.[16] In the separator, the aqueous phase containing ^{68}Zn is retained by the hydrophobic membrane and can be re-routed back into the cyclotron target cell via a closed loop. The organic phase enriched with ^{68}Ga permeates through the membrane, and the radionuclide can be back-extracted (stripped) into 0.1 M HCl, delivering aqueous [^{68}Ga]$GaCl_3$ for radiolabeling.

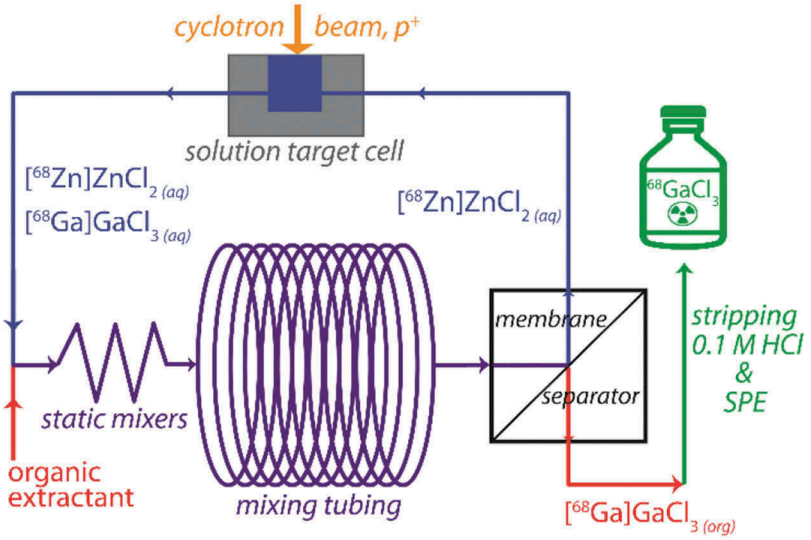

Figure 1. A schematic depicting a conceptual apparatus for continuous production of ^{68}Ga using the ^{68}Zn(p,n)^{68}Ga nuclear reaction in a cyclotron solution target. Fluidically, the target is coupled to the ^{68}Ga-separation step consisting of liquid-liquid extraction of ^{68}Ga into the organic phase followed by back-extraction (stripping) into 0.1 M HCl. The aqueous phase, containing ^{68}Zn is returned into the cyclotron solution target for irradiation.

The long-term goal of our program is to develop a continuous and automated production of PET radiometals by integrating modern fluidic techniques and process analytical technology tools (PAT) into cyclotron liquid targetry. In this contribution, we present a proof-of-concept study, where we focused on developing an efficient chemical system for in-flow separation of Ga from Zn by evaluating a number of extractants and diluents at different concentration of $ZnCl_2$ and HCl used in the ^{68}Ga liquid target production. The performance of the optimized extraction system was discussed in a context of Ga/Zn extraction efficiency in batch and flow, initial Zn and HCl concentration, phase cross-contamination, and cyclotron solution target integration. We also present a predictive computational model describing the solution equilibrium for the relevant Ga and Zn species as they partition between the aqueous and organic phases.

Experimental

Materials

Anisole, diethyl ether (Et_2O, b.p. = 35°C, log P = .87), n-butyl methyl ether (n-BuOMe, b.p. = 70°C, log P = 1.54), tetrahydropyran (THP, b.p. = 88°C, log P = .95), α,α,α-trifluorotoluene (TFT), toluene, 1,2-dichloroethane (DCE), multi-element standard solution 1 for ICP (TraceCert in 10% HNO_3), citric acid, $ZnCl_2$, and $FeCl_3$, were reagent grade and purchased from Sigma Aldrich. n-Dibutyl ether (n-Bu_2O, b.p. = 141°C, log P = 2.99) and diisopropyl ether ($^{i}Pr_2O$, b.p. = 69°C, log P = 1.49) were purchased from Merck. Heptane was purchased from VWR Chemicals. n-Hexyl methyl ether (n-HexOMe, b.p. = 125°C, log P = 2.21) and n-amyl ether (n-Am_2O, b.p. = 187°C, log P = 3.38) were purchased from abcr GmbH. High purity hydrochloric acid (37%, trace metal basis) from Honeywell was used. All purchased chemicals were used without further purification. Zinc foil (250 µm, 99.9% trace metals basis) and copper foil (500 µm, 99.98% trace metal basis) were purchased from Sigma Aldrich. TK200 resin was purchased from TrisKem. Pall PTFE membranes were used for all experiments; perfluoroalkoxy alkane (PFA) diaphragms were purchased from McMaster Carr. All PFA tubing was purchased from Idex Health and Science. PTFE static mixers were purchased from Stamixco. The 15 mL plastic centrifuge tubes with screw caps (SuperClear) were purchased from VWR. The 10 mL and 25 mL Hamilton glass syringes were purchased from Sigma Aldrich.

Radionuclide production and separation

The radionuclides zinc-65 (^{65}Zn, $t_{½}$: 244 d) and ^{67}Ga were used to quantify the Zn and Ga extraction. The radionuclides were produced on a GE 16.5 MeV PETtrace cyclotron by the ^{nat}Cu(p,n)^{65,63}Zn and ^{nat}Zn(p,n)^{66,67,68}Ga nuclear reactions, respectively, using a solid target with stacked zinc (250 µm, 750–831 mg) and copper (500 µm, 301–341 mg) foils. The target was irradiated for 120–160 minutes at 10 µA. Subsequently, the target was allowed to decay for at least 18–24 h before further handling to minimize the amount of the co-produced shorter-lived radionuclides ^{63}Zn ($t_{½}$ 38 min), ^{68}Ga ($t_{½}$ 68 min), and gallium-66 ($t_{½}$ 9.5 h). The zinc foil containing around 50 MBq of ^{67}Ga at end of bombardment was dissolved in 3 mL of conc. HCl, and the concentration of HCl was adjusted to 3 M or 6 M. 10–50 µL of this solution was then added per mL to the stock solution of $ZnCl_2$ also prepared in 3 M or 6 M hydrochloric acid, resulting in an activity concentration of 100–300 kBq/mL (^{67}Ga). The copper foil, containing around 5–10 MBq of ^{65}Zn at end of bombardment, was dissolved in 1.7 mL of concentrated HNO_3 at 60°C. The deep blue solution was evaporated to dryness at 150°C using vigorous argon flow. The blue solid was re-dissolved in 2.5 mL of 1 M HCl and loaded onto TK200 resin (3 g). The resin was washed with 1 M HCl, which removed all the copper (a total of 14 mL), and then with water, which eluted the ^{65}Zn (a total of 25 mL). The fractions containing the highest amount of ^{65}Zn were collected, the solution was evaporated to dryness, dissolved in 2 mL 3 M hydrochloric acid, and added (10–20 µL per mL) to the 5.6 M or 1 M $ZnCl_2$ stock solution containing the gallium radionuclides. The resulting

solution, containing 100–300 kBq/mL of both ^{67}Ga and ^{65}Zn, simulating a cyclotron-irradiated liquid target mixture was used as the aqueous phase for the LLE. To quantify Cu, Mn, and Co, we used the ^{64}Cu, ^{54}Mn, and ^{60}Co radionuclides, respectively. These were provided by Prof. Xiaolin Hou, except for ^{64}Cu, which was supplied from the medical production at our site using the GE PETtrace cyclotron.

Instrumentation and methods

Ga and Zn were quantified by gamma spectroscopy of the ^{67}Ga and ^{65}Zn using a Princeton Gammatech LGC 5 or Ortec GMX 35195-P germanium detector, calibrated using certified barium-133 and europium-152 sources. The same instrumentation was used to measure activities from ^{64}Cu, ^{54}Mn, and ^{60}Co. An Eppendorf 5702 centrifuge was used to assist in phase separation. Fe was quantified using a Thermo Scientific iCAP 6000 Series ICP Optical Emission Spectrometer. The membrane separator module was purchased from Zaiput Flow Technologies. All experiments used 0.2 μm membrane pore size, 0.002" (0.051 mm) diaphragm, two 10-element static mixers, and 108 cm mixing tube. The solutions for the continuous membrane-based separation were pumped using KDS 100 Legacy Syringe pumps. For batch experiments, the phase mixing was performed using an IKA ROCKER 3D digital shaker. The quantitative NMR (qNMR) was performed on an Agilent 400 MR spectrometer operating at 400.445 MHz (^{1}H) as described elsewhere.[17]

Phase equilibrium and liquid-liquid extraction of Ga and Zn in 5.6 M $ZnCl_2$/HCl – Et_2O system

For the phase equilibrium studies (Figure 4 A), nine centrifuge tubes were each charged with 3 mL of 5.6 M $ZnCl_2$ made in 0, 0.5, 1, 1.5, 2, 2.5, 3, 3.5, or 4 M HCl solution, respectively, and subsequently 3 mL of Et_2O (pre-saturated with the HCl solution of the corresponding strength) was added. The mixture was shaken for 30 minutes and centrifuged at 4000 rpm to separate the phases. The level of the two phases was marked on the centrifuge tubes with a pen, and the tubes were emptied and dried. Water was added up to the marks and weighted to calculate the volume of the organic and aqueous phase after the mixing. For the LLE studies (Figure 4 B) five centrifuge tubes were each charged with 1.3 mL of 5.6 M $ZnCl_2$ – made in 0.05, 0.6, 1, 2, or 3 M HCl solution, respectively, also containing ^{67}Ga and ^{65}Zn radionuclides and mixed with 1.3 mL of HCl-saturated Et_2O for 30 minutes. The phases were separated after being centrifuged at 4000 rpm. The activity of ^{67}Ga and ^{65}Zn in the aqueous and in the organic phases were measured by gamma spectroscopy.

Phase separation: diluent study

The 6 M HCl and 3 M HCl solutions used for the experiments were made by diluting concentrated HCl with D_2O. A 1.3 mL 5.6 M $ZnCl_2$ in 6 M HCl solution was added to each of seven centrifuge tubes. The level of the solution in the centrifuge tubes at upright position was marked with a pen. A 1 mL aliquot of one of the seven ethers, Et_2O, $^{i}Pr_2O$, THP, *n*-Bu_2O, *n*-BuOMe, *n*-HexOMe or *n*-Am_2O, was added to the tubes. After shaking the tubes for one minute, the aqueous and the ether phases became partially or completely miscible. Then, toluene was added to the tubes as a diluent to increase the phase separation between the aqueous and the organic phase. Toluene was added until the aqueous phase had the same volume as before the mixing with ether, which was noted by comparing the level of the aqueous phase with the mark on the tube. The same procedure was used to test different diluents, where 1.3 mL of 5.6 M $ZnCl_2$ in 6 M HCl solution was added to each of four centrifuge tubes and 1 mL THP was added to each tube. One of four different diluents, anisole, DCE, TFT, or heptane, was added to the tubes until the volume of the aqueous phase was the same as before the mixing. This study with THP and the same diluents as well as toluene was repeated with a 5.6 M $ZnCl_2$ in 3 M HCl solution. The phases were separated after the addition of sufficient amount of diluent. To quantify the amount of ether and diluent in the aqueous phase, we used qNMR. To that end, 0.7 mL of each aqueous phase was transferred to separate NMR tubes, and 15–20 mg citric acid was added to each sample as internal calibrant.

Batch extraction

For the batch LLE of gallium, seven centrifuge tubes were charged with 1.3 mL of 5.6 M $ZnCl_2$ made in 3 M HCl solution, also containing ^{67}Ga and ^{65}Zn. To this, 3 mL of one of the seven ethers, Et_2O, $^{i}Pr_2O$, THP, Bu_2O, *n*-BuOMe, *n*-HexOMe, or *n*-Am_2O, mixed with TFT (1/2 v/v) was added. The tubes were shaken for 30 minutes, centrifuged at 4000 rpm, and the phases were separated. The activity of ^{67}Ga and ^{65}Zn in each phase was quantified by gamma spectroscopy. The batch LLEs with all seven ethers with TFT (1/2 v/v) were repeated with a solution of 5.6 M $ZnCl_2$ made in 6 M HCl. The extraction of Mn and Co were studied using the same procedure, where ^{54}Mn and ^{60}Co were added to the 5.6 M $ZnCl_2$ in 3 M HCl solution. Batch LLEs with 1 mL of 1 M $ZnCl_2$ made in 6 M HCl, also containing ^{67}Ga and ^{65}Zn radionuclides were also performed under the same conditions and same organic solvent mixtures.

The Ga extraction efficiencies (EE(%)) were calculated from the activities of ^{67}Ga in the organic phase divided by the total activities in the aqueous and organic phase as shown in

$$EE(\%) = \frac{^{67}Ga_{org}}{^{67}Ga_{org} + ^{67}Ga_{aq}} \times 100\% \quad (1)$$

The Zn extraction was calculated in the same way using the radioactivities of ^{65}Zn. The percent Ga recovery and the percent Zn contamination were calculated as the activity of ^{67}Ga and ^{65}Zn in the 0.1 M HCl stripping solution divided by the activities of the respective radionuclides in the aqueous solution before the extraction and stripping.

Flow extraction

A 3-stage separation of gallium from zinc using liquid-liquid extraction in flow is presented in Figure 2. In stage 1 (extraction), the aqueous feed consisted of a solution of 1 M $ZnCl_2$ made in 6 M HCl, also containing ^{67}Ga and ^{65}Zn radionuclides, and the aqueous phase contained a 1/2 (v/v) mixture of *n*-BuOMe/TFT. In stage 2, the 8 M HCl was used as an aqueous phase to selectively remove Zn from the organic phase (scrubbing). In stage 3 radiogallium was back-extracted from the organic into the aqueous phase (stripping). For the purpose of screening and optimization studies, either a single-stage extraction or a double-stage extraction and stripping was used. In these experiments, the aqueous feed consisted of a solution of either 5.6 M $ZnCl_2$ made in 3 M HCl or a solution of 1 M $ZnCl_2$ made in 6 M HCl. A 1/2 (v/v) mixture of Et_2O, $^{i}Pr_2O$, THP, *n*-BuOMe, *n*-HexOMe, *n*-Bu_2O, or *n*-Am_2O with TFT was used as the organic phase. The fluidics were driven by two separate syringe pumps equipped with the Hamilton glass syringes, which were filled with the organic (4.5–9 mL) and the aqueous (1.5–3 mL) phases. The aqueous flow rate was 15 mL/h, and the organic flow rate was 45 mL/h for all experiments. The two phases passed through PFA tubing (1/16″ OD, 0.03″ ID) and combined in a PEEK tee. The phases were mixed by two 10 element PTFE static mixers placed inside a short piece of PFA tubing (1/8″ OD, 1/16″ ID). The two phases were further mixed in a 108 cm long PFA tubing (1/16″ OD, 0.03″ ID) mixing loop by steady slug flow and passed into the membrane separator.

The membrane separator with integrated pressure control (SEP-10) is commercially available from Zaiput Flow Technologies and is similar to one described in detail by Adamo et al.[14] In the membrane separator, the organic phase permeated the hydrophobic membrane (PTFE/PP, 0.2 μm pore size and 139 μm thickness) and passed through the permeate outlet, while the aqueous phase was retained and passed through the retentate outlet (Figure 3). The 0.002” PFA diaphragm in the membrane separator worked as integrated pressure control, and complete phase separation between the aqueous and the organic phase was obtained with the chosen membrane and diaphragm. Samples of the aqueous and the organic phase were collected after the LLE and the activity were measured using gamma spectroscopy.

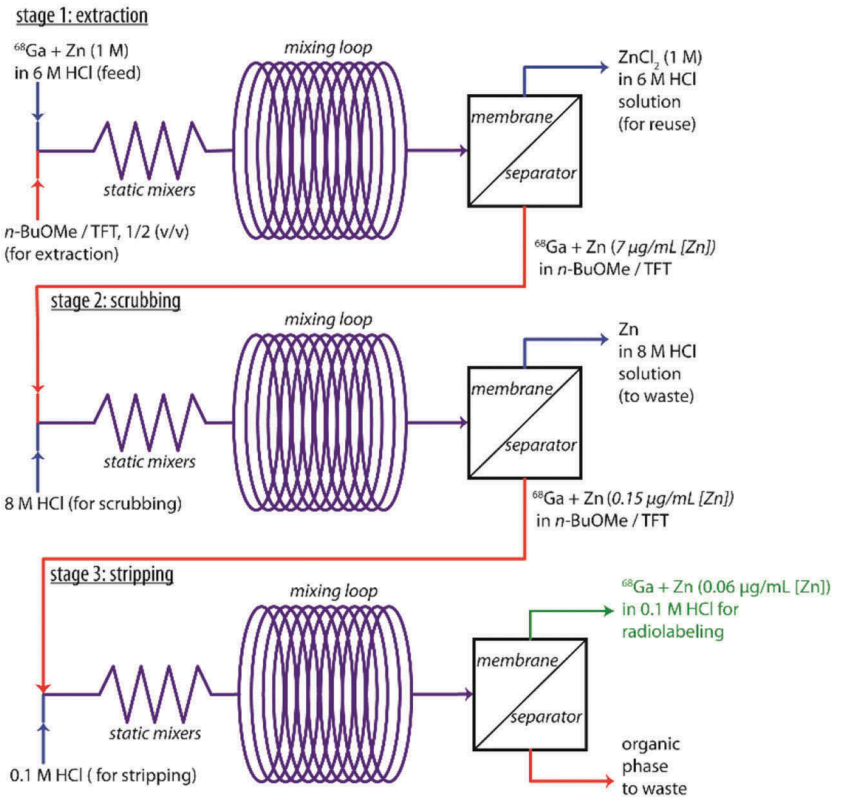

Figure 2. A schematic depicting the liquid-liquid extraction in flow of ^{66,67,68}Ga = *Ga and Zn using the 1/2 (v/v) mixture of *n*-BuOMe/TFT, and hydrochloric acid, also containing 1 M $ZnCl_2$, and including scrubbing of residual Zn with 8 M HCl and back-extraction of *Ga into 0.1 M HCl. The process was performed stepwise.

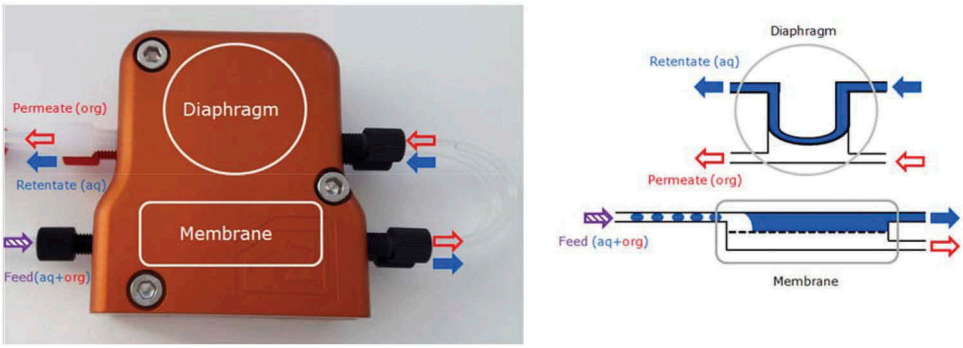

Figure 3. A photograph (left) and a schematic (right) depicting the membrane separator used in this study. The aqueous phase is shown in blue (retained phase) and the organic phase is shown in white (permeated phase).

Fe extraction

The LLE in flow with $^{i}Pr_2O$/TFT (1/2) as organic phase was repeated, but 9 mM $FeCl_3$ was added to the 5.6 M $ZnCl_2$ in 3 M HCl solution. The aqueous phase before and after the LLE was analyzed by ICP-OES.

Copper extraction

7 MBq ^{64}Cu was added to the 5.6 M $ZnCl_2$ in 3 M HCl solution and the LLE in flow with $^{i}Pr_2O$/TFT (1/2) was repeated. The extraction of ^{64}Cu was measured by gamma spectroscopy.

Computational methods

All gas-phase and COSMO calculations were performed using the TURBOMOLE 7.3 suite of programs using the resolution of the identity approximation (RI).[19] The gas-phase structures were optimized at the RI BP/def2-TZVPD level, and the convergence to the ground state was verified by running analytical frequency calculations. The single-point gas-phase energies were then re-evaluated at the RI MP2/def2-TZVPP level. The COSMO files were obtained at the RI BP/def2-TZVPD level in the COSMO phase with a smooth radii-based isosurface cavity, and the convergence to the ground state was verified by running numerical frequency calculations. The resulting COSMO files were used to perform solution thermodynamics calculations using COSMOtherm, Version C30, Release 18; (COSMOlogic GmbH & Co. KG), yielding the free energies of solvation, sigma surfaces, and sigma profiles.[20]

Results and discussion

System design

The continuous production of ^{68}Ga necessitates a judicious choice of the chemical composition of the cyclotron target solution and the extraction system. For the radionuclide production, the $[^{68}Zn]Zn(NO_3)_2/HNO_3$ solution has recently become the system of choice over $[^{68}Zn]ZnCl_2$/HCl, as HNO_3 reduces pressure buildup during the cyclotron irradiation.[11] However, when the requirement for the LLE is factored in, a solution based on $[^{68}Zn]ZnCl_2$/HCl appears preferable due to superior extractability of $GaCl_3$ vs. $Ga(NO_3)_3$. $ZnCl_2$ is also significantly more soluble than $Zn(NO_3)_2$ (408 vs. 120 g/100 mL, correspondingly),[21] which allows one to probe a wider range of zinc concentrations. We considered the composition of the organic phase to be equally important. First and foremost, it should provide for high extractability of ^{68}Ga into the organic phase and excellent ^{68}Ga vs. ^{68}Zn selectivity but at the same time allow for efficient stripping of $[^{68}Ga]GaCl_3$ back into the aqueous phase. The second critical parameter is the mutual phase contamination, which often occurs during LLE and can be significant at high electrolyte concentrations. A failure to prevent the contamination of the aqueous phase with the organic phase could lead to pressure build-up and soot formation during the cyclotron irradiation of the target solution. Furthermore, the aqueous and organic phases with partial miscibility tend to have low interfacial tension, which might cause a phase breakthrough during the membrane separation step.[15]

The earlier work established that dialkyl ethers, and in particular Et_2O and $^{i}Pr_2O$, efficiently and selectively extracted gallium from 5–7 M hydrochloric acid solutions in batch.[18,22–26] In view of the dialkyl ethers being generally nontoxic, readily available, low boiling-point liquids with significant variation in hydrophobicity, we decided to evaluate this class of compounds for further development in LLE and membrane-based separation of Ga from Zn. Since the *Ga production yield and its extractability, as well as the *Ga vs. Zn selectivity, is expected to depend on zinc and HCl concentrations, we decided to explore both high (5.6 M) and low (1 M) concentrations of $ZnCl_2$ and HCl (3 M vs. 6 M).

Phase equilibrium at high (5.6 M) $ZnCl_2$ concentration

THP, Et_2O, *n*-BuOMe, $^{i}Pr_2O$, *n*-HexOMe, *n*-Bu_2O, and *n*-Am_2O ethers were chosen as the extractants. The preliminary experiments showed that the presence of concentrated $ZnCl_2$

dramatically influenced the equilibrium between the aqueous and organic phases. A single phase was observed by mixing equal volumes of Et_2O and a 5.6 M solution of $ZnCl_2$ prepared in 6 M HCl. Lowering the concentration of HCl to 5 M, and then to 4 M still produced a single phase. At 3.5 M HCl, two phases finally separated, but extensive migration of aqueous phase into the organic phase was observed (Figure 4 A, circles, green trace) and confirmed by the qNMR. Lowering the concentration of HCl further led to an exponential decrease in $V(Et_2O)/V(aq)$ and consequently to a decrease in the migration of aqueous phase into the organic phase. Remarkably, this trend was opposite to what was reported in the literature in the absence of $ZnCl_2$ (Figure 4 A, squares, teal trace).[18,22] Gratifyingly, the presence of 5.6 M $ZnCl_2$ had a positive influence on radiogallium extraction. Already at 3 M HCl in the presence of 5.6 M $ZnCl_2$, 80% of radionuclide could be extracted into Et_2O, whereas without $ZnCl_2$, the extraction efficiencies in 3 M HCl were reported to be below 20%.[18] Regrettably, we found that together with the aqueous phase, more than 60% of $ZnCl_2$ was co-extracted into the organic phase (Figure 4 B). The reason for increased solubility of the 5.6 M $ZnCl_2$ in the ether phase is unclear at the moment. One can speculate that at high concentrations neutral and mostly covalent oligomeric chains $(ZnCl_2–H_2O)_n$ start to form and migrate into the ether phase.

Encouraged by the medium-to-high levels of radiogallium extraction and the tolerance of cyclotron target to concentrated (5.6–10 M) $ZnCl_2$ solution reported earlier by Jensen and Clark,[9] we felt that LLE in flow could be further developed while the unfavorable phase equilibrium and high co-extraction of $ZnCl_2$ could be combatted with a prudent choice of extractant and diluent. Our strategy was to find a suitable diluent that provided for a reliable phase separation with no or little mutual phase contamination while keeping high gallium extraction efficiency and *Ga vs. Zn selectivity. Given its low capacity to dissolve water,[27] toluene was initially chosen as a diluent for screening the liquid-liquid phase equilibrium in the series of ethers mixed with 5.6 M $ZnCl_2$ prepared in 6 M HCl. This strategy proved to be successful: Figure 5 (left Y-axis) shows the amount of toluene that had to be added to suppress the migration of the aqueous phase into the organic phase. THP, together with Et_2O, had the highest affinity for the aqueous phase (log P = .95 and 0.87, correspondingly), while n-Bu_2O and n-Am_2O (log P = 2.99 and 3.38, correspondingly) required no or little diluent and could be used neat for extraction. The qNMR of the aqueous phase showed that upon equilibration, less than 10% of the ether migrated into the aqueous phase even for the most hydrophilic ethers (Figure 5, right Y-axis). Next, we optimized the nature of the diluent by screening a series of hydrophobic solvents against THP, chosen to challenge the aqueous/organic phase equilibria as a hydrophilic ether. In a panel of diluents selected from five major classes of organic

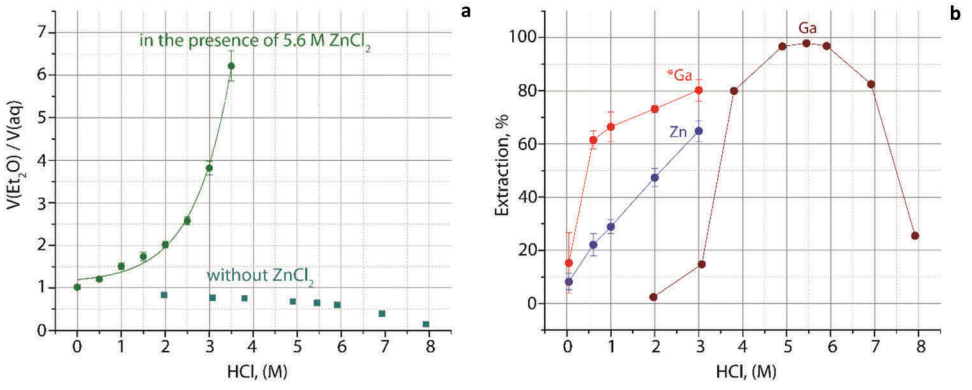

Figure 4. A: Volume changes on equilibrating equal volumes of Et_2O and HCl of various strengths in the presence (5.6 M, circles) and absence (squares) of $ZnCl_2$. B: Liquid-liquid extraction of radiogallium (^{66,67,68}Ga = *Ga, red) and zinc (^{65}Zn, blue) with Et_2O from HCl solutions of various strengths in the presence of 5.6 M $ZnCl_2$, and the extraction of Ga in the absence of $ZnCl_2$, as reported by Swift (maroon).[18] Error bars represent the standard deviation of two consecutive measurements.

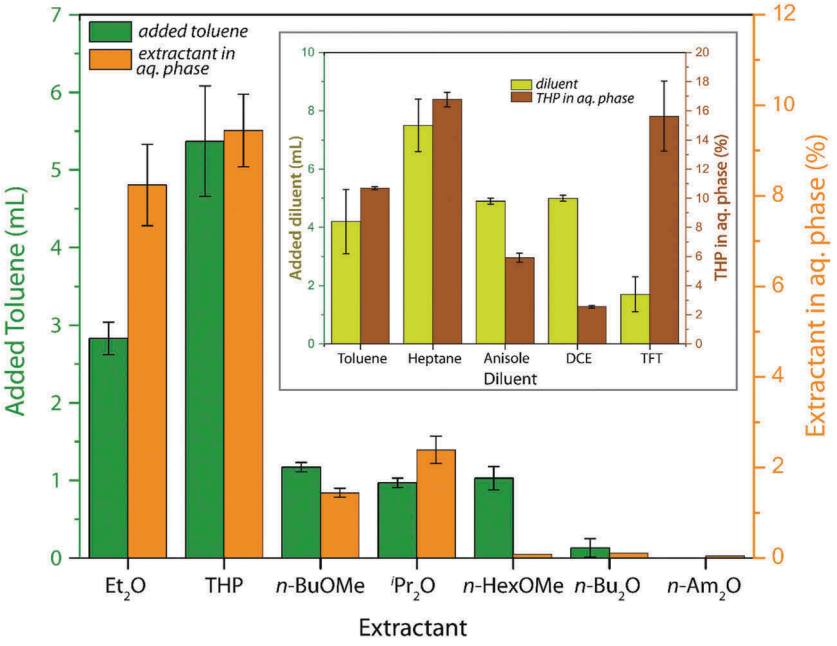

Figure 5. The influence of diluent on the liquid-liquid phase equilibrium containing organic phase and 5.6 M $ZnCl_2$ prepared in 6 M HCl. Main: The amount of toluene added to the ethereal phase required to reconstitute the initial 1.3 mL of the aqueous phase. Inset: The amount of diluent added to the THP phase required to reconstitute the initial 1.3 mL of the aqueous phase. Error bars represent the standard deviation of two consecutive measurements.

solvents and represented by toluene, anisole, DCE, TFT and heptane, TFT was the most effective, requiring only 1.7 mL to reconstitute the initial 1.3 mL of the aqueous phase (Figure 5, inset, left Y-axis).

Although the amount of THP in the aqueous phase remained substantial at 6 M HCl (Figure 5, inset, right Y-axis), at 3 M HCl it dropped to 4%, suggesting that a judicious choice of the extractant would allow us to further suppress the phase contamination (Fig. S1, Supporting Information).

Batch and in-flow extractions at high (5.6 M) $ZnCl_2$ concentration

Having established TFT as an optimal diluent, we investigated the *Ga and Zn extractions in batch. At 6 M HCl, a 1/2 (v/v) mixture of TFT and one of the seven ethers in the screening set allowed for radiogallium extraction efficiencies above 80% (Fig. 6, red circles). $^{i}Pr_2O$ and *n*-BuOMe were found to be the best performers extracting up to 97% of radiogallium in 6 M HCl. As expected, the extraction efficiencies decreased in 3 M HCl, with $^{i}Pr_2O$/TFT mixture able to extract 77% of *Ga and 1% of Zn (Fig. 6, red and blue triangles). Only 0.3% of $^{i}Pr_2O$ and no TFT was found migrating into the aqueous phase. Among all ethers, THP co-extracted the highest amount of zinc from both 6 M and 3 M HCl.

Next, we translated the batch experiments into fully continuous flow experiments using the apparatus depicted in Figure 2 (single-stage extraction only). The low mutual phase contamination observed in batch at 3 M HCl prompted us to explore LLE in flow of *Ga and Zn from the 5.6 M $ZnCl_2$/3 M HCl solution using optimized flow conditions established previously.[15] The organic phase consisted of a 2/1 (v/v) mixture of TFT used as a diluent and Et_2O, THP, $^{i}Pr_2O$, and *n*-BuOMe used as the extractants. In all cases, clean phase separation was achieved, and the radiogallium was selectively extracted into the organic phase. The organic phase could then be either collected or directly re-routed into the second separation module, where 0.1 M HCl was used as the aqueous phase for stripping. Within the experimental errors, the results of the LLE in flow mirrored those

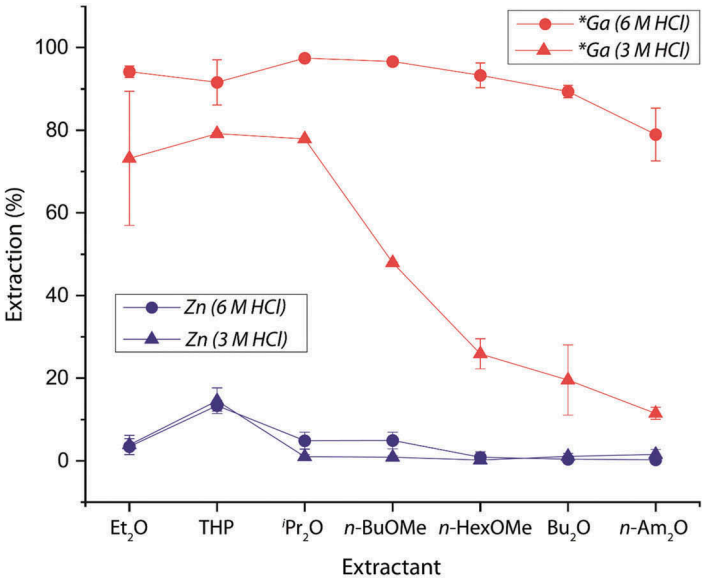

Figure 6. ^{66,67,68}Ga = *Ga (red, two top traces) and Zn (blue, two bottom traces) extractions in batch using a 1/2, (v/v) mixture of ether/TFT. The aqueous phase is formed by 5.6 M $ZnCl_2$ prepared either in 6 M HCl (circles) or in 3 M HCl (triangles). Error bars represent the standard deviation of two consecutive measurements.

obtained in the batch experiments: the THP showed the highest radiogallium extraction, but also the lowest *Ga vs. Zn selectivity (Table 1, entry 2). Measuring the LLE in flow performance over time, we noted that in all cases except *n*-BuOMe (50%), 70% of radiogallium was extracted within the first 2 minutes, and the extraction was complete in under 6 minutes. The *Ga stripping efficiencies were uniformly high (> 95%) across the series, but little selectivity was observed for *Ga vs. Zn stripping. For practical implementations, $^{i}Pr_2O$ seems to strike the best balance between the levels of radiogallium and zinc extraction.

Batch and in-flow extractions at low (1 M) $ZnCl_2$ concentration

Turning now to low $ZnCl_2$ concentration, we found that 1 M $ZnCl_2$ prepared in 6 M HCl and combined with a 1/2 (v/v) mixture of ether/TFT yielded a well-separated biphasic mixture with no mutual phase contamination. Table 2 shows that *Ga extractions in batch at 1 M $ZnCl_2$ were on average on the same level as those obtained from the 5.6 M $ZnCl_2$/6 M HCl, but appreciably higher than those obtained from 5.6 M $ZnCl_2$/3 M HCl. Importantly, the co-extraction of zinc was one order of magnitude lower for the non-hydrophobic ethers, likely due to increased chloride per zinc equivalents ratio, which promoted the formation of non-extractable $ZnCl_4^{2-}$ [28] (Table 2 entries 1–4).

Table 1. Liquid-liquid extraction and stripping of ^{66,67,68}Ga = *Ga and Zn in flow using a 1/2 (v/v) mixture of ether/TFT (extraction) and 0.1 M HCl (stripping). The aqueous phase was formed by 5.6 M $ZnCl_2$ prepared in 3 M HCl. Errors represent the standard deviation of three consecutive measurements.

Entry	Ether	*Ga extraction, %	Zn extraction, %	Ga stripping, %	Zn stripping, %	Ga recovery, %	Zn contamination, %
1	Et_2O	81.4 ± 2.6	4.2 ± 0.7	99.7 ± 0.7	91.0 ± 8.2	81.1 ± 2.6	3.8 ± 0.8
2	THP	89.6 ± 3.7	26.2 ± 8.6	99.3 ± 2.8	98.1 ± 4.4	88.9 ± 4.5	25.7 ± 8.5
3	$^{i}Pr_2O$	76.3 ± 1.9	1.9 ± 1.6	97.8 ± 2.4	93.4 ± 6.3	74.6 ± 2.6	1.7 ± 1.5
4	*n*-BuOMe	51.8 ± 1.8	2.1 ± 0.3	98.5 ± 3.1	76.5 ± 3.8	51.0 ± 2.4	1.6 ± 0.2

Table 2. Liquid-liquid extraction of ^{66,67,68}Ga = *Ga and Zn in batch and in flow using a 1/2 (v/v) mixture of ether/TFT. The aqueous phase was formed by 1 M $ZnCl_2$ prepared in 6 M HCl. Errors represent the standard deviation of two consecutive measurements.

		Batch		Flow	
Entry	Extractant	*Ga %	Zn %	*Ga %	Zn %
1	Et_2O	96.4 ± 1.7	0.3 ± 0.2	98.9 ± 0.2	0.2 ± 0.2
2	THP	98.0 ± 1.1	1.7 ± 0.5	97.4 ± 2.0	1.5 ± 0.5
3	$^{i}Pr_2O$	93.1 ± 1.1	0.4 ± 0.5	97.5 ± 1.3	0.1 ± 0.1
4	*n*-BuOMe	98.0 ± 0.4	0.5 ± 0.7	95.7 ± 2.0	$5 \cdot 10^{-3} \pm 3 \cdot 10^{-3}$
5	*n*-HexOMe	93.9 ± 1.6	0.4 ± 0.2	90.6 ± 3.5	$2 \cdot 10^{-3} \pm 2 \cdot 10^{-4}$
6	Bu_2O	84.8 ± 4.9	0.3 ± 0.2	87.3 ± 0.4	0.01 ± 0.01
7	*n*-Am_2O	73.6 ± 1.4	0.5 ± 0.1	80.4 ± 1.5	$2 \cdot 10^{-3} \pm 1 \cdot 10^{-3}$

Next, all seven ethers were chosen for translation in flow. Running LLE in flow under the optimized conditions reported in Table 1 resulted in smooth and reproducible phase separation with no phase breakthrough. The radiogallium extractions were complete within 6 minutes, and the yields were consistent with the batch extractions (Table 2).

Co-extraction of other metals

Iron is an environmentally ubiquitous metal and is often present as a contaminant during radionuclide production. It will also competitively chelate to many gallium chelators.[29] Therefore, it was important to access the co-extraction of Fe^{III} into the solvent system optimized for the liquid-liquid extraction of gallium. An in-flow extraction of 9 mM $FeCl_3$ dissolved in 5.6 M $ZnCl_2$/3 M HCl with $^{i}Pr_2O$/TFT, 1/2, (v/v) resulted in 66 ± 2% of Fe extraction into the organic phase and 98% stripping into 0.1 M HCl. The lack of *Ga vs. Fe selectivity demonstrated by our optimized system was not surprising given the high Lewis acidity and strong propensity to form organic-soluble $HMCl_4$ species by both cations (M = Ga, Fe).[30] Small amounts of various chelating Cu, Co, and Mn radionuclidic impurities are also commonly found in the cyclotron-irradiated samples of zinc solutions.[13] In contrast to Fe extraction, Cu was extracted only at 0.04%, and no detectable extraction was observed for Mn and Co.

COSMO-RS model for extraction of Ga and Zn

Although experimental studies on liquid-liquid extraction of Ga using ethers have a long history, no model explaining equilibrium in the Ga/HCl/ether system has been put forward. An earlier attempt to correlate the extractability of Ga with a dielectric constant of an ether was unsuccessful, and a participation of an extractant in coordination to the metal was conjectured.[24] A broader question of Ga vs. Zn selectivity arises in the context of LLE of the two metals following cyclotron production of *Ga where the concentrations of HCl and zinc may vary during irradiation due to high temperatures and radiolysis. The speciation of Ga and Zn under different HCl concentrations was studied in detail using titration,[23,31] X-ray scattering, Raman,[32] and EXAFS spectroscopy.[28] These studies provide an opportunity to inform theory about the Ga and Zn species most likely to be present in solution, which coupled with an appropriate computational technique can pave the way to a predictive quantitative model.

The conductor-like screening model for real solvents (COSMO-RS) is one of such computational methodologies. Known for its algorithmic simplicity, numerical stability and robustness COSMO-RS combines first-principle quantum chemistry with statistical thermodynamics. The detailed description of COSMO-RS can be found elsewhere,[33] but in short, in a first step, a molecule is geometry-optimized in a homogeneous conductor environment yielding the surface polarization charge densities as a molecular descriptor and a measure of a molecular surface polarity. These calculations are performed using density functional theory. In the next step, statistical thermodynamics is used to

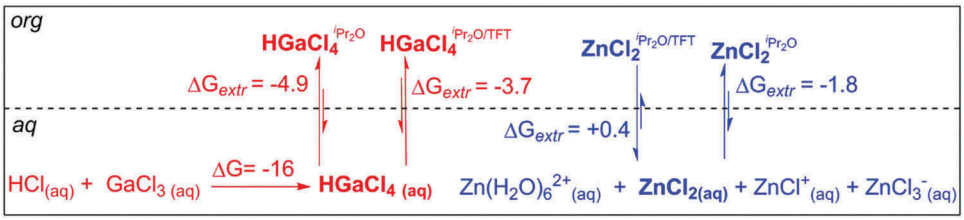

Scheme 1. The solution equilibrium for the relevant gallium and zinc species in the aqueous and organic phases as calculated at COSMO-RS-FINE/RI-MP2 level.[34] The values are in kcal/mol.

quantify intramolecular interaction energies as interactions of polarization charge densities, ultimately yielding chemical potentials of a given species in the system. Thus, COSMO-RS treats a solute and a solvent on the same footing and contains relatively few empirical terms, which allows one to use it outside of parametrization.

Having developed an efficient and reliable experimental method for selective LLE of radiogallium in the presence of zinc, we turned to construct a predictive theoretical model for extraction. The first step was to establish the main extractable species, and these could be gleaned from earlier experimental studies. The works of Reznik and Nachtrieb indicate that in the 3–6 M HCl range, gallium extracts into tributyl phosphate or $^{i}Pr_2O$ as a 1/1 mixture of HCl/$GaCl_3$, presumably in the form of the chlorogallic acid, $HGaCl_4$.[23,31] Indeed, we found $HGaCl_4$ to be a potential-energy minimum in both gas and COSMO phases, and its formation from HCl and $GaCl_3$ was predicted to go to completion in the aqueous phase (ΔG = – 16 kcal/mol, Scheme 1). In line with the experiment, the solution thermodynamics calculations found $^{i}Pr_2O$ to be a much better solvent for $HGaCl_4$ than water, with the difference in the free energy of solvation calculated at – 4.9 kcal/mol.

Examination of the COSMO sigma surface of $HGaCl_4$ reveals that it is dominated by the weakly negatively charged Ga–Cl moieties (Figure 7, yellow-green surface). A better insight into why $^{i}Pr_2O$ is an excellent solvent for $HGaCl_4$ can be obtained by examining their respective sigma profiles, which give a relative amount of surface with a given polarity σ. Figure 7 shows that the weakly negatively charged part of $HGaCl_4$ represented by peak *H* is well solvated by a weakly positively charged C–H moieties of $^{i}Pr_2O$ (peaks *F* and *G*). The positively charged H-atom of $HGaCl_4$ (peak *C*) is solvated by the negatively charged O-atom of $^{i}Pr_2O$, (peak *J*). Therefore, the sigma profiles of $HGaCl_4$ and $^{i}Pr_2O$ are complementary, translating into high free energy of solvation (ΔG_{solv} = – 9.9 kcal/mol) and high extractability into the organic phase.

The speciation of the $ZnCl_2$ solutions is more complex. The previous EXAFS and Raman studies conclude that in 7.5 M solution $ZnCl_2$ is present as an almost equimolar mixture of $Zn(H_2O)_6^{2+}$, $ZnCl_2$, $ZnCl^+$, and $ZnCl_3^{-}$.[32] The charged zinc species are not directly extractable into the ether phase, but as a neutral species, $ZnCl_2$ is expected to be solvated by $^{i}Pr_2O$. The examination of $ZnCl_2$ sigma profile reveals that a substantial part of its negatively charged sigma surface is outside of the main $^{i}Pr_2O$ solvation (Figure 7, peak I). Furthermore, the peaks A and B, corresponding to the high-density surface charge around Zn^{2+} have no matching solvent counterparts. Consequently, the transfer of $ZnCl_2$ from the aqueous into the organic phase is less favorable than for Ga (–1.8 kcal/mol vs. – 4.9 kcal/mol), hence lower extraction. As the concentration of external HCl increases, more $ZnCl_2$ is expected to form, driving higher zinc extraction. This is consistent with our experimental observations, where a significant extractability of Zn into Et_2O was observed at higher acid concentrations (Figure 4 B). The thermodynamics changes when TFT is added to the extractant. While the Ga extraction into the organic phase remains exergonic (ΔG_{extr} = – 3.7 kcal/mol), the Zn extraction becomes endergonic (ΔG_{extr} = + 0.4 kcal/mol) keeping the Zn in the aqueous phase. Thus, the less polar TFT acts not only as a diluent preventing mutual phase contamination and increasing the interfacial tension but also as a metal solvation modulator, leading to increased Ga vs. Zn extraction selectivity. With the COSMO-RS model in hand, we computed the LLE of Ga and Zn under the batch extraction conditions (Figure 8). An excellent agreement with the experiment was achieved for the

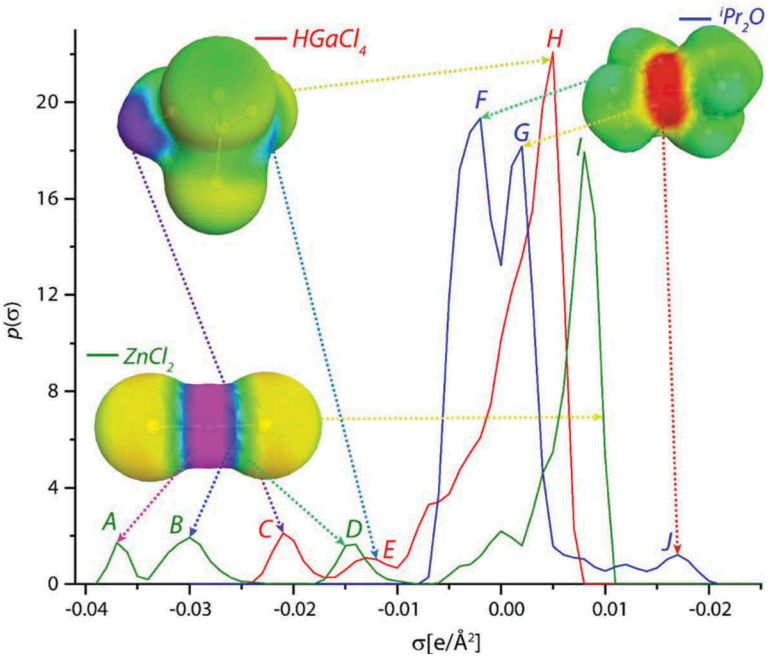

Figure 7. The depiction of COSMO sigma surfaces (polarization charge densities) and sigma profiles for $HGaCl_4$, $ZnCl_2$, and $^{i}Pr_2O$.

extraction of Ga into the C4–C7 ethers measured for both high (5.6 M) and low (1 M) $ZnCl_2$ concentrations in 6 M HCl as evidenced by a mean unsigned error of prediction (MUE, 2.8% and 4.0% correspondingly). The corresponding MUE for the hydrophobic ethers (*n*-Bu_2O and *n*-Am_2O) was somewhat higher at 13.2% and 10.1%.

Experimentally, when 1 M $ZnCl_2$ was prepared in 6 M HCl, the extraction of zinc was very low (Table 2), which is consistent with its speciation diagram dominated by the non-extractable $ZnCl_4^{2-}$ due to the higher Cl/Zn ratio.[28] Therefore, the modeling of Zn extraction was performed using high (5.6 M) concentrations, where the presence of neutral $ZnCl_2$ can be substantial. This yielded the MUE of extraction prediction for Zn at 3.4%, with THP giving the largest error at 7%. It is important to emphasize that while the current modeling efforts considered HCl as a reagent, critical in determining the chemical form of the extracted metal species, its contribution as a solvent was neglected, as no COSMO model for HCl in solution exists. This underscores the importance of developing a COSMO-RS model for concentrated hydrochloric acid, which will help to further improve the quality of predicting the liquid-liquid equilibrium in acidic media.

Advantages, limitations and further development of LLE in flow

Under optimized conditions the LLE in flow is a fast, reproducible and robust operation at both high and low $ZnCl_2$ concentrations. Preliminary experiments conducted in our laboratory indicate that a cyclotron solution target with niobium body and foil, which was also used by Jensen et al.,[9] exhibited good corrosion resistance during short (≤30 minutes), low current (≤10 μA) cyclotron irradiation of both the 5.6 M $ZnCl_2$/3 M HCl and 1 M [^{68}Zn]$ZnCl_2$/6 M HCl solutions when running as an open system. The irradiation of the latter solution for 10 min at 10 μA yielded 350 MBq/μA of activity, which corresponded to a 79% of the theoretical saturation yield as calculated from the experimental cross sections using SRIM software. While both processes can be considered potentially suitable for implementation within the

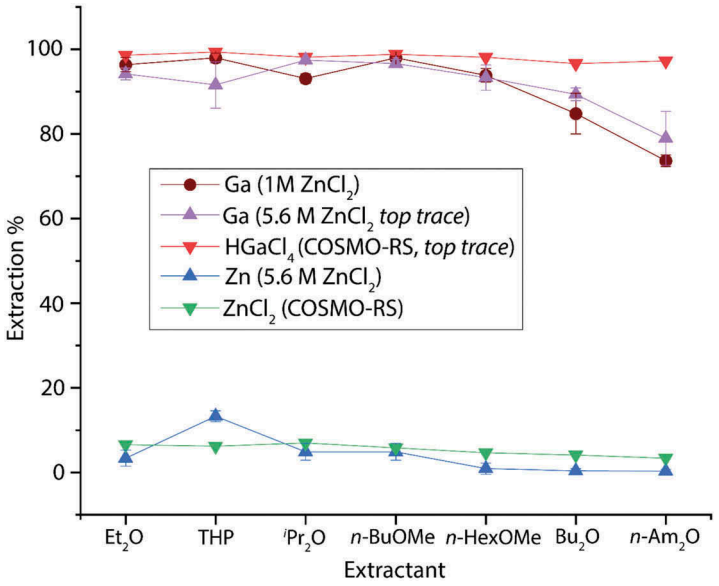

Figure 8. The comparison of experimental (circles and upward triangles) and calculated (downward triangles) extraction of gallium and zinc. The organic phase: 1/2 $^{i}Pr_2O$/TFT, (v/v), the aqueous phase: 5.6 M or 1 M $ZnCl_2$ in 6 M HCl. The calculations were performed at the COSMO-RS-FINE level of theory.[33] Error bars represent the standard deviation of two consecutive experimental measurements.

primary recirculation loop, the appreciably higher *Ga and lower Zn extractions from the 1 M [^{68}Zn]$ZnCl_2$/6 M HCl mixture make it a preferred candidate for development. In fact, we showed that when implemented as a single-stage LLE in flow and followed by scrubbing of residual Zn with 8 M HCl and back-extraction of *Ga into 0.1 M HCl, the method could deliver radiogallium in 90% yield and reduce the final zinc contamination to an estimated 0.06 µg/mL, which, at typical ^{68}Ga-production yields could meet the current requirements of the European Pharmacopeia monograph[35] (Figure 2). If required, any additional purification can be performed downstream the primary recirculation loop using one of the SPE-based purification protocols described elsewhere.[11–13] When compared to the existing methods of ^{68}Ga productions using liquid targets, the ability of the continuous process to recycle ^{68}Zn on the fly could translate into significant savings. With the current ^{68}Zn prices at ~$1/mg, one can expect to reduce the price of a batch by $200–$700. The continuous production also means the process can be stopped and re-started at any time. This could lead to an easy batch size scaling and dose-on-demand production.[36] On the other hand, one of the challenges inherent to the process is that there will be a limit of how many times the target solution can be recirculated without a significant loss of yield or accumulating too many impurities. Implementation of in flow-compatible PAT tools such as Raman and near infrared spectroscopy would be important, as it could provide critical process understanding and inform the regulators about science and quality risk-based management within the framework of the FDA's Quality-by-Design as applied to continuous production of ^{68}Ga.[37]

Conclusions

In conclusion, we found that radiogallium can be efficiently extracted from $ZnCl_2$ solutions in batch and in flow using a membrane-based liquid-liquid separator with integrated pressure control. For extractions from concentrated (5.6 M) solutions of $ZnCl_2$ prepared in 3 M HCl, a 1/2 (v/v) mixture of $^{i}Pr_2O$/TFT is preferred, extracting 76.3 ± 1.9% of radiogallium and 1.9 ± 1.6% of Zn. When 1 M solutions of $ZnCl_2$ is prepared in 6 M HCl, the extraction of radiogallium and *Ga vs. Zn selectivity

is appreciably higher. In this case, a 1/2 (v/v) mixture of *n*-BuOMe/TFT is the system of choice, extracting 95.7 ± 2.0% of radiogallium and co-extracting only 0.005 ± 0.003% of Zn. Trifluorotoluene (TFT) plays a key role in controlling the interfacial tension between the aqueous and the organic phases, and their miscibility, which is critical for successful operation of membrane-based separation of the liquid phases in flow. The COSMO-RS model developed for this system confirms that the ethers act as solvation extractants for the metals and that TFT modulates Ga and Zn solvation, thus increasing the *Ga vs. Zn extraction selectivity. HCl appears to control the speciation of gallium and zinc, and a higher concentration of HCl is beneficial for extraction. Assuming $HGaCl_4$ and $ZnCl_2$ to be the species extractable in the organic phase, the COSMO-RS theory predicts the extraction of gallium and zinc with the MUE of prediction at 4.0% and 3.4% respectively. The high efficiency and selectivity of the radiogallium LLE in flow and its compatibility with commercial cyclotron liquid targets encourages further development of the $ZnCl_2$/HCl-based system, thus paving the way towards fully automated continuous production of ^{68}Ga.

Conflict of Interest

The author declare that there is no conflict of interest regarding the publication of this article.

Funding

The research was supported by the Independent Research Fund Denmark, Grant [8022-00111B].

References

[1] Bekerman, C.; Hoffer, P. B.; Bitran, J. D. The Role of Gallium-67 in the Clinical Evaluation of Cancer. *Semin. Nucl. Med.* 1984, *14*, 296–323. DOI: 10.1016/S0001-2998(84)80005-7.
[2] Even-Sapir, E.; Israel, O. Gallium-67 Scintigraphy: A Cornerstone in Functional Imaging of Lymphoma. *Eur. J. Nucl. Med. Mol. Imaging*. 2003, *30*, S65–S81. DOI: 10.1007/s00259-003-1164-7.
[3] Vorster, M.; Buscombe, J.; Saad, Z.; Sathekge, M. Past and Future of Ga-citrate for Infection and Inflammation Imaging. *Curr. Pharm. Des.* 2018, *24*, 787–794. DOI: 10.2174/1381612824666171129200611.
[4] Mojtahedi, A.; Thamake, S.; Tworowska, I.; Ranganathan, D.; Delpassand, E. S. The value of 68Ga-DOTATATE PET/CT in diagnosis and management of neuroendocrine tumors compared to current FDA approved imaging modalities: a review of literature. *Am. J. Nucl. Mol. Imaging*. 2014, *4*, 426–434.
[5] Witkowska-Patena, E.; Mazurek, A.; Dziuk, M. 68Ga-PSMA PET/CT imaging in recurrent prostate cancer: Where are we now? *Cent. European J. Urol.* 2017, *70*, 37–43.
[6] Velikyan, I.;. 68Ga-based Radiopharmaceuticals: Production and Application Relationship. *Molecules*. 2015, *20*, 12913–12943. DOI: 10.3390/molecules200712913.
[7] Chakravarty, R.; Chakraborty, S.; Ram, R.; Vatsa, R.; Bhusari, P.; Shukla, J.; Mittal, B. R.; Dash, A. Detailed evaluation of different 68Ge/68Ga generators: an attempt toward achieving efficient 68Ga radiopharmacy. *J. Labelled Compd. Radiopharm.* 2016, *59*, 87–94. DOI: 10.1002/jlcr.v59.3.
[8] Engle, J. W.; Lopez-Rodriguez, V.; Gaspar-Carcamo, R. E.; Valdovinos, H. F.; Valle-Gonzalez, M.; Trejo-Ballado, F.; Severin, G. W.; Barnhart, T. E.; Nickles, R. J.; Avila-Rodriguez, M. A. Very High Specific Activity 66/68Ga from Zinc Targets for PET. *Appl. Radiat. Isot.* 2012, *70*, 1792–1796. DOI: 10.1016/j.apradiso.2012.03.030.
[9] Jensen, M.; Clark, J., in *Proceedings of 13th International Workshop on Targetry and Target Chemistry*, Danmarks Tekniske Universitet, Risø Nationallaboratoriet For Bæredygtig Energi, Denmark. 2011, pp. 288–292.
[10] Moreira, H. M. R.;, Cyclotron Production of 68Ga Using a 68Zn-Based Liquid Target, MSc thesis, University of Coimbra, 2013.
[11] Pandey, M. K.; Byrne, J. F.; Jiang, H.; Packard, A. B.; DeGrado, T. R. Cyclotron production of 68Ga via the 68Zn(p,n)68Ga reaction in aqueous solution. *Am. J. Nucl. Mol. Imaging*. 2014, *4*, 303–310.
[12] Alves, V.; Do Carmo, S.; Alves, F.; Abrunhosa, A. Automated Purification of Radiometals Produced by Liquid Targets. *Instruments*. 2018, *2*, 17. DOI: 10.3390/instruments2030017.
[13] Riga, S.; Cicoria, G.; Pancaldi, D.; Zagni, F.; Vichi, S.; Dassenno, M.; Mora, L.; Lodi, F.; Morigi, M. P.; Marengo, M. Production of Ga-68 with a General Electric PETtrace Cyclotron by Liquid Target. *Phys. Med.* 2018, *55*, 116–126. DOI: 10.1016/j.ejmp.2018.10.018.

[14] Adamo, A.; Heider, P. L.; Weeranoppanant, N.; Jensen, K. F. Membrane-Based, Liquid–Liquid Separator with Integrated Pressure Control. *Ind. Eng. Chem. Res.* 2013, *52*, 10802–10808. DOI: 10.1021/ie401180t.
[15] Pedersen, K. S.; Imbrogno, J.; Fonslet, J.; Lusardi, M.; Jensen, K. F.; Zhuravlev, F. Liquid–Liquid Extraction in Flow of the Radioisotope Titanium-45 for Positron Emission Tomography Applications. *React. Chem. Eng.* 2018, *3*, 898–904. DOI: 10.1039/C8RE00175H.
[16] Abiev, R. S.; Dymov, A. V. Modeling the Hydrodynamics of Slug Flow in a Minichannel for Liquid-liquid Two-phase System. *Theor. Found. Chem. Eng.* 2013, *47*, 299–305. DOI: 10.1134/S0040579513040180.
[17] Pauli, G. F.; Chen, S.-N.; Simmler, C.; Lankin, D. C.; Gödecke, T.; Jaki, B. U.; Friesen, J. B.; McAlpine, J. B.; Napolitano, J. G. Importance of Purity Evaluation and the Potential of Quantitative 1H NMR as a Purity Assay. *J. Med. Chem.* 2014, *57*, 9220–9231. DOI: 10.1021/jm401509e.
[18] Swift, E. H.;. A New Method for the Separation of Gallium from Other Elements. *J. Am. Chem. Soc.* 1924, *46*, 2375–2381. DOI: 10.1021/ja01676a004.
[19] *TURBOMOLE V7.3 2018*, a development of University of Karlsruhe and Forschungszentrum Karlsruhe GmbH, 1989–2007, *TURBOMOLE GmbH*, since 2007; available from: http://www.turbomole.com.
[20] Eckert, F.; Klamt, A. Fast Solvent Screening via Quantum Chemistry: COSMO-RS Approach. *AIChE J.* 2002, *48*, 369–385. DOI: 10.1002/(ISSN)1547-5905.
[21] Lide, D.;, Ed.. *CRC Handbook of Chemistry and Physics*; CRC Press, United States. 2003.
[22] Irving, H. M.; Rossotti, F. J. C. The Solvent Extraction of Group IIIB Metal Halides. *Analyst*. 1952, *77*, 801–812. DOI: 10.1039/an9527700801.
[23] Nachtrieb, N. H.; Fryxell, R. E. The Extraction of Gallium Chloride by Isopropyl Ether. *J. Am. Chem. Soc.* 1949, *71*, 4035–4039. DOI: 10.1021/ja01180a047.
[24] Brooks, R. R.; Lloyd, P. J. Influence of Molecular Structure on the Liquid/Liquid Extraction of the Chloro-Complexes of Gallium and Indium with Aliphatic Ethers. *Nature*. 1961, *189*, 375. DOI: 10.1038/189375a0.
[25] Lewis, M. R.; Reichert, D. E.; Laforest, R.; Margenau, W. H.; Shefer, R. E.; Klinkowstein, R. E.; Hughey, B. J.; Welch, M. J. Production and purification of gallium-66 for preparation of tumor-targeting radiopharmaceuticals. *Nucl. Med. Biol.* 2002, *29*, 701–706.
[26] Brown, L. C. Chemical Processing of Cyclotron- Produced 67Ga. *Appl. Radiat. Isot.* 1971, *22*, 710–713. DOI: 10.1016/0020-708X(71)90082-2.
[27] Kirchnerová, J.; Cave, G. C. B. The Solubility of Water in Low-dielectric Solvents. *Can. J. Chem.* 1976, *54*, 3909–3916. DOI: 10.1139/v76-562.
[28] D'Angelo, P.; Zitolo, A.; Ceccacci, F.; Caminiti, R.; Aquilanti, G. Structural characterization of zinc(II) chloride in aqueous solution and in the protic ionic liquid ethyl ammonium nitrate by X-ray absorption spectroscopy. *J. Chem. Phys.* 2011, *135*, 1–7.
[29] Nurchi, V. M.; Crisponi, G.; Lachowicz, J. I.; Medici, S.; Peana, M.; Zoroddu, M. A. Chemical Features of in Use and in Progress Chelators for Iron Overload. *J. Trace Elem. Med. Biol.* 2016, *38*, 10–18. DOI: 10.1016/j.jtemb.2016.05.010.
[30] Nachtrieb, N. H.; Conway, J. G. The Extraction of Ferric Chloride by Isopropyl Ether. I. *J. Am. Chem. Soc.* 1948, *70*, 3547–3552. DOI: 10.1021/ja01191a004.
[31] Reznik, A.; Zekel, L. Zh. Tributyl-phosphate extraction of gallium from hydrochloric-acid solutions. *Neorg. Khim.* 1979, *24*, 1025–1032.
[32] Maeda, M.; Ito, T.; Hori, M.; Johansson, G. The Structure of Zinc Chloride Complexes in Aqueous Solution. *Z. Naturforsch.* 1996, *51*, 63–70.
[33] Klamt, A.;. The COSMO and COSMO-RS Solvation Models. *Wiley Interdiscip. Rev. Comput. Mol. Sci.* 2011, *1*, 699–709. DOI: 10.1002/wcms.56.
[34] Hellweg, A.; Eckert, F. Brick by brick computation of the Gibbs free energy of reaction in solution using quantum chemistry and COSMO-RS. *AIChE J.* 2017, *63*, 3944–3954.
[35] *European Pharmacopoeia 9.0*; Council of Europe, Strasbourg, 2013. pp 1148–1149.
[36] Arima, V.; Pascali, G.; Lade, O.; Kretschmer, H. R.; Bernsdorf, I.; Hammond, V.; Watts, P.; De Leonardis, F.; Tarn, M. D.; Pamme, N.;; et al. Radiochemistry on chip: towards dose-on-demand synthesis of PET radiopharmaceuticals. *Lab Chip*. 2013, *13*, 2328–2336. DOI: 10.1039/c3lc50269d.
[37] Yu, L. X.; Amidon, G.; Khan, M. A.; Hoag, S. W.; Polli, J.; Raju, G. K.; Woodcock, J. Understanding Pharmaceutical Quality by Design. *Aaps J.* 2014, *16*, 771–783. DOI: 10.1208/s12248-014-9598-3.

Appendix C - NMR spectra

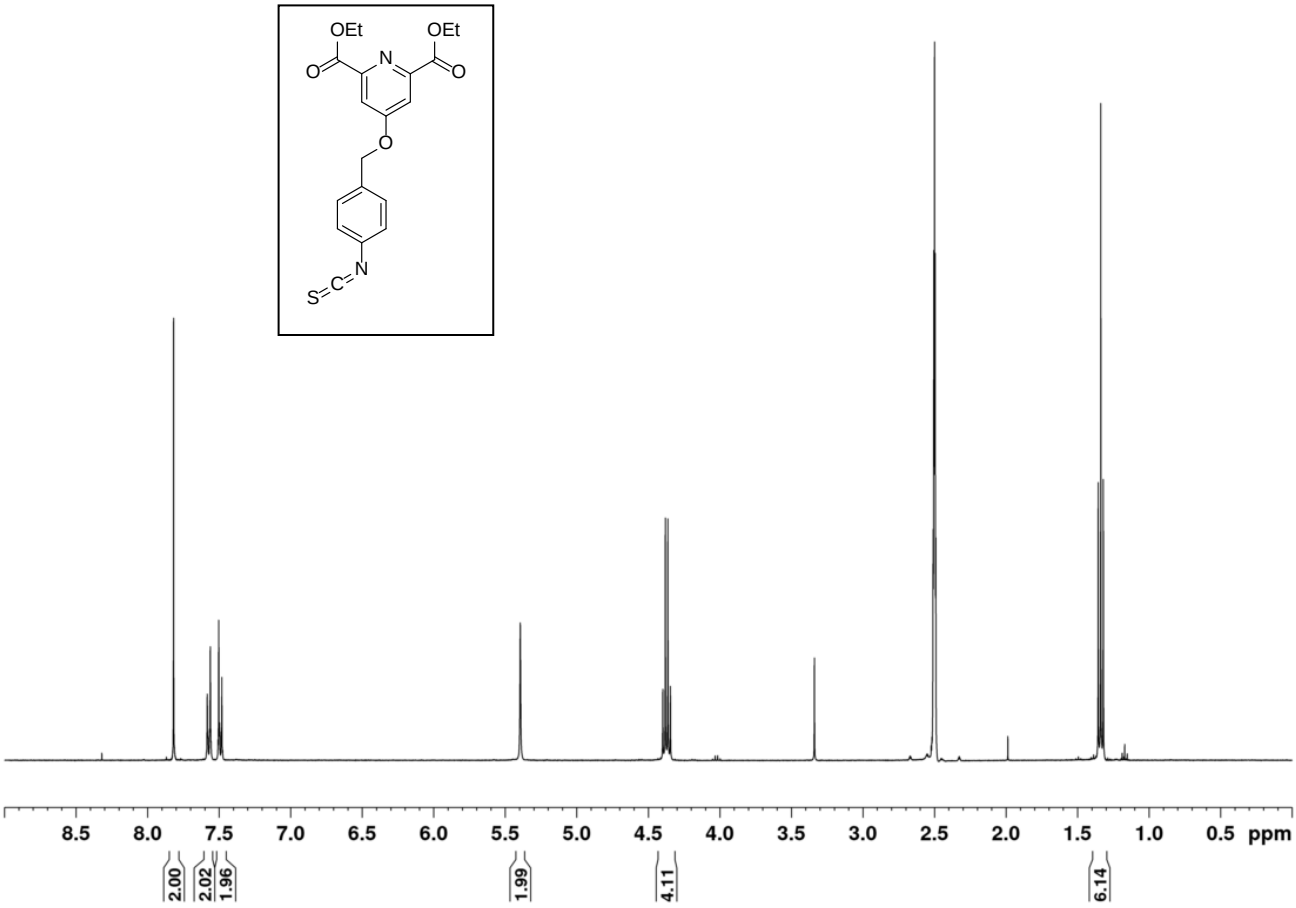

Figure 1A: ^{1}H NMR (400 MHz, DMSO-d_6) spectrum of compound **4** (Figure 48).

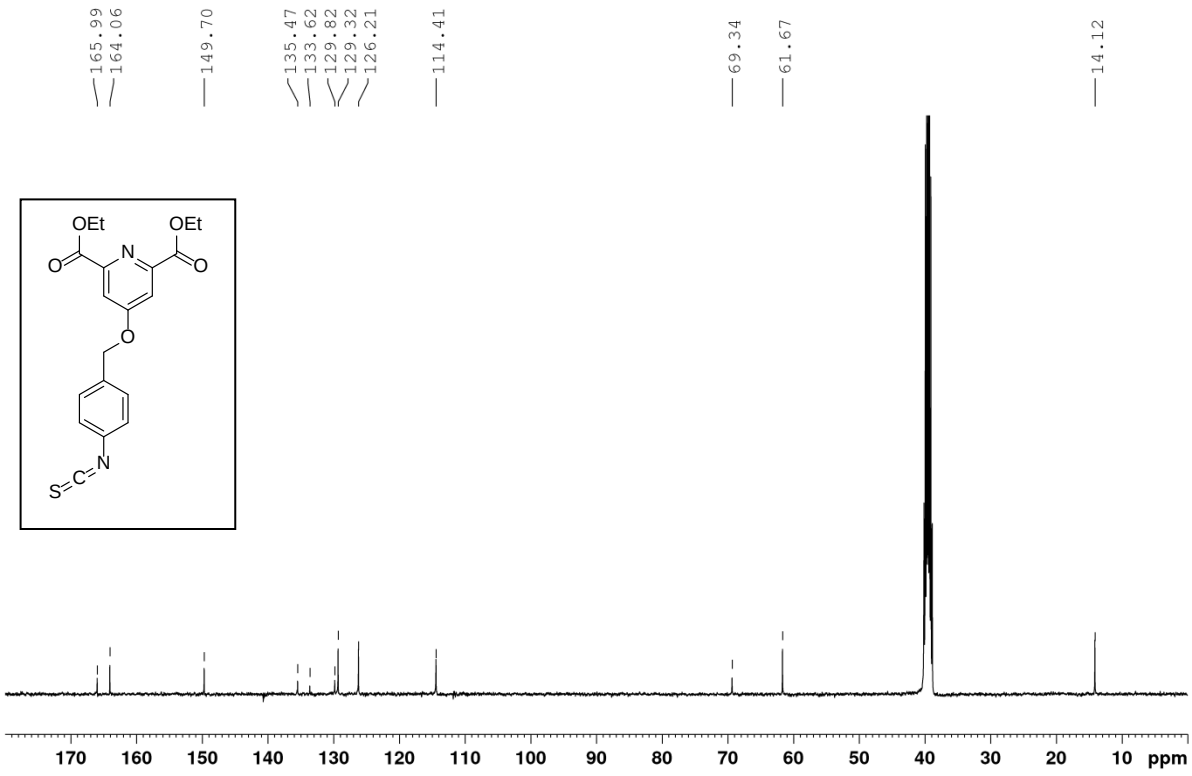

Figure 2A: ^{13}C NMR (100 MHz, DMSO-d_6) spectrum of compound **4** (Figure 48).

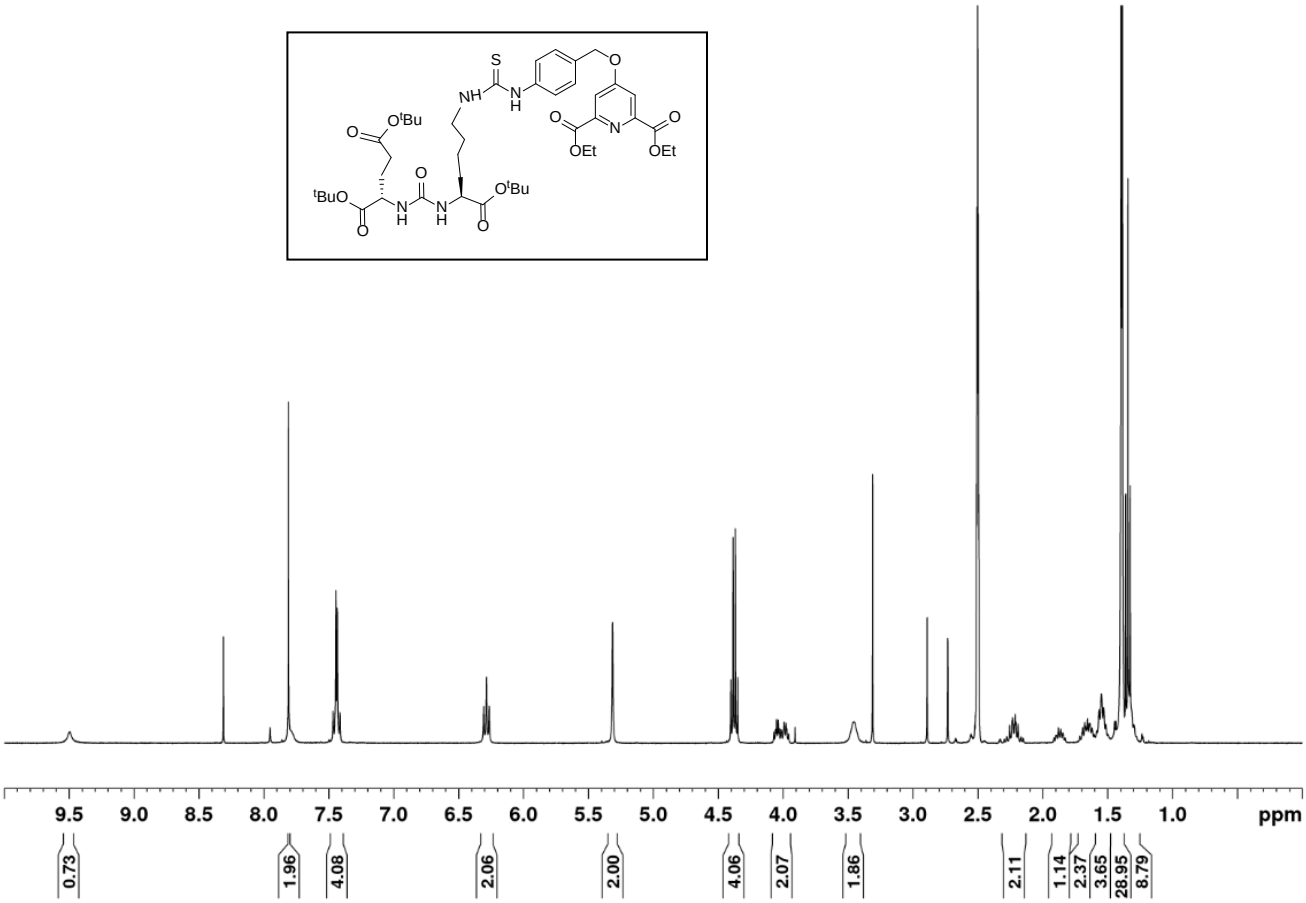

Figure 3A: ^{1}H NMR (400 MHz, DMSO-d_6) spectrum of compound **7** (Figure 48).

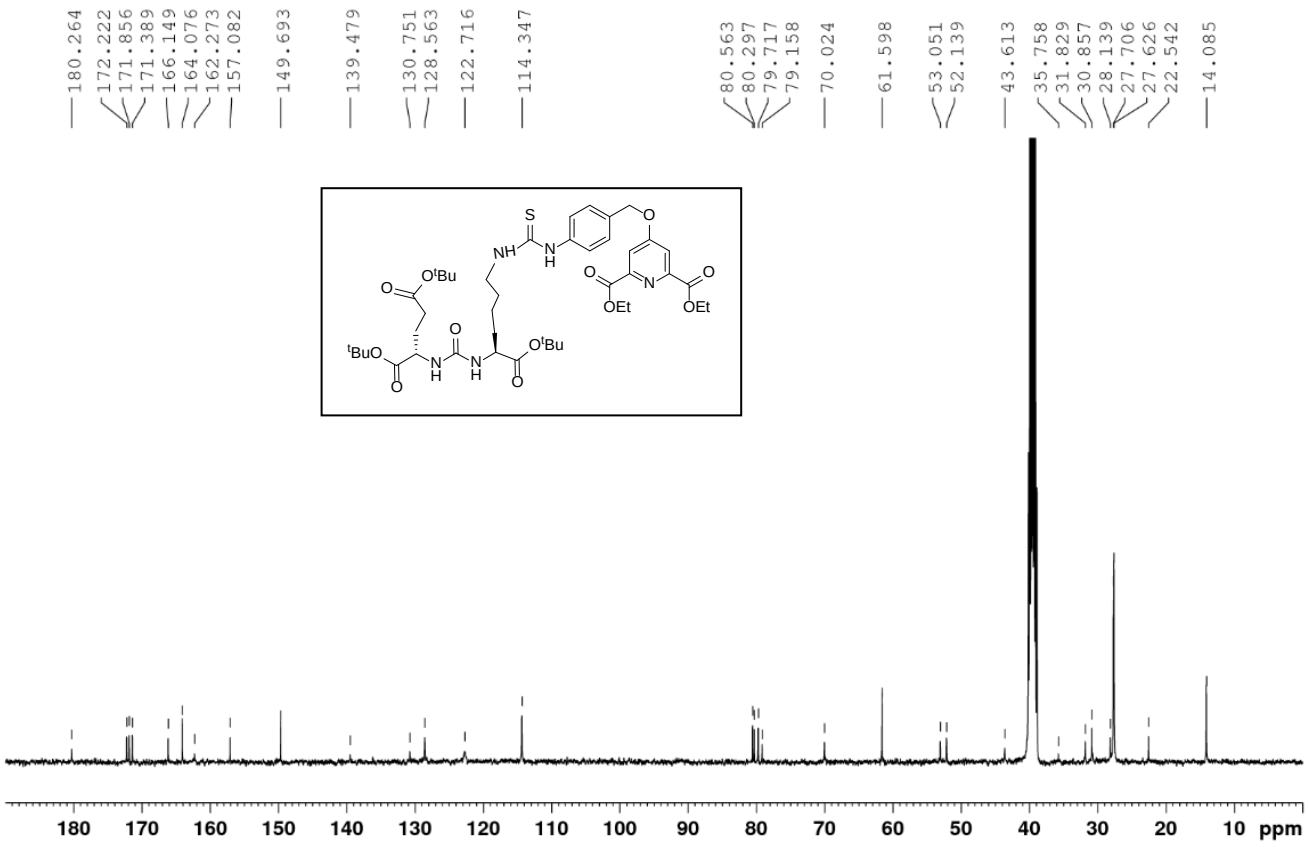

Figure 4A: ^{13}C NMR (100 MHz, DMSO-d_6) spectrum of compound **7** (Figure 48).

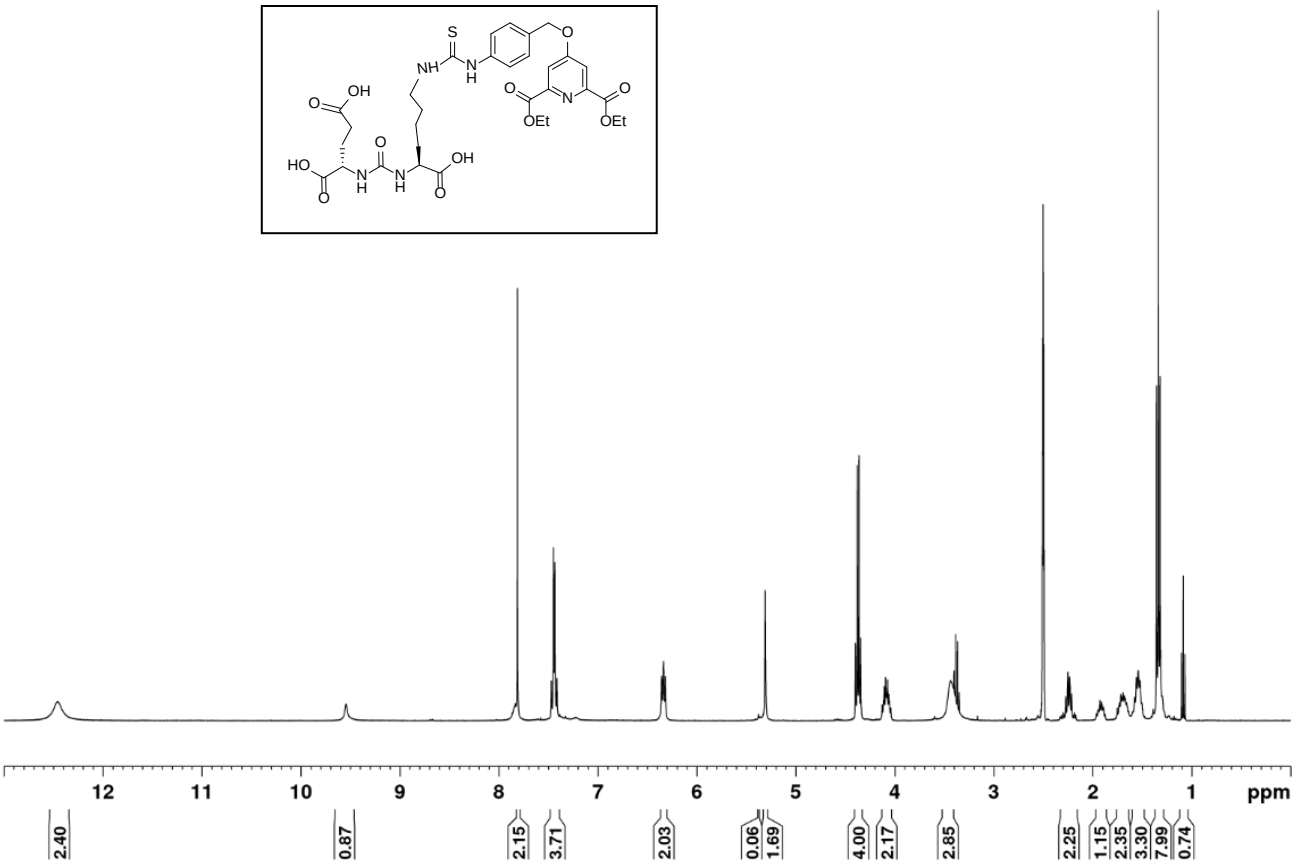

Figure 5A: ^{1}H NMR (400 MHz, DMSO-d_6) spectrum of compound **8** (Figure 48).

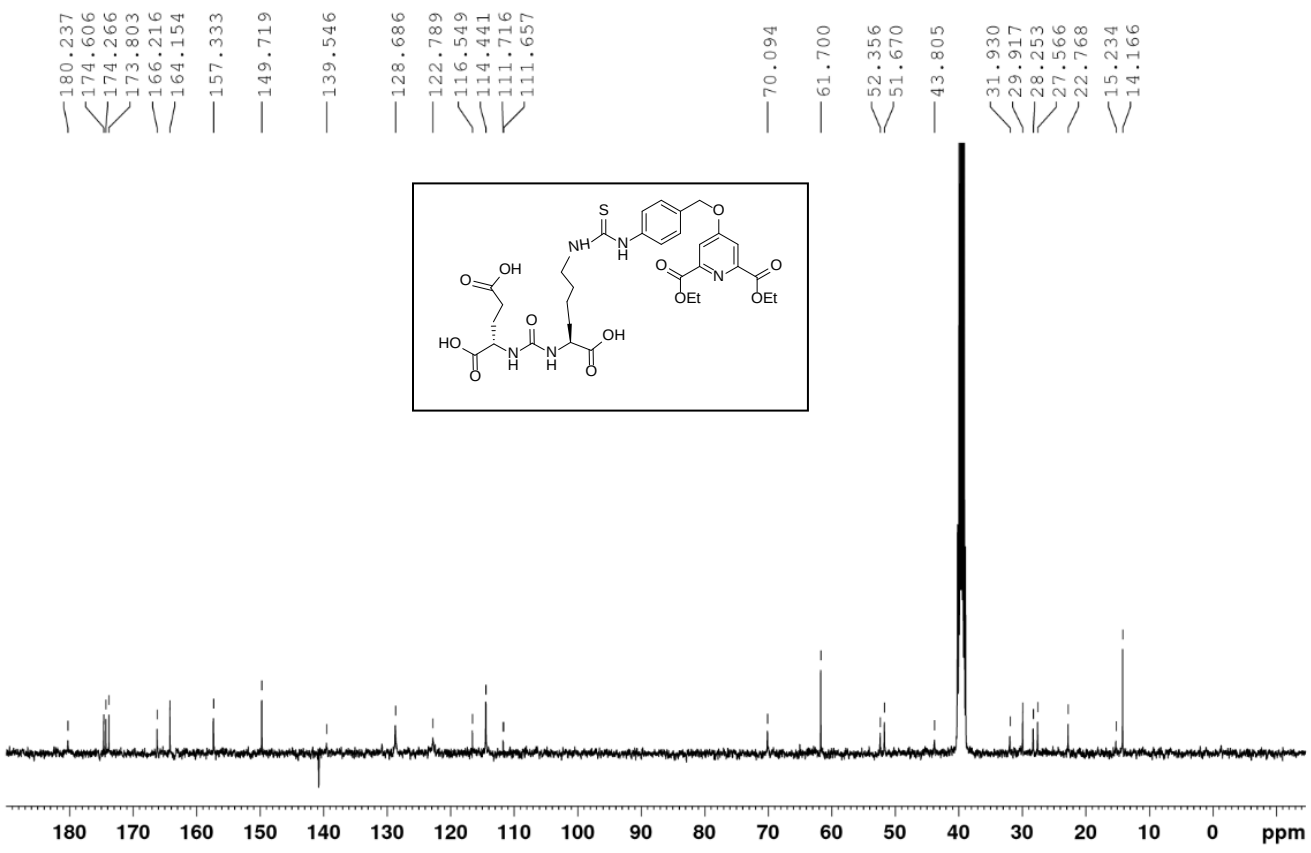

Figure 6A: ^{13}C NMR (100 MHz, DMSO-d_6) spectrum of compound **8** (Figure 48).

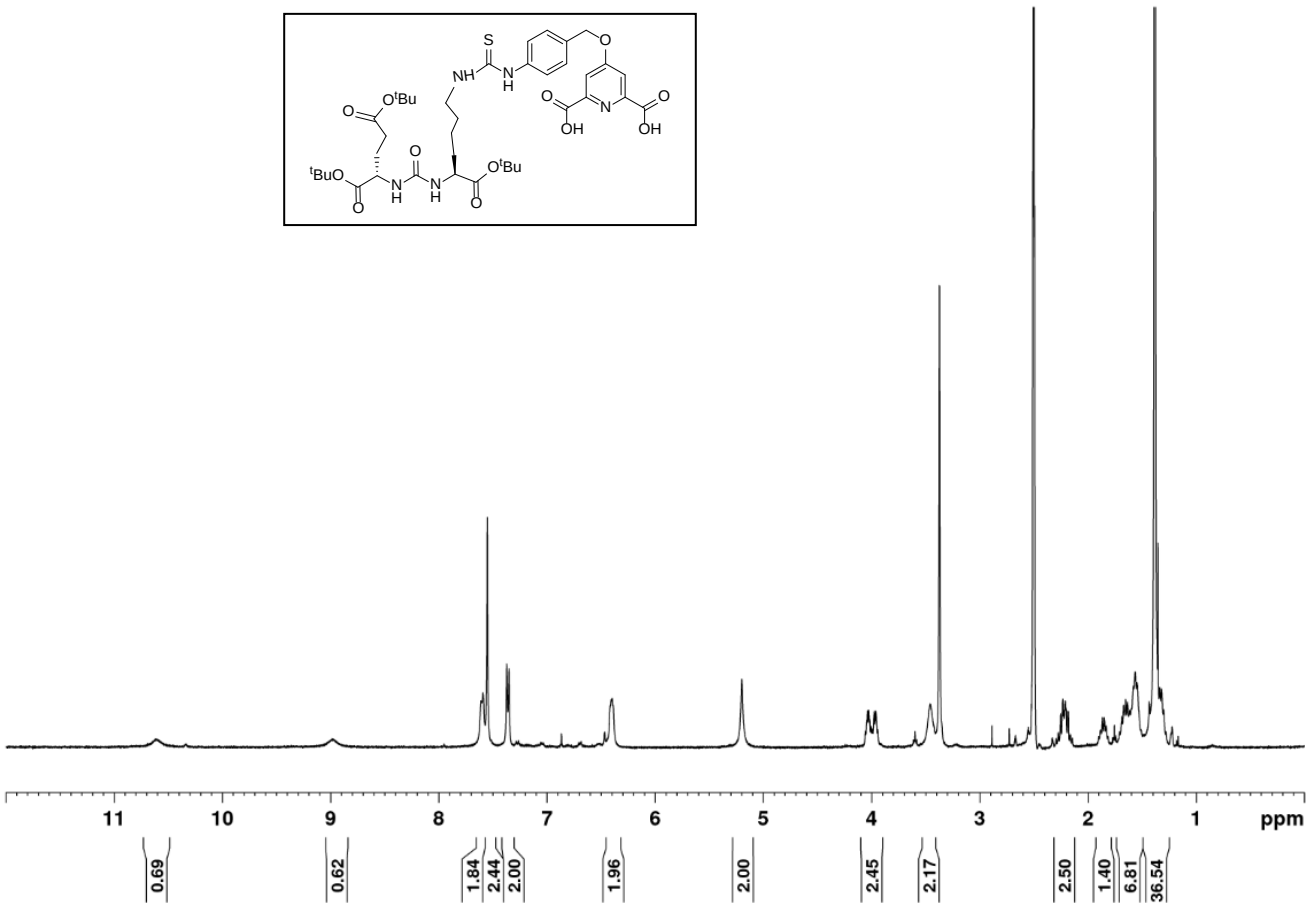

Figure 7A: ^{1}H NMR (400 MHz, DMSO-d_6) spectrum of compound **9** (Figure 48).

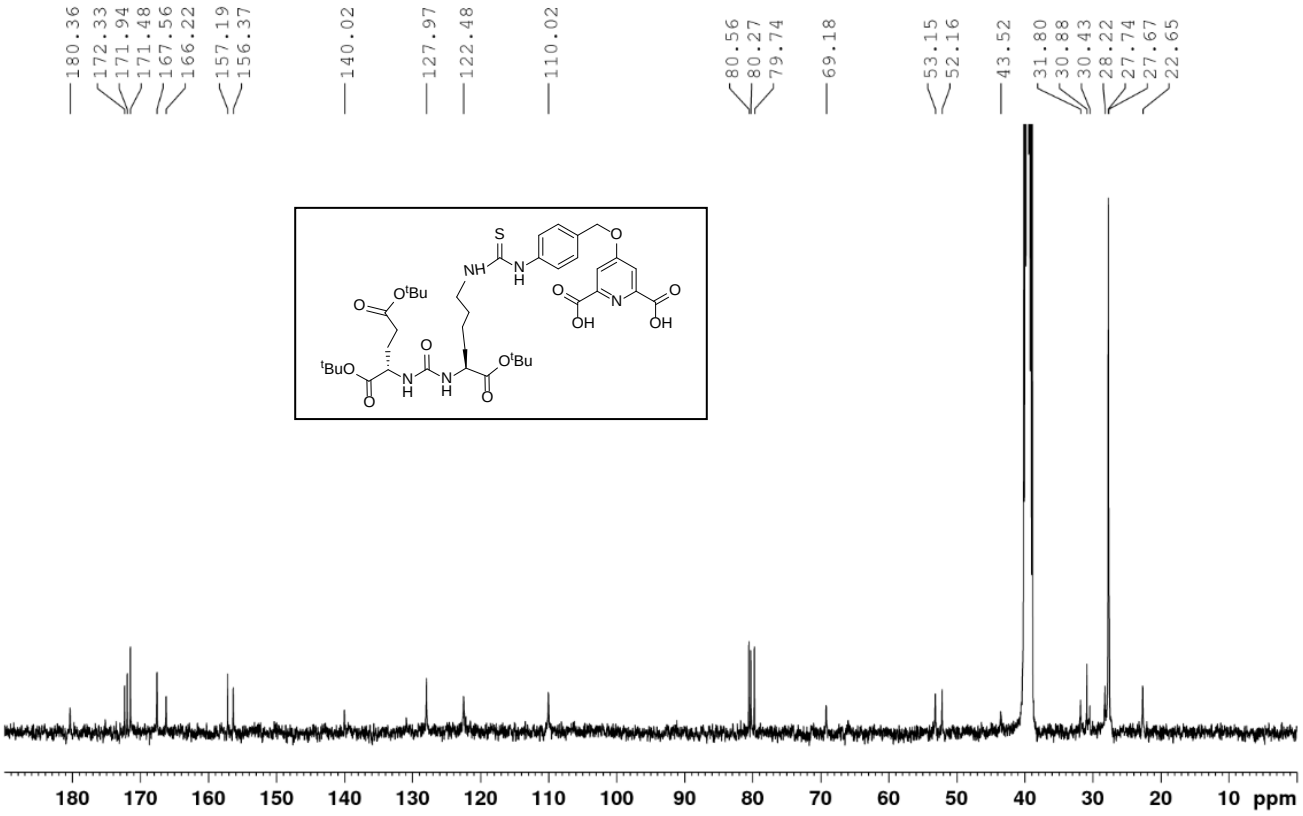

Figure 8A: ^{13}C NMR (100 MHz, DMSO-d_6) spectrum of compound **9** (Figure 48).

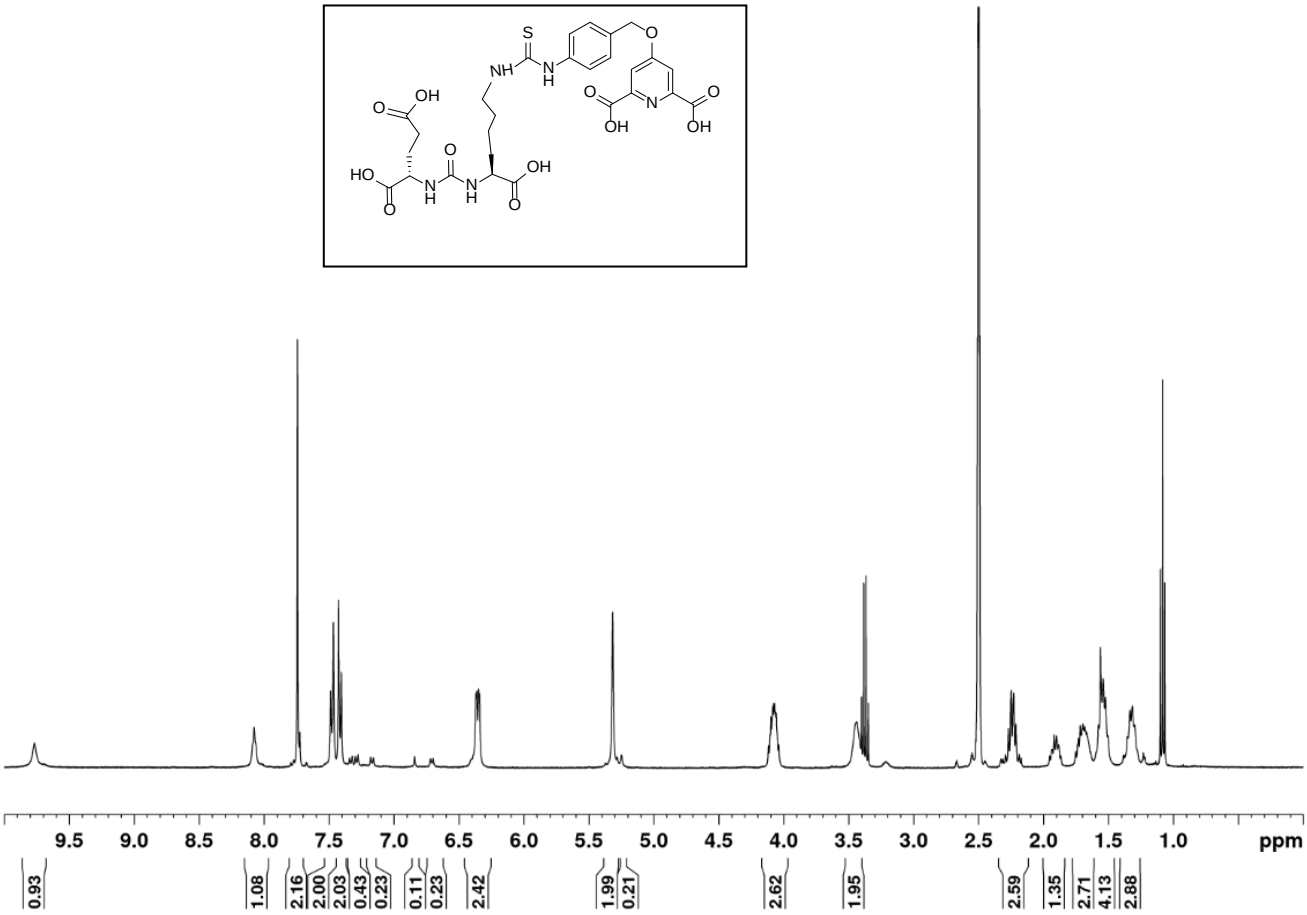

Figure 9A: ^{1}H NMR (400 MHz, DMSO-d_6) spectrum of compound **CA-PSMA** synthesized from compound **9** (Figure 48).

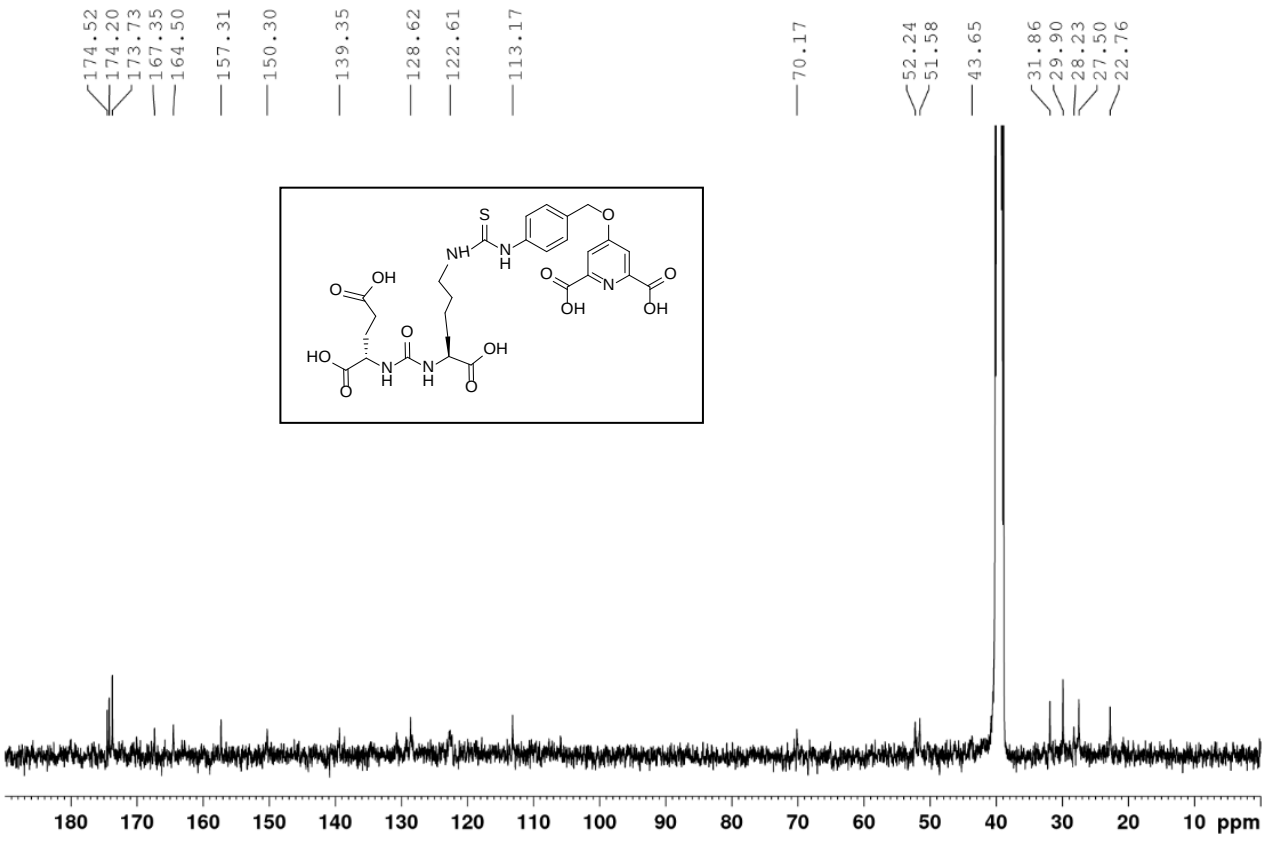

Figure 10A: ^{13}C NMR (100 MHz, DMSO-d_6) spectrum of compound **CA-PSMA** synthesized from compound **9** (weak signal at 180 ppm from the thiourea carbon atom) (Figure 48).

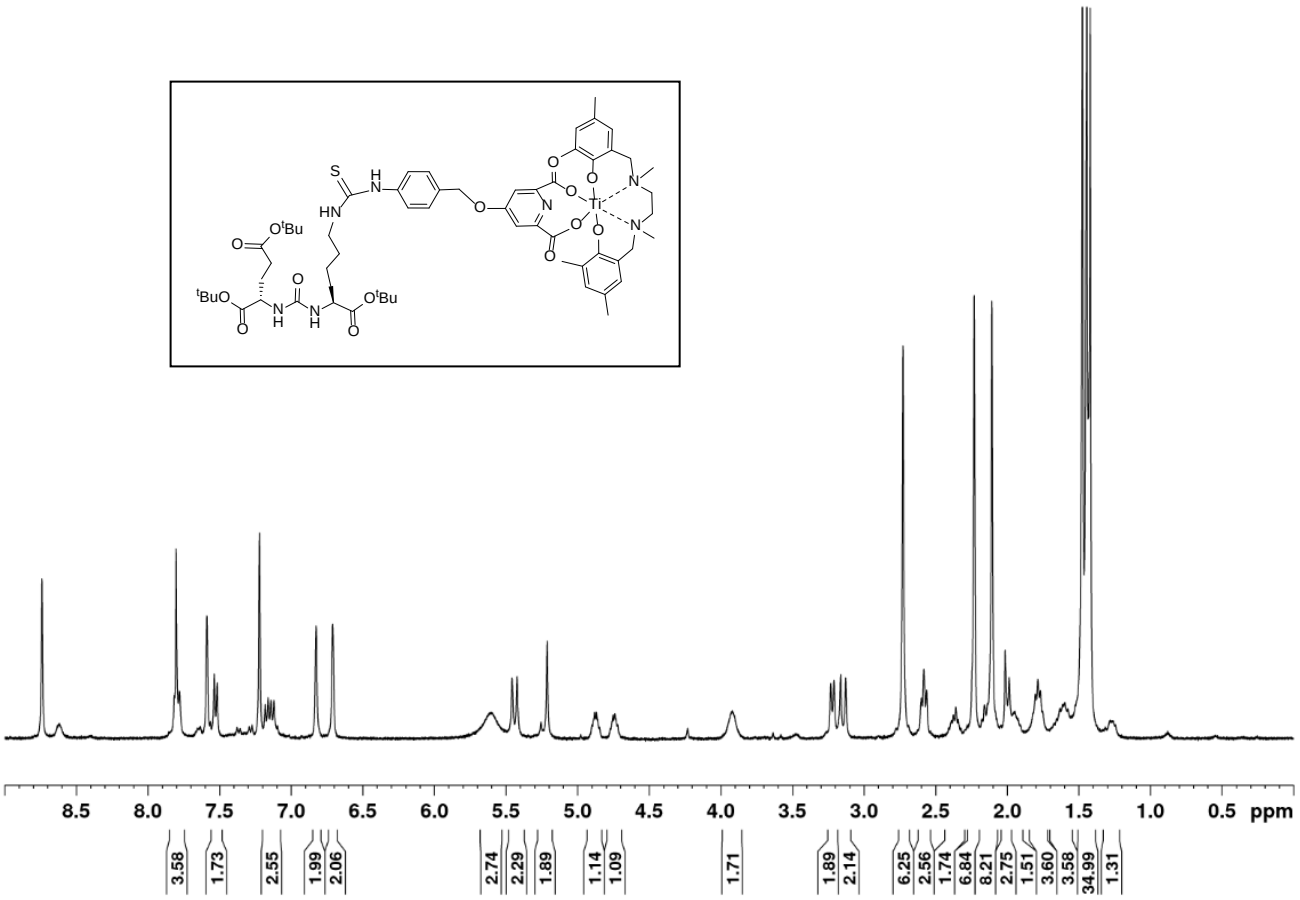

Figure 11A: ^{1}H NMR (400 MHz, pyridine-d_5) spectrum of compound **11** (Figure 49).

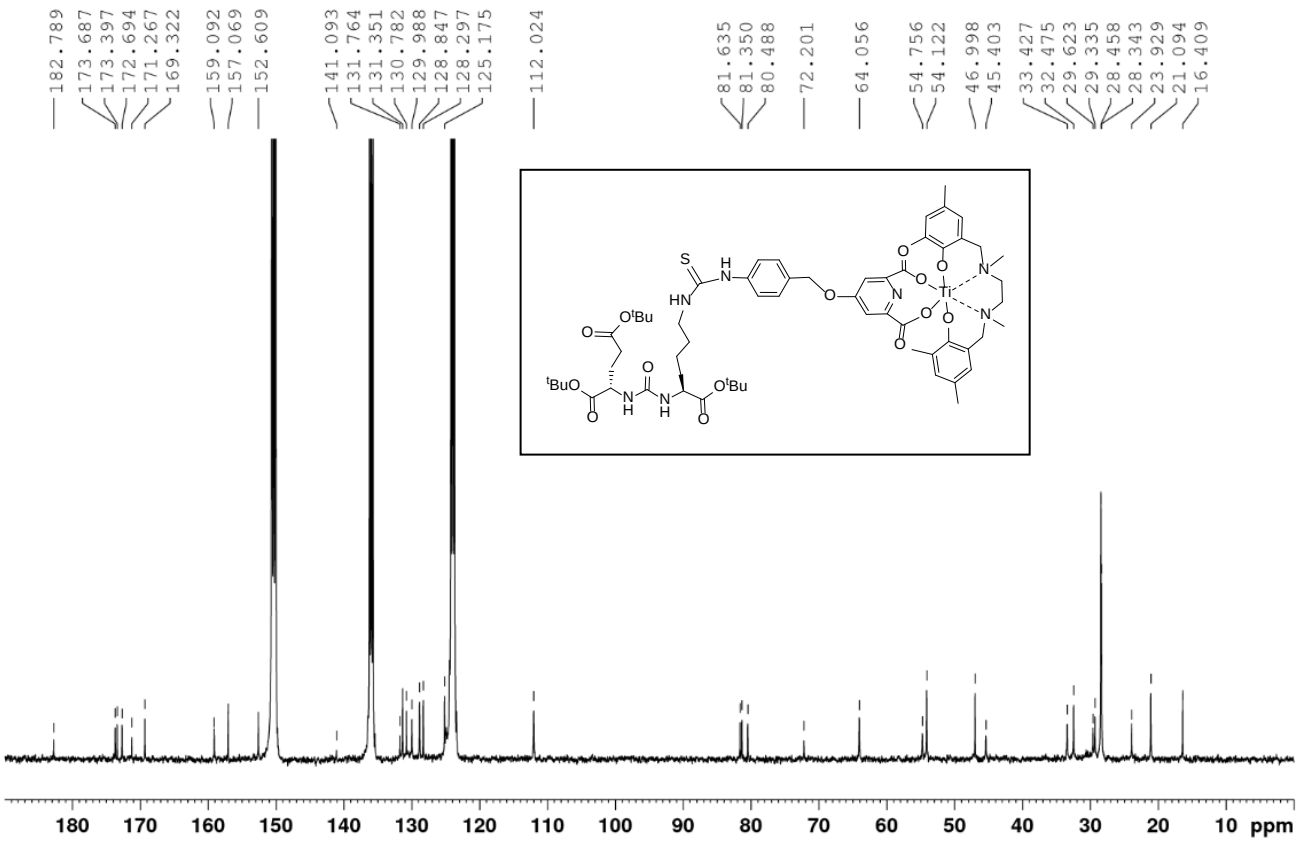

Figure 12A: ^{13}C NMR (100 MHz, pyridine-d_5) spectrum of compound **11** (Figure 49).

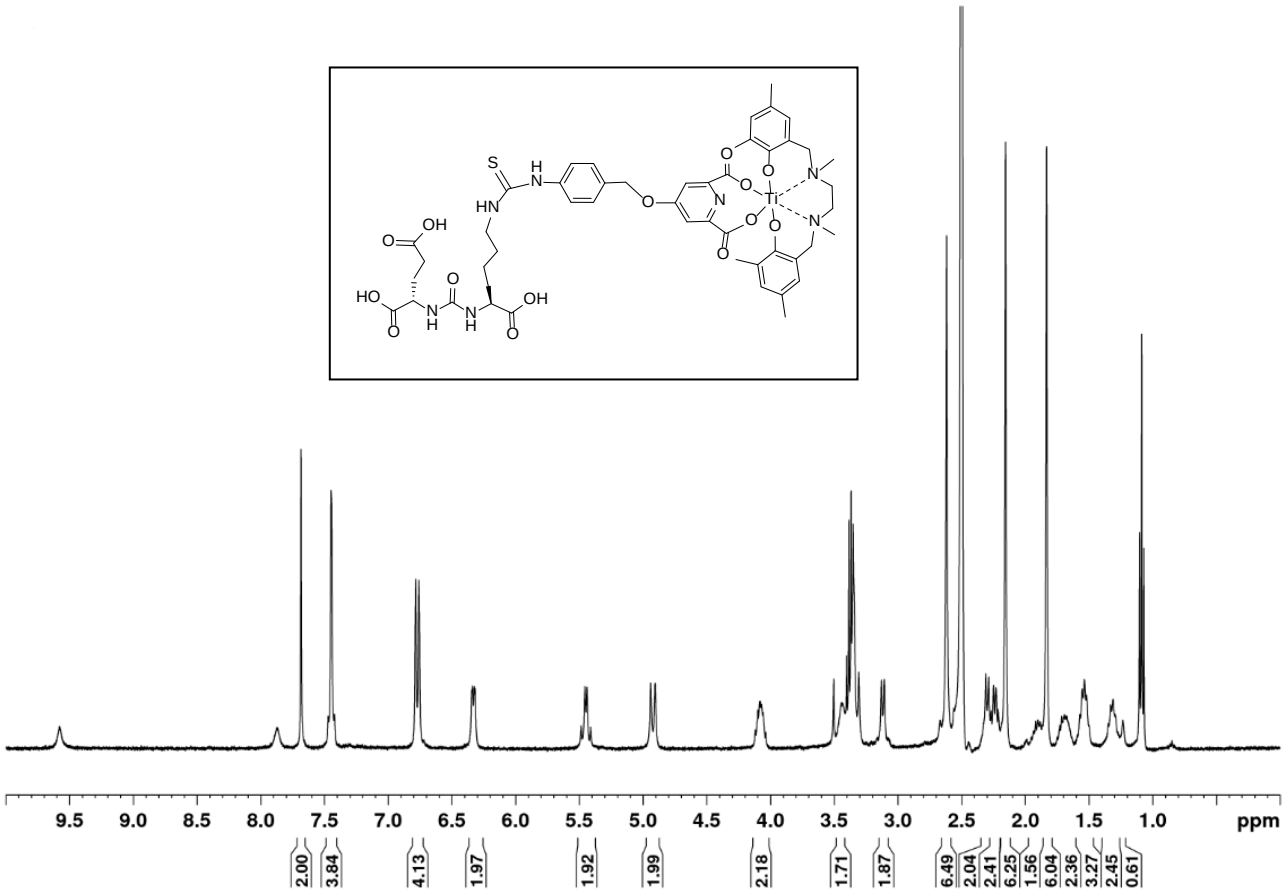

Figure 13A: ^{1}H NMR (400 MHz, DMSO-d_6) spectrum of **Ti-CAS-PSMA** synthesized from **CA-PSMA** and compound **10** (Figure 49).

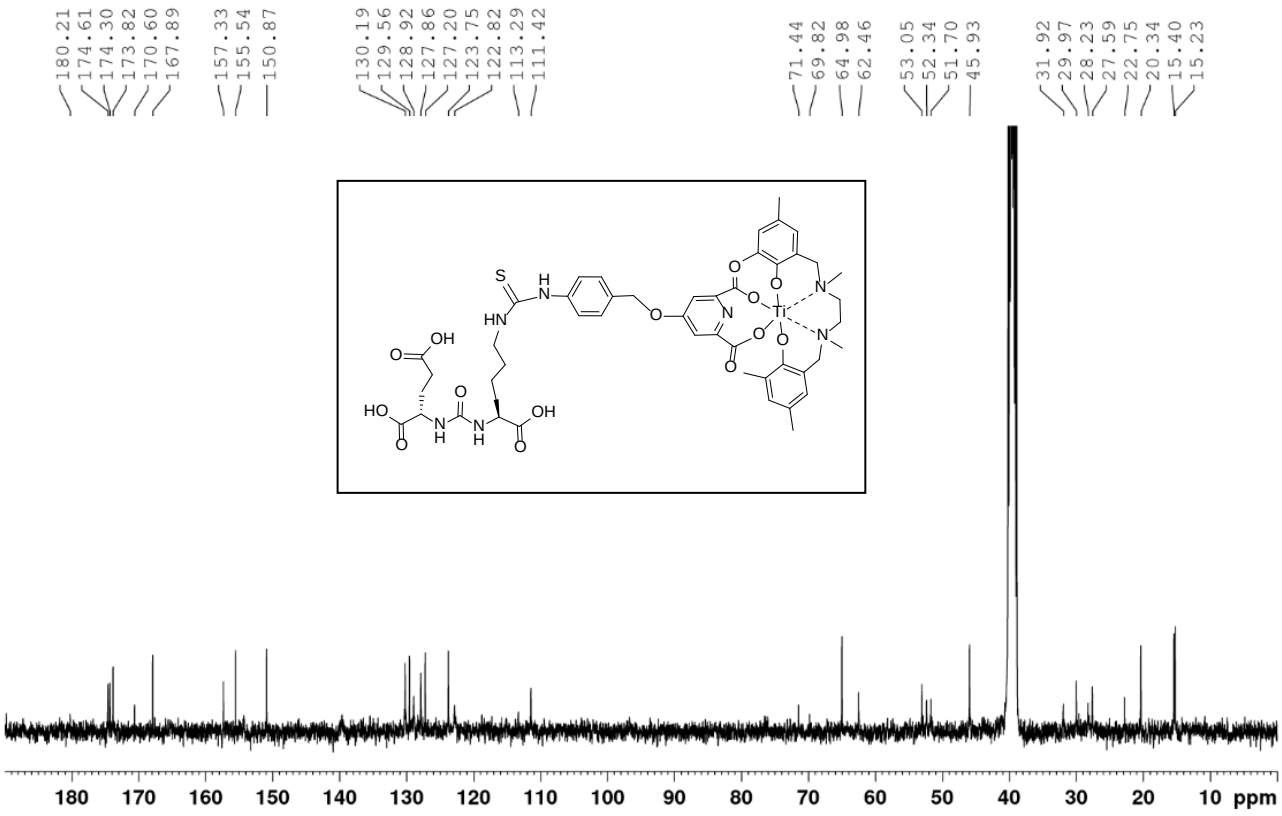

Figure 14A: ^{13}C NMR (100 MHz, DMSO-d_6) spectrum of **Ti-CAS-PSMA** synthesized from **CA-PSMA** and compound **10** (Figure 49). Two weak peaks at 139 ppm and 135 ppm were seen.